Deletion of Sarco(endo)plasmic Reticulum Ca^{2+}-ATPase Regulatory Proteins: Impacts on Energy Metabolism and Obesity

by

Daniel Gamu

A thesis

presented to the University of Waterloo

in fulfillment of the

thesis requirement for the degree of

Doctor of Philosophy

in

Kinesiology

Waterloo, Ontario, Canada, 2017

Examining Committee Membership

The following served on the Examining Committee for this thesis. The decision of the Examining Committee is by majority vote.

External Examiner	NAME: Dr. Christopher G.R. Perry, PhD Title: Assistant Professor, School of Kinesiology and Health Science, York University
Supervisor(s)	NAME: Dr. A. Russell Tupling, PhD Title: Professor, Associate Chair for Undergraduate Studies, Department of Kinesiology, University of Waterloo
Internal Members	NAME: Dr. Marina Mourtzakis, PhD Title: Associate Professor, Associate Chair, Applied Research, Partnerships and Outreach, Department of Kinesiology, University of Waterloo
	NAME: Dr. Joe Quadrilatero, PhD Title: Associate Professor, Associate Chair of Graduate Studies, Department of Kinesiology, University of Waterloo
Internal-external Member	NAME: Dr. Jamie Joseph, PhD Title: Associate Professor, School of Pharmacy, University of Waterloo

Author's Declaration

I hereby declare that I am the sole author of this thesis. This is a true copy of the thesis, including any required final revisions, as accepted by my examiners.

I understand that my thesis may be made electronically available to the public.

Abstract

The sarco(endo)plasmic reticulum (SR) Ca^{2+}-ATPase (SERCA) is responsible for maintaining low cytosolic [Ca^{2+}] through the ATP-dependent pumping of Ca^{2+} ions from the cytosol into the SR lumen. SERCA activity has the potential to be a critical regulator of body mass and adiposity given that it is estimated to contribute upwards of 20% of daily energy expenditure (Smith *et al.* 2013. *PLoS One*. 8: e68924). Two well-characterized regulators of SERCAs are the homologous proteins sarcolipin (SLN) and phospholamban (PLN), which reduce its Ca^{2+} affinity/maximal activity either on their own or through a ternary super-inhibitory complex (Asahi *et al*. 2002. *J Biol Chem*. 277: 26725-26728). Our group has shown that SLN uncouples SERCA function within oxidative skeletal muscle (Bombardier *et al.* 2013. *FEBS Lett*. 587: 1687-1692), and mice lacking SLN ($Sln^{-/-}$) are susceptible to diet-induced obesity (Bombardier *et al*. 2013. *FASEB J*. 27: 3871-3878). However, it remains unclear whether skeletal muscle PLN has a similar role in regulating SERCA efficiency and diet-induced thermogenesis. Furthermore, double knock-out (DKO) mice for both SLN and PLN display a cardiac phenotype distinct from either single KO model (Shanmugam *et al*. 2011. *Cardiovasc Res*. 89: 353-361), suggesting the combined action of SLN and PLN, possibly even the super-inhibitory complex, is integral for regulating cardiac Ca^{2+}-handling. Given that both SERCA regulators are expressed within oxidative muscle, and even within the same muscle fibre (Fajardo *et al*. 2013. *PLoS One*. 8: e84304), potential exists for their combined role in the regulation of SERCA efficiency within skeletal muscle, and consequently whole-body metabolism.

The two major objectives of this thesis were to: 1) determine whether skeletal muscle PLN reduces SERCA efficiency and is involved in diet-induced thermogenesis, and 2) characterize the impact of dual SLN/PLN ablation on skeletal muscle SERCA efficiency, whole-body metabolism and susceptibility to obesity. To address objective 1) we utilized *Pln*$^{-/-}$ and wild-type (WT) littermates, and to address objective 2) we utilized DKO (*Sln*$^{-/-}$/*Pln*$^{-/-}$) and WT (*Sln*$^{+/+}$/*Pln*$^{+/+}$) control mice. We hypothesized that 1) PLN would uncouple SERCA function and *Pln*$^{-/-}$ mice would develop an obesogenic phenotype, and 2) DKO mice would have improved SERCA efficiency within skeletal muscle and as a result be susceptible to an obesogenic phenotype.

We chose to focus our examination using the soleus (SOL), as this muscle endogenously expresses PLN. *Pln*$^{-/-}$ mice showed no changes in histological variables or SR protein expression within SOL, including SLN. While PLN ablation increased maximal Ca^{2+}-ATPase activity ~33% ($P < 0.01$), SERCA pumping efficiency was similar to that of WT littermates, suggesting that PLN does not uncouple Ca^{2+}-uptake from ATP hydrolysis in oxidative muscle. Not surprisingly then, whole-body metabolic rate, metabolic efficiency, glucose tolerance, fat pad mass and adiposity were comparable between WT and *Pln*$^{-/-}$ littermates following 8 weeks of high-fat feeding (42% kcal from fat). This lack of an obesogenic phenotype in *Pln*$^{-/-}$ was not the result of compensation from other known mechanisms of diet-induced thermogenesis, namely skeletal muscle SLN or brown adipose tissue (BAT) uncoupling protein (UCP)-1 expression. Furthermore, cumulative food consumption was also similar between *Pln*$^{-/-}$ mice and WT littermates. Interestingly, SOL PLN expression of high-fat fed WT mice was reduced ~60% ($P < 0.05$) compared to chow-fed controls. Furthermore, there was a tendency (*P*

= 0.07) for high-fat feeding to increase the non-inhibitory phosphorylated form of PLN, together suggesting that the physical interaction of PLN with SERCA is reduced by caloric surfeit. These results indicate that, unlike SLN, skeletal muscle PLN does not increase the energy demand of SERCA to pump Ca^{2+} and is not involved in adaptive diet-induced thermogenesis.

We next examined Ca^{2+}-handling within the SOL of DKO mice. To our surprise, maximal Ca^{2+}-ATPase activity tended ($P = 0.06$) to be lower in DKO SOL. However, we observed a fast-to-slow fibre type shift within DKO SOL, along with hypertrophy of type I and IIA fibres ($P < 0.05$). Correspondingly, SERCA2a protein expression was elevated ($P < 0.05$), while SERCA1a was reduced ($P < 0.05$) in DKO SOL. Thus, the reduction of maximal SERCA function in DKO mice likely reflects an overall reduction of total SERCA density resulting from the fibre type shift of these animals. Despite these changes, SERCA efficiency tended ($P = 0.08$) to be higher in DKO SOL, consistent with the absence of SLN, and suggests a lower energy demand of SERCA to pump Ca^{2+} in these mice. Interestingly, 24-hr whole-body metabolic rate (ml O_2/kg body mass/hr) was ~4% higher ($P < 0.05$) in DKO mice, although they were also more ($P < 0.05$) spontaneously active during metabolic measurements. Unlike hypothesized, DKO mice were in fact protected against diet-induced obesity compared to WT control animals as noted by their lower dietary mass gain, smaller subcutaneous/visceral fat pad mass, and lower adiposity index when fed both a chow or HFD for 8 weeks ($P < 0.05$). Protection of DKO mice against obesity was unrelated to energy intake, as cumulative food consumption was similar to that of WT control mice. Interestingly, weekly metabolic efficiency was lower ($P < 0.05$) in DKO mice across 8 weeks of chow feeding and

between weeks 1 to 5 of the HFD, suggesting greater energy expenditure of these animals. Although HFD-fed DKO mice were more spontaneously active during metabolic measurements both pre- and post-HFD ($P < 0.05$), whole-body energy expenditure was greater ($P < 0.05$) post-HFD in DKO mice, even during states of physical inactivity; therefore, greater cage activity can only partly explain their lean phenotype. Although SERCA isoforms were altered within DKO SOL in both chow- and HFD-fed animals as described above, no genotype differences were observed in the expression of proteins involved in SR Ca^{2+} release or storage, regardless of diet. PLN protein expression was again reduced in WT SOL by ~55% ($P < 0.05$) in response to the HFD, in addition to increasing its non-inhibitory phosphorylated form ($P < 0.05$). Furthermore, while BAT UCP-1 protein expression of WT and DKO mice was increased ~25% ($P < 0.01$) in response to the HFD, no genotype differences in UCP-1 expression existed. Thus, protection against obesity was not the result of any change in skeletal muscle or BAT proteins measured in response to dual SLN/PLN ablation.

This thesis revealed several novel findings. First, we show that physiological levels of PLN protein within oxidative skeletal muscle do not uncouple SERCA function. Not surprisingly then, *Pln*$^{-/-}$ animals were not susceptible to an excessively obese phenotype when given a "Westernized" HFD, which is distinctly different from that previously shown for *Sln*$^{-/-}$ mice. Secondly, we showed that PLN protein expression is responsive to calorie surfeit. Specifically, high-fat feeding reduced PLN's interaction with SERCA by both decreasing its expression and increasing its non-inhibitory phosphorylated form. These data are in line with a growing body of literature suggesting that SLN and PLN serve distinct physiological roles within skeletal muscle. We

conclude that, unlike SLN, PLN is not involved in skeletal muscle adaptive diet-induced thermogenesis. Thirdly, we show that the combined regulation of SERCA by SLN and PLN are required for the regulation of muscle fibre-type and size as noted by the fast-to-slow fibre-type shift and hypertrophy of type I and IIA fibres with DKO SOL. Lastly, despite the inability to activate SLN-mediated thermogenesis, DKO animals were surprisingly protected against obesity. While not examined here, the muscular phenotype of DKO animals is consistent with the activation of cytosolic Ca^{2+}-signaling proteins. Given that *in vivo* SR Ca^{2+} load is likely to be higher in DKO skeletal muscle, this may result in a greater SR gradient favoring SR Ca^{2+} leak and subsequent activation of cytosolic Ca^{2+}-signaling proteins. Furthermore, a futile cycle of SR Ca^{2+}-leak and re-uptake may explain, in part, hypermetabolic phenotype and protection against obesity of DKO mice.

Acknowledgements

First, I would like to thank my supervisor Dr. A Russell Tupling. Russ, even after thinking about what I will write here for so long, I can't adequately express the magnitude of my gratitude towards you. Unbeknownst to me at the time, meeting you in 2008 was without doubt a watershed moment in my life. So many amazing things have happened to me since beginning my graduate studies in your lab, both professionally and personally. Thank you for your unwavering support, guidance, immense patience, and willingness to share a scientific discussion. You are a role model that I strive to emulate.

I would also like to thank my thesis advisory committee, Dr. Marina Mourtzakis and Dr. Joe Quadrilatero. I'm grateful to have had the opportunity to learn so much from each of you through your amazing classes and discussions (both formal and informal). Thank you for challenging me to become a better scientist and helping shape my academic personality. To Marg Burnett and Denise Hay, you both are such incredible people. Your tireless dedication to the department and students is truly appreciated. We simply would not be able to do what we do without each of you. Thank you to Jing Ouyang for the technical support, and to the animal care technicians (Nancy, Jean, Martin, and Angela) for their compassionate care of all the research animals involved in this study.

My time in Waterloo has been filled with memories that I will hold close to my heart for the rest of my life, memories that are the direct result of the people I've met in the Kinesiology department. I believe that the best way to grow is to surround oneself by individuals vastly superior in knowledge and skill. To Dr. Eric Bombardier, Dr. Ian Smith, Dr. Chris Vigna, and Dr. Val Fajardo, you each have created such a high standard that I continuously try to reach, both at Waterloo and beyond. But more importantly, thank you for your friendship. I wish you all continued success in your respective careers and can't wait to share a pint (many pints) and a laugh (many laughs) again! To Emma, Riley, Brad, Cat, Frenk, Paige and all past Tupling lab members, the lab has always felt like an extended family and that is because of each of you. A very special thanks to Brad and Emma for their help in completing this thesis, your dedication and work ethic are truly appreciated and will serve you well. To the members of the Quadrilatero and Mourtzakis labs over the past years, you have taken me into your homes, fed me, made me a part of your monumental life events, shared countless laughs (and just as many beers), and fed me. From the bottom of my heart, thank you for your friendship and making my time in Waterloo one that I look back on so fondly. You will always be welcome in our home!

To my family, without you this would simply not have been possible. Mum and Dad, Jon and I are the men we are today because of you. I can't even begin to express what your love and support means to me. Thank you for allowing us to pave our own way, even if it is an unconventional one. Your encouragement, especially during hard times, has been the catalyst for me to finish my graduate career. I hope that I can be the parent to my son that you both have been to us. I love you both so much. Jon, I don't think I would have even entertained doing a PhD if not for you. One day I hope to be as

intelligent, eloquent, insightful, and analytical as you are. Thank you for pushing me, always. I'm so fortunate to have you as my brother and best friend. I love you Jono. Rachel and Jack, you are my heart and soul. Each and every day I hope to do right by you both. Red, meeting you in the hallway outside of the physiology lab changed my life. I've thought about you every single day since, and now we get to build our life together. You inspire me as a parent, a partner, an academic, and so much more. You and Jack are the love of my life.

Dedication

This thesis is dedicated to my beautiful little redhead Jack. I hope to always make you proud and inspire you to challenge yourself, even if it means falling flat on your face the first time.

Table of Contents

List of Figures

List of Tables

List of Abbreviations

AA – amino acid

ATP – adenosine triphosphate

AUC – area under the curve (in reference to glucose tolerance test)

BAT – brown adipose tissue

$[Ca^{2+}]_f$ – cytosolic free Ca^{2+} concentration

CaMK - Ca^{2+}/calmodulin-dependent protein kinase

CaN - calcineurin

CLAMS – comprehensive lab animal monitoring system

CPA - cyclopiazonic acid (SERCA-specific inhibitor)

CSA – cross sectional area

CSQ - calsequestrin

DHPR - dihydropyrodine receptor

DIT – diet-induced thermogenesis

DKO – sarcolipin/phospholamban double knock-out mice

EDL – extensor digitorum longus

Epidid – epididymal fat pad

FDB - flexor digitorum brevis

HEK-293 – human embryonic kidney 293 cells

HFD – high-fat diet

Ing – inguinal fat pad

KO – knock-out

LV – left ventricle

MHC – myosin heavy chain

pCa - $-\log_{10}([Ca^{2+}]_f)$

pCa_{50} – Ca^{2+} affinity: pCa value at half-maximal ATPase activity

PKA – protein kinase A

PLN - phospholamban

Pln$^{-/-}$ - phospholamban deficient mice

Pln^{OE} – phospholamban overexpressing mice

PMSF - phenylmethylsulfonyl fluoride buffer

PTU - propylthiouracil

RER – respiratory exchange ratio

Retro – retroperitoneal fat pad

RyR – ryanodine receptor

SERCA – sarco(endo)plasmic reticulum Ca^{2+}-ATPase

SLN - sarcolipin

Sln$^{-/-}$ - sarcolipin deficient mice

SOL - soleus

SR – sarcoplasmic reticulum

T3 – triiodothyronine

T4 - L-thyroxine

UCP – uncoupling protein

V_{Max} – maximal rate of catalytic activity

VO_2 – O_2 consumption rate (ml O_2/kg body mass/hr)

WT – wild-type

CHAPTER 1

Review of the Literature, Statement of the Problem and Hypotheses

Introduction

Obesity has risen to epidemic proportions and imposes a significant financial burden to global health care systems (1) due to its associated prevalence with diseases like type 2 diabetes, hypertension, cardiovascular diseases, and various cancers (2). Clinically, individuals with a body mass index (BMI: kg/m^2) of 30 or above are obese, while those with a BMI between 25-29 are considered overweight (2). The maintenance of body mass and development of obesity can be understood from a thermodynamic perspective. Body mass is maintained when caloric intake is matched by caloric expenditure (i.e. energy balance). However, when caloric intake exceeds that of expenditure (i.e. positive energy balance), the resulting caloric surplus is stored as fat in adipose tissue depots, and when this surplus continues for a prolonged period of time, obesity and associated metabolic complications can develop. Conversely, body mass can be reduced when caloric expenditure exceeds that of intake (i.e. negative energy balance). Mathematically, this model of obesity is easy to understand; however, the physiological determinants that regulate energy balance are dynamic as they can be altered by environmental factors (e.g. diet, activity, ambient temperature).

Exploiting naturally occurring mechanisms that govern metabolic rate to increase energy expenditure has long been a conceptually palatable idea to reduce obesity and associated comorbidities. In homeothermic endotherms, several important mechanisms regulate internal body temperature and mass in the face of environmental stress, the best characterized of which is mitochondrial uncoupling within brown adipose tissue (BAT).

BAT: the Classical Regulator of Adaptive Thermogenesis

Adaptive thermogenesis refers to a regulated change in energy expenditure in response to alterations in ambient temperature or food availability (3, 4), allowing maintenance of physiological function during thermal or dietary perturbation. Adaptive thermogenesis can be further subdivided as 1) shivering thermogenesis, and 2) non-shivering thermogenesis. Classically, adaptive thermogenesis has been studied in response to cold exposure (3). In this context, shivering thermogenesis refers to heat production originating from continual muscular contraction in order to maintain body temperature during acute cold exposure. However, contraction cannot continue indefinitely and eventually ceases, although body temperature continues to be maintained (3). Non-shivering thermogenesis refers to the ability to maintain continued heat production in the absence of shivering, and in rodents originates primarily from BAT mitochondrial uncoupling protein (UCP)-1 (3).

UCP-1 is found within the inner mitochondrial membrane of brown adipocytes, and uncouples mitochondrial respiration by dissipating the hydrogen gradient formed across the inner mitochondrial membrane during electron transport (3). The resultant heat released during this process originates from the conversion of potential osmotic energy, as H^+ ions flow down their electrochemical gradient into the mitochondrial matrix. In order to maintain cellular adenosine triphosphate (ATP) stores in the face of a continually dissipated H^+ gradient, catabolism of energy substrates (e.g. carbohydrate and fat) must increase to produce enough reducing equivalents (i.e. NADH, $FADH_2$) required for the maintenance of proton motive force, a process further releasing heat. As expected, UCP-1 knock-out (KO) mice are cold-sensitive due to an inability to recruit BAT-mediated thermogenesis (5). Furthermore, UCP-1 KO mice develop obesity when

housed at thermoneutrality (~30°C) (6). In this latter context, the activation of energy expenditure by diet is referred to as diet-induced thermogenesis (DIT), the purpose of which is to regulate body mass and metabolic function.

While UCP-1 may be a major regulator of thermogenesis in rodents (3, 6), its relevance to the pathogenesis or amelioration of human obesity remains debated (7-11). Thus, discovery of other adaptive thermogenic mechanisms that regulate body mass has been of particular interest to the field. Specifically, mechanisms within skeletal muscle may play a major role in the development of obesity (12-17).

The Main Sources of Skeletal Muscle Energy Consumption: A Brief Discussion

Skeletal muscle has the capacity to contribute considerably to daily energy expenditure given that it comprises ~40% of adult body mass (18). During neural activation of a skeletal muscle fibre, depolarization of the sarcolemmal and t-tubular membranes result in the release of Ca^{2+} from the sarcoplasmic reticulum (SR) lumen into the cytosol (19) (**Figure 1.1**). Upon release, Ca^{2+} ions bind to the thin filament regulatory protein troponin C, causing a conformational change in tropomyosin and exposing myosin binding sites along the actin filament (19). Once exposed, myosin then interacts with actin forming cross-bridges, and the hydrolysis of ATP by the myosin ATPase provides the energy required for sarcomere shortening (i.e. muscular contraction). In order for the muscle fibre to then relax, Ca^{2+} must be pumped from the cytosol back into the SR lumen, an ATP-dependent process mediated by the

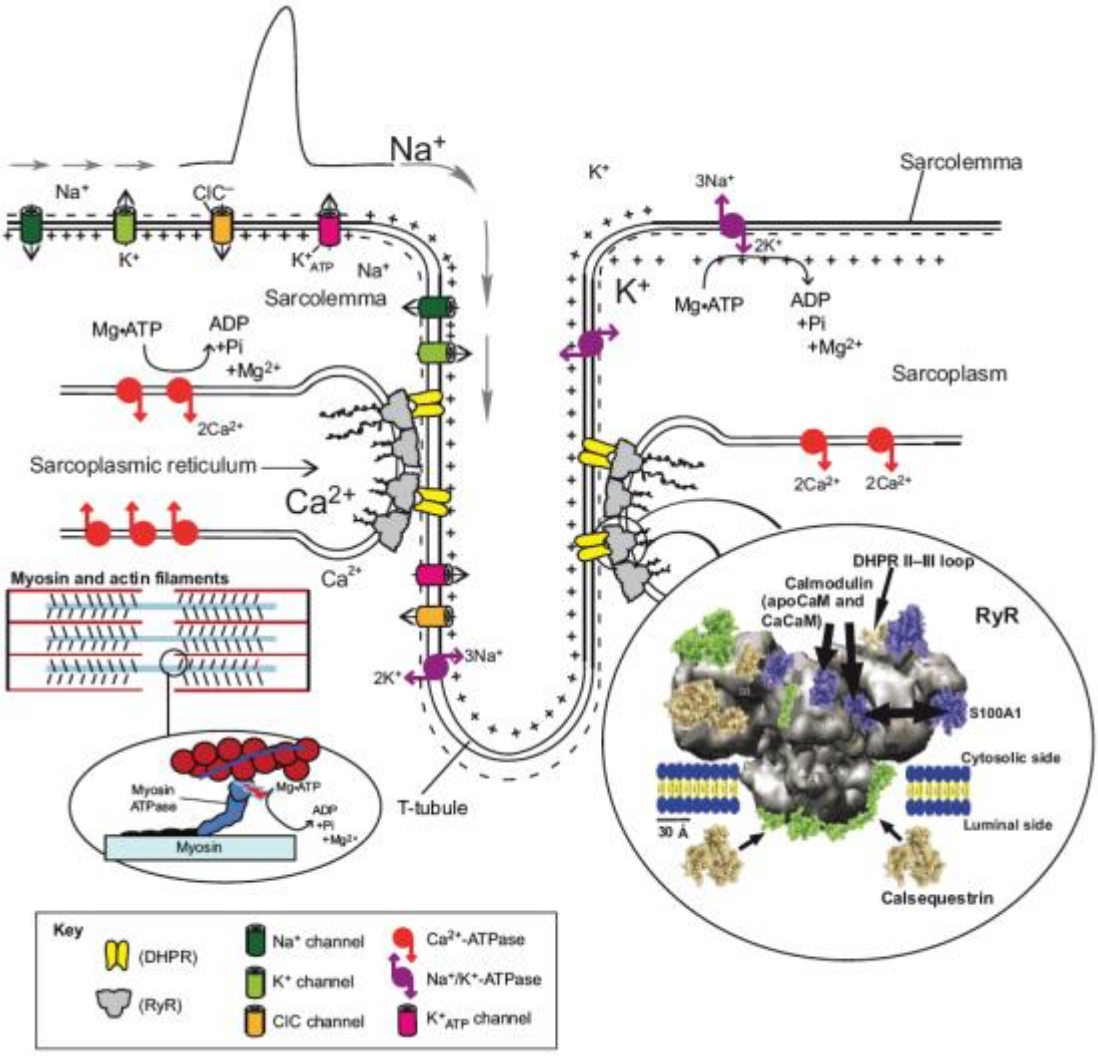

Figure 1.1. Molecular events of skeletal muscle contraction and relaxation, including sites of ATP utilization. Depolarization of the sarcolemma propagates into the t-tubule and is sensed by the dihydropyrodine receptor (DHPR), which is physically coupled to the ryanodine receptor (RyR), together forming the Ca^{2+}-release unit. A conformational change in the DHPR results in the release of Ca^{2+} from the sarcoplasmic reticulum (SR) through the RyR. The subsequent rise in cytosolic Ca^{2+} allows the interaction between actin and myosin filaments, and the hydrolysis of ATP by the myosin ATPase enables shortening of the sarcomere (left insert). The ATP-dependent pumping of Ca^{2+} ions back into the SR lumen by the Ca^{2+}-ATPase results in sarcomere relaxation. Once inside the SR, Ca^{2+} ions become bound to the luminal Ca^{2+} binding protein calsequestrin, which physically associates with the RyR (right insert). Na^+ and K^+ gradients are restored by the Na^+/K^+-ATPase, allowing for subsequent sarcolemmal and t-tubular depolarization. Image taken from MacIntosh *et al* (20).

sarco(endo)plasmic reticulum Ca^{2+}-ATPase (SERCA) (21). Finally, the electrochemical gradients of Na^+ and K^+ are returned by the action of the Na^+/K^+-ATPase to allow for continual depolarization of the muscle fibre (22). During isometric contraction, the contributions of the myosin ATPase, SERCA, and Na^+/K^+-ATPase are estimated to contribute ~65-80%, 10-25%, and 5-10% towards ATP consumption, respectively (18). While the processes of muscle contraction, relaxation, and resetting of ion gradients inevitably control adaptive shivering thermogenesis, mounting evidence indicates that the energy consumed by SERCA is a dynamically regulated process, controlling core temperature and body mass in response to environmental stress.

SERCA Structure and Muscular Isoforms

SERCAs are 110 kDa SR integral membrane proteins of the P-type ATPase family, named so because of the transfer of the γ–phosphate group of ATP to a highly conserved aspartate residue (Asp351), forming a phospho-protein intermediate (23). SERCAs contain a large cytoplasmic headpiece consisting of three domains: nucleotide-binding, phosphorylation and actuator (21) (**Figure 1.2**). A short stalk region connects this headpiece to a transmembrane domain consisting of 10 α-helicies, of which 2 Ca^{2+} binding sites are situated within helices 4-6 and 8 (21). As its name implies, binding of ATP occurs within the nucleotide-binding domain, and along with the occupancy of 2 Ca^{2+} ions within their transmembrane binding sites, permit a conformation that transfers ATP's γ–phosphate to Asp351 located within the phosphorylation domain (24). This conformation places strain on the actuator domain, causing its angular rotation and eventual gating of Ca^{2+} ions into the SR lumen (24) (described below).

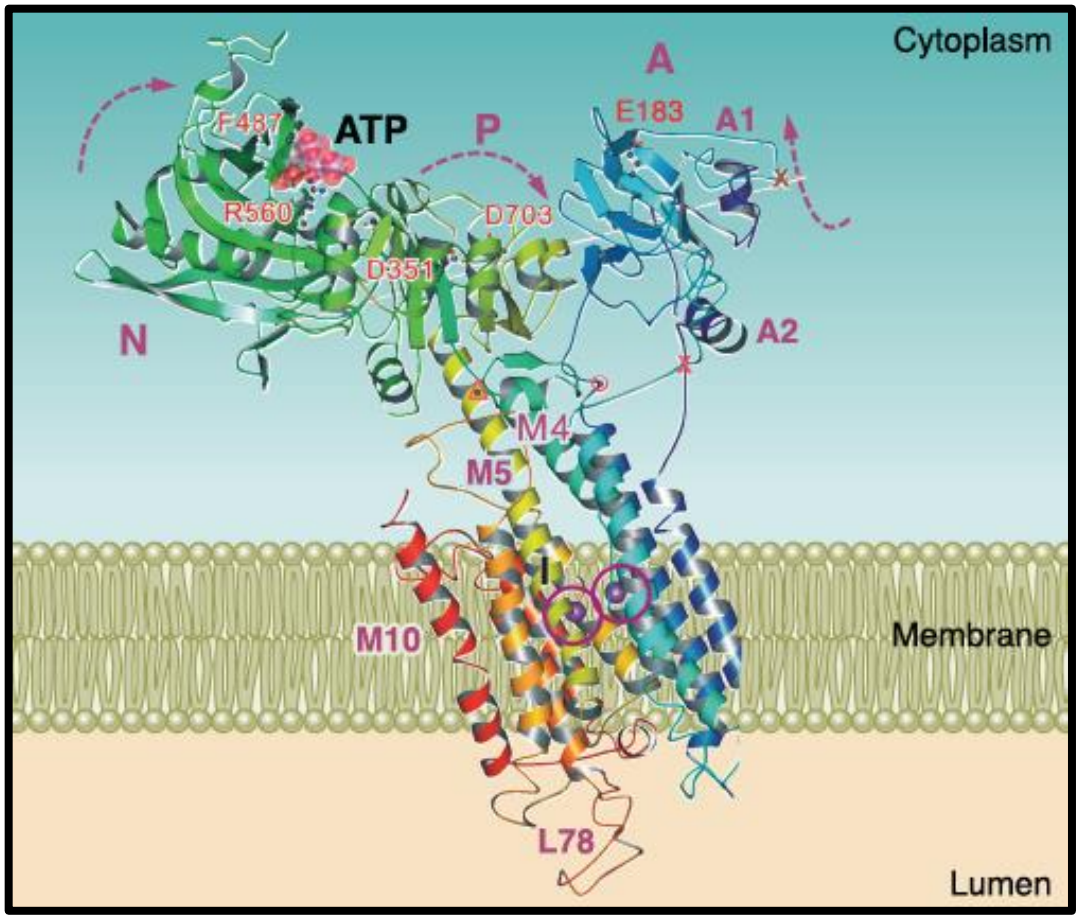

Figure 1.2. Three-dimensional ribbon diagram of SERCA in the Ca^{2+}-bound E1 state. The large cytoplasmic headpiece consists of the nucleotide-binding domain (N), phosphorylation domain (P) containing aspartate 351 (D351), and the actuator domain (A). Two Ca^{2+} binding sites (circled in purple) reside within the transmembrane domain, which consists of 10 α-helices (M1-10, not all labeled). ATP is also displayed residing within the N domain. Image was taken from Brini and Carafoli (24).

A number SERCA isoforms exist and are expressed in both muscle and non-muscle tissues, arising from developmental and tissue-specific alternative splicing of the *ATP2A1-3* genes: SERCA1a/b, SERCA2a-c, and SERCA3a-f (25). SERCA2a is the major isoform expressed in adult cardiac muscle (26), but SERCA expression patterns are slightly more complex within skeletal muscle. Traditionally, SERCA1a is the major isoform co-expressed with myosin heavy chain type II comprising the fast-twitch muscle phenotype, while SERCA2a is co-expressed with myosin heavy chain type I comprising the slow-twitch muscle phenotype (27). However, recent work with human single skeletal muscle fibres by our group has revealed this phenotypic expression pattern not to be as dichotomous as previously believed, with some type I fibres co-expressing SERCA1a and some type II fibres co-expressing SERCA2a (28). Despite subtle differences in gene and amino acid sequence (29), no intrinsic difference in the rate of Ca^{2+}-uptake exist between SERCA2a and SERCA1a (30). Instead, a higher protein density of SERCA1a within fast-twitch fibres can account for faster rates of Ca^{2+}-uptake and relaxation (27).

SERCAs are Major Regulators of Muscular [Ca^{2+}] and Energy Consumption

In addition to initiating muscular relaxation, SERCAs are the major protein responsible for maintaining a low basal cytosolic free Ca^{2+} concentration ($[Ca^{2+}]_f$), despite a Ca^{2+} gradient $>10^4$ across the SR, favoring Ca^{2+} efflux (31, 32). Given that SERCAs contain 2 Ca^{2+} binding sites and one ATP binding site, the theoretical optimal stoichiometry of Ca^{2+} pumping is 2 Ca^{2+} ions pumped for every 1 ATP hydrolyzed (i.e. coupling ratio of 2:1). Ca^{2+} pumping occurs through a series of complex conformational

changes as SERCAs progress through their catalytic cycle (**Figure 1.3**; reactions 1-6). SERCAs exist in one of two major conformational states, namely E_1 or E_2. In the E_1 state, SERCA's two Ca^{2+} binding sites face the cytosol with a high Ca^{2+} affinity (33). Upon binding of cytosolic Ca^{2+}, Asp351 located within SERCA's phosphorylation domain is autophosphorylated by ATP (34), forming a high-energy phospho-protein intermediate (33) (**Figure 1.3**; reactions 1-2). Following phosphorylation, SERCAs transition into their low-energy phospho-protein E_2 state, in which the two Ca^{2+} binding sites face the SR lumen with low Ca^{2+} affinity (33) (**Figure 1.3**; reaction 3). Once the two Ca^{2+} ions are released, inorganic phosphate contained on Asp351 is exchanged for H_2O and SERCAs transition back to their E_1 state (33), completing the catalytic cycle (**Figure 1.3**; reactions 4-6). Under physiological conditions, the theoretical optimal coupling of 2 Ca^{2+} per 1 ATP can be lowered due to the presence of several alternate reactions of the catalytic cycle; that is to say, Ca^{2+} pumping by SERCAs can become less energetically efficient.

When luminal $[Ca^{2+}]_f$ is high (e.g. during rest or relaxation), Ca^{2+} ions may bind or remain bound to the E_2 conformational state and be carried back into the cytosol when SERCAs transition to their E_1 conformation; this loss of luminal Ca^{2+} ions occurs without the concomitant synthesis of ATP, and is referred to as uncoupled Ca^{2+} efflux or passive leak (35, 36) (**Figure 1.3**; reactions 7-9). Similarly, when luminal $[Ca^{2+}]_f$ is high, the rate at which SERCAs transition from E_1 to E_2 may be slowed, increasing the number of pumps found in the Ca^{2+}-bound E_1 conformation, and promoting the cleavage of P_i without the translocation of Ca^{2+} ions, which is referred to as uncoupled ATPase activity (35, 36) (**Figure 3**; reaction 10). Additionally, Ca^{2+} ions may fall off of the pump

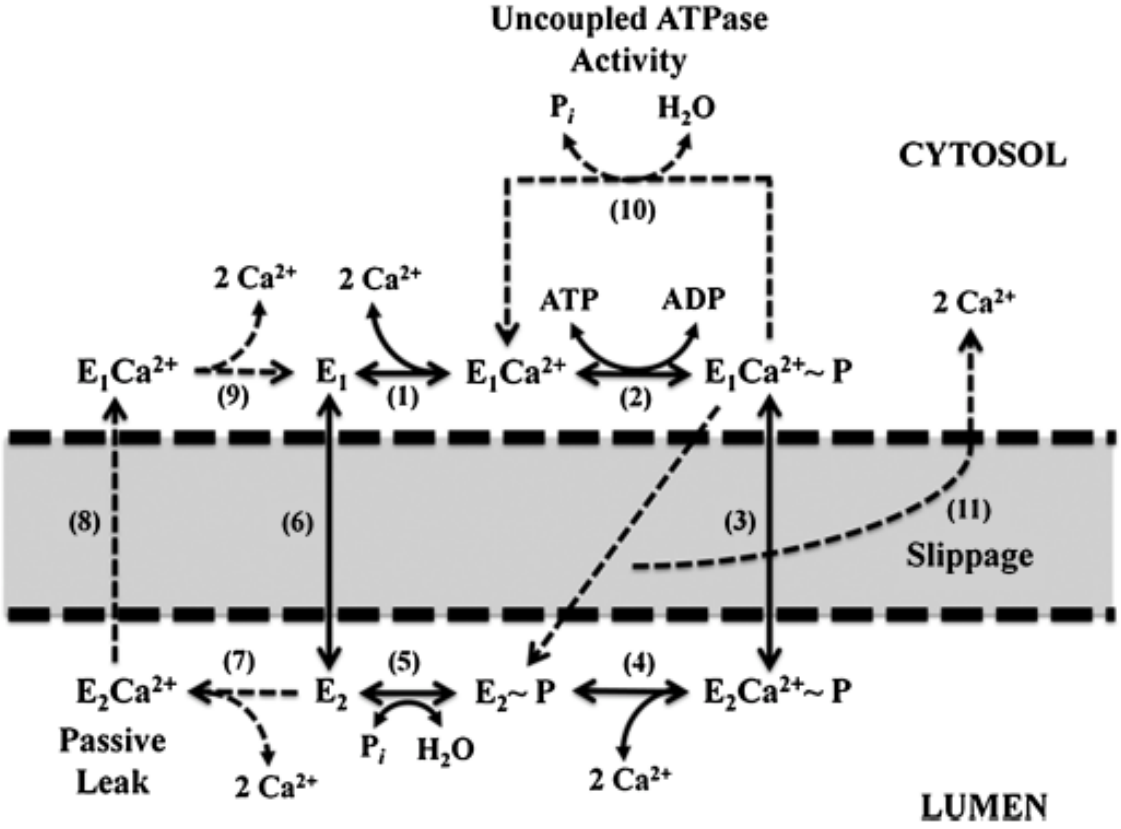

Figure 1.3. Schematic representation of SERCA's catalytic cycle (solid arrows) during Ca^{2+} pumping (reactions 1-6), including the alternate reactions (dashed arrows) of passive Ca^{2+} leak (reactions 7-9), uncoupled ATPase activity (reaction 10), and slippage (reaction 11). Figure taken from Gamu *et al* (15).

following ATP hydrolysis but prior to translocation during the E_1 to E_2 transition, called slippage (35, 37) (**Figure 1.3**; reaction 11). Slippage may be a feature of the physical interaction of SERCA with its regulatory protein sarcolipin (discussed below) (12-14, 37, 38). All of these alternative reactions would result in the activation of SERCA activity, requiring continual consumption of ATP in order to maintain a low cytosolic $[Ca^{2+}]_f$, the result being a lowering of the theoretical optimal coupling ratio of 2:1.

Given the large SR gradient favoring efflux of Ca^{2+} and that alternate reactions exist that reduce SERCA pumping efficiency, it is not surprising that consumption of ATP by SERCAs comprise a large proportion of resting (i.e. non-contracting) energy expenditure of skeletal muscle (39-42). Our group has recently used intact mouse skeletal muscles along with indirect calorimetry to determine the contribution of SERCA-mediated Ca^{2+} pumping to resting energy expenditure of muscle (42). Smith and colleagues (42) indirectly inhibited SERCA activity through blockade of SR Ca^{2+} release from the ryanodine receptor (RyR) by exposing muscles to high cellular Mg^{2+}. Following Mg^{2+} treatment, O_2 consumption of both slow- and fast-twitch muscles declined ~42-48% relative to their basal rates (42), a drop representing the specific contribution of SERCA-mediated Ca^{2+} pumping to basal energy expenditure. Interestingly, this suggests that there is a constant requirement to pump Ca^{2+} across the SR, even when muscles are idle. When extrapolated to the whole body level, SERCA activity may account for ~12-15% of whole-body basal energy expenditure and ~15-20% of total daily energy expenditure in man (42). What's more, mounting evidence shows that SERCA's contribution to muscle and whole-body energy expenditure is dynamically regulated through its interaction with small SR regulatory proteins.

Regulation of SERCA Function by Sarcolipin (SLN) and Phospholamban (PLN)

SERCA activity is regulated through its physical interactions with several small proteins, the most well characterized of which are SLN and PLN (**Figure 1.4A**). SLN is a 31 amino acid (AA) SR integral membrane protein containing a cytoplasmic N-terminal domain (AAs 1-7), transmembrane domain (AAs 8-26) and small C-terminal tail (AAs 27-31) that protrudes into the SR lumen (43). PLN is a larger 52 AA integral membrane protein containing two major cytoplasmic domains, namely IA (AAs 1-20) and IB (AAs 21-30), and a transmembrane domain (AAs 31-52) (43). Both SLN and PLN bind within the same transmembrane groove of SERCA (**Figure 1.4B**) to inhibit Ca^{2+}-uptake and thus the rate of relaxation within cardiac atria (44) and ventricle (45-47), respectively, and within oxidative skeletal muscles (48, 49). While monomers of either protein inhibit SERCA, PLN also forms non-inhibitory storage pentamers (50). SLN has been proposed to form higher order multimers (51, 52), but this has yet to be demonstrated *in vivo*, nor is its physiological impact clear. Additionally, a super-inhibitory ternary complex can form when both SLN and PLN are bound in tandem to the pump, inhibiting Ca^{2+}-uptake to a greater extent than either regulator alone (53). Because SLN and PLN can exist within the same muscle fibre (28), the possibility of a PLN/SLN/SERCA ternary complex to regulate Ca^{2+}-uptake exists *in vivo*.

In vitro, inhibition by either regulatory protein is reduced when $[Ca^{2+}]_f$ increases, likely dissociating them from SERCA. However, cross-linking studies show SLN to be more resistant to the dissociative effects of $[Ca^{2+}]$ as it can still bind to SERCA at high $[Ca^{2+}]$, whereas PLN cannot (12, 54, 55). Furthermore, PLN function is acutely regulated through phosphorylation by protein kinase A (PKA) and Ca^{2+}/calmodulin-dependent

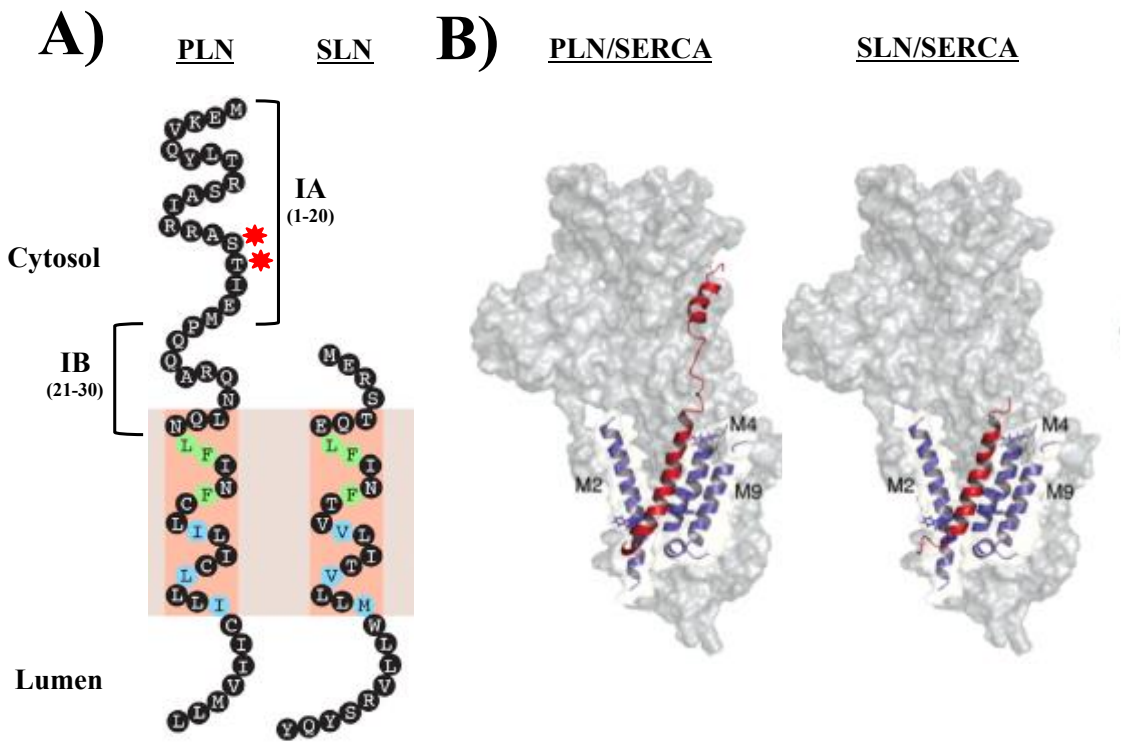

Figure 1.4. Structure and interaction with SERCA is similar between PLN and SLN. **A)** Primary sequence of PLN and SLN shown imbedded within the sarcoplasmic reticulum. PLN's cytosolic domains (including the comprised amino acid numbers) are labeled. The putative phosphorylation sites Ser16 and Thr17 are indicated by red stars. Conserved residues between PLN and SLN within their transmembrane α-helices are indicated in green (identical) or blue (similar). Image is from Anderson *et al* (56) and subsequently modified. **B)** Both PLN and SLN (depicted in red) bind within the same transmembrane groove on SERCA (transmembrane α-helices shown in blue). Image taken from Traaseth *et al* (57) and subsequently modified.

protein kinase II (CaMKII) at serine-16 and threonine-17, respectively (58), increasing SERCA activity (**Figure 1.4A**). In fact, PLN has been shown to mediate the positive lusitropic effect of the β-agonist isoproterenol in both rodent myocardium (45-47) and oxidative skeletal muscle (48). Several studies in the mouse heart have suggested that, like PLN, SLN partly mediates the enhanced contractile response to β-agonism (44, 59). Some *in vitro* evidence indicates that threonine-5 of SLN is a potential phosphorylation site for CaMKII (60). However, it remains to be seen whether reversible phosphorylation in response to Ca^{2+}-dependent or adrenergic signals *in vivo* are regulatory mechanisms controlling the function of SLN, and subsequently SERCA, within skeletal muscle.

Muscular SLN and PLN Expression Patterns: Clarification of Conflicting Evidence

Expression patterns of SLN and PLN are chamber-specific in the heart, with SLN abundant in the atria and PLN abundant in the ventricles where both are co-expressed with SERCA2a (58). Babu *et al* (44) have reported SLN protein within the ventricle and PLN within the atrium of mice, albeit at lower expression levels than their native chambers. However, in skeletal muscle the expression patters of SLN and PLN are slightly more ambiguous, possibly owing to species-specific differences (61) and methods of detection (28, 49, 56). In adult wild-type (WT) mice, SLN protein expression has been found in slow-oxidative muscles such as the soleus (SOL) and red gastrocnemius (12, 49, 62-65) and in fast-glycolytic muscles like the extensor digitorum longus (EDL) (49, 64, 66, 67). However, the degree of SLN expression appears to display a phenotypic pattern, with greater protein expression found within oxidative muscle groups (49, 64).

PLN protein has been shown to exist in oxidative muscle of WT mice (28, 65, 67), although not all reports corroborate this finding (49, 63, 68). Additionally, some groups have shown PLN protein expression within the EDL (66, 67). Our group has demonstrated PLN protein to be detectable only on polyvinylidene difluoride membranes and not nitrocellulose (28), which may explain previous reports of its absence in oxidative muscle (49, 63, 68). Furthermore, the presence of PLN in glycolytic muscle groups previously observed (66, 67) may result from non-specific binding when using PLN antibodies (28, 49), possibly resulting in false-positive confirmation of PLN. To further muddy the waters, Anderson and colleagues (56) recently reported that SLN and PLN gene expression does not occur in adult appendicular skeletal muscles in mice, instead suggesting that SERCAs are regulated almost exclusively by a newly identified regulator named myoregulin. However, several of these studies (49, 56, 63, 66-68) are at odds with the initial report of PLN in murine skeletal muscle, in which PLN knock-out mice demonstrated a contractile phenotype within SOL and not the EDL (48). This suggests, at the very least, the degree of PLN protein expression within skeletal muscles is higher in slow-oxidative muscle groups compared to fast-glycolytic muscles. In support of this, single-fibre Western blotting of human vastus lateralis muscle has shown PLN protein expression to be greater in type I fibres, although PLN is still found in type IIA fibres, albeit to a lower degree (28).

Biochemical Impact of SLN and PLN on SERCA Function

Numerous gain- and loss-of-function studies utilizing reconstituted liposomes, heterologous cell-expression systems, and transgenic animals have demonstrated that

both proteins function as negative regulators of SERCA activity by reducing its affinity for Ca^{2+}, inhibiting the rate of SR Ca^{2+}-uptake when bound to the pump (45, 49, 55, 56, 65, 69-75). However, the specific biochemical impact that either protein has on SERCA function can be complicated by the model system used, the specific measure of SERCA function and how it is expressed, to name but a few. It is important to note that two distinct measurements of SERCA function can be made *in vitro*. Both SERCA's Ca^{2+}-dependent rate of ATP hydrolysis (i.e. ATPase activity) and Ca^{2+} ion transport (i.e. Ca^{2+}-uptake activity) can be assayed separately to examine kinetic variables of SERCA's catalytic activity (e.g. maximal activity and affinity). While the translocation of Ca^{2+} ions is certainly dependent on ATP hydrolysis by the pump, the two are not necessarily coupled under all conditions (discussed above). SLN was initially reported to reduce the Ca^{2+} affinity of SERCA1 when co-expressed in HEK-293 cells, in addition to increasing the maximal rate (V_{max}) of Ca^{2+}-induced Ca^{2+}-uptake (69). However, this same group subsequently reported no impact of SLN on the V_{max} of SERCA1a or SERCA2a despite it reducing the Ca^{2+} affinity of either SERCA isoform (76), a finding recently confirmed by Anderson and colleagues (56). Using similar methods, others have reported SLN to reduce the V_{max} of Ca^{2+}-uptake with no impact on SERCA's Ca^{2+} affinity (54), or no affinity change reported (55). Additionally, Sahoo and colleagues (55) found that SLN had no impact on the kinetic parameters of Ca^{2+}-dependent ATP hydrolysis of SERCA1, despite it reducing the V_{max} of Ca^{2+}-uptake. The generation of the SLN knock-out mouse ($Sln^{-/-}$) (44) has been a valuable tool to test physiological levels of SLN protein expression and its impact on SERCA and muscle function. $Sln^{-/-}$ mice initially displayed an increase in the V_{max} of Ca^{2+}-uptake within the atria, along with improved Ca^{2+} affinity

in both atrial and ventricular homogenates (44). These mice were subsequently shown to have greater SERCA Ca^{2+} affinity within oxidative skeletal muscles, despite SLN having no impact on the V_{max} of Ca^{2+}-dependent ATP hydrolysis (49). Interestingly, ectopic over-expression of SLN in rat SOL reduced the V_{max} of Ca^{2+}-uptake with no change in SERCA's Ca^{2+} affinity (77), suggesting that there is a population of Ca^{2+} pumps that remain uninhibited by SLN in oxidative muscle of larger rodents. Despite the apparent confusing results of SLN on SERCA function *in vitro*, rodent studies have consistently shown that SLN reduces cardiac (44, 59, 78) and skeletal muscle (49, 77) contractility, consistent with a lowering of SERCA's Ca^{2+} affinity and slowing of the rate of SR Ca^{2+}-uptake.

Unlike SLN, there is more consistency observed on the impact of PLN on the kinetic parameters of SERCA function. A number of studies co-expressing PLN and SERCA in HEK-293 cells demonstrated that PLN reduces the Ca^{2+} affinity of SERCA without affecting the V_{max} of Ca^{2+}-dependent Ca^{2+}-uptake or ATP hydrolysis rates (55, 56, 69, 76). In agreement with these cell-based studies, SERCA's Ca^{2+} affinity is enhanced without changes in the V_{max} of Ca^{2+}-uptake within hearts of PLN knock-out ($Pln^{-/-}$) mice (45, 79-81). Conversely, SERCA's Ca^{2+} affinity is reduced within the hearts of PLN over-expressing (Pln^{OE}) mice (74, 82). Within skeletal muscles, the specific impact of PLN on SERCA kinetics is less clear, possibly owing to the presence of multiple fibre-types and SERCA isoforms. Ectopic over-expression of PLN in mice lowers the Ca^{2+} affinity within fast-glycolytic muscles without change in the V_{max} of Ca^{2+}-uptake (71), whereas impaired Ca^{2+} affinity and maximal Ca^{2+}-induced ATP hydrolysis rate have recently been reported within slow-oxidative muscles of Pln^{OE} mice

(65). Surprisingly, no measurements of SERCA enzymatic function have been made in skeletal muscles of *Pln*$^{-/-}$ mice.

The SR and SERCA: a Nexus for Muscle-Based Thermogenesis

Muscular contraction and relaxation result in heat generation, which is important during cold exposure (discussed above). The contribution of the SR itself to thermogenesis can be seen in the inherited disorder malignant hyperthermia, which can result from the mutation of several Ca^{2+}-handling proteins, causing excessive SR Ca^{2+} leak while individuals are under anesthesia (83). Severe muscular contracture results in life-threatening hyperpyrexia, requiring treatment with the RyR antagonist dantrolene to prevent Ca^{2+} release and indirectly stop ATP usage by the myosin and Ca^{2+}-ATPases. While this is a pathological state, several similar examples of futile Ca^{2+}-cycling exist in nature, with the purpose of regulating tissue temperature. Some deep-sea diving fishes possess an ocular "heater organ", consisting of dense SR and t-tubular networks devoid of myofiliments that continually release and re-uptake Ca^{2+} ions to regulate brain and eye temperature (84). A similar mechanism may also exist within the flexor digitorum brevis (FDB) muscle of mice, which does not participate in shivering thermogenesis (85, 86). Prolonged cold exposure (4°C for 4-5 wks) results in disassociation of the channel stabilizing subunit calstabin-1 (also known as FKBP12) from RyR1 (86), resulting in SR Ca^{2+} leak. Cold-adapted FDB muscles show increases in markers of mitochondrial biogenesis (85), possibly resulting from activation of Ca^{2+}-dependent signaling pathways in response to RyR destabilization. Regardless, cold-induced SR Ca^{2+} leak would result in SERCA-mediated Ca^{2+}-uptake to maintain SR Ca^{2+} load, inevitably contributing to

thermogenesis. While these are examples of futile Ca^{2+} cycling, emerging evidence has shown that uncoupling of SERCA Ca^{2+} transport is an integral control point of muscular energy expenditure.

Two *in vitro* studies by the same group first demonstrated that the SERCA/SLN relationship is thermogenic in nature (37, 38). Using reconstituted lipid vesicles, experimentally increasing the molar ratio of SLN to SERCA reduced vesicular Ca^{2+} accumulation markedly without effect on SERCA ATP consumption (37), in addition to increasing the amount of heat released per mol of ATP hydrolyzed by SERCA during Ca^{2+} pumping (38). This uncoupling of SERCA Ca^{2+} transport from ATP hydrolysis was attributed to SLN's ability to promote "slippage" of Ca^{2+} ions from the pump (37). Sahoo and colleagues (55) have used HEK-293 cells co-transfected with SLN and rat SERCA1 to show that SLN reduces the rate of Ca^{2+} transport without impacting ATP consumption, suggesting that SLN reduces SERCA's pumping efficiency. In agreement with these *in vitro* studies, our group has used the *Sln*$^{-/-}$ model to show that skeletal muscle SLN does in fact uncouple SERCA function *in vivo* (14). In the presence of a vesicular Ca^{2+} gradient, the apparent coupling ratio (i.e. Ca^{2+} transported/ATP hydrolyzed) within oxidative muscle was greater in *Sln*$^{-/-}$ mice relative to WT controls due to a lower rate of ATP usage (14). As a result, the contribution of SERCA activity to resting energy expenditure of isolated non-contracting muscle was ~13% lower in *Sln*$^{-/-}$ mice (14). In agreement with this, *Sln*$^{-/-}$ mice expend less energy during sub-maximal treadmill exercise and are unable to maintain body temperature upon acute cold-exposure while shivering (12, 13, 54), indicating that SLN uncouples SERCA Ca^{2+} pumping even during muscular contraction. Physiologically, this means that more ATP is required to pump

Ca^{2+} across the SR when SERCA is bound to SLN. Thus, energy is "wasted" in the presence of SLN as it is diverted away from that needed to translocate Ca^{2+} into the SR lumen, regardless if muscle is active or idle.

Not surprisingly, our group (13, 16, 17) and others (12, 87) have shown $Sln^{-/-}$ mice to develop diet-induced obesity resulting from efficient SERCA metabolism. Interestingly, SLN protein expression increases in response to diet-induced obesity within slow-oxidative muscle of WT mice, suggesting SLN is recruited to increase the energy demand of SERCA Ca^{2+} pumping to regulate body mass and metabolism. In agreement with this, Sln^{OE} mice are hyper-metabolic at thermoneutrality and subsequently resistant to diet-induced obesity (88). These studies have provided convincing evidence that skeletal muscle SLN plays a major role in diet-induced adaptive thermogenesis, a role previously thought in rodents to be exclusive to UCP-1 (6).

Given that SLN and PLN are traditionally thought to be functionally homologous (43), it is reasonable to hypothesize that PLN too may function to regulate SERCA efficiency and whole-body metabolism; however, very few studies have attempted to examine this. Within the left ventricle, SERCA2a's apparent coupling ratio is lower (i.e. less efficient) in WT relative to $Pln^{-/-}$ mice at low extravesicular $[Ca^{2+}]_f$, and treatment of WT ventricular homogenate with catalytic PKA to phosphorylate PLN increases SERCA2a's efficiency (80). This suggests that ventricular Ca^{2+} pumping is energetically more costly when PLN is bound to SERCA2a. Based on these findings, it is surprising then that *ex vivo* O_2 consumption is higher in work-preforming $Pln^{-/-}$ hearts despite greater SERCA efficiency (89). This increase in cardiac energy expenditure occurs despite similar force production and heart rate with PLN ablation (45, 89), although one

report has found heart rate to be elevated in *Pln*$^{-/-}$ mice (90). One possibility for the greater cardiac energy demand despite more efficient Ca^{2+} pumping of *Pln*$^{-/-}$ hearts may be the enhancement of SERCA2a's Ca^{2+} affinity in these mice. With the release of SR Ca^{2+} during each beat, the greater Ca^{2+} affinity of SERCA2a would result in more Ca^{2+} ions being pumped back into the SR (and thus more ATP consumption) at the expense of those needed for cross-bridge activation in *Pln*$^{-/-}$ mice. Consequently, it is possible that more total Ca^{2+} must be released from the SR to generate a given amount of force, resulting in more total ATP usage during the cardiac cycle and greater myocardial O_2 consumption. This suggestion is consistent with right-shifted cardiac force-frequency curve and higher critical heart rate (i.e. heart rate that elicits maximal rate of force production) of *Pln*$^{-/-}$ mice (90).

More recently, Sahoo and colleagues (54, 55) have examined whether skeletal muscle PLN plays a role in regulating SERCA efficiency and adaptive thermogenesis *in vivo*. In contrast to *Sln*$^{-/-}$ mice, acute cold exposure (4°C for 8 hrs) did not reduce core body temperature of *Pln*$^{-/-}$ animals, even if interscapular BAT was surgically removed (54). The authors concluded from this study that PLN differs functionally from SLN and does not participate in SERCA uncoupling. However, the experimental paradigm of acute cold exposure may be insufficient to reveal a thermogenic relationship between PLN and SERCA. Shivering is the first mechanism to defend body temperature when exposed to cold, and in rodents will be the major source of heat production well in excess of 8 hrs (3). Additionally, these authors demonstrated that unlike SLN, PLN's physical interaction with SERCA is diminished when $[Ca^{2+}]_f$ exceeds 1 μM (54). Therefore, it is possible that rising cytosolic $[Ca^{2+}]_f$ that occurs with continual muscular contraction may

abolish the physical interaction between PLN and SERCA, preventing uncoupling of SERCA in response to acute cold exposure. Furthermore, these mice were raised and housed at room temperature (54), a thermal stress that may have necessitated compensation from other mechanisms (e.g. SLN, UCP-1) that could protect core temperature in the absence of PLN. Moreover, this group did not observe an uncoupling effect of PLN like that of SLN during co-transfection experiments with HEK-293 cells (55). It is not clear why these results differ from those of Frank and colleagues (80), possibly due to the model system used (HEK-293 vs. cardiac left ventricle), the specific SERCA isoform interaction examined (rat SERCA1 vs. mouse SERCA2a), and the degree of PLN/SERCA protein expression between the model systems. Currently, no study has examined whether PLN plays a role in skeletal muscle-based adaptive diet-induced thermogenesis.

Promoting SERCA's Alternate Reactions: Insights from Thyroid Dysfunction and Ambient Thermal Stress

Although little is known whether PLN truly regulates the efficiency of SERCA *in vivo*, there is, at the very least, an association between its expression and states of hyper- and hypo-metabolism. Thyroid hormones are known to regulate both skeletal muscle and cardiac Ca^{2+}-handling by controlling the expression of various SR proteins (91), and thyroid dysfunction alters whole-body energy expenditure (92). Experimental induction of hyperthyroidism (a hypermetabolic state) by the administration of L-thyroxine (T4) or triiodothyronine (T3) has been reported to decrease the expression of PLN within both cardiac and skeletal muscle of experimental animals (93-99). Furthermore, T3/T4 injection decreases SLN mRNA expression in both the atria and SOL of mice (98, 99).

Together, these studies suggest that the physical interaction of both SLN and PLN is diminished by T3/T4 signaling, and the resulting increase in metabolism with hyperthyroidism is not the result of uncoupling of SERCA-mediated Ca^{2+} transport through their physical interaction with the pump. Although the influence of thyroid hormones on metabolism of peripheral tissues is extensive, they do directly impact SERCA thermogenesis. Surprisingly, T4 administration has been shown to increase the amount of heat released from SR vesicles during Ca^{2+}-pumping (94, 100), this despite a presumed reduction in the interaction of SLN/PLN with the pump. Conversely, propylthiouracil (PTU) induced hypothryroidism (a hypometabolic state) has been shown to increase the expression of both PLN and SLN within the heart (94, 98), while reducing the amount of heat released from the SR during Ca^{2+} pumping (94). Again, the blunting of SERCA thermogenesis while simultaneously increasing the expression of SLN/PLN with hypothyroidism is surprising in light of their previously reported ability to uncouple Ca^{2+} transport from ATP hydrolysis (14, 37, 38, 55, 80).

Interestingly, cold-exposure produces a similar effect on PLN and SERCA thermogenesis to that seen with hyperthyroidism. In rabbits, prolonged cold acclimation (4°C for 72 hrs) reduces cardiac PLN protein expression and increases its phosphorylated (i.e. non-inhibitory) form, while concomitantly increasing the amount of heat released from SR vesicles during Ca^{2+} pumping (94). Within oxidative skeletal muscle of cold-adapted rabbits, SERCA1a protein expression is increased along with SR heat production (101). Although SLN or PLN were not measured in this study, both SERCA ATPase and Ca^{2+}-uptake rates were enhanced in cold adapted muscle (101). Together, the increase in SERCA content and function suggest that the SERCA/SLN and SERCA/PLN ratio (an

indication of their inhibitory function) were at the very least unchanged. Thus, it is unlikely that uncoupling of SERCA through SLN or PLN's physical interaction with the pump is responsible for the cold-induced thermogenic response of the SR. Not surprisingly then, left ventricular gene expression of SERCA2a is reduced while PLN is increased in rats that are acclimated to 34°C for 1 month (102). These studies indicate that SR remodeling and SERCA thermogenesis are not only determined by thyroid status, but are physiologically regulated in response to changes in energy demand. A major question is what mechanism(s) could account for the change in SERCA thermogenesis in these studies, especially if its interaction with SLN and PLN is diminished.

As discussed above, several alternate reactions of SERCA's catalytic cycle could explain an increase in the heat released by the SR while pumping Ca^{2+} if SERCAs physical interaction with its regulators is diminished, specifically uncoupled ATPase activity and/or passive Ca^{2+} leak (**Figure 1.3**), both of which require luminal $[Ca^{2+}]_f$ to be high. Given that hyperthyroidism and cold-exposure appear to improve Ca^{2+}-handling in part by reducing SERCA's inhibition from SLN or PLN, this may consequently increase SR Ca^{2+} load and subsequently drive SERCA's alternate reactions, particularly passive Ca^{2+} leak. Both SLN (44, 59, 78, 103) and PLN (47, 74, 104) reduce the peak amount of Ca^{2+} released by the SR during cardiac muscle activation, resulting from a lower SR Ca^{2+} load due to inhibition of SERCA pumping by either protein (103-107). Not surprisingly then, SLN/PLN double knock-out (DKO) mice (i.e. $Sln^{-/-}/Pln^{-/-}$) have higher atrial and ventricular SR Ca^{2+} content compared to WT control animals (108). While a greater SR Ca^{2+} load may benefit contractile force production, a functional consequence *in vivo* may be an increased Ca^{2+} gradient across the SR favoring its loss. Indeed, Ca^{2+} release events

in the form of spontaneous Ca^{2+} waves, Ca^{2+}-sparks, or SR Ca^{2+} leak are increased in frequency and or/amplitude in the absence of SERCA inhibition by either PLN (105-107, 109-113) or SLN (103). Consequently, ATP consumption by SERCAs must increase to continually sequester Ca^{2+} ions lost from the SR to prevent its cytotoxic accumulation, a mechanism of futile Ca^{2+} cycling akin to that of ocular heater organs of fish or FDB fibres of mice described above. Thus, it is possible that either SLN or PLN could indirectly contribute to energy metabolism in a distinct manner other than uncoupling of SERCAs through their physical interaction (i.e. slippage). Given that SLN and PLN share considerable homologous function and may possibly compensate for one another, it would be reasonable for such futile SR Ca^{2+} cycling to occur within the muscles of DKO mice.

Statement of the Problem

A number of recent studies have shown SLN to be a critical regulator of muscle-based thermogenesis, protecting mice from cold exposure and the development of excessive diet-induced obesity. SLN is proposed to uncouple SERCA-mediated Ca^{2+} transport from ATP hydrolysis through its physical interaction with the pump, inducing "slippage" of Ca^{2+} ions from their binding sites during SERCA's catalytic cycle. While there is considerable similarity in the gene/protein sequence, structure, and biochemical impact on SERCA function between SLN and PLN, it is unclear whether PLN regulates energy metabolism and participates in diet-induced adaptive thermogenesis within skeletal muscle. To date, conflicting information exists on PLN's ability to regulate the energetic efficiency of SERCA (55, 80). Additionally, only one report has attempted to

examine whether PLN participates in adaptive thermogenesis, showing *Pln*$^{-/-}$ mice not to develop hypothermia during acute cold stress (54). However, acute cold challenge may not be a sufficient physiological stressor to examine whether PLN regulates adaptive thermogenesis (as discussed above); thus, it remains unclear whether *Pln*$^{-/-}$ mice have an obesogenic phenotype similar to that previously shown for *Sln*$^{-/-}$ mice resulting from an inability to uncouple SERCAs. Furthermore, it is possible that SLN functionally compensates for the loss of PLN within skeletal muscles of *Pln*$^{-/-}$ animals, contributing to the absence of a hypometabolic phenotype in these mice. Lastly, similar to that previously shown within the heart (44), both SLN and PLN protein have been found within oxidative skeletal muscle (48, 49), and even within the same muscle fibre (28). Interestingly, DKO mice (i.e. *Sln*$^{-/-}$*/Pln*$^{-/-}$) display a cardiac muscular phenotype distinct from either single knock-out model alone (108); however the combined impact of SLN and PLN on SERCA function within skeletal muscle is not known. Given that SLN and PLN are believed to be homologous in function, the possibility arises that either protein can compensate for the other's loss, particularly within skeletal muscles where both are endogenously found. Therefore, the major goals of this thesis were to characterize the role of PLN, and the combined role of SLN and PLN together, in regulating skeletal muscle SERCA Ca^{2+} pumping efficiency, energy balance, and diet-induced obesity in mice.

STUDY 1:

Objectives:

1) Previous reports have produced equivocal findings regarding endogenous expression patterns of PLN within skeletal muscle. The first objective was simply to confirm the presence/absence of PLN protein expression within cardiac, oxidative, and glycolytic muscle groups.
2) Our group has previously shown Ca^{2+}-uptake rates, maximal ATPase activity, and Ca^{2+}-affinity of SERCA to be reduced within skeletal muscle of Pln^{OE} mice (65). The second objective was to determine the impact of PLN ablation on SERCA function and Ca^{2+}-affinity within cardiac, oxidative, and glycolytic muscle. Additionally, because of the similarities between SLN and PLN, we also wanted to determine whether PLN reduces Ca^{2+} pumping efficiency (i.e. coupling) of SERCA.
3) To date, no examination of SLN has been made within skeletal muscle of $Pln^{-/-}$ mice, nor is it known whether PLN ablation alters muscle fibre-type characteristics. The third objective was to determine if compensatory changes in Ca^{2+}-handling proteins (particularly SLN) or fibre-type characteristics occur within oxidative skeletal muscle of $Pln^{-/-}$ mice.
4) SLN ablation does not alter whole-body metabolism, glucose handling, or body mass in chow-fed mice at room temperature, despite $Sln^{-/-}$ mice being susceptible to diet-induced obesity (12-14). The fourth objective was to examine the impact of PLN ablation on body mass, baseline whole-body metabolic rate and glucose tolerance.

Hypotheses:

1) PLN protein expression will be abundant within cardiac left ventricle, to a lesser degree within oxidative skeletal muscle (i.e. SOL), and will be undetectable within glycolytic skeletal muscle (i.e. EDL).
2) Relative to WT control animals, *Pln*$^{-/-}$ mice will show improvements in SERCA function (measured as Ca^{2+}-dependent Ca^{2+}-uptake rate and maximal ATP hydrolysis rate) and increased Ca^{2+}-affinity within cardiac left ventricle and the SOL, but not the EDL. *Pln*$^{-/-}$ mice are also hypothesized to have increased SERCA efficiency within the LV and SOL compared to WT littermates.
3) *Pln*$^{-/-}$ mice will not display any changes in the expression of Ca^{2+}-handling proteins or fibre-type characteristics within oxidative skeletal muscle.
4) Body mass, whole-body metabolic rate, and glucose tolerance will be unaltered in chow-fed *Pln*$^{-/-}$ mice relative to WT control animals.

STUDY 2:

Objectives:

1) We have previously shown *Sln*$^{-/-}$ mice to be susceptible to diet-induced obesity due to an inability to recruit SLN-mediated uncoupling of SERCA within oxidative skeletal muscle (13). The first objective was to determine if *Pln*$^{-/-}$ mice are susceptible to excessive diet-induced obesity relative to WT littermates when fed a high-fat "Westernized" diet.
2) In response to high-fat feeding, *Sln*$^{-/-}$ mice have a lower whole-body metabolic rate and impaired glucose tolerance relative to WT littermates (12, 13, 16, 17).

The second objective was to examine the impact of high-fat feeding on whole-body metabolic rate and glucose handling in *Pln*$^{-/-}$ mice.

3) SLN protein expression increases in response to high-fat feeding within oxidative skeletal muscle of WT mice (12, 13). The third objective was to determine if skeletal muscle PLN protein expression is increased by consumption of a high-fat diet, and whether any compensatory changes occur in Ca^{2+}-handling proteins or BAT UCP-1 in high-fat fed *Pln*$^{-/-}$ mice.

Hypotheses:

1) Relative to WT littermates, *Pln*$^{-/-}$ mice will develop excessive diet-induced obesity, characterized by excessive mass gain, adiposity, and glucose intolerance following high-fat feeding due to an inability to recruit PLN-mediated uncoupling of SERCA within oxidative skeletal muscle. This will occur despite the consumption of a similar amount of total calories. Chow-fed control WT and *Pln*$^{-/-}$ littermates will be phenotypically indistinguishable from one another.
2) Compared with WT littermates, whole-body metabolic rate will be reduced and glucose tolerance will be impaired in *Pln*$^{-/-}$ mice following high-fat feeding.
3) Within oxidative skeletal muscle of WT mice, PLN protein expression will increase in high-fat fed WT mice relative to chow-fed controls. Furthermore, no compensatory diet-induced changes in skeletal muscle Ca^{2+}-handling proteins or BAT UCP-1 will occur with high-fat feeding in *Pln*$^{-/-}$ mice relative to WT animals.

STUDY 3:

Objectives:

1) SERCA function is drastically improved within cardiac muscle of DKO mice compared with WT controls (108). Both SLN and PLN can be found within oxidative skeletal muscle (e.g. SOL), and even within the same single skeletal muscle fibre (28, 48, 49). The first objective was to examine SERCA function, Ca^{2+}-affinity, and efficiency (as measured in **Study 1**) within oxidative muscle of DKO mice.
2) DKO mice present with hypertrophy of left ventricular myocytes (108), suggesting the combined effects of SLN and PLN regulate muscle morphology. The second objective was to determine whether changes in the expression of Ca^{2+}-handling proteins, fibre-type size and distribution occur within oxidative skeletal muscle of DKO mice.
3) SERCA Ca^{2+} pumping efficiency can be modulated through its interaction with its regulatory proteins (15, 114), potentially contributing to whole-body metabolic homeostasis. The third objective was to examine body mass, baseline whole-body metabolic rate and glucose tolerance of DKO mice.

Hypotheses:

1) Compared to WT control mice, SERCA Ca^{2+}-dependent Ca^{2+}-uptake rate and maximal Ca^{2+}-dependent ATP hydrolysis rate will be increased within the SOL of DKO animals, along with SERCA's Ca^{2+}-affinity. Furthermore, DKO animals will display greater SERCA pumping efficiency within the SOL relative to WT control animals.

2) DKO mice will not display any changes in the expression of Ca^{2+}-handling proteins, fibre size or fibre-type distribution within oxidative skeletal muscle.
3) Body mass, whole-body metabolic rate, and glucose tolerance will be unaltered in chow-fed DKO mice relative to WT control animals.

STUDY 4:

Objectives:

1) Both SLN (14) and PLN (80) have been reported to reduce the energetic efficiency of SERCA mediated Ca^{2+} pumping within muscular tissues of mice. The first objective was to determine whether DKO mice are susceptible to excessive diet-induced obesity relative to WT control animals.
2) *Sln*$^{-/-}$ mice present with a whole-body hypometabolic phenotype in response to high-fat feeding only due to an inability to recruit inefficient Ca^{2+} pumping (12, 13). The second objective was to examine the impact of high-fat feeding on the whole-body metabolic phenotype of DKO mice.
3) Deletion of SLN and PLN may lead to inadvertent changes in muscular Ca^{2+}-handling or other known regulators of diet-induced thermogenesis. The third objective was to determine whether consumption of a high-fat diet results in any compensatory changes in the expression of major Ca^{2+}-handling proteins within oxidative skeletal muscle or BAT UCP-1 within DKO mice.

Hypotheses:

1) Relative to WT control animals, DKO mice will develop excessive diet-induced obesity characterized by excessive mass gain, adiposity, and glucose intolerance

following high-fat feeding, despite consuming a similar amount of total calories. Chow-fed control WT and DKO mice will be phenotypically indistinguishable from one another.

2) Compared with WT controls, whole-body metabolic rate will be reduced in DKO mice following high-fat feeding due to an inability of these animals to recruit uncoupling of SERCA in response the diet. Metabolic rate will remain unchanged in chow-fed WT and DKO control animals.
3) Compared with WT control animals, no compensatory high-fat diet-induced changes in the expression of skeletal muscle Ca^{2+}-handling proteins or BAT UCP-1 will occur in DKO mice.

CHAPTER 2

Impact of PLN Ablation on Whole-Body Metabolism and Skeletal Muscle Ca^{2+}-Handling

Introduction

Phospholamban (PLN) is a small 52 amino acid integral membrane protein of the sarcoplasmic reticulum (SR) that regulates the sarco(endo)plasmic reticulum Ca^{2+}-ATPase (SERCA) within heart and oxidative skeletal muscle (43, 48). When bound to SERCA, PLN reduces SERCA's affinity for Ca^{2+}, slowing the rate of ATP-dependent translocation of Ca^{2+} into the SR lumen and the rate of muscular relaxation (48, 69). Sarcolipin (SLN), a functional homologue of PLN found in both cardiac and skeletal muscle (43), has gained considerable attention for its ability to uncouple SERCA ATP hydrolysis from Ca^{2+} transport through its physical interaction with the pump, contributing to energy metabolism in mice (12-14, 37, 38, 55). Indeed, mice lacking SLN (*Sln*$^{-/-}$) develop an excessively obese phenotype when fed a high-fat diet (12, 13), whereas those over-expressing SLN are protected from diet-induced obesity (88). Thus, mechanisms that reduce the energetic efficiency of Ca^{2+} transport within skeletal muscle represent a plausible method to reduce body mass and the development of obesity.

Within cardiac left ventricle (LV), PLN has been reported to reduce the efficiency of Ca^{2+} pumping by SERCA (80), similar to that of skeletal muscle SLN; however, some recent studies have challenged this finding (54, 55). Unlike *Sln*$^{-/-}$ mice, Sahoo and colleagues (54) found that those lacking PLN (*Pln*$^{-/-}$) are able to maintain core body temperature when acutely exposed to cold (i.e. 4°C for 8 hrs). The authors concluded that since body temperature was not compromised in *Pln*$^{-/-}$ mice, PLN does not reduce the efficiency of Ca^{2+} pumping and is functionally distinct from SLN (54). However, no assessment of SERCA's Ca^{2+} pumping efficiency (i.e. coupling: Ca^{2+} pumped/ATP hydrolyzed) within skeletal muscle of *Pln*$^{-/-}$ was made in that study. Muscular shivering

is the first line of thermal defense during cold exposure (3), and the resultant rise in cytosolic Ca^{2+} that occurs with shivering is likely to dissociate PLN from SERCA (54, 55), making uncoupling less likely to be observed if it is a function of the physical interaction between the two proteins. Additionally, PLN binding to SERCA is alleviated when it is phosphorylated by protein kinase A (PKA) at serine-16 (43), increasing the rate of Ca^{2+}-uptake and improving contractile function during states of β-adrenergic activation (e.g. cold exposure). Therefore, the previously used experimental paradigm of acute cold exposure to assess PLN's role in thermogenesis may be confounded by disrupting its physical interaction with SERCA and thus the ability to uncouple Ca^{2+} transport from ATP hydrolysis. Furthermore, unlike PLN, SLN has a greater affinity for SERCA as noted by its ability to cross-link to the pump in the face of increasing [Ca^{2+}] (54, 55). Thus, it is not surprising that differences in thermal protection arise between *Sln*$^{-/-}$ and *Pln*$^{-/-}$ mice while shivering. Currently, it is unclear whether physiological levels of PLN within skeletal muscle can uncouple SERCA, nor is it known what impact PLN ablation has on whole-body metabolism.

Several other important questions remain with respect to the impact of PLN ablation *in vivo*. Initially, *Pln*$^{-/-}$ mice demonstrated a clear improvement in muscular contractility within the heart and oxidative slow-twitch muscle such as the soleus (SOL), but not glycolytic fast-twitch muscle like the extensor digitorum longus (EDL) (46, 48, 89). This improvement is due to the relatively high degree of endogenous PLN expression within the LV, while PLN is present in oxidative slow-twitch skeletal muscle, albeit to a much lesser degree than in the heart; no functional improvement within glycolytic fast-twitch muscle in response to PLN ablation is likely due to its absence

endogenously in this tissue (46, 48, 61, 89, 115, 116). However, a number of reports have raised confusion regarding the presence of PLN within skeletal muscle of mice *in vivo* (28, 48, 49, 56, 63, 65-68). Confirming PLN's basic muscular distribution will be important to ascertain its potential quantitative impact towards whole-body metabolism.

While the chamber-specific expression pattern within the heart and muscular distribution of PLN and SLN may suggest that SERCA regulation by either protein is mutually exclusive, our group has demonstrated that co-expression of both proteins occurs within the same muscle group in mice (65), and even within the same skeletal muscle fibre in humans (28). It is possible that ablation of one protein in mice may be compensated for by the other, especially given their similar gene/protein sequence and functional impact on SERCAs (43). In light of this, no examination of SLN expression within skeletal muscle of $Pln^{-/-}$ mice has yet been made, which will be critical in determining the impact of PLN *per se* on energy metabolism. Furthermore, we have reported that over-expression of PLN within oxidative muscle of mice results in previously unrecognized myopthay, characterized by a fast-to-slow shift in myosin heavy chain isoform within the SOL and changes in the expression of several Ca^{2+}-handling proteins, including SLN (65, 68). Others have shown that over-expressing SLN within skeletal muscle results in metabolic changes of glycolytic muscle groups (88). Not surprisingly, genetic manipulation of several Ca^{2+}-handling proteins can alter the contractile and metabolic phenotype of skeletal muscle (117-121), which may have downstream impacts on processes involved in energy metabolism. To this end, while compensatory changes in Ca^{2+}-handling and contractile proteins have been made within

the hearts of *Pln*$^{-/-}$ mice (46, 89), no comprehensive examination has been made within skeletal muscle of these animals (48, 54).

The major objective of this study was to examine the role of physiological levels of PLN protein expression on SERCA Ca^{2+} pumping efficiency within skeletal muscle and consequently whole-body metabolism using the *Pln*$^{-/-}$ model. Additionally, we sought to confirm the tissue distribution pattern of PLN protein expression in representative oxidative and glycolytic muscles in hopes of clarifying several conflicting reports within the literature. Lastly, it was of interest to determine whether PLN ablation resulted in changes in the expression of major SR Ca^{2+}-handling proteins or fibre-type characteristics of skeletal muscle. We hypothesized that, like SLN, endogenous levels of PLN protein would reduce the Ca^{2+} pumping efficiency of SERCAs within skeletal muscle, but would not alter whole-body metabolism in mice held at room temperature. Furthermore, we predicted that *Pln*$^{-/-}$ skeletal muscle would not display any compensatory changes in the expression of SR proteins or muscle fibre-type characteristics compared with WT littermates.

Methods

Experimental Animals and Genotyping

Heterozygous breeding pairs (i.e. $Pln^{+/-}$, strain genetic background: mix of C57BL/6, C3H, and 129S2/SvPas) were purchased from Mutant Mouse Regional Resource Centers (MMRRC; strain name: STOCK Pln^{tm1Egk}/Mmmh, stock number: 000027-MU) and used to establish a $Pln^{-/-}$ colony at the University of Waterloo. Animals were group housed at room temperature (~22°C) under a 12:12-hr reverse light/dark cycle, and given *ad libitum* access to standard rodent chow (8640 Teklad 22/5 Rodent Diet, Teklad Diets, Madison, WI) and water. Genotyping of experimental animals was done according to MMRRC instructions by digesting ear clippings using a commercially available kit (PureLink® Genomic DNA Mini Kit, ThermoFisher Scientific) and appropriate forward and reverse primers (**Appendix A: Table A1**). All experiments were conducted using 3-6 month old homozygous male PLN knock-out ($Pln^{-/-}$) and WT ($Pln^{+/+}$) littermate controls. Studies were approved by the University of Waterloo Animal Care Committee and carried out in accordance with the Canadian Council on Animal Care.

Whole-Body Metabolic Rate and Glucose Tolerance

For one week prior to experimentation, all animals were singly housed in clear plastic cages with wire mesh bottoms, and provided powdered rodent chow and water *ad libitum* to mimic housing conditions of the metabolic chambers. Indirect calorimetry was used to determine the impact of PLN ablation on whole-body metabolism using the

Comprehensive Lab Animal Monitoring System (CLAMS; Oxymax Series, Columbus Instruments, Columbus, OH). Once a week for three consecutive weeks, WT (n = 14) and *Pln*$^{-/-}$ (n = 10) mice (3-4 mo old) were housed (~22°C, 12:12-hr reverse light/dark cycle) within the CLAMS over a 48-hr period. Data collected from the first 24-hr were discarded to eliminate the effects of handling stress on metabolic variables. O_2 consumption rate (ml O_2 consumed/kg body mass/hr), respiratory exchange ratio (RER: VCO_2/VO_2) and metabolic heat production (kcal/hr/mouse) were monitored every 26-min over the following 24-hr period. Spontaneous cage activity was measured using infrared beam breaks (i.e. counts). Activity was expressed as total activity in x- and z-planes, and ambulatory activity, which was determined by the breaking of 2 successive beams in the x-plane. Metabolic rate was expressed as the average over the 24-hr collection period, and during states of activity (>2 ambulatory counts, dark phase: 0800 hr – 2000 hr) and inactivity (≤2 ambulatory counts, light phase: 2000 hr- 0800 hr) as done previously by our group (13).

Glucose tolerance was measured using an intraperitoneal glucose tolerance test following an overnight fast (~16 hrs). Blood (~5-10 μL) was sampled from a tail vein and analyzed for glucose using a standard diabetic glucometer (Accu-Chek Aviva, Roche Diagnostics) at 0, 30, 60, and 120 min following an injection of 10% D-glucose (1g/kg body mass) (13, 16).

Tissue Collection

All chemicals were purchased from BioShop Canada Inc. (Burlington, ON, Canada) unless indicated otherwise. Animals (5-6 month old) were euthanized by

cervical dislocation and muscles were excised, cleaned of connective and extraneous tissue, and placed in ice-cold phenylmethylsulfonyl fluoride (PMSF; Sigma-Aldrich, Oakville, ON, Canada) buffer (pH: 7.5). PMSF buffer contained in mM: 250 sucrose, 5 HEPES, 0.2 PMSF, and 0.2% (w/v) NaN_3 (Fisher Scientific, Fair Lawn, NJ). Due to tissue requirements for the various conditions of the Ca^{2+}-uptake and Ca^{2+}-ATPase assays (described below), left and right appendicular muscles from 2-3 animals of each genotype were pooled together (n = 5/genotype). SOL, EDL, and LV muscles were homogenized 1:10 (w/v) in ice-cold PMSF buffer using a glass-on-glass Dounce homogenizer, after which aliquots were frozen in liquid nitrogen and stored at -80°C until needed.

Ca^{2+}-Dependent Ca^{2+}-ATPase Activity

Ca^{2+}-dependent Ca^{2+}-ATPase activity (μmol ATP/g protein/minute) was measured in muscle homogenates using an NADH-linked spectrophotometric assay as previously described by our group (122) and outlined in **Appendix A** (**Figure A1**). ATPase buffer (pH: 7.0) contained in mM: 200 KCl, 20 HEPES, 10 NaN_3, 1 EGTA, 15 $MgCl_2$ (Sigma-Aldrich), 10 phosphoenolpyruvate (BioVectra, Charlottetown, PE, Canada), and 5 ATP (Sigma-Aldrich). Parallel reactions were run for each sample in the presence (1 μM) and absence of the Ca^{2+}-specific ionophore A23187 (Sigma-Aldrich, product #: C7522) within the reaction mixture. In the absence of the Ca^{2+} ionophore, vesicular Ca^{2+} accumulates and can induce back-inhibition of SERCA pumping (123), which more closely mimics the physiological condition of intact muscle. Following the addition (18 U/mL) of the auxiliary enzymes lactate dehydrogenase (Sigma-Aldrich, product #: L2625-25KU) and pyruvate kinase (Sigma-Aldrich, product #: 10 128 163

001), muscle homogenates were added to the reaction cocktail, which was then partitioned into 15 Eppendorf tubes containing various volumes of $CaCl_2$, giving free Ca^{2+} concentrations ($[Ca^{2+}]_f$) ranging from pCa (i.e. $-\log_{10}[Ca^{2+}]_f$) ~7.5-4.5. An additional tube (pCa: 4.5) contained 0.12 mM of the highly specific SERCA inhibitor cyclopiazonic acid (CPA; Sigma-Aldrich, product #: C1530), which was used to determine background activity and subtracted from each reaction mixture. Duplicates (100 µl) from each reaction tube were added to a clear round-bottom 96-well plate, and reactions were started by the addition of 0.3 mM NADH (Sigma-Aldrich, product #: 12166339), after which the decreasing rate of NADH absorbance at 340 nm was read for 30 min at 37°C.

To determine the exact $[Ca^{2+}]_f$ present in each reaction well, 1.2 µM of the Ca^{2+}-sensitive ratiometric dye Indo-1 (Biotium, Freemont, CA) was added to the reaction cocktail and partitioned into opaque Eppendorf tubes as above. Two additional tubes containing either zero $CaCl_2$ or 100 mM $CaCl_2$ were included as minimum and maximum measurements, respectively. Triplicates (100 µl) of each reaction tube were added to an opaque 96-well plate and incubated in the dark for 30 min at 37°C, and were read at an excitation wavelength of 355 nm using a fluorometric plate reader. Due to its peak absorbance wavelength and fluorescent properties, NADH was omitted from the reaction mixture. The emission maxima for the Ca^{2+}-free (G) and Ca^{2+}-bound (F) states of Indo-1 were measured at 485 nm and 405 nm, respectively, and the ratio (R) of F to G was used to calculate $[Ca^{2+}]_f$ according to the following equation (124):

$$\textbf{Equation 1}: \ [Ca^{2+}]_f = K_d \cdot (G_{max}/G_{min})\,(R - R_{min})/(R_{max} - R)$$

where K_d (250 nM) is the equilibrium constant for the interaction between Indo-1 and Ca^{2+} in homogenate (124), G_{max} is the maximum value of G (i.e. zero $CaCl_2$ well), G_{min} is the minimum value of G upon the addition of 100 mM $CaCl_2$ (i.e. max Ca^{2+} well), R_{min} is the minimum value of R (i.e. zero $CaCl_2$ well) and R_{max} is the maximum value of R upon the addition of 100 mM $CaCl_2$ (i.e. max Ca^{2+} well).

Activity curves were plotted as ATPase rate against pCa values using non-linear regression (GraphPad Prism software). The apparent Ca^{2+} affinity (i.e. pCa_{50}: pCa value at half-maximal ATPase activity) was calculated using the sigmoidal dose-response equation:

$$\textbf{Equation 2}: Y = Y_{bot} + (Y_{top} - Y_{bot})/(1 + 10^{(LogCa50 - x)\ X\ n_H})$$

where Y_{bot} is the value at the bottom of the plateau, Y_{top} is the value at the top of the plateau, $LogCa_{50}$ is the logarithm of pCa_{50} and n_H is the Hill coefficient.

Ca^{2+}-Dependent Ca^{2+}-Uptake Activity

Ca^{2+}-dependent Ca^{2+}-uptake rate (μmol Ca^{2+}/g protein/minute) was measured in muscle homogenates in both the presence and absence of the precipitating anion oxalate. Similar to the absence of ionophore described above, the removal of oxalate from the assay more closely resembles the physiological condition of intact muscle as it allows vesicular Ca^{2+} to accumulate and induce back-inhibition of SERCA pumping (123). Ca^{2+}-uptake was measured using the Ca^{2+}-sensitive fluorescent dye Indo-1 and fluorometer equipped with dual-emission monochromators and Felix software (Photon Technology International, Birmingham, NJ) (65). When excited at 355 nm, the emission

maxima for the Ca^{2+}-free state of Indo-1 is 485 nm and that for the Ca^{2+}-bound state is 405 nm.

Ca^{2+}-uptake buffer (pH: 7.0) contained 100 mM KCl, 20 mM HEPES, 10 mM NaN_3, 5 μM TPEN (Sigma-Aldrich), 10 mM $MgCl_2$, and 5 mM oxalate (Sigma-Aldrich, or absent). Reactions (2 mL final volume) took place at 37°C in a 4-sided cuvette under constant stirring. Following the addition of buffer, homogenate (~60-120 μl), 1 μl $CaCl_2$ (10 mM), and Indo-1 (1.5 μM), SERCA-mediated Ca^{2+}-uptake was initiated by the addition of ATP (5 mM). Once the reaction had plateaued (i.e. vesicles filled), Ca^{2+} was allowed to leak from the vesicles following the addition of the SERCA-specific inhibitor CPA (0.02 mM), after which 145 μl of EGTA (5 mM) and 30 μl of $CaCl_2$ (100 mM) were added to achieve maximally free and Ca^{2+}-bound states of Indo-1, respectively.

Equation 2 was used to determine change in $[Ca^{2+}]_f$ by time (i.e. Ca^{2+}-uptake rate), after which curves were smoothed over 21 points using a Savitsky-Goloay algorithm. Ca^{2+}-uptake rates were measured using linear regression ±100 nM at the following $[Ca^{2+}]_f$: 1000 nM (pCa 6.0), 500 nM (pCa 6.3), and 250 nM (pCa 6.6). The apparent coupling ratio of SERCA was determined by dividing each Ca^{2+}-dependent uptake rate by the Ca^{2+}-dependent ATPase rate under each condition (i.e. presence/absence of Ca^{2+} gradient).

Western Blotting

Primary antibodies against PLN (2D12, product #: MA3-922), ryanodine receptor (RyR; 34C, product #: MA3-925), dihydropyrodine receptor (DHPR) α-1 subunit (1A, product #: MA3-920), calsequestrin (CSQ; VIIID12, product #: MA3-913) and

SERCA2a (2A7-A1, product #: MA3-919) were purchased from ThermoScientific (Rockford, IL). The primary antibody against SERCA1a (A52) was a generous gift from Dr. David MacLennan (University of Toronto) (125), while that directed against the C-terminal luminal tail of SLN (LVRSYQY) was custom made from Lampire Biological Laboratories (Pipersville, PA) (65). All appropriate secondary antibodies were purchased from Santa Cruz Biotechnology (Santa Cruz, CA). Samples were solubilized in 1X Laemmli buffer containing SDS, and separated on glycine or tricine gels by SDS-PAGE. All proteins were wet transferred on ice for 1 hour onto polyvinylidene difluoride (PVDF) membranes (0.2 μm pore size) except SLN, which was transferred to nitrocellulose membranes (0.2 μm pore size) (126). Following transfer, membranes were blocked in TRIS-buffered saline (pH: 7.5) containing 0.1% Tween-20 (v/v) (TBST) and 5% (w/v) skim milk powder for 1 hour at room temperature. All primary, secondary, and detection conditions for each protein are outlined in **Appendix A** (**Table A2**). Densitometry analysis was done using GeneSnap software (Syngene; Frederick, MD), and protein load was confirmed using Ponceau S staining for normalization of densitometry values.

Protein content of muscle homogenates used for Ca^{2+}-ATPase/uptake assays and Western blotting was determined by the bicinchoninic acid assay (Sigma-Aldrich) using bovine serum albumin (Sigma-Aldrich) as a standard.

Immunofluorescent Staining of Muscle Fibre-Type

SOL muscles from 5-6 mo old WT (n = 6) and *Pln*$^{-/-}$ (n = 8) mice were excised and embedded in Tissue-Tek® O.C.T. Compound (VWR, Mississauga, ON, Canada)

frozen in isopentane cooled in liquid nitrogen then stored at -80°C until needed. Samples were cut into 10 μm thick cross sections at -20°C using a cryostat (Thermo Electronic). Fibre-type analysis was based on immunofluorescent identification of myosin heavy chain (MHC) isoform as previously described (127). Primary antibodies against MHCI (BA-F8) and MHCIIA (SC-71) were purchased from Developmental Studies Hybridoma Bank (University of Iowa). Secondary antibodies (Invitrogen, Carlsbad, CA) against MHCI and IIA were Alexa Fluor® conjugated 350 IgG_{2b} (blue) and 488 IgG_1 (green), respectively. Muscle cross sections were visualized with an Axio Observer Z1 microscope (Carl Ziess) equipped with standard filters (red, green, blue), an AxioCam HRm camera, and Axio Vision software (Carl Ziess). Using this configuration, type I fibres appear blue, type IIA fibers appear green, and type IIX fibres appear black. Pure and hybrid fibre counts were quantified across an entire muscle cross-section, while fibre-specific cross-sectional area (CSA) was determined by averaging ~20 fibres of each type from various portions of a cross-section using ImageJ software.

Statistical Analysis

Given the large body of evidence showing PLN inhibits SERCA function, Ca^{2+}-dependent Ca^{2+}-ATPase and Ca^{2+}-uptake rates along with Ca^{2+}-affinity measurements were analyzed using a 1-tailed Student's T-test (independent samples). Glucose tolerance data were analyzed with a 1-way repeated measures ANOVA. All other comparisons were made with a 2- tailed Student's T-test (independent samples). Statistical significance was considered at $P \leq 0.05$. All data presented are mean ± S.E.

Results

Whole-Body Metabolic Phenotype

Body mass (**Figure 2.1 A**) of 3-4 mo old male *Pln*$^{-/-}$ mice was similar ($P = 0.360$) to their WT littermates. No differences were seen in whole-body metabolic rate when energy expenditure (**Figure 2.1 B/C**) was expressed as O_2 consumption rate relative to body mass (i.e. ml O_2/kg/hr) or as absolute heat production (i.e. kcal/hr/mouse) (**Figure 2.1 D**). However, *Pln*$^{-/-}$ mice tended ($P = 0.06$) to have lower absolute heat production when measured over 24 hours. Despite this tendency, total spontaneous cage activity (**Figure 2.1 E**) and ambulation (**Figure 2.1 F**) were similar between *Pln*$^{-/-}$ and WT mice. Lastly, RER, an index of whole-body substrate utilization, was unaltered by PLN ablation (**Figure 2.1 G**).

Glucose tolerance, expressed as blood glucose during an intraperitoneal glucose tolerance test (**Figure 2.2 A**) or area under the glucose curve (**Figure 2.2 B**) did not differ between WT and *Pln*$^{-/-}$ littermates.

Fibre-Type Distribution and Muscle PLN Protein Expression

While PLN is present abundantly within cardiac LV, conflicting reports exist as to its presence within skeletal muscles (discussed above). Thus, we felt it necessary to qualitatively examine PLN protein expression within representative oxidative and glycolytic muscles in our own hands (**Figure 2.3 A**). PLN protein was abundant within LV, being easily detected at just 1 μg protein load. Within SOL, 20 μg of protein was

required to detect PLN, whereas it was undetected at this protein load within EDL. As expected, PLN protein was undetected in all muscles of *Pln*$^{-/-}$ mice.

Given the presence of PLN protein within SOL, we sought to determine whether its ablation altered skeletal muscle fibre-type expression pattern (**Figure 2.3 B/C**). While the SOL fibre-type distribution pattern of WT and *Pln*$^{-/-}$ animals differed somewhat to that reported for C57Bl/6J mice (127), no genotype differences were found in the percentage of type I ($P = 0.178$), type IIA ($P = 0.294$), type II A/X ($P = 0.153$), or type IIX ($P = 0.282$) fibres (**Figure 2.3 C**). Furthermore, fibre-specific CSA (μm^2) of type IA (0.517) or type IIA ($P = 0.339$) fibres were unaffected by PLN ablation (**Figure 2.3 D**). CSA of type IIA/X and IIX fibres were not analyzed due to their low abundance.

Cardiac and Skeletal Muscle Ca^{2+}-Dependent Ca^{2+}-ATPase Activity

In the presence of the Ca^{2+} ionophore A23187, maximal Ca^{2+}-dependent Ca^{2+}-ATPase activity (V_{Max}; μmol/g prot/ min) was significantly higher ($P < 0.05$) within the LV of *Pln*$^{-/-}$ mice (**Figure 2.4 A/B**), whereas it was unaffected ($P = 0.413$) in the absence of Ca^{2+} ionophore (**Figure 2.4 C/D**). Consistent with its inhibitory role in the heart, pCa_{50} within LV of *Pln*$^{-/-}$ mice was significantly lower compared to WT animals in both the presence ($P < 0.0001$) and absence ($P < 0.05$) of a Ca^{2+} ionophore (**Table 2.1**). Like that of the LV, V_{Max} within SOL was significantly greater ($P < 0.01$) in *Pln*$^{-/-}$ mice compared to WT littermates in the presence of a Ca^{2+} ionophore (**Figure 2.5 A/B**), and tended ($P = 0.057$) to be greater in its absence (**Figure 2.5 C/D**). However, pCa_{50} was not different between WT and *Pln*$^{-/-}$ littermates within SOL, regardless of the presence ($P = 0.395$) or absence ($P = 0.228$) of a Ca^{2+} ionophore (**Table 2.1**). Consistent with the

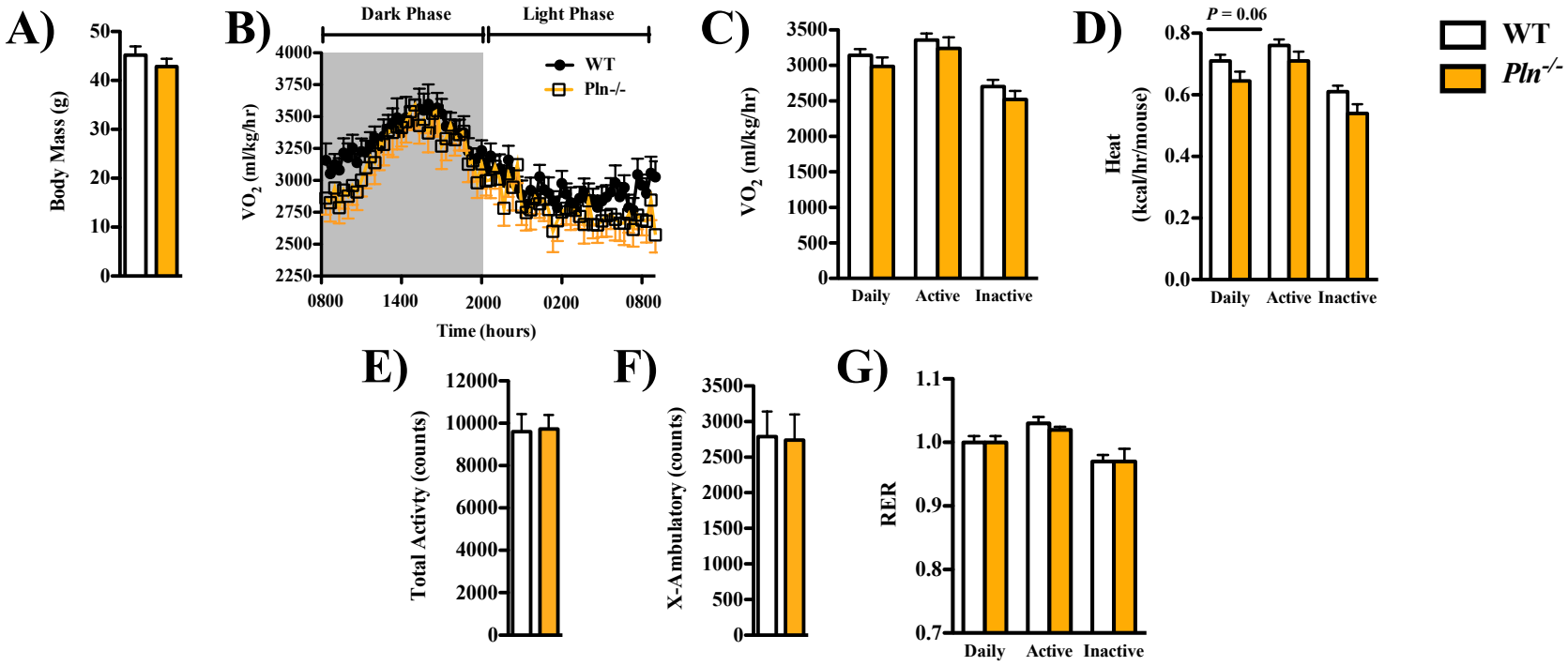

Figure 2.1. Whole-body metabolic parameters of 3-4 month old wild-type (WT; n = 14) and PLN knock-out (*Pln*$^{-/-}$; n = 10) mice. **A)** Animal body mass (g). **B)** Metabolic rate expressed as oxygen consumption rate (VO_2: ml O_2/kg body mass/hr) over a full 24 hour light/dark cycle. **C)** VO_2 averaged over 24 hours (daily), during states of cage activity (active: 0800 hrs - 2000 hrs (dark phase), >2 ambulatory activity counts) and inactivity (inactive: 2000 hrs - 0800 hrs (light phase), ≤2 ambulatory activity counts). **D)** Metabolic rate expressed as absolute heat production rate (kcal/hr/mouse). **E)** Total spontaneous cage activity (counts) over 24-hours. **F)** Ambulatory cage activity (counts) in the X plane over 24 hours. **G)** Respiratory exchange ratio (RER: VCO_2/VO_2). Values are mean ± S.E.

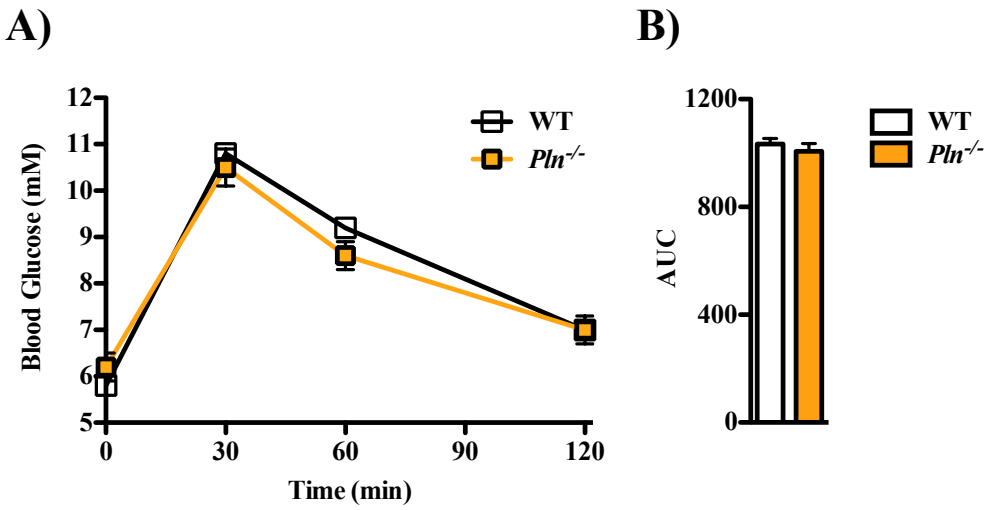

Figure 2.2. Whole-body glucose tolerance of 3-4 month old wild-type (WT; n = 25) and PLN knock-out (*Pln*$^{-/-}$; n = 13) mice. **A)** Blood glucose (mM) during an intraperitoneal glucose tolerance test. **B)** Glucose tolerance expressed as area under the curve (AUC). Values are mean ± S.E.

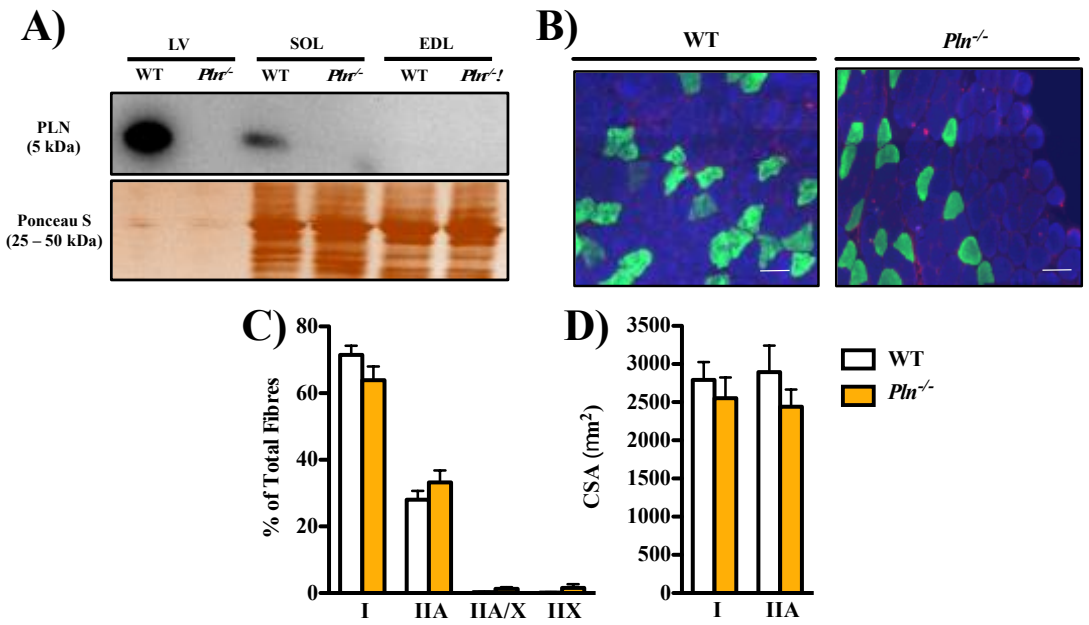

Figure 2.3. Fibre-type distribution and muscle PLN expression. **A)** PLN expression across representative muscle tissues. In wild-type (WT) animals, PLN is detected within cardiac left ventricle (LV) at 1 µg protein load, 20 µg protein load in soleus (SOL), is undetectable at 20 µg protein load in extensor digitorum longus (EDL), and is absent in all *Pln*$^{-/-}$ muscles. **B)** Representative SOL immunofluorescent cross-sectional images based on myosin heavy chain (MHC) isoform staining (blue = type I, green = type IIA, black = type IIX). Scale bars are set to 50 µm. **C)** Fibre-type distribution pattern (% of total fibres) of WT (n = 6) and *Pln*$^{-/-}$ (n = 8) SOL. **D)** Fibre-type specific cross sectional area (µm^2) within SOL. Values are mean ± S.E.

inability to detect PLN protein within the EDL of WT mice, V_{Max} was unaltered by PLN ablation regardless of the presence ($P = 0.497$) or absence ($P = 0.423$) of a Ca^{2+} ionophore (**Appendix A: Figure A2**). Furthermore, pCa_{50} did not differ between genotype, regardless of ionophore presence ($P = 0.426$) or absence ($P = 0.438$) (**Appendix A: Table A3**).

Cardiac and Skeletal Muscle Ca^{2+}-Dependent Ca^{2+}-Uptake Activity and SERCA Efficiency

As expected, oxalate-supported Ca^{2+}-uptake rates were significantly greater ($P < 0.05$) within the LV of *Pln*$^{-/-}$ mice across all pCa values compared with WT littermates (**Figure 2.6 A**). Following vesicle Ca^{2+} loading and subsequent addition of CPA, LV SR Ca^{2+} leak rate was reduced in *Pln*$^{-/-}$ animals (**Figure 2.6 B**); however, it should be noted that the starting $[Ca^{2+}]_f$ tended ($P = 0.09$) to be lower for *Pln*$^{-/-}$ mice (WT vs. *Pln*$^{-/-}$: 2285 ± 151 nM vs. 1959 ± 80 nM, data not shown). We next examined SERCA's Ca^{2+} pumping efficiency (i.e. apparent coupling ratio) within the LV. We reasoned that the high degree of PLN protein expression and virtual absence of SLN within this chamber would allow us the best opportunity to examine whether PLN reduces SERCA's pumping efficiency. Coupling ratios were measured in the absence of a vesicular Ca^{2+} gradient (i.e. presence of oxalate during Ca^{2+}-uptake and ionophore during Ca^{2+}-ATPase assays) as previous reports have used similar assay conditions (55, 80), but produced equivocal results. To our surprise, the apparent coupling ratio at pCa 6.0 was significantly lower ($P < 0.05$) in *Pln*$^{-/-}$ LV relative to WT littermates; however, SERCA's efficiency at pCa 6.3 and 6.6 did not differ between genotype (**Figure 2.7**).

Despite our confirmation of the presence of PLN within the SOL and its impact on SERCA ATPase function, SOL Ca^{2+}-uptake rates did not differ between WT and *Pln*$^{-/-}$ mice in the absence (**Figure 2.8 A**) or presence (**Figure 2.8 C**) of a vesicular Ca^{2+}-gradient across the pCa values measured. Furthermore, SOL SR Ca^{2+} leak rates under either condition were unchanged by PLN ablation (**Figure 2.8 B/D**). Our group has previously shown SLN to reduce SERCA's energetic efficiency within the SOL in the presence of a vesicular Ca^{2+} gradient (14). We next measured SERCA's Ca^{2+} pumping efficiency within the SOL in both the presence and absence of a vesicular Ca^{2+} gradient to ensure the effect of PLN on SERCA coupling was dependent on vesicular Ca^{2+} accumulation. No differences in the apparent coupling ratio within the SOL of WT and *Pln*$^{-/-}$ mice were found across pCa values or assay conditions (**Figure 2.9 A/B**).

Ca^{2+}-uptake rates and coupling ratios were not measured within the EDL due to the absence of PLN protein expression in this muscle and subsequent lack of an impact on SERCA ATPase function.

Skeletal Muscle SR Protein Expression

Major proteins involved in the storage, release, and uptake of Ca^{2+} within oxidative slow-twitch muscle were examined to determine whether they were impacted by PLN ablation. Within the SOL, no change in the expression of RyR ($P = 0.333$), DHPR ($P = 0.471$), SERCA1a ($P = 0.369$), SERCA2a ($P = 0.252$), CSQ ($P = 0.486$), or SLN ($P = 0.367$) were observed between *Pln*$^{-/-}$ mice and WT littermates (**Figure 2.10 A/B**).

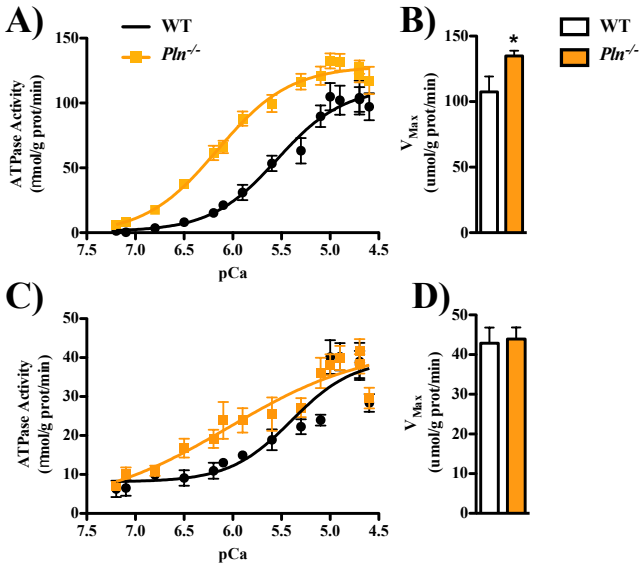

Figure 2.4. Ca^{2+}-dependent Ca^{2+}-ATPase activity (µmol/g protein/min) within left ventricle homogenates of wild-type (WT; n = 5) and *Pln*$^{-/-}$ mice (n = 6). **A)** ATPase activity curves measured in the presence of the Ca^{2+}-specific ionophore A23187 (i.e. leaky vesicles). **B)** Maximal ATPase activity (V_{Max}) of leaky vesicles. **C)** ATPase activity curves measured in the absence of the Ca^{2+}-specific ionophore A23187 (i.e. intact vesicles). **D)** V_{Max} of intact vesicles. *Significantly different (P <0.05) from WT. Values are mean ± S.E.

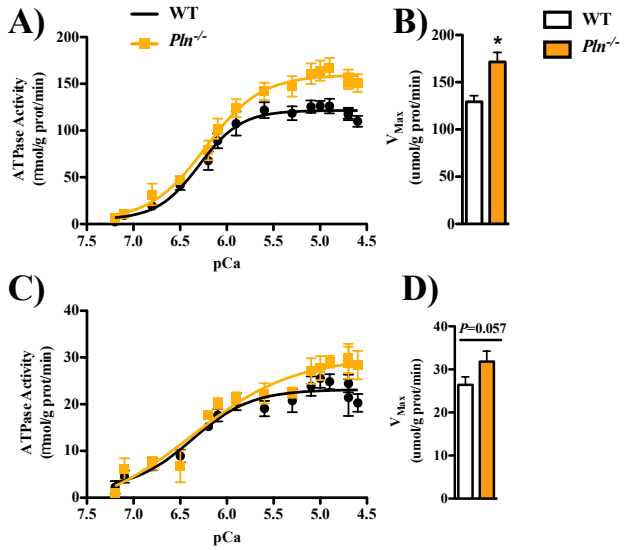

Figure 2.5. Ca^{2+}-dependent Ca^{2+}-ATPase activity (µmol/g protein/min) within soleus homogenates of wild-type (WT) and *Pln*$^{-/-}$ mice (n = 5/group). **A)** ATPase activity curves measured in the presence of the Ca^{2+}-specific ionophore A23187 (i.e. leaky vesicles). **B)** Maximal ATPase activity (V_{Max}) of leaky vesicles. **C)** ATPase activity curves measured in the absence of the Ca^{2+}-specific ionophore A23187 (i.e. intact vesicles). **D)** V_{Max} of intact vesicles. *Significantly different (P <0.05) from WT. Values are mean ± S.E.

Table 2.1. Ca^{2+} affinity (i.e. pCa_{50}: pCa at half maximal ATPase activity) of wild-type (WT) and *Pln*$^{-/-}$ mice (n = 5/group) in various tissues measured in the presence (i.e. leaky vesicles) and absence (i.e. intact vesicles) of the Ca^{2+}-specific ionophore A23187.

		pCa_{50}	
Condition	**Tissue**	**WT**	***Pln*$^{-/-}$**
Leaky	LV	5.54 ± 0.03	6.16 ± 0.03#
	SOL	6.28 ± 0.06	6.25 ± 0.07
Intact	LV	5.37 ± 0.10	6.00 ± 0.23*
	SOL	6.25± 0.07	6.57 ± 0.23

LV: left ventricle, SOL: soleus

* Significantly different than WT ($P < 0.05$)

Significantly different than WT ($P < 0.0001$)

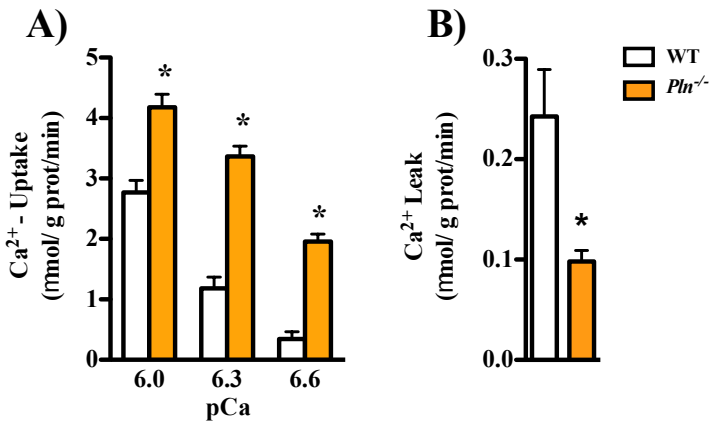

Figure 2.6. Ca^{2+}-dependent Ca^{2+}-uptake and leak rates (µmol/g protein/min) within left ventricle of wild-type (WT) and *Pln*$^{-/-}$ mice (n = 5/group). **A)** Oxalate-supported Ca^{2+}-uptake rates at various pCa (i.e. $-\log_{10}([Ca^{2+}_f])$) values. **B)** Ca^{2+} leak rate of oxalate-supported vesicle filling following the addition of the SERCA-specific inhibitor CPA. *Significantly different (P <0.05) from WT. Values are mean ± S.E.

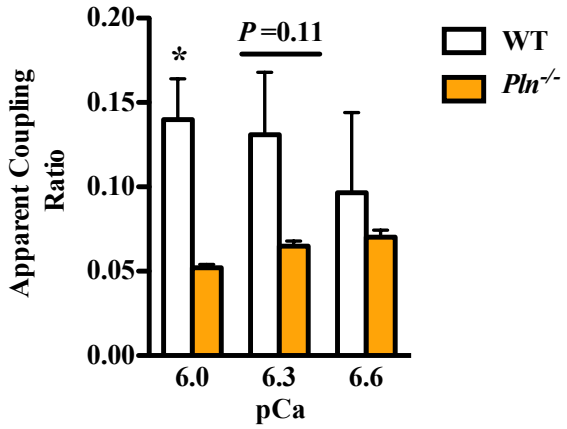

Figure 2.7. SERCA Ca^{2+}-pumping efficiency (i.e. coupling ratio: Ca^{2+}-uptake rate/ Ca^{2+}-ATPase rate) within the left ventricle of wild-type (WT) and *Pln*$^{-/-}$ mice (n = 5/group). Coupling ratios were measured across of range of pCa values (i.e$-\log_{10}([Ca^{2+}_f])$) in the absence of a vesicular Ca^{2+} gradient (i.e. presence of oxalate during Ca^{2+}-uptake and the Ca^{2+} ionophore A23187 during Ca^{2+}-ATPase measurements). *Significantly different (P <0.05) from WT. Values are mean ± S.E.

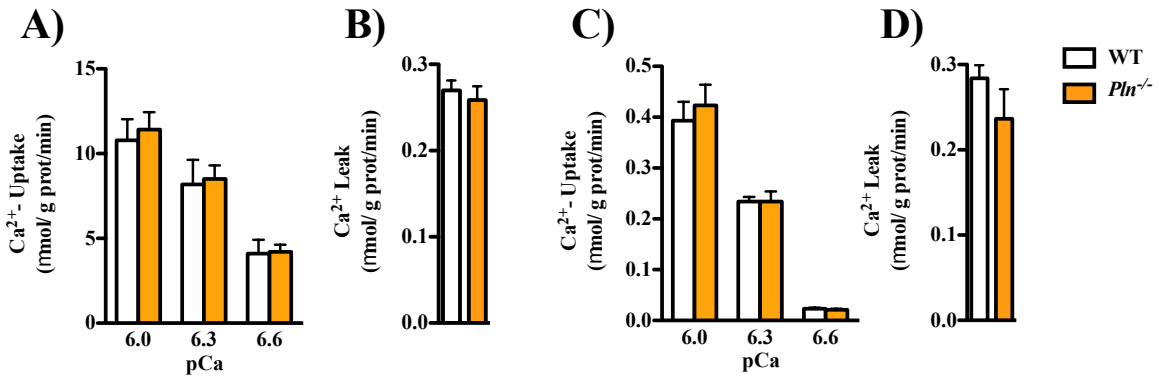

Figure 2.8. Ca^{2+}-dependent Ca^{2+}-uptake and leak rates (µmol/g protein/min) within the soleus of wild-type (WT) and *Pln*$^{-/-}$ mice (n = 3-5/group). **A)** Oxalate-supported Ca^{2+}-uptake rates at various pCa (i.e. $-\log_{10}([Ca^{2+}_f])$) values. **B)** Ca^{2+} leak rate of oxalate-supported vesicle filling following the addition of the SERCA-specific inhibitor CPA. **C)** Ca^{2+}-uptake rates in the absence of the precipitating anion oxalate. **D)** Ca^{2+} leak in the absence of oxalate following the addition of CPA. Values are mean ± S.E.

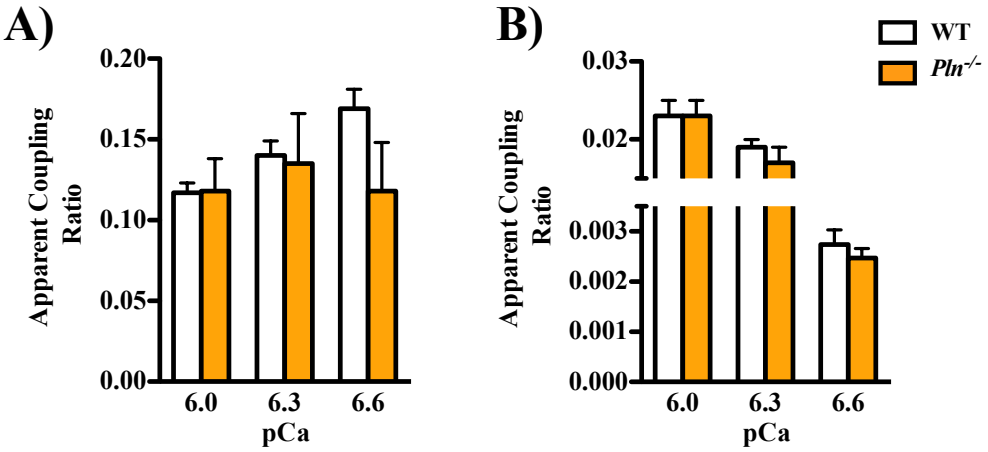

Figure 2.9. SERCA Ca^{2+}-pumping efficiency (i.e. coupling ratio: Ca^{2+}-uptake rate/ Ca^{2+}-ATPase rate) within soleus of wild-type (WT) and *Pln*$^{-/-}$ mice (n = 3-5/group). Coupling ratios were measured across of range of pCa values (i.e. $-\log_{10}([Ca^{2+}_f])$). **A)** SERCA efficiency measured in the absence of a vesicular Ca^{2+} gradient (i.e. presence of oxalate during Ca^{2+}-uptake and the Ca^{2+} ionophore A23187 during Ca^{2+}-ATPase measurements). **B)** SERCA efficiency measured in the presence of a vesicular Ca^{2+} gradient (i.e. absence of oxalate during Ca^{2+}-uptake and ionophore during Ca^{2+}-ATPase measurements). Values are mean ± S.E.

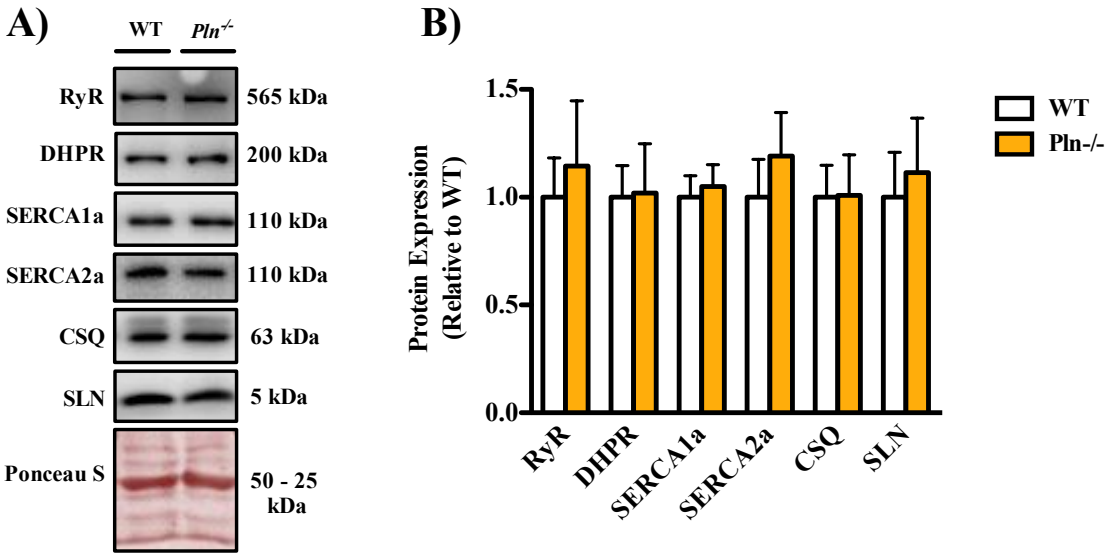

Figure 2.10. Sarcoplasmic reticulum Ca^{2+}-handling protein expression is unaltered by PLN ablation. **A)** Representative Western blots of 5-6 mo old wild-type (WT) and *Pln*$^{-/-}$ mice (n = 7-11/group). Equal protein load was confirmed using Ponceau S staining. **B)** Protein expression relative WT mice. Values are mean ± S.E.

Discussion

Ca^{2+} pumping contributes significantly to skeletal muscle metabolism (42), and SLN has been shown to increase the energy required by SERCAs to pump Ca^{2+} ions by uncoupling Ca^{2+} transport form ATP hydrolysis (14, 37, 38). To this end, SR proteins baring structural resemblance to SLN and that can physically interact with the pump, such as PLN, may have a similar function in regulating skeletal muscle energy metabolism. Several recent studies have concluded that PLN is functionally distinct from SLN, and that only SLN can regulate the energy requirement of SERCA activity (54, 55). In light of this, the impact of physiological levels of PLN protein expression on skeletal muscle SERCA efficiency and whole-body metabolism remains unclear. Furthermore, while PLN ablation does not appear to be involved in cold-induced adaptive thermogenesis (54), it is not known whether this results from compensation by other SR proteins involved in muscular energy expenditure, particularly SLN. Thus, the major objectives of this study were to characterize the impact of PLN ablation on skeletal muscle SERCA pumping efficiency and whole-body metabolism, along with potential compensatory changes in SR protein expression and muscle phenotype of $Pln^{-/-}$ mice. As hypothesized, whole-body energy expenditure of $Pln^{-/-}$ mice did not differ to that of WT littermates housed at room temperature. Unlike previously shown for SLN, PLN did not reduce the pumping efficiency of SERCA within oxidative skeletal muscle across various $[Ca^{2+}]_f$, nor did it reduce SERCA's efficiency within the LV at low $[Ca^{2+}]_f$ in which PLN's physical interaction with the pump is greatest. To our surprise, SERCAs were less coupled within the LV of $Pln^{-/-}$ mice at higher $[Ca^{2+}]_f$ suggesting a greater energy requirement to pump Ca^{2+}. Furthermore, as hypothesized PLN ablation did not alter the

phenotype of oxidative skeletal muscle, nor did it result in compensation by SLN or other measured SR proteins. These findings demonstrate that PLN does not reduce the energetic efficiency of SERCA, specifically at $[Ca^{2+}]_f$ close to resting levels within striated muscle. Thus, our results are in line with the growing body of evidence that SLN and PLN may serve functionally distinct roles within skeletal muscle.

Whole-Body Metabolic Phenotype

To date, no examination of whole-body metabolic rate has been made in *Pln*$^{-/-}$ mice despite previous reports on PLN's ability to uncouple SERCA being equivocal (55, 80). Herein, we showed that both body mass normalized and absolute energy expenditure were unaffected by global PLN ablation in mice held at room temperature. Although we hypothesized a role of PLN in regulating Ca^{2+} pumping energetics, the lack of an effect on whole-body energy expenditure with PLN ablation is not entirely surprising. Despite SLN's ability to uncouple SERCA, both muscle-specific and whole body metabolic rate of *Sln*$^{-/-}$ mice are not lower relative to WT animals when held under identical housing/feeding conditions (14). Even when *Sln*$^{-/-}$ mice are housed at thermoneutrality, metabolic rate is similar to that of WT control mice (62, 87); phenotypic differences in energy expenditure only arise under diet- or cold-induced stress (12, 13, 16, 54). The lack of a change in whole-body energy expenditure of *Pln*$^{-/-}$ mice was unrelated to any compensatory adaptation in spontaneous physical activity or substrate oxidation. Together, the lack of an effect of PLN ablation on body mass are consistent with these CLAMS variables. Although body composition was not measured in 3-4 month old mice, whole-body glucose tolerance was similar between genotypes,

which may suggest that adiposity too was unaltered in *Pln*$^{-/-}$ mice (see **Chapter 3** for body composition data).

Muscular PLN Distribution, Fibre-Type Characteristics, and SR Protein Expression

A number of studies have reported conflicting information regarding the presence of PLN within oxidative and glycolytic muscle (28, 48, 49, 56, 63, 65-68). Here, we readily detected PLN within cardiac LV and confirm its presence within the SOL, whereas it was undetectable in the EDL of WT mice. These results are consistent with the initial report of PLN on skeletal muscle contractile function, which demonstrated that *Pln*$^{-/-}$ mice only display an improvement in contractility within the SOL, not the EDL (48). Furthermore, this distribution pattern of PLN is consistent with the notion that it preferentially regulates SERCA2a *in vivo* (61, 128). Our group has shown that a population of skeletal muscle fibres in human vastus lateralis does in fact co-express SERCA1a and PLN (28), challenging the long held view that PLN only regulates SERCA2a. However, it is unclear from this study exactly which fibres within the SOL PLN resides. Although others have reported the presence of PLN protein within the EDL of mice (66, 67), we do not show that here. One possibility for this may be that PLN is only detectible at higher protein loads within this muscle than that used here. However, we found no biochemical impact of PLN ablation on SERCA function within the EDL. Thus, it is reasonable to conclude from our results and others (48) that PLN protein is low or completely absent, and serves no endogenous role in regulating SERCA1a function within this muscle *in vivo*.

Ca^{2+}-signaling is integral in regulating the contractile and metabolic phenotype of skeletal muscle (129). Within the SOL, PLN overexpressing mice display a fast-to-slow shift in MHC expression, along with atrophy of type I fibres and compensatory hypertrophy of IIA fibres (65, 68). Thus, changing the activation state of SERCA *in vivo* can drastically alter muscle phenotype. To date, the impact of PLN ablation on muscle fibre-type characteristics is unknown. Thus, we chose to answer this using the SOL, as we not only detect PLN within this muscle, but also demonstrated a biochemical impact on SERCA function. As hypothesized, *Pln*$^{-/-}$ mice showed no change in either the fibre-type distribution or fibre-specific CSA, suggesting that the endogenous amount of PLN protein and its subsequent effect on SERCA function is not required for Ca^{2+}-dependent pathways governing fibre-type distribution and size. Similarly, *Sln*$^{-/-}$ mice do not display any change in fibre-type, fibre size, or oxidative capacity within the SOL (49, 130, 131). Although it is unclear whether overexpression of SLN affects SOL fibre-type characteristics, ectopic overexpression of SLN within glycolytic muscles does in fact increase oxidative capacity (88). Thus, the inhibition of SERCA resulting from overexpression of either regulatory protein likely raises basal cytosolic $[Ca^{2+}]_f$ beyond cellular buffering to activate Ca^{2+}-dependent pathways governing muscular phenotype, whereas their individual ablation likely does not drastically alter buffering of resting $[Ca^{2+}]_f$ beyond a point that affects signaling pathways.

Similar to the fibre-type data, SR protein expression was not altered in *Pln*$^{-/-}$ mice, suggesting that the capacity for Ca^{2+}-uptake, storage, and release is unaltered within oxidative muscle by PLN ablation. Our findings here confirm the initial report of PLN in the SOL, which showed no changes in RyR or SERCA expression in *Pln*$^{-/-}$ animals (48).

Importantly, this is the first study to examine the impact of PLN deletion on SLN protein expression within skeletal muscle, which we show to be unchanged in *Pln*$^{-/-}$ mice. While this may suggests that SLN protein expression does not compensate for the loss of PLN, we cannot rule out an enhancement in the physical interaction of SLN with SERCA in the absence of PLN given that a ternary SLN/PLN/SERCA complex can form (28, 53). Regardless, the previously reported ability of *Pln*$^{-/-}$ mice to withstand cold challenge (54) appears not to be the result of a compensatory up-regulation of SLN protein within oxidative skeletal muscle.

Our SR protein expression results within oxidative muscle differ somewhat to other tissues and models. Although PLN ablation was previously shown not to alter the ultrastructure or the expression of SERCA2a and CSQ of ventricular muscle, RyR protein expression was reduced in *Pln*$^{-/-}$ LV (46). It is unclear why this latter finding differs from the skeletal muscle findings here and those of Slack and colleagues (48), but could be the result of tissue-specific changes in Ca^{2+} signaling. Furthermore, overexpression of PLN within the SOL increases SERCA2a protein and surprisingly, SLN (65). Thus, examining a potential role of PLN in studies of muscle-based thermogenesis through overexpression within slow-twitch muscle may preclude its utility.

SERCA Function and Efficiency

Consistent with our Western blotting results and those previously examining myocardial and skeletal muscle contractile function (46, 48), ablation of PLN improved SERCA ATPase activity within LV and SOL, but not EDL. This is the first report demonstrating that endogenous levels of PLN reduce SERCA ATPase V_{Max} within

muscle. The only other report to measure cardiac ATPase function found that while Ca^{2+} affinity was increased in *Pln*$^{-/-}$ mice, V_{Max} was not (80). Several differences exist between our assay conditions and that previously examining SERCA ATPase activity of *Pln*$^{-/-}$ heart. Whereas we have utilized crude homogenate from LV only, Frank and colleagues (80) used SR-enriched membranes from both left and right ventricles that were supplemented with both oxalate and the RyR blocker ruthenium red to prevent SR Ca^{2+} release. The addition of a Ca^{2+} ionophore in our assay ensures that luminal Ca^{2+} will not accumulate to induce back-inhibition of SERCA activity, and that extravesicular $[Ca^{2+}]_f$ remains constant and will not subsequently limit SERCA pumping during the course of the assay. It is possible that blockade of Ca^{2+} release in oxalate-supported preparations limits SERCA, particularly when measured at higher $[Ca^{2+}]_f$ where there will be a greater degree of luminal Ca^{2+} accumulation, thus reducing SERCA activity through back inhibition. Back inhibition in this instance is likely to disproportionately affect SERCA in *Pln*$^{-/-}$ mice given their enhanced ability to sequester Ca^{2+}. In agreement with this, SERCA ATPase activity measured previously begins to plateau at pCa ~6.25 in *Pln*$^{-/-}$ preparations (80), whereas we continue to observe increasing activity in both genotypes well past this pCa value. Regardless, our results here are consistent with our group's previous finding that V_{Max} is depressed in the SOL of PLN overexpressing mice (65). While mechanistically unclear how PLN reduces V_{Max}, it does not appear to be the result of an increase in SERCA protein expression in *Pln*$^{-/-}$ muscle, which we show to be unchanged in the SOL, and others have shown for SERCA2a within the LV (89). Interestingly, SERCA2a protein is even elevated in the SOL of PLN overexpressing mice despite depressed ATPase V_{Max} (65).

As expected, LV Ca^{2+} affinity was enhanced with PLN ablation, but surprisingly this was not the case within the SOL of *Pln*$^{-/-}$ mice. This discrepancy is likely the result of PLN content being much higher in LV compared to the SOL. Recently, we have shown that muscle remodeling in response to both functional overload and unloading of the plantaris and SOL, respectively, both increase SLN protein expression and correspondingly depress ATPase V_{Max} (130). However, this up-regulation of SLN is without effect on Ca^{2+} affinity in these muscles (130). Similarly, overexpression of SLN within rat SOL was shown to depress V_{Max} of Ca^{2+}-uptake but did not reduce Ca^{2+} affinity (77). These findings in skeletal muscles of rodent models differ from co-transfection studies using HEK-293 cells, which demonstrate a reduction in Ca^{2+} affinity by either SERCA regulator (55, 69, 76). It is important to note, however, that the molar ratios of either regulator to SERCA in these heterologous cell studies range from 2:1 to 5:1 (55, 69, 76). As SLN and PLN protein expression is much greater in cardiac compared to skeletal muscle, the lack of an increase of Ca^{2+} affinity within the SOL in response to PLN deletion likely reflects the relatively low degree of endogenous PLN protein (thus PLN:SERCA ratio) within this muscle of WT mice.

Consistent with higher ATPase activity, oxalate-supported Ca^{2+}-uptake rates were faster in LV homogenates from *Pln*$^{-/-}$ mice. Although we are unable to obtain a measure of Ca^{2+} affinity from this assay, it is important to state that we were able to consistently measure Ca^{2+}-uptake at low $[Ca^{2+}]_f$ (50 – 150 nM) in *Pln*$^{-/-}$ LV, whereas in WT mice we could not, suggestive of greater Ca^{2+} affinity with PLN ablation. Interestingly, the rate of Ca^{2+} release following steady state filling was markedly lower in *Pln*$^{-/-}$ LV in response to SERCA inhibition. Using a similar assay system to that herein, Aschar-Sobbi and

colleagues (113) found that inhibiting PLN function by the addition of PKA or a PLN anti-body increased passive Ca^{2+} leak from canine cardiac SR, and postulated that this resulted from Ca^{2+} leak through a PLN pentameric ion channel. While our results here may provide the first direct evidence of such a mechanism given the absence of a perntameric channel is associated with reduced SR Ca^{2+} leak in *Pln*$^{-/-}$ LV homogenate, it is important to note that LV RyR expression is reduced in these animals (46, 89), which would also contribute to the reduced rate of passive Ca^{2+} leak observed. Caution should be taken when interpreting our *in vitro* passive leak results, as one may logically conclude that its reduction with PLN ablation would reduce the ATP requirement of SERCA for reuptake as less Ca^{2+} is lost from the SR. The luminal $[Ca^{2+}]_f$ in our assay is not reflective of that *in vivo*, which has been demonstrated to be higher in response to PLN ablation, driving a larger gradient for Ca^{2+} leak (30, 64, 72, 100, 103, 121, 128). Thus, the physiological relevance and the bioenergetic impact of the reduced rate of passive leak within *Pln*$^{-/-}$ LV remain unclear.

To our surprise, *Pln*$^{-/-}$ SOL showed no improvement in the rates of Ca^{2+}-uptake in either the presence or absence of oxalate across the measured pCa values. However, we also found that SOL ATPase activity was not different between WT and *Pln*$^{-/-}$ mice in the presence/absence of ionophore at the exact same pCa values measured for Ca^{2+}-uptake (data not shown), despite a higher V_{Max} with PLN ablation. Unfortunately, we were unable to achieve reliable Ca^{2+}-uptake rates in the observed range of PLN's impact on ATPase V_{Max}; therefore, we cannot rule out that SOL Ca^{2+}-uptake rates are not faster at higher $[Ca^{2+}]_f$. Lack of improved rates of Ca^{2+}-uptake within the SOL of *Pln*$^{-/-}$ mice is in stark contrast to PLN overexpressing animals, which shows a marked depression in this

muscle (65). However, *Sln*$^{-/-}$ mice also show no change in SOL Ca^{2+}-uptake at low $[Ca^{2+}]_f$ (14), consistent with our results herein. While these findings appear to contradict previous studies showing that both PLN and SLN reduce Ca^{2+} affinity and uptake rate, it is likely the lack of improvement in SERCA function relates to the low molar ratio of either regulator within the SOL (described above).

Conflicting evidence currently exists within the literature with respect to PLN's ability to uncouple SERCA (55, 80). We chose to first examine PLN's impact on SERCA pumping efficiency using LV, as this provided us a tissue rich in PLN protein. Further, we chose to analyze LV coupling in the absence of a vesicular Ca^{2+} gradient to best compare our results with previous studies (55, 80). Unlike that shown by Frank and colleagues (80), we found that PLN did not reduce SERCA's pumping efficiency at low $[Ca^{2+}]_f$, in which a physical interaction between these proteins occurs. Much to our surprise and contrary to our hypothesis, the LV coupling ratio was reduced at pCa 6.0 in response to PLN ablation, suggesting that SERCA2a pumping efficiency is Ca^{2+}-dependent and more energetically inefficient at higher $[Ca^{2+}]_f$ within LV of *Pln*$^{-/-}$ mice. Interestingly, we may not be the first group to observe such an effect of PLN on SERCA coupling. Sahoo and colleagues (55) used HEK-293 cells transfected with SERCA alone or in combination with wither SLN or PLN at a molar ratio of 1:2 to compare their effects on Ca^{2+}-uptake and ATP hydrolysis rates. While SLN was shown to depress Ca^{2+}-uptake without effect on ATPase rates suggesting uncoupling of SERCA by SLN, PLN appeared to have little effect on Ca^{2+}-uptake while drastically reducing ATPase rate suggesting enhanced coupling of SERCA by PLN, particularly at pCa 6.0 (see figures 2B/C and 3B/C in (55)). Our findings here and those of Sahoo *et al* (55) may explain why energy

expenditure of isolated work-performing *Pln*$^{-/-}$ hearts are nearly twice as high as those of WT littermates (89), a finding at odds with this same group's report of PLN uncoupling SERCA2a within the heart (80). Unfortunately due to technical restraints we were unable to measure LV Ca^{2+}-uptake in the absence of oxalate; therefore we cannot unequivocally rule out that PLN might decrease SERCA pumping efficiency under physiological conditions in this muscle.

Our group has shown that endogenous amounts of SLN protein reduce SERCA's apparent coupling ratio within mouse SOL, specifically at $[Ca^{2+}]_f$ near resting levels within skeletal muscle (14). Thus, we next examined whether PLN ablation reduced SERCA efficiency within the SOL of mice. Unlike that previously shown for SLN, we found that skeletal muscle PLN had no impact of Ca^{2+}-pumping efficiency at any measured pCa value, regardless of whether a vesicular Ca^{2+} gradient was allowed to form. In light of no change in either submaximal Ca^{2+}-uptake or ATP hydrolysis rates between WT and *Pln*$^{-/-}$ SOL, it is not surprising then that coupling ratios were similar between genotypes. This again could relate to the small amount of PLN protein expressed within this muscle relative to that of the LV. Regardless, we find no evidence of reduced pumping efficiency at $[Ca^{2+}]_f$ close to resting levels within skeletal muscle, wherein the physical interaction between PLN and SERCA is likely to be greatest. This study adds further evidence to the assertion that PLN and SLN may serve functionally distinct roles within skeletal muscle. Furthermore, that endogenous amounts of PLN protein within skeletal muscle do not uncouple SERCA is consistent with the ability of *Pln*$^{-/-}$ mice to withstand acute cold challenge, as this stressor recruits thermogenesis originating primarily from skeletal muscle SLN and BAT UCP-1 (54). However,

although endogenous amounts to PLN do not uncouple SERCA within muscle and alter whole-body metabolism in mice, this does not preclude PLN from a role in adaptive thermogenesis, specifically in response to prolonged cold-exposure or diet-induced obesity wherein there is a need to expand the capacity of thermogenic mechanisms to regulate energy metabolism. Given that SLN protein expression increases several-fold within oxidative muscle in response to a high-fat diet and prolonged cold exposure (12, 13, 63), the possibility still exists that PLN too is recruited by these physiological stressors to adaptively regulate SERCA metabolism.

Conclusion

While PLN and SLN share considerable sequence homology and biochemical impact on SERCA catalytic activity, we show here that endogenous levels of PLN protein do not uncouple SERCA-mediated Ca^{2+}-transport from ATP hydrolysis, particularly at $[Ca^{2+}]_f$ near that of resting skeletal muscle, which is distinctly different from SLN. Consequently, whole-body metabolism is unaltered in *Pln*$^{-/-}$ mice housed at room temperature. Furthermore, we show that ablation of PLN does not alter muscular phenotype or the expression of other Ca^{2+}-handling proteins within oxidative skeletal muscle, including SLN. Although this study adds to the notion that PLN and SLN are functionally distinct (132), the role of PLN in adaptive thermogenesis remains unclear.

CHAPTER 3

Examination of Diet-Induced Obesity in *Pln*$^{-/-}$ Mice

Introduction

Obesity is associated with numerous comorbidities including type 2 diabetes, hypertension, cardiovascular diseases, and various cancers (2). Thus, finding ways to reduce adiposity is not only critical to manage the financial burden of treating obesity-related disorders, but also for the management of optimal metabolic function and health. Obesity results from a chronic energy imbalance, such that energy intake exceeds that of expenditure. Mammals possess mechanisms capable of regulating energy expenditure to maintain body temperature or body mass in response to changes in ambient temperature or diet, a process referred to as adaptive thermogenesis. In rodents, the most well characterized adaptive thermogenic mechanism is uncoupling of the mitochondrial proton gradient by uncoupling protein (UCP)-1 within brown and beige/brite fat (3, 133). Despite the now confirmed presence of brown fat within adult humans (7, 8), its absolute mass is variable (9), and its role in obesity management, while promising, is still debated (10, 11). This has prompted the search for other adaptive thermogenic mechanisms. Skeletal muscle is a prime candidate tissue due to its large contribution to overall body mass and metabolic rate (18).

UCP-3 is homologous in structure to UCP-1 (134), and uncouples mitochondrial respiration within skeletal muscle (135, 136). However, unlike mice lacking UCP-1 which are both cold-sensitive and susceptible to diet-induced obesity when housed at thermoneutral temperature (5, 6, 62, 87), those lacking UCP-3 show no hypometabolic phenotype (135, 136). The perplexing ability of skeletal muscle UCP-3 to uncouple respiration without an overt impact on energy balance suggests that its physiological regulation differs from that of UCP-1 and it has roles other than adaptive thermogenesis.

More recently, the sarcoplasmic reticulum (SR) has emerged as a critical organelle involved in skeletal muscle-based adaptive thermogenesis (15).

The SR is the major storage site of myocellular Ca^{2+} and the main protein responsible for maintaining SR and cytosolic [Ca^{2+}] is the sarco(endo)plasmic reticulum Ca^{2+}-ATPase (SERCA), which pumps Ca^{2+} ions into the SR lumen at the expense of ATP. Given that SERCA contains 2 Ca^{2+} binding sites and a single ATP-binding site, its theoretical optimal stoichiometry for Ca^{2+}-pumping is 2 Ca^{2+} ions per ATP hydrolyzed. Within skeletal muscle, SERCA function is regulated by several proteins, the best characterized of which are sarcolipin (SLN) and phospholamban (PLN), which inhibit the rate of Ca^{2+}-uptake by reducing SERCA's Ca^{2+} affinity and/or maximal activity (137). SLN has garnered attention for its ability to uncouple Ca^{2+} transport from ATP hydrolysis, increasing the energy required by SERCA to pump Ca^{2+} (14, 37, 38). Our group (13, 16, 17) and others (12) have shown that mice lacking SLN ($Sln^{-/-}$) are susceptible to excessive diet-induced obesity and glucose intolerance. Interestingly, the expression of SLN protein is increased 3-4 fold within oxidative muscle in response to high-fat feeding (12, 13), suggesting that uncoupling of SERCA is recruited as a mechanism to regulate adiposity and metabolism. Not surprisingly, mice over-expressing SLN are hypermetabolic and protected from diet-induced obesity (88). Furthermore, SLN participates in cold-induced thermogenesis, as $Sln^{-/-}$ mice are unable to maintain their body temperature when acutely cold challenged (12, 54). Together, these studies have provided convincing evidence that SLN is integral for both cold- and diet-induced adaptive thermogenesis originating from skeletal muscle, a role previously believed to be

exclusive to brown fat (3, 6). Currently, no study has examined whether PLN is involved in skeletal muscle-based diet-induced adaptive thermogenesis.

PLN and SLN share considerable similarity in their amino acid sequence (43), and both bind to the same transmembrane groove of SERCA to inhibit Ca^{2+}-uptake and muscle contractility (48, 49, 57). As such, they have historically been believed to be functional homologues of one another (43); however, this notion has recently been challenged (54, 55). Initially, PLN was shown to uncouple SERCA function within the heart (80); however, this has recently been challenged using several models. In HEK-293 cells transfected with SERCA alone or in combination with SLN or PLN, Sahoo and colleagues (55) showed that only SLN reduced the rate of Ca^{2+} translocation without impacting the rate at which SERCA consumes ATP, suggesting PLN does not uncouple SERCA. In agreement with this, we used *Pln*$^{-/-}$ mice to show that physiological levels of PLN protein expression do not alter SERCA Ca^{2+}-pumping efficiency within oxidative muscle (**Chapter 2**). It is important to note, however, that endogenous PLN protein content within oxidative muscle is relatively low and has little impact on SERCA function at [Ca^{2+}] near that of resting levels of muscle (**Chapter 2**) where SLN has been shown to exert effects on SERCA efficiency (14).

To date, only one study has attempted to examine whether skeletal muscle PLN participates in adaptive thermogenesis (54). In response to an acute cold-challenge (4°C for 8 hrs), Sahoo and colleagues (54) found that unlike *Sln*$^{-/-}$ mice, *Pln*$^{-/-}$ animals were capable of maintaining their body temperature, leading the authors to conclude PLN does not participate in adaptive thermogenesis. However, this experimental model may not be sufficient to observe a potential thermogenic effect on PLN for several reasons. First,

muscular contraction can activate kinases that rapidly phosphorylate numerous targets, including PLN (138). Protein kinase A (PKA) and Ca^{2+}/calmodulin-dependent protein kinase II (CaMKII) phosphorylate serine-16 (Ser16) and threonine-17 (Thr17) of PLN, respectively (58), inhibiting PLN function; these kinases are likely to target PLN during periods of increased shivering thermogenesis. Secondly, unlike SLN, PLN appears to have a lower affinity for SERCA as shown by its diminished ability to crosslink to the pump in the face of increasing [Ca^{2+}] (54, 55). It is possible that the rising cytosolic [Ca^{2+}] that occurs with repeated muscular contracture could prevent PLN from physically interacting with SERCA. Lastly, we showed previously that endogenous levels of PLN protein expression within oxidative skeletal muscle does not impact SERCA efficiency or alter whole-body metabolism in mice (**Chapter 2**). While muscular SLN protein expression increases in response to physiological stressors like prolonged cold-exposure and diet-induced obesity (12, 13, 63), acute cold stress is unlikely to increase PLN protein expression. Thus, while skeletal muscle PLN is not required acutely during shivering thermogenesis, this does not preclude its involvement in adaptive diet-induced thermogenesis. It is important to note that while a mouse model of PLN overexpression within oxidative muscle exists, these mice display a previously unrecognized myopathy accompanied paradoxically by SLN overexpression (65), the deletion of which further worsens the myopathy phenotype (139). Therefore, the utility of PLN overexpressing mice in studies of adaptive thermogenesis is highly questionable.

The objective of this study was to determine whether skeletal muscle PLN is involved in diet-induced adaptive thermogenesis. Given that SLN and PLN share considerable sequence homology and regulate SERCA in a similar manner, we

hypothesized that *Pln*$^{-/-}$ mice would be susceptible to an exaggerated diet-induced obesity phenotype, similar to that previously shown for *Sln*$^{-/-}$ mice (12, 13). Furthermore, we hypothesized that, like SLN, PLN protein expression would be increased within oxidative skeletal muscle by the consumption of a high-fat diet.

Methods

Experimental Animals and Genotyping

Experimental animals were group housed at room temperature (~22°C) under a 12:12-hr reverse light/dark cycle, and given *ad libitum* access to standard rodent chow (8640 Teklad 22/5 Rodent Diet, Teklad Diets, Madison, WI) and water. Animal genotyping was done as previously described in **Chapter 2**. All experiments were conducted using 3-4 month old homozygous male PLN knock-out ($Pln^{-/-}$) and wild-type (WT: $Pln^{+/+}$) littermate controls. Following genotype identification, mice were individually housed under the same environmental and feeding conditions described above. All studies were approved by the University of Waterloo Animal Care Committee and carried out in accordance with the Canadian Council on Animal Care.

Experimental Diets and Diet-Induced Obesity

Individually housed mice were given *ad libitum* access to water and either standard rodent chow (as above) or a "Westernized" high-fat diet (HFD) containing 42% kcal from fat, 42.7% kcal from carbohydrate, and 15.2% kcal from protein (TD 88137; Harlan Teklad, Madison, WI) for 8 weeks to induce obesity. Sample sizes for each group were as follows: WT chow: 12, $Pln^{-/-}$ chow: 7, WT HFD: 13, and $Pln^{-/-}$ HFD: 6. Body mass and food consumption were monitored weekly throughout the 8-week period. Food consumption was determined by weighing food pellets on top of the cage hopper and subtracting the difference remaining, along with any that had fallen into the cage bedding after each week. Whole-body metabolic efficiency, an indirect measurement of energy

expenditure (6, 87), was calculated by dividing the total mass gained over 8 weeks for each animal by their total food consumption (i.e. g mass gained/ MJ food consumed). To calculate this, food consumption (g) was converted to MJ using the caloric density (kcal/g) of each diet provided by the manufacturer and the conversion 1 kcal = 0.00418 MJ.

Whole-body Energy Expenditure and Glucose Tolerance

Before initiation of the dietary treatments, all animals were acclimated for one week to clear plastic cages with wire mesh bottoms, and provided powdered rodent chow and water *ad libitum* as described in **Chapter 2**. Prior to and following the experimental diets, animals were placed in the Comprehensive Lab Animal Monitoring System (CLAMS; Oxymax Series, Columbus Instruments, Columbus, OH) to measure O_2 consumption rate (ml O_2 consumed/kg body mass/hr), respiratory exchange ratio (RER: VCO_2/VO_2), metabolic heat production (kcal/hr/mouse), and spontaneous cage activity. Variables were expressed over 24-hours, and during states of activity and inactivity as described in **Chapter 2**. For high-fat fed animals, powdered HFD was placed in the feed canisters during post-diet CLAMS measurements.

Glucose tolerance was measured pre- and post-diet using an intraperitoneal glucose tolerance test following an overnight fast (~16 hrs). Blood (~5-10 μL) was sampled from a tail vein and analyzed for glucose using a standard diabetic glucometer (Accu-Chek Aviva, Roche Diagnostics) at 0, 30, 60, and 120 min following an injection of 10% D-glucose (1g/kg body mass) (13, 16). A detailed schematic of the experimental timeline and measurements can be found in **Appendix B** (**Figure B1**).

Blood and Tissue Collection

All chemicals were purchased from BioShop Canada Inc. (Burlington, ON, Canada) unless indicated otherwise. Post-diet, animals were fasted 4 hours prior to euthanasia by an anesthetic overdose of sodium pentobarbital (0.65 mg/kg body mass). Blood was collected via cardiac puncture using a heparinized syringe and allowed to clot on ice for ~10 min before being centrifuged at 5000 x g for 10 min. Serum was then collected, frozen in liquid nitrogen, and stored at -80°C until required.

Epididymal (Epidid), retroperitoneal (Retro), and inguinal (Ing) fat pads were removed and weighed for the determination of adiposity. A visceral adiposity index was calculated as 100 X [(Epidid + Retro pads)/ body mass] as previously done by our group (13). Organs (kidney, heart, liver) were also removed, cleaned and weighed. Soleus (SOL) and extensor digitorum longus (EDL) muscles were excised, cleared of connective tissue and weighed. The SOL was placed in ice-cold phenylmethylsulfonyl fluoride (PMSF; Sigma-Aldrich, Oakville, ON, Canada) buffer (pH: 7.5) containing in mM: 250 sucrose, 5 HEPES, 0.2 PMSF, and 0.2% (w/v) NaN_3 (Fisher Scientific, Fair Lawn, NJ). The SOL was then homogenized 1:10 (w/v) in ice-cold PMSF buffer using a glass-on-glass Dounce homogenizer, aliquots frozen in liquid nitrogen and stored at -80°C until needed. Interscapular brown adipose tissue (BAT) was cleared of extraneous white adipose tissue and muscle, weighed, and flash frozen in liquid nitrogen. Prior to use, BAT samples were thawed in ice-cold PMSF buffer, minced, and homogenized 1:4 (w/v) in PMSF for Western blotting (13).

Western Blotting

All antibodies and Western blotting protocols were carried out as described previously in **Chapter 2** and outlined in **Appendix A Table A2**. Protein content of muscle and BAT homogenates was determined by the bicinchoninic acid assay (Sigma-Aldrich, Oakville, ON, Canada) using bovine serum albumin (Sigma-Aldrich) as a standard.

Serum Catecholamines

Serum epinephrine and norepinephrine concentrations (ng/mL) were determined by high-performance liquid chromatography (HPLC) using the methods of Weicker and colleagues (140) as modified by Green *et al.* (141). Briefly, ~200 μl of thawed plasma was mixed in an Eppendorf tube containing 20 mg of acid washed Al_2O_3 (Sigma-Aldrich), 400 μl of buffer (pH: 8.7) containing 2 M Tris and 2% (w/v) EDTA, ~637 pg of 3,4-dihydroxybenzylamine (internal standard), and mixed for 10 min for catecholamine adsorption. Samples were then washed with distilled water and desorbed from Al_2O_3 with the addition of 0.1 M perchloric acid. Following centrifugation, 50 μl of the supernatant was injected into a Waters 2465 HPLC (Mississauga, ON, Canada) at 1.2 mL/min and separated using a Supelcosil (#58230U) columun (C18, 15 cm, 5 μm particle size). The mobile phase (pH: 3.5) consisted of 50 mM sodium acetate, 20 mM citric acid, 2 mM sodium octane sulfate, 1 mM di-*n*-butylamine, 100 μM EDTA dissolved in 96:4 (v/v) water:methanol. Serum catecholamines were compared against freshly made epinephrine (Sigma-Aldrich, product #: E4375) and norepinephrine (Sigma-Aldrich,

product #: A9512) standards, whose retention times were 5.26 min and 4.27 min, respectively.

Statistical Analysis

Dietary mass gain of chow- and HFD-fed animals, glucose tolerance, and CLAMS variables were analyzed using a 2-way ANOVA with repeated measures. Cumulative food intake, metabolic efficiency, tissue mass, adiposity, tissue protein expression, and serum catecholamines were analyzed with a 2-way ANOVA. When appropriate, post-hoc comparisons were made using a Newman-Keuls test to examine specific mean differences. Dietary PLN expression of WT mice (i.e. chow vs. HFD) was analyzed using a 2-tailed Student's t-test (independent samples). Statistical significance was considered at $P \leq 0.05$. All data presented are mean ± S.E.

Results

Dietary Mass Gain, Food Consumption and Metabolic Efficiency

As expected, high-fat fed animals gained significantly more mass relative to chow-fed counterparts (**Figure 3.1 A**) over the 8-week diet (main effect of diet: HFD > chow, $P < 0.0001$); however, the amount of weight gained was similar between WT and *Pln*$^{-/-}$ mice under both chow and HFD conditions. While cumulative 8-week calorie intake (MJ consumed) was greater in high-fat fed animals (main effect of diet: HFD > chow, $P < 0.0001$), no genotype difference in food intake existed in either chow- or HFD-fed mice (**Figure 3.1 B**). Following the 8th week of the diet, metabolic efficiency (i.e. g body mass gained/cumulative MJ food consumed) was significantly higher in high-fat fed animals (main effect of diet: HFD > chow, $P < 0.0001$), but as above, no differences existed between WT and *Pln*$^{-/-}$ littermates on either a chow or HFD (**Figure 3.1 C**).

Metabolic Phenotype

In high-fat fed animals, whole-body energy expenditure normalized to body mass (i.e. ml O_2/kg/hr) was significantly reduced post-diet (main effect of HFD: post < pre, $P < 0.001$) by ~18%, ~19%, and ~15% when measured over 24-hrs, during states of activity, and during states of inactivity, respectively (**Figure 3.2 A/B**). No differences in relative energy expenditure were observed between WT and *Pln*$^{-/-}$ mice pre- or post-HFD. Conversely, absolute energy expenditure measured as heat production (i.e. kcal/hr/mouse) was significantly greater post-diet (main effect of HFD: post > pre, $P < 0.0001$) by ~17%, ~14%, and ~20% when measured over 24-hrs, during states of activity,

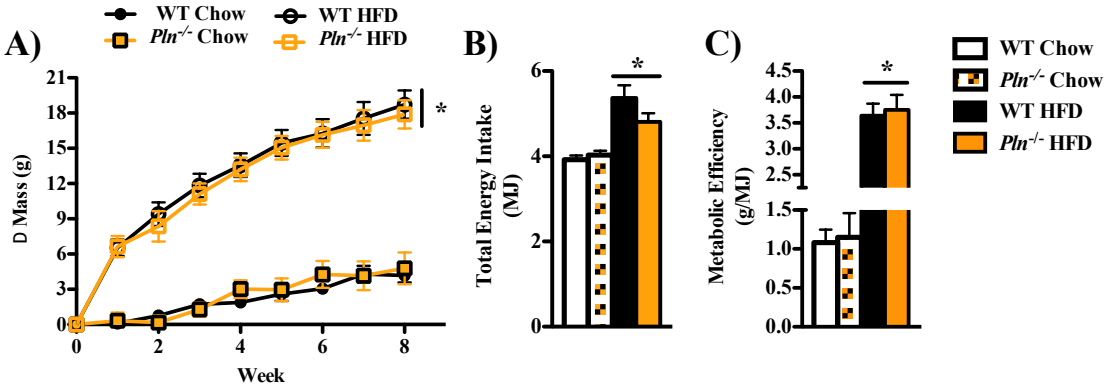

Figure 3.1. PLN ablation does not predispose mice to diet induced obesity. **A)** Dietary mass gain (g) of wild-type (WT) or *Pln*$^{-/-}$ mice over 8 weeks of a chow or high-fat diet (HFD) (n = 6-13/group). **B**) Cumulative 8-week food consumption (MJ). **C)** Metabolic efficiency (g mass gained/MJ food consumed) following the 8 week dietary treatment. * Significant main effect ($P < 0.0001$) of diet (HFD > chow). Values are mean ± S.E.

and during states of inactivity, respectively (**Figure 3.2 C**). As above, absolute heat production rate did not differ pre- or post-HFD between WT and *Pln*$^{-/-}$ mice. Total spontaneous cage activity (**Figure 3.2 D**) or cage ambulation (**Figure 3.2 E**) of high-fat fed mice did not differ pre- or post-diet, regardless of genotype. Lastly, whole-body substrate usage indicated a shift towards greater fat oxidation during all measurement states consistent with the consumption of the HFD, as RER was significantly lower post-diet in both genotypes (main effect of HFD: post < pre, $P < 0.0001$) (**Figure 3.2 F**). PLN ablation itself did not impact substrate usage pre- or post-HFD when measured over 24-hrs ($P = 0.903$), during states of activity ($P = 0.463$), or during states of inactivity ($P = 0.944$).

Whole-Body Glucose Tolerance and Dietary Catecholamine Response

Whole-body glucose tolerance pre- and post-HFD is shown in **Figure 3.3**. As expected, animals became glucose intolerant following the 8-week HFD relative to pre-dietary levels, as evidenced by the significantly greater blood glucose levels across all time points measured (main effect of HFD: post > pre, $P < 0.0001$) (**Figure 3.3 A**). This was also shown when glucose tolerance was expressed as area under the curve (AUC) (**Figure 3.3 B**), which was ~27% greater post-HFD relative to pre-dietary levels (main effect of HFD: post > pre, $P < 0.001$). No differences in blood-glucose concentration existed between *Pln*$^{-/-}$ and WT mice at any time point pre- or post-HFD, or when glucose tolerance was expressed as AUC.

We previously showed a compensatory rise in circulating catecholamines following high-fat feeding in *Sln*$^{-/-}$ mice (13). Thus, it was of interest to determine

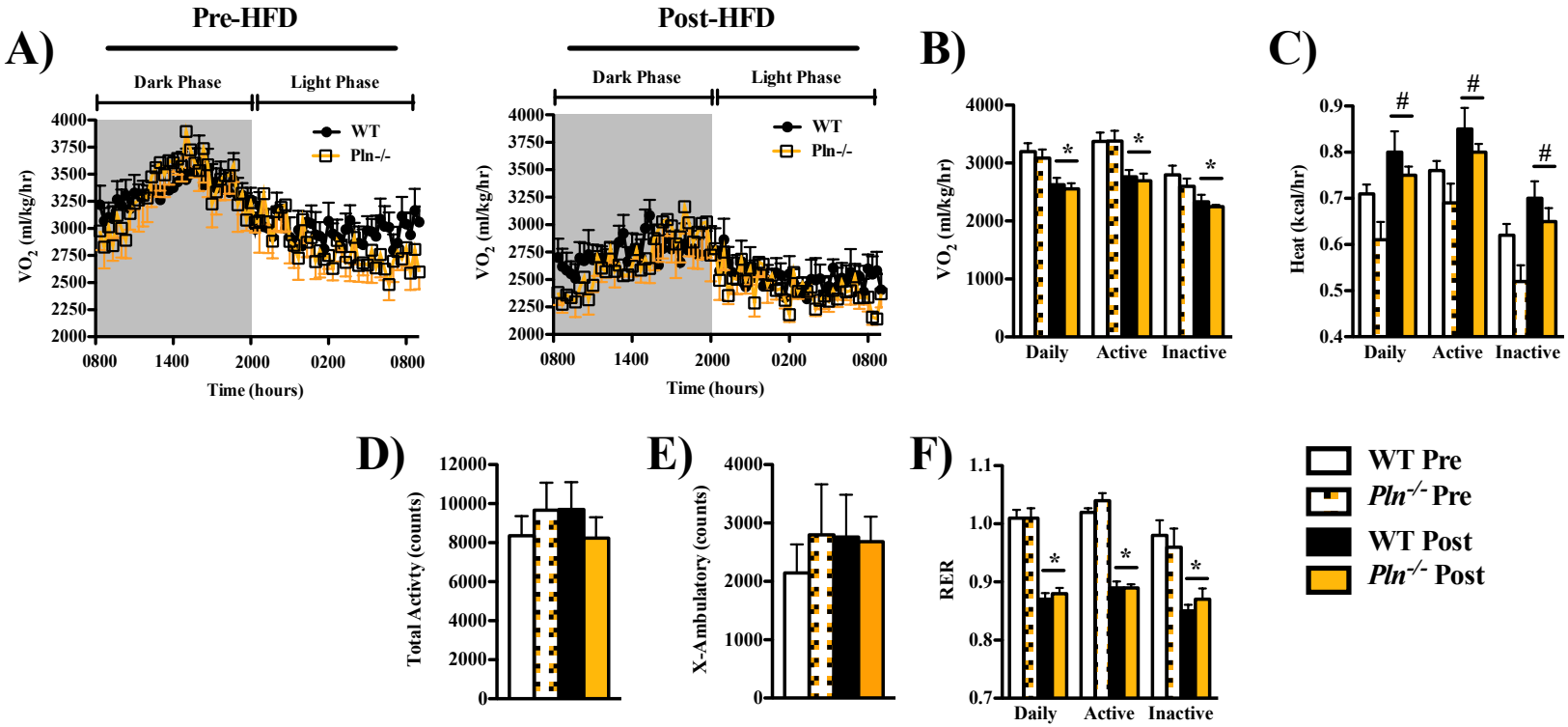

Figure 3.2. Metabolic phenotype of wild-type (WT) and *Pln*$^{-/-}$ mice in response to an 8-week high-fat diet (HFD). **A)** Metabolic rate expressed as oxygen consumption rate (VO_2: ml O_2/kg body mass/hr) over a full 24 hour light/dark cycle before (Pre) and following (Post) the 8-week HFD. **B)** VO_2 averaged over 24 hours (daily), during states of cage activity (active: 0800 hrs - 2000 hrs (dark phase), >2 ambulatory activity counts) and inactivity (inactive: 2000 hrs - 0800 hrs (light phase), ≤2 ambulatory activity counts). **C)** Metabolic rate expressed as absolute heat production rate (kcal/hr/mouse). **D**) Total spontaneous cage activity (counts) over 24-hours. **E)** Ambulatory cage activity (counts) in the X plane over 24 hours. **F)** Respiratory exchange ratio (RER: VCO_2/VO_2). * Significant main effect ($P < 0.001$) of diet (Post < Pre). # Significant main effect ($P < 0.001$) of diet (Post > Pre). Values are mean ± S.E.

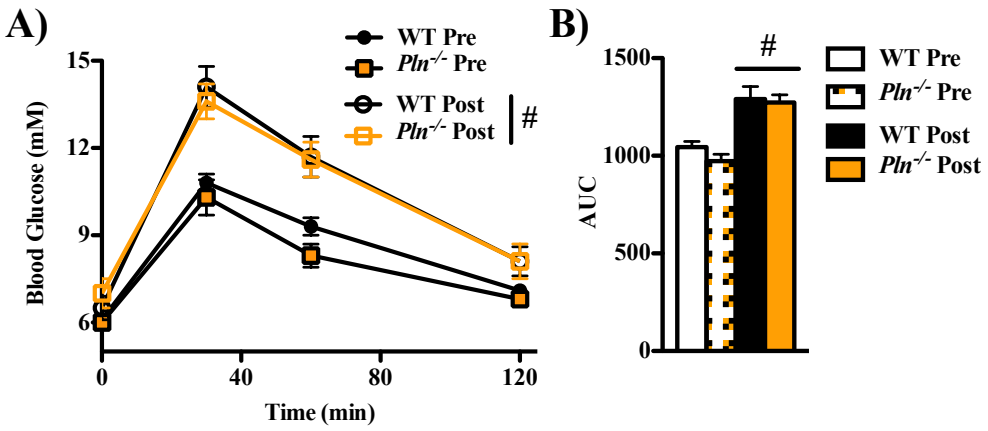

Figure 3.3. Glucose tolerance of WT (n = 13) and *Pln*$^{-/-}$ (n = 6) mice before (Pre) and after (Post) an 8 week high-fat diet (HFD). **A)** Blood glucose (mM) during and intraperitoneal glucose tolerance test pre- and post-HFD. **B)** Glucose tolerance expressed as area under the curve (AUC) of animals pre- and post-HFD. # Significant main effect ($P < 0.0001$) of diet (Post > Pre). Values are mean ± S.E.

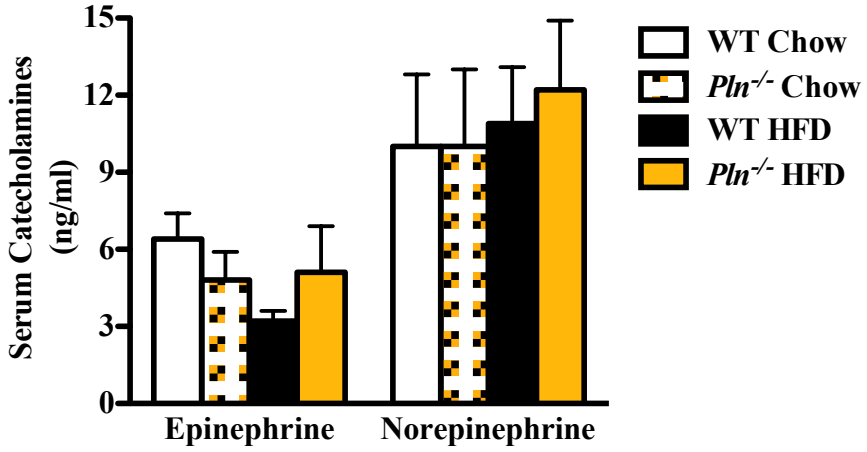

Figure 3.4. Serum epinephrine and norepinephrine concentrations (ng/ml) of wild-type (WT) and *Pln*$^{-/-}$ mice following 8 weeks of a chow or high-fat diet (HFD) (n = 6 - 13/group). Values are mean ± S.E.

whether this also occurred in response to PLN ablation. Serum epinephrine and norepinephrine following 8 weeks of chow- or high-fat feeding are shown in **Figure 3.4**. Neither epinephrine nor norepinephrine levels were affected by diet or genotype.

Organ, Muscle and Fat Mass

Kidney, heart, and liver masses (both absolute and normalized to body mass) of chow and high-fat fed animals are listed in **Table 3.1**. Relative to chow-fed controls, HFD-fed animals had a significantly greater kidney and liver mass (main effect of diet: HFD > chow, $P < 0.05$); however, gross heart mass was not different between chow and high-fat fed mice. Interestingly, $Pln^{-/-}$ mice had smaller kidneys, regardless of diet (main effect of genotype: $Pln^{-/-}$ < WT, $P < 0.05$). When normalized to body mass, high-fat feeding significantly reduced kidney and heart masses (main effect of diet: HFD < chow, $P < 0.05$), but increased relative liver mass (main effect of diet: HFD > chow, $P < 0.05$). There was no impact of PLN ablation on normalized organ masses, regardless of diet.

SOL mass was similar between chow and HFD-fed mice ($P = 0.197$) and was not impacted by PLN ablation ($P = 0.703$) (**Figure 3.5 A**). Likewise, EDL mass was not affected by diet ($P = 0.970$) or genotype ($P = 0.232$) (**Figure 3.5 A**). As expected, high-fat feeding significantly increased (main effect of diet: HFD > chow, $P < 0.01$) the masses of the epididymal (+30%), and retroperitoneal (+73%) fat depots, while the inguinal fat depot was over 2-fold larger (**Figure 3.5 B**); however, fat depot mass was not affected by animal genotype. Consistent with this, the adiposity index (**Figure 3.5 C**) of high-fat fed animals was ~ 17% greater (main effect of diet: HFD > chow, $P < 0.05$)

Table 3.1. Organ masses of WT and *Pln*$^{-/-}$ mice following 8 weeks of a chow or high-fat diet (HFD) (n = 6-13/group). Values are presented as absolute mass (g) and organ mass as a percentage of total body mass (% mass). *P*-values are listed for the main effect of genotype (WT vs. *Pln*$^{-/-}$), diet (Chow vs. HFD), and the genotype/diet interaction when analyzed by a 2-way ANOVA. Values are mean ± S.E.

	Chow		HFD		Genotype	Diet	Interaction
	WT	*Pln*$^{-/-}$	WT	*Pln*$^{-/-}$	*P*-Value		
Mass (g)							
Kidney	0.430 ± 0.036	0.384 ± 0.016	0.383 ± 0.013	0.321 ± 0.010	< 0.05	< 0.05	0.774
Heart	0.247 ± 0.020	0.251 ± 0.018	0.237 ± 0.010	0.233 ± 0.005	0.995	0.399	0.785
Liver	1.900 ± 0.124	2.117 ± 0.118	4.739 ± 0.268	4.421 ± 0.468	0.853	<0.05	0.333
% Mass							
Kidney	0.915 ± 0.069	0.784 ± 0.051	0.557 ±0.056	0.540 ± 0.022	0.243	< 0.05	0.369
Heart	0.528 ± 0.037	0.527 ± 0.048	0.386 ± 0.018	0.391 ± 0.015	0.965	< 0.05	0.886
Liver	4.119 ± 0.125	4.270 ± 0.168	7.093 ± 0.639	7.342 ± 0.631	0.714	< 0.05	0.930

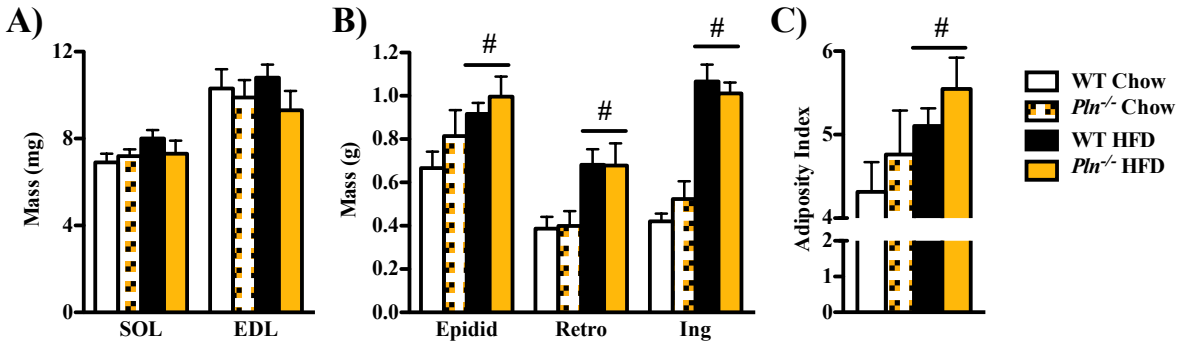

Figure 3.5. Skeletal muscle and adipose depot mass of wild-type (WT) and *Pln*$^{-/-}$ mice following 8 weeks of a chow or high-fat diet (HFD) (n = 6-13/group). **A)** Soleus (SOL) and extensor digitorum (EDL) mass (mg). **B)** Epididymal (Epidid), retroperitoneal (Retro), and inguinal (Ing) fat pad masses (g). **C)** Adiposity index (as described in "Methods"). # Significant main effect ($P < 0.05$) of diet (HFD > Chow). Values are mean ± S.E.

relative to chow-fed counterparts, while no differences ($P = 0.233$) between WT and *Pln*$^{-/-}$ mice existed on either diet.

SR Protein Expression

It was of interest to us to determine whether any compensatory changes in the expression of proteins involved in SR Ca^{2+} release, uptake, and storage existed within oxidative muscle in the absence of PLN, and in response to caloric surfeit. SOL muscle protein expression of RyR ($P = 0.287$), DHPR ($P = 0.968$), SERCA1a ($P = 0.591$), SERCA2a ($P = 0.820$), CSQ ($P = 0.593$) and SLN ($P = 0.459$) were similar between *Pln*$^{-/-}$ and WT mice, regardless of whether they were fed a chow or HFD (**Figure 3.6 A/B**). Although SOL DHPR content increased ~37% with high-fat feeding, this was not statistically significant ($P = 0.149$). Surprisingly, SOL SLN expression declined ~38% (main effect of diet: HFD < chow, $P < 0.05$) in both WT and *Pln*$^{-/-}$ mice in response to the HFD relative to chow-fed controls (**Figure 3.6 A/B**).

Currently, no examination of the dietary response of PLN in skeletal muscle has been made in the context of diet-induced obesity. Thus, it was a priority to determine whether a Westernized diet impacted the protein expression of PLN in a muscle group that also expresses SLN. Interestingly, high-fat feeding significantly reduced ($P < 0.05$) PLN protein expression in WT mice by ~60% relative to chow-fed controls (**Figure 3.6 C/D**). Furthermore, while total phosphorylated PLN was significantly ($P < 0.05$) decreased with high-fat feeding, the relative degree of Ser16/Thr17 phosphorylation of PLN tended ($P = 0.07$) to increase with high-fat feeding (**Figure 3.6 C/D**). Together,

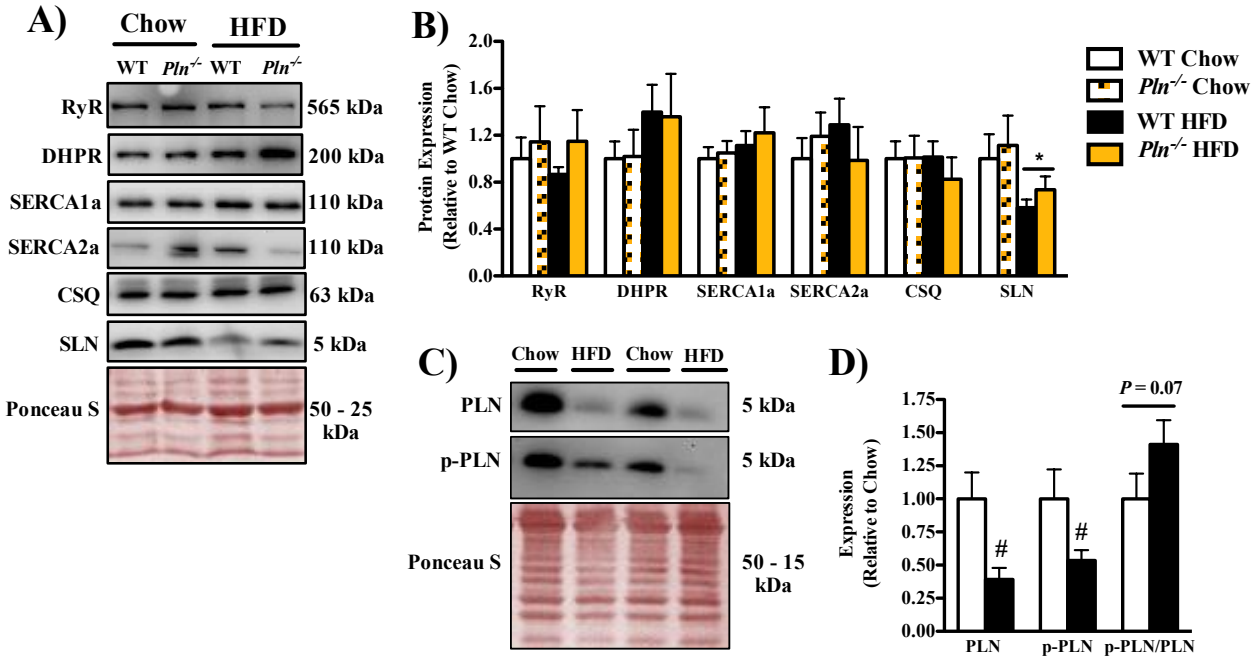

Figure 3.6. Expression of soleus Ca^{2+}-handling proteins following 8 weeks of a chow or high-fat diet (HFD). **A)** Representative Western blots of chow and high-fat fed WT and *Pln*$^{-/-}$ mice (n = 6-13/group). Equal protein load was confirmed using Ponceau S staining. **B)** Protein expression relative to chow-fed WT mice. **C)** Representative Western blots of monomeric PLN and phosphorylated monomeric PLN (p-PLN) of chow, and high-fat fed WT mice. **D**) PLN expression relative to chow-fed mice. * Significant main effect ($P < 0.05$) of diet (HFD < Chow). # Significantly different ($P < 0.05$) from WT Chow. Values are mean ± S.E.

these data suggest that the high-fat feeding reduces the inhibitory interaction of PLN with SERCA within oxidative skeletal muscle.

BAT Mass and UCP-1 Expression

BAT is a major thermogenic organ that participates in diet-induced adaptive thermogenesis by dissipating the mitochondrial proton gradient through UCP-1 (3). Thus, we sought to examine whether a compensatory role of BAT/UCP-1 existed with PLN ablation. Absolute BAT mass increased ~2.8-fold in high-fat fed animals (main effect of diet: HFD > chow, $P > 0.0001$) relative to chow-fed controls (**Figure 3.7 A**). When BAT mass was normalized to animal body mass (**Figure 3.7 B**), high-fat feeding again resulted in a significant expansion in BAT tissue (main effect of diet: HFD > chow, $P > 0.0001$). However, no differences in absolute or normalized BAT mass existed between WT or *Pln*$^{-/-}$ littermates, regardless of dietary intervention. Furthermore, while UCP-1 protein expression was increased ~21% by high-fat feeding (main effect of diet: HFD > chow, $P > 0.01$), no genotype differences existed between either chow- or HFD-fed animals (**Figure 3.7 C/D)**.

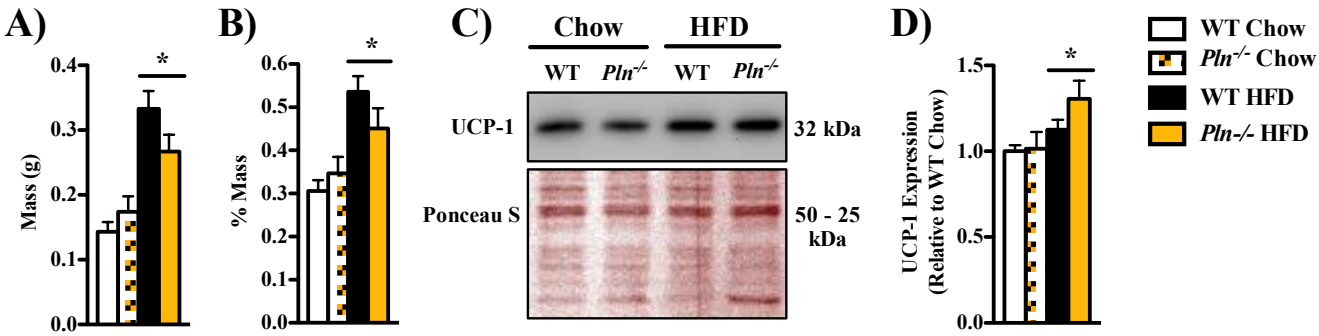

Figure 3.7. Adaptive response of brown adipose tissue (BAT) is unaffected by PLN ablation. **A)** BAT mass (g) of wild-type (WT) and *Pln*$^{-/-}$ mice following an 8 weeks of a chow or high-fat diet (HFD) (n = 6-13/group). **B)** BAT mass expressed as a percentage of animal body mass (% mass). **C)** Representative Western blot of BAT UCP-1. Equal protein load was confirmed using Ponceau S staining. **D)** BAT UCP-1 protein expression relative to chow-fed WT mice. * Significant main effect ($P < 0.05$) of diet (HFD > Chow). Values are mean ± S.E.

Discussion

Ca^{2+}-pumping by SERCA is a major contributor to skeletal muscle metabolic rate (42), and the SERCA regulatory protein SLN increases the energy demand of SERCA-mediated Ca^{2+} pumping within oxidative skeletal muscle (14). As such, SLN has emerged as a critical regulator of muscle-based adaptive thermogenesis, protecting mice from acute cold exposure and the development of diet-induced obesity (12, 13, 16, 17, 54, 88). Historically, SLN and PLN have been thought to be functional homologues of one another given their structural resemblance and similar impacts on SERCA activity and consequently muscle function (48, 49, 76, 77). Additionally, both are endogenously expressed within oxidative skeletal muscle in WT mice (65), and even co-expressed within a population of the same single skeletal muscle fibres of humans (126). While one group has previously been shown PLN to reduce the energetic efficiency of SERCA (80), our lab (**Chapter 2**) and others (55) have not found this. Therefore, despite our previous study (**Chapter 2**) it remained unclear whether skeletal muscle PLN was recruited by diet to uncouple SERCA in a manner similar to SLN, as *Sln*$^{-/-}$ mice only develop an obesogenic phenotype when fed a HFD (12, 13). Given its similarities to SLN, we sought to determine whether skeletal muscle PLN participates in adaptive diet-induced thermogenesis. Unlike hypothesized, *Pln*$^{-/-}$ mice displayed no obesogenic phenotype compared with WT littermates, as noted by their similar diet-induced mass gain, adiposity, and development of glucose intolerance. Consistent with this, energy expenditure of high-fat fed mice was unaltered by PLN ablation. Furthermore, the expression of major skeletal muscle Ca^{2+}-handling proteins and BAT UCP-1 were similar between WT and *Pln*$^{-/-}$ mice, indicating that the absence of an obesogenic phenotype was

not due to compensation from other thermogenic mechanisms in PLN deficient animals. Surprisingly, the protein expression of both SLN and PLN within oxidative skeletal muscle declined in response to high-fat feeding. Despite this, PLN ablation *per se* did not predispose mice to excessive diet-induced obesity, which is in stark contrast to SLN ablation. The findings here are consistent with those of **Chapter 2** and Sahoo and colleagues (55), demonstrating that PLN does not uncouple SERCA-mediated Ca^{2+} transport from ATP hydrolysis, and add further evidence to the assertion that SLN and PLN serve functionally distinct purposes within skeletal muscle.

Whole-Body Metabolism, Dietary Mass Gain and Adiposity

As expected, consumption of a "Westernized" diet resulted in considerable mass gain over the 8 week period in both WT and *Pln*$^{-/-}$ mice compared to chow-fed controls, the magnitude of which was similar to that previously found by our group using the same HFD (13, 16, 17). Consistent with the similar dietary mass gain, cumulative food consumption was not different between WT and *Pln*$^{-/-}$ littermates, indicating that global loss of PLN did not result in a compensatory change of energy intake as a mechanism to maintain energy balance. Not surprisingly then, metabolic efficiency was unaltered by PLN ablation, suggesting that energy expenditure during the diets were similar between WT and *Pln*$^{-/-}$ littermates. This was confirmed by our CLAMS experiments, which demonstrated that body-mass normalized and absolute energy expenditure, along with spontaneous cage activity, were comparable between genotypes. While adiposity was expectedly greater in fat-fed animals, neither the subcutaneous/visceral fat depots nor the adiposity index were affected by PLN ablation. Consequently, there was a comparable

development of diet-induced glucose intolerance post-HFD in all animals, consistent with a comparable development of obesity between WT and *Pln*$^{-/-}$ littermates. While insulin sensitivity was not measured here, consumption of a "Westernized" diet is known to inhibit skeletal muscle insulin signaling through the accretion of intramuscular bioactive lipid species and a pro-inflammatory cytokine profile resulting from obesity (142, 143). Since these factors are related to the degree of positive energy balance and adiposity, it is reasonable to expect that there was a comparable development of diet-induced insulin resistance in both genotypes.

Our finding that *Pln*$^{-/-}$ animals lack an excessively obese phenotype when provided a HFD contrasts quite drastically with that of *Sln*$^{-/-}$ mice (12, 13, 16, 17). Under identical housing and feeding conditions, we have previously shown *Sln*$^{-/-}$ animals to gain more mass, develop greater adiposity, and become more glucose intolerance despite consuming a similar amount of calories from a HFD to that of WT littermates (13, 16, 17). This phenotype is also accompanied by a depression in whole-body metabolic rate resulting from the inability of *Sln*$^{-/-}$ mice to recruit SLN-mediated uncoupling of SERCA in response to high-fat feeding (13). Not surprisingly then, mice overexpressing SLN within skeletal muscle are hypermetabolic when housed at thermoneutrality and consequently resistant against the development of diet-induced obesity (88). Consistent with the development of excessive diet-induced obesity with SLN ablation only, *Sln*$^{-/-}$ mice become hypothermic in response to acute cold exposure, whereas this is not the case for *Pln*$^{-/-}$ animals (12, 54, 62). The consistency between the cold- and diet-induced hypometabolic phenotype of *Sln*$^{-/-}$ mice, and lack thereof in *Pln*$^{-/-}$ mice, is in agreement with our previous findings that skeletal muscle SLN (14), not PLN (**Chapter 2**), is

capable of uncoupling SERCA. Our findings herein add further evidence to the viewpoint that SLN and PLN serve functionally distinct purposes within skeletal muscle, particularly during states of metabolic stress.

Organ and Skeletal Muscle Mass

PLN ablation has previously been reported not to affect cardiac mass or ultrastructure (45, 46, 89), consistent with our findings here that both absolute and relative heart masses were unchanged in *Pln*$^{-/-}$ mice. Likewise, while high-fat feeding increased absolute liver mass, no genotype differences existed in liver size. Surprisingly, *Pln*$^{-/-}$ animals displayed smaller kidneys, regardless of diet. While unclear why this was the case, relative kidney mass was the same between WT and *Pln*$^{-/-}$ mice. Our findings that the relative masses of all organs were similar between WT and *Pln*$^{-/-}$ littermates, is likely reflective of the comparable diet-induced mass/adiposity gain between these animals.

In **Chapter 2**, we found no effect of PLN ablation on fibre-type distribution pattern or fibre-specific size of the SOL, a muscle that expresses PLN protein. In agreement with this, gross SOL mass was unaltered by PLN ablation, regardless of whether animals were fed a control or HFD. Given that PLN protein was not detectable within the EDL (**Chapter 2**), it was not surprising that no change in gross EDL mass existed between WT and *Pln*$^{-/-}$ littermates, regardless of their diet. In contrast to *Pln*$^{-/-}$ animals, mice overexpressing PLN within slow-twitch muscle show a drastic reduction of SOL mass and activation of Ca^{2+}-dependent proteolytic enzymes resulting from chronic SERCA inhibition (65). Our findings here and those of **Chapter 2** indicate that

endogenous levels of PLN protein to not impact skeletal muscle mass, and further corroborate that the HFD-induced mass gain of *Pln*$^{-/-}$ mice is reflective of an equivalent expansion of adipose tissue to that of WT littermates.

Tissue Protein Expression and Circulating Catecholamines

In **Chapter 2**, we found the expression of various proteins involved in Ca^{2+}-uptake, storage, and release to be unaltered within the SOL in response to PLN ablation. This was again the case here, as *Pln*$^{-/-}$ mice showed no disproportional change in SR proteins or BAT UCP-1 in response to high-fat feeding, indicating that the lack of an obesogenic phenotype of these mice was not related to any compensatory changes in the proteins measured. Similar to these results, *Sln*$^{-/-}$ mice show no changes in SOL SERCA1a, SERCA2a, CSQ, or BAT UCP-1 in response to diet-induced obesity (12, 13). Together, these studies indicate that ablation of either protein does not result in skeletal muscle SR remodeling, which could complicate the interpretation of their respective phenotypes. The most surprising finding from this study was the diet-induced decline of both SLN and PLN protein content within oxidative skeletal muscle. In the SOL, SLN protein expression has been reported to increase ~3-4-fold in response to caloric surfeit (12, 13, 87), although not all studies have shown such a robust diet-induced induction of SLN protein within WT skeletal muscle (144). In agreement with these studies, transgenic overexpression of SLN is protective against diet-induced obesity in mice (88). One possible explanation for the disparity in the diet-induced SLN response found here is the strain background of the mice, which is 129S and not C57BL/6J like that previously used (12, 13, 87). Not surprisingly, cardiac contractile parameters have been shown to

differ among various strains of mice (90), which may relate to intrinsic differences in muscular Ca^{2+}-handling. Interestingly, endogenous levels of SLN protein expression within the SOL appear to be lowest in C57BL/6J animals compared to WT mice of other strains (**Appendix B**: **Figure B2**); it is possible that optimal HFD-induced uncoupling by SLN may occur at a lower protein expression in 129S mice, and increasing SLN further may hinder muscle function with diet-induced obesity. While previous studies may suggest a positive correlation between the amount of SLN protein and muscular energy expenditure, this may not always be the case. In WT mice, O_2 consumption rate of isolated intact SOL muscles is similar to that of *Sln*$^{-/-}$ littermates (13). Furthermore, while SLN protein expression is greater in myocytes cultured from obese compared to lean individuals, basal energy expenditure is comparable between the groups and, surprisingly, SLN-dependent energy expenditure is lower in myocytes from obese humans (145). Thus, the amount of SLN present may not be the sole predictor of its ability to uncouple SERCA in response to diet-induced obesity. It is also possible that despite our observation of lower SLN protein following the HFD, the amount actually bound to SERCA may be higher, eliminating a need to increase SLN's total capacity. Unfortunately, because muscle specific energy expenditure was not measured here, we cannot definitively say that the reduction in SLN protein expression resulted in lower muscle energy expenditure, or more specifically, that the fraction of energy consumed by SERCA was lower in response to the HFD.

Similar to the dietary response of SLN, SOL PLN protein was also reduced by high-fat feeding. In fact, analysis of WT mice from our group's first report on SLN's role in obesity (13) revealed a similar decline in SOL PLN content in response to high-fat

feeding (146). In addition to a reduction of PLN content, PLN Ser16/Thr17 phosphorylation tended to be higher in the SOL of high-fat fed WT mice. This tendency could not be explained by a rise in circulating catecholamines, which were unaltered by diet or genotype. However, skeletal muscle-specific norepinephrine turnover can be modified by diet in rodents (147), suggesting that adrenergic control of SR proteins, including PLN phosphorylation, could occur independent of a change in circulating catecholamines. Together, this response of PLN to high-fat feeding indicates its physical interaction with SERCA is diminished with obesity. While the physiological role of this change is unclear from this study, it is in line with our findings from **Chapter 2** and those of others (55), which demonstrate that PLN is not an uncoupler of SERCA. Interestingly, other physiological/hormonal states associated with increased energy expenditure, such as prolonged cold exposure and hyperthyroidism, are associated with similar changes in muscular PLN phosphorylation and expression (93-95, 97, 148), and more surprisingly an increase in SERCA thermogenesis (94, 100). While it is tempting to speculate that a decline in PLN protein expression *per se* is thermogenic, the mechanism of how this might occur is unclear and awaits experimentation.

Conclusion

Unlike what has previously been observed with whole-body ablation of SLN (12, 13, 16), mice deficient in PLN are not susceptible to the development of diet-induced obesity and glucose intolerance when provided *ad libitum* access to a HFD. The lack of an obeogenic phenotype in *Pln*$^{-/-}$ animals is not the result of compensation by other thermogenic mechanisms originating from BAT or skeletal muscle (i.e. UCP-1 and SLN,

respectively). Our findings herein are in accordance with previous reports by our group (**Chapter 2**) and others (55) demonstrating that PLN does not uncouple SERCA. Furthermore, phenotypic consistency exists between the lack of excessive obesity shown here and the previously demonstrated ability of *Pln*$^{-/-}$ mice to withstand cold-stress, whereas *Sln*$^{-/-}$ animals display a stereotyped hypometabolic phenotype in response to calorie overload and acute cold-stress (12, 13, 16, 54). Thus, our findings add further support to the growing body of evidence that SLN and PLN serve functionally distinct purposes within skeletal muscle.

CHAPTER 4

Characterization of Dual SLN/PLN Ablation on Whole-Body Metabolism and Ca^{2+}-Handling Within Oxidative Skeletal Muscle

Introduction

Within skeletal muscle, cellular Ca^{2+} plays a critical role in excitation-contraction coupling and as a second messenger to co-ordinate gene transcription in response to various physiological stimuli. While intracellular Ca^{2+}-signaling proteins, including the Ca^{2+}/calmodulin (CaM)-dependent phosphatase calcineurin (CaN) and CaM kinases (CaMKs), are responsible for controlling the metabolic and contractile phenotype of skeletal muscle (129, 149), the major regulator of cytosolic and sarcoplasmic reticulum (SR) [Ca^{2+}] is the sarco(endo)plasmic reticulum Ca^{2+}-ATPase (SERCA). SERCAs are 110 kDa integral membrane proteins of the SR responsible for the ATP-dependent transfer of Ca^{2+} ions from the cytosol into the SR lumen (21). Two isoforms exist within skeletal muscle, SERCA2a which is co-expressed with myosin heavy chain (MHC) type I, and SERCA1a which is co-expressed with MHC type II, comprising the slow- and fast-twitch muscular isoforms, respectively (27). Although no intrinsic difference in the rate of Ca^{2+}-pumping exists between isoforms (30), the density of SERCA1a within fast-twitch fibres is greater than that of SERCA2a within slow-twitch fibres (27), allowing for faster rates of Ca^{2+}-uptake and contractile kinetics.

Two well-described regulators of SERCA function are sarcolipin (SLN) and phospholamban (PLN) (43), both of which slow the rate of Ca^{2+}-uptake by reducing SERCA's affinity for Ca^{2+} and/or decreasing maximal SERCA activity, consequently reducing muscular contractility (48, 49, 76, 77). Their expression pattern in the heart is chamber-specific, with SLN abundant in the atria and PLN abundant in the ventricle (58); however, some have detected SLN within the left ventricle and PLN within the atria using SR-enriched preparations, albeit at lower levels than their native chambers (44).

Within mice, SLN and PLN are both present in oxidative muscles, whereas in glycolytic muscles SLN is expressed to a lower degree and PLN is absent (48, 49). In human vastus lateralis, both can even be co-expressed within the same single skeletal muscle fibre, although PLN is more abundant in type I fibres while SLN is greater in type IIA fibres (28).

Interestingly, genetic manipulation of either SERCA regulator can alter the phenotype of skeletal muscle. Mice overexpressing PLN (Pln^{OE}) within type I fibres display a fast-to-slow fibre type shift within the soleus (SOL), atrophy of type I fibres, and compensatory hypertrophy of type IIA fibres (65, 68). Furthermore, Pln^{OE} animals present with a previously unrecognized centronuclear myopathy-like phenotype (65, 68). While overexpression of SLN driven by the human α-actin promoter has been reported not to affect fibre-type distribution within glycolytic skeletal muscle, it does increase fatigue resistance (64) and oxidative capacity in high-fat fed animals (88). Remodeling of either the contractile or metabolic phenotype in these murine models is presumably due to the activation of Ca^{2+}-dependent signaling pathways in response to chronic SERCA inhibition. However, loss of either PLN or SLN in mice does not alter skeletal muscle fibre type distribution, and at least for PLN, fibre size (49). Within the heart, the impact of SLN or PLN ablation is slightly more complex. Similar to skeletal muscle, mice lacking PLN do not display altered gross cardiac morphology or ventricular ultrastructure (45, 46). While SLN ablation in mouse has been reported not to affect atrial or ventricular morphology (44), this same group has also found atrial fibrosis to be increased in $Sln^{-/-}$ mice (103). Surprisingly, double knock-out (DKO) of both SLN and PLN results in left ventricular hypertrophy and predisposes aged mice to cardiac

dysfunction, this despite improved SERCA function (108). While these knock-out studies suggest that physiological levels of either protein may not alter cellular [Ca^{2+}] and subsequent downstream signaling to a large extent, the combinatorial loss of both within the heart can. Along this line, co-expression of both SLN and PLN with SERCA in HEK-293 cells results in super-inhibition of Ca^{2+}-uptake, as both Ca^{2+}-affinity and maximal SERCA activity are markedly reduced compared to either regulator alone (76). Interestingly, SLN prevents the formation of non-inhibitory PLN pentamers, maintaining it in its inhibitory momomeric form (76). Moreover, a ternary complex of SLN/PLN/SERCA is capable of forming (53), indicating a complex interplay between SLN and PLN to regulate SERCA function. It is possible that a super-inhibitory complex serves a critical physiological function in regulating cardiac Ca^{2+}-handling, as noted by the pathological cardiovascular phenotype of DKO mice. Given that both SERCA regulators are found in oxidative muscle an even within the same muscle fibre (28, 65), their combined physiological impact on skeletal muscle is less clear.

Ca^{2+}-handling is not only important for signaling pathways controlling skeletal muscle morphology and metabolic phenotype, but also for energy metabolism (42). SERCA activity is estimated to account for upwards of 48% of basal energy expenditure in isolated resting skeletal muscle (42), and several regulatory proteins have been demonstrated to increase SERCA's ATP requirement to pump Ca^{2+} ions (14, 37, 38, 150). The regulatory interaction between SERCA and SLN is thermogenic in nature as SLN uncouples Ca^{2+} transport from ATP hydrolysis, making SERCA less energetically efficient at pumping Ca^{2+} (14, 37, 38, 54, 55). Despite more efficient Ca^{2+}-pumping, mice lacking SLN (*Sln*$^{-/-}$) do not display lower skeletal muscle and whole-body energy

expenditure (14), but are susceptible to diet-induced obesity and hypothermia (12, 13, 16, 17). Unlike SLN, our group (**Chapter 2**) and others (55) find no evidence that PLN uncouples SERCA function. Not surprisingly then, whole-body metabolic rate is unaltered in mice lacking PLN (*Pln*$^{-/-}$), nor are these animals susceptible to diet-induced obesity or cold-intolerance like that of *Sln*$^{-/-}$ mice (54). While it is logical then to predict SERCA efficiency to be higher in DKO mice due exclusively to the absence of SLN, SERCA efficiency is also influenced by SR content (see **Chapter 1: Figure 1.3**), which is higher in DKO mice (108), and not just through physical interaction with its regulatory proteins. Thus, the impact of dual SLN/PLN ablation on SERCA pumping efficiency, and subsequently whole-body metabolism, remains to be seen.

Given that DKO mice display a cardiac phenotype distinct from either single gene knock-out model, we sought to examine the impact of dual SLN/PLN ablation on oxidative skeletal muscle morphology, as it expresses both of these proteins endogenously. Furthermore, we wanted to characterize the impact of the loss of these SERCA regulatory proteins on Ca^{2+}-handling, SERCA efficiency, and whole-body metabolism. We hypothesized that DKO mice would display an improvement in muscular Ca^{2+}-handling resulting from the loss of SERCA inhibitors, along with an increase in SERCA Ca^{2+} pumping efficiency within oxidative skeletal muscle. We predicted that despite an increase in SERCA pumping efficiency of these mice, whole-body metabolic rate would not be altered. Lastly, as has been previously shown for both *Sln*$^{-/-}$ and *Pln*$^{-/-}$ models, we hypothesized that fibre-type characteristics of oxidative DKO skeletal muscle would be comparable to that of wild-type (WT) control animals.

Methods

Experimental Animals and Genotyping

Mice carrying the targeted PLN knock-out allele are those described in **Chapter 2** and **Chapter 3**, and those carrying the targeted SLN knock-out allele (strain: C57Bl/6J) have been previously described by our group (13, 49). Genotyping of the *Pln* WT and targeting alleles were done as described in **Chapter 2** and **Chapter 3**, and *Sln* WT and targeting alleles were done according to Tupling and colleagues (49) using appropriate forward and reverse primers (**Appendix A**: **Table A1**). Generation of DKO mice was achieved by crossing heterozygous mice of each colony (i.e. $Sln^{+/-}$ and $Pln^{+/-}$) according to the schema described in **Appendix C** (**Figure C1**). This strategy yielded homozygous founder WT (i.e. $Sln^{+/+}/Pln^{+/+}$) and DKO (i.e. $Sln^{-/-}/Pln^{-/-}$) mice, which were then used to establish separate WT and DKO lines. Animals were group housed at room temperature (~22°C) under a 12:12-hr reverse light/dark cycle, and given *ad libitum* access to standard rodent chow (8640 Teklad 22/5 Rodent Diet, Teklad Diets, Madison, WI) and water. All experiments were conducted using 3-6 month old male mice and were approved by the University of Waterloo Animal Care Committee and carried out in accordance with the Canadian Council on Animal Care.

Whole-Body Metabolic Rate and Glucose Tolerance

For one week prior to experimentation, all animals were singly housed in clear plastic cages with wire mesh bottoms, and provided powdered rodent chow and water *ad libitum* to mimic housing conditions of the metabolic chambers. Indirect calorimetry was

used to determine the effects of dual SLN/PLN ablation on whole-body metabolism using the Comprehensive Lab Animal Monitoring System (CLAMS; Oxymax Series, Columbus Instruments, Columbus, OH). Once a week for three consecutive weeks, WT (n = 43) and DKO (n = 44) mice (3-4 months old) were housed within the CLAMS over a 48-hr period (~22°C, 12:12-hr reverse light/dark cycle). Data collected from the first 24-hr were discarded to eliminate the effects of handling stress on metabolic variables. O_2 consumption rate (ml O_2 consumed/kg body mass/hr), respiratory exchange ratio (RER: VCO_2/VO_2) and metabolic heat production (kcal/hr/mouse) were monitored every 26-min over the following 24-hr period. Spontaneous cage activity was measured using infrared beam breaks (i.e. counts) in the x- and z-planes of the cage. Cage activity was expressed as total activity in both planes, and ambulatory activity, which was determined by the breaking of 2 successive beams in the x-plane. Metabolic rate was expressed as the average over the 24-hr collection period, and during states of activity (>2 ambulatory counts, dark phase: 0800 hr – 2000 hr) and inactivity (≤2 ambulatory counts, light phase: 2000 hr- 0800 hr) as done previously in **Chapter 2** and **Chapter 3**.

Glucose tolerance was measured using an intraperitoneal glucose tolerance test following an overnight fast (~16 hrs). Blood (~5-10 μL) was sampled from a tail vein and analyzed for glucose using a standard diabetic glucometer (Accu-Chek Aviva, Roche Diagnostics) at 0, 30, 60, and 120 min following an injection of 10% D-glucose (1g/kg body mass) (13, 16).

Tissue Collection

All chemicals were purchased from BioShop Canada Inc. (Burlington, ON, Canada) unless indicated otherwise. A separate group of experimental animals (5-6 month old) were euthanized by cervical dislocation and soleus (SOL) was excised, cleaned of connective and extraneous tissue, and placed in ice-cold phenylmethylsulfonyl fluoride (PMSF; Sigma-Aldrich, Oakville, ON, Canada) buffer (pH: 7.5). PMSF buffer contained in mM: 250 sucrose, 5 HEPES, 0.2 PMSF, and 0.2% (w/v) NaN_3 (Fisher Scientific, Fair Lawn, NJ). Due to tissue requirements for the various conditions of the Ca^{2+}-ATPase and Ca^{2+}-uptake assays (described below), left and right SOL muscles from 2-3 animals of each genotype were pooled together (n = 6/genotype), homogenized 1:10 (w/v) in ice-cold PMSF buffer using a glass-on-glass Dounce homogenizer, aliquots frozen in liquid nitrogen and stored at -80°C until needed.

Ca^{2+}-Dependent Ca^{2+}-ATPase Activity

Ca^{2+}-dependent Ca^{2+}-ATPase activity was measured in muscle homogenates using an NADH-linked spectrophotometric assay as previously described by our group (122) and outlined in **Appendix A** (**Figure A1**). ATPase buffer (pH: 7.0) contained in mM: 200 KCl, 20 HEPES, 10 NaN_3 (Fisher Scientific), 1 EGTA, 15 $MgCl_2$ (Sigma-Aldrich), 10 phosphoenolpyruvate (BioVectra, Charlottetown, PE, Canada), and 5 ATP (Sigma-Aldrich). Parallel reactions were run for each sample in the presence (1 μM) and absence of the Ca^{2+}-specific ionophore A23187 (Sigma-Aldrich, product #: C7522) within the reaction mixture. In the absence of the Ca^{2+} ionophore, vesicular Ca^{2+} accumulates and can induce back-inhibition of SERCA pumping (123), which more closely mimics the physiological condition of intact muscle. Following the addition (18

U/mL) of the auxiliary enzymes lactate dehydrogenase (Sigma-Aldrich, product #: L2625-25KU) and pyruvate kinase (Sigma-Aldrich, product #: 10 128 163 001), muscle homogenates were added to the reaction cocktail, which was then partitioned into 15 Eppendorf tubes containing various volumes of $CaCl_2$, giving $[Ca^{2+}]$ ranging from pCa (i.e. $-\log_{10}[Ca^{2+}]_f$) ~7.5-4.5. An additional tube (pCa 4.5) contained 0.12 mM of the highly specific SERCA inhibitor cyclopiazonic acid (CPA; Sigma-Aldrich, product #: C1530), which was used to determine background activity and subtracted from each reaction mixture. Duplicates (100 µl) from each reaction tube were added to a clear round-bottom 96-well plate and reactions were started by the addition of 0.3 mM NADH (Sigma-Aldrich, product #: 12166339), after which the decay rate of NADH absorbance at 340 nm was read for 30 min at 37°C.

To determine the exact $[Ca^{2+}]_f$ present in each reaction well, 1.2 µM of the Ca^{2+}-sensitive fluorescent dye Indo-1 (Biotium, Freemont, CA) was added to the reaction cocktail and partitioned into opaque Eppendorf tubes as above. Two additional tubes containing either zero $CaCl_2$ or 100 mM $CaCl_2$ were included as minimum and maximum measurements, respectively. Triplicates (100 µl) of each reaction tube were added to an opaque 96-well plate and incubated in the dark for 30 min at 37°C, and were read at an excitation wavelength of 355 nm using a fluorometric plate reader. Due to its peak absorbance wavelength and fluorescent properties, NADH was omitted from the reaction mixture. The emission maxima for the Ca^{2+}-free (G) and Ca^{2+}-bound (F) states of Indo-1 were measured at 485 nm and 405 nm, respectively, and the ratio (R) of F to G was used to calculate $[Ca^{2+}]_f$ according to the following equation (124):

$$\textbf{Equation 1}: [Ca^{2+}]_f = K_d \cdot (G_{max}/G_{min})\,(R - R_{min})/(R_{max} - R)$$

where K_d (250 nM) is the equilibrium constant for the interaction between Indo-1 and Ca^{2+} in homogenate (124), G_{max} is the maximum value of G (i.e. zero $CaCl_2$ well), G_{min} is the minimum value of G upon the addition of 100 mM $CaCl_2$ (i.e. max Ca^{2+} well), R_{min} is the minimum value of R (i.e. zero $CaCl_2$ well) and R_{max} is the maximum value of R upon the addition of 100 mM $CaCl_2$ (i.e. max Ca^{2+} well).

Activity curves were plotted as ATPase rate against the negative logarithm of $[Ca^{2+}]_f$ (i.e. pCa) using non-linear regression (GraphPad Prism software). The apparent Ca^{2+} affinity (i.e. pCa_{50}: pCa value at half-maximal ATPase activity) was calculated using the sigmoidal dose-response equation:

$$\textbf{Equation 2}: Y = Y_{bot} + (Y_{top} - Y_{bot})/(1 + 10^{(LogCa50 - x)\ X\ n_H})$$

where Y_{bot} is the value at the bottom of the plateau, Y_{top} is the value at the top of the plateau, $LogCa_{50}$ is the logarithm of pCa_{50} and n_H is the Hill coefficient.

Ca^{2+}-Dependent Ca^{2+}-Uptake Activity

Ca^{2+}-dependent Ca^{2+}-uptake was measured from pooled SOL homogenates in both the presence and absence of the precipitating anion oxalate. Similar to the absence of ionophore described above, the removal of oxalate from the assay medium more closely resembles the physiological condition of intact muscle as it allows vesicular Ca^{2+} to accumulate and induce back-inhibition of SERCA pumping (123). Ca^{2+}-uptake was measured using the Ca^{2+}-sensitive fluorescent dye Indo-1 (Biotium, Freemont, CA) and fluorometer equipped with dual-emission monochromators and Felix software (Photon Technology International, Birmingham, NJ) (65). When excited at 355 nm, the emission

maxima for the Ca^{2+}-free state of Indo-1 is 485 nm and that for the Ca^{2+}-bound state is 405 nm.

Ca^{2+}-uptake buffer (pH: 7.0) contained 100 mM KCl, 20 mM HEPES, 10 mM NaN_3 (Fisher Scientific), 5 μM TPEN (Sigma-Aldrich), 10 mM $MgCl_2$ (Sigma-Aldrich), and 5 mM oxalate (Sigma-Aldrich, or absent). Reactions (2 mL final volume) took place at 37°C in a 4-sided cuvette under constant stirring. Following the addition of buffer, homogenate (~40-80 μl), 1 μl $CaCl_2$ (10 mM), and Indo-1 (1.5 μM), SERCA-mediated Ca^{2+}-uptake was initiated by the addition of ATP (5 mM). Once the reaction had plateaued (i.e. vesicles filled), Ca^{2+} was allowed to leak from the vesicles following the addition of the SERCA-specific inhibitor CPA (0.02 mM), after which 145 μl of EGTA (5 mM) and 30 μl of $CaCl_2$ (100 mM) were added to achieve maximally free and Ca^{2+}-bound states of Indo-1, respectively. **Equation 1** was used to determine the change in $[Ca^{2+}]_f$ by time (i.e. Ca^{2+}-uptake rate), after which curves were smoothed over 21 points using a Savitsky-Goloay algorithm. Ca^{2+}-uptake rates were measured using linear regression ±100 nM at the following $[Ca^{2+}]_f$: 2000 nM (pCa 5.7), 1000 nM (pCa 6.0), 500 nM (pCa 6.3), and 250 nM (pCa 6.6). The apparent coupling ratio of SERCA was determined by dividing each Ca^{2+}-dependent uptake rate by the Ca^{2+}-dependent ATPase rate under each condition (i.e. presence or absence of Ca^{2+} gradient).

Western Blotting

Primary antibodies against ryanodine receptor (RyR; 34C, product #: MA3-925), dihydropyrodine receptor (DHPR) α-1 subunit (1A, product #: MA3-920), calsequestrin (CSQ; VIIID12, product #: MA3-913) and SERCA2a (2A7-A1, product #: MA3-919)

were purchased from ThermoScientific (Rockford, IL). The primary antibody against SERCA1a (A52) was a generous gift from Dr. David MacLennan (University of Toronto) (125). All appropriate secondary antibodies were purchased from Santa Cruz Biotechnology (Santa Cruz, CA). Samples were solubilized in 1X Laemmli buffer containing SDS, and separated on glycine gels by SDS-PAGE. All proteins were wet transferred on ice for 1 hour onto polyvinylidene difluoride (PVDF) membranes (0.2 μm pore size). Following transfer, membranes were blocked in TRIS-buffered saline (pH: 7.5) containing 0.1% Tween-20 (v/v) (TBST) and 5% (w/v) skim milk powder for 1 hour at room temperature. All primary, secondary, and detection conditions for each protein are outlined in **Appendix A** (**Table A2**). Densitometry analysis was done using GeneSnap software (Syngene; Frederick, MD), and protein load was confirmed using Ponceau S staining for normalization of densitometry values.

Protein content of muscle homogenates used for Ca^{2+}-ATPase/uptake assays and Western blotting was determined by the bicinchoninic acid assay (Sigma-Aldrich) using bovine serum albumin (Sigma-Aldrich) as a standard.

Immunofluorescent Staining of Muscle Fibre-Type

SOL muscles from 5-6 month old WT (n = 10) and DKO mice (n = 9) were excised, embedded in Tissue-Tek® O.C.T. Compound (VWR, Mississauga, ON, Canada), frozen in isopentane cooled in liquid nitrogen, and stored at -80°C until needed. Samples were then cut into 10 μm thick cross sections at -20°C using a cryostat (Thermo Electronic). Fibre-type analysis was based on immunofluorescent identification of MHC isoform as previously described (127). Primary antibodies against MHCI (BA-F8) and

MHCIIA (SC-71) were purchased from Developmental Studies Hybridoma Bank (University of Iowa). Secondary antibodies (Invitrogen, Carlsbad, CA) against MHCI and IIA were Alexa Fluor® conjugated 350 IgG_{2b} (blue) and 488 IgG_1 (green), respectively. Muscle cross sections were visualized with an Axio Observer Z1 microscope (Carl Ziess) equipped with standard filters (red, gree, blue), an AxioCam HRm camera, and Axio Vision software (Carl Ziess). Using this configuration, type I fibres appear blue, type IIA fibers appear green, and type IIX fibres appear black. Pure and hybrid fibre counts were quantified across an entire muscle cross-section, while fibre-specific cross-sectional area (CSA) was determined by averaging ~20 fibres of each type from various portions of a cross-section using ImageJ software.

Statistical Analysis

Whole-body glucose tolerance data were measured using a one-way ANOVA with repeated measures. CLAMS variables, immunohistochemical data, and Western blot data were measured with a 2-tailed Student's T-test (independent samples). Given that SLN and PLN are known to inhibit SERCA function, all SERCA enzyme and coupling variables were analyzed with a 1-tailed Student's T-test (independent samples). Statistical significance was considered at $P \leq 0.05$. All data presented are mean ± S.E.

Results

Whole-Body Metabolic Phenotype

Body mass (**Figure 4.1 A**) of 3-4 month old male DKO mice was not significantly different ($P = 0.12$) from WT control animals. Surprisingly, when energy expenditure was expressed as O_2 consumption rate relative to body mass (i.e. ml O_2/kg/hr) (**Figure 4.1 B/C**), DKO mice showed a significantly higher metabolic rate ($P < 0.05$) when measured over a 24-hr period. While there was a tendency ($P = 0.07$) for DKO mice to have a greater normalized metabolic rate during active states, no genotype difference was observed during states of inactivity ($P = 0.315$). When energy expenditure was expressed as absolute heat production (i.e. kcal/hr/mouse) (**Figure 4.1 D**), no differences were found between WT and DKO animals when measured over a 24-hr period ($P = 0.488$), during states of activity ($P = 0.419$), or during states of inactivity ($P = 0.371$). Interestingly, DKO animals were more active ($P < 0.001$), as seen by their greater total spontaneous cage activity (**Figure 4.1 E**) and ambulation (**Figure 4.1 F**). Lastly, RER (VCO_2/VO_2), an index of whole-body substrate selection, did not differ between WT and DKO mice during any measurement period (**Figure 4.1 G**).

Interestingly, DKO mice displayed fasting hyperglycemia as noted by their significantly ($P < 0.01$) higher blood glucose before receiving a glucose bolus (WT vs. DKO: 5.3 ± 0.1 mM vs. 5.8 ± 0.2 mM). The glucose tolerance test revealed a main effect of genotype ($P < 0.05$), with DKO mice having higher blood glucose concentration, irrespective of time point (**Figure 4.2 A**), and correspondingly these mice had a larger ($P < 0.05$) area under the glucose curve (**Figure 4.2 B**). However, when measurement of

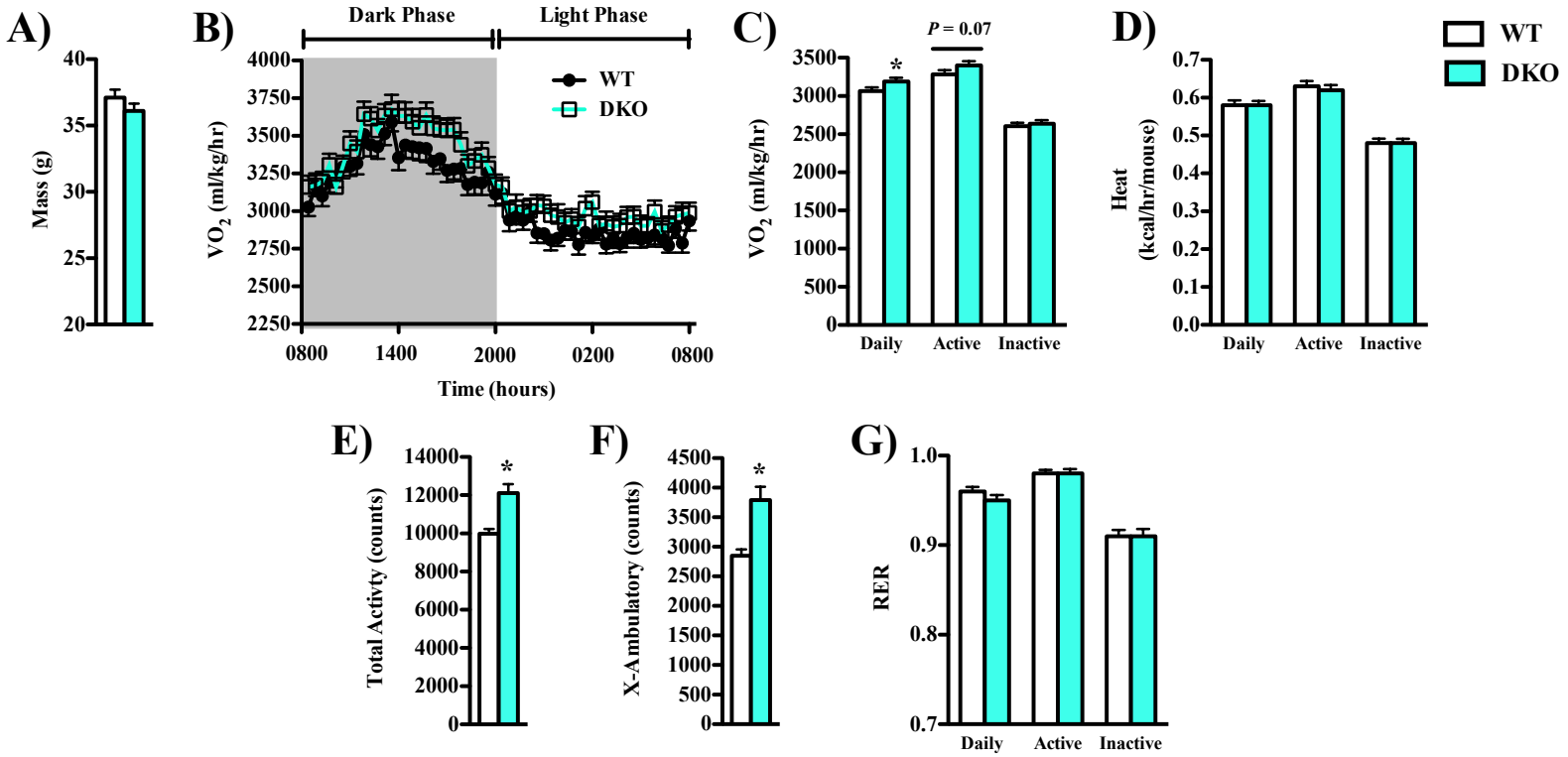

Figure 4.1. Whole-body metabolic parameters of 3-4 month old wild-type (WT; n = 43) and double knock-out (DKO; n = 44) mice. **A)** Animal body mass (g). **B)** Metabolic rate expressed as oxygen consumption rate (VO_2: ml O_2/kg body mass/hr) over as full 24 hour light/dark cycle. **C)** VO_2 averaged over 24 hours (daily), during states of cage activity (active: 0800 hrs - 2000 hrs (dark phase), >2 ambulatory activity counts) and inactivity (inactive: 2000 hrs - 0800 hrs (light phase), ≤2 ambulatory activity counts). **D)** Metabolic rate expressed as absolute heat production rate (kcal/hr/mouse). **E)** Total spontaneous cage activity (counts) over 24-hours. **F)** Ambulatory cage activity (counts) in the X plane over 24 hours. **G)** Respiratory exchange ratio (RER: VCO_2/VO_2). **G)** Respiratory exchange ratio (RER: VCO_2/VO_2). * Significantly different than WT ($P < 0.05$). Values are mean ± S.E.

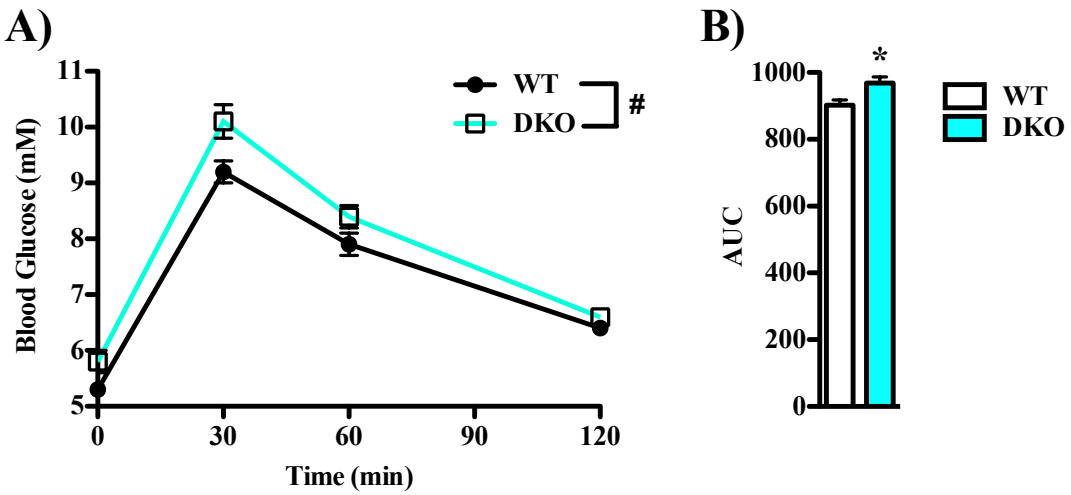

Figure 4.2. Whole-body glucose tolerance of 3-4 month old wild-type (WT; n = 39) and double knock-out (DKO; n = 38) mice. **A)** Blood glucose (mM) during and intraperitoneal glucose tolerance test. **B)** Glucose tolerance expressed as area under the curve (AUC). # Significant main effect ($P < 0.05$) of genotype (DKO > WT). *Significantly different than WT ($P < 0.05$). Values are mean ± S.E.

AUC was adjusted for their initial fasting blood glucose (**Appendix C**: **Figure C2**) **(**i.e. blood glucose at time point 0), AUC was similar between WT and DKO animals (P = 0.361), suggesting the response to the glucose bolus *per se* was unaffected by SLN/PLN ablation.

Fibre-Type Distribution and SERCA Isoform Expression of Oxidative Muscle

We have previously shown that transgenic manipulation of SERCA inhibitors can alter skeletal muscle fibre-type characteristics (65). Thus, it was of interest to determine whether dual ablation of SLN and PLN results in changes in SOL fibre-type distribution given that both are endogenously expressed within this muscle. Interestingly, DKO animals displayed a fast-to-slow fibre-type shift within the SOL (**Figure 4.3 A/B**). DKO mice had a greater number ($P < 0.05$) of type I fibers, while type IIA fibers were reduced ($P < 0.05$). No differences were found in the proportion of type IIX fibres between genotypes. Furthermore, DKO animals displayed fibre-type hypertrophy within the SOL (**Figure 4.3 C**). Cross- sectional area (CSA) of type I fibres was significantly greater ($P < 0.01$), as was that of type IIA fibres ($P < 0.01$). No difference in CSA existed for type IIX fibres between WT and DKO mice ($P = 0.344$).

Consistent with the fast-to-slow fibre-type shift in DKO SOL, SERCA isoform expression was correspondingly altered by dual SLN/PLN ablation (**Figure 4.4 A/B**). SERCA2a expression was significantly increased ($P < 0.01$) by ~1.6-fold in DKO mice, while SERCA1a was correspondingly reduced by ~23% ($P < 0.05$). No other changes in SR proteins were observed within the SOL of DKO animals.

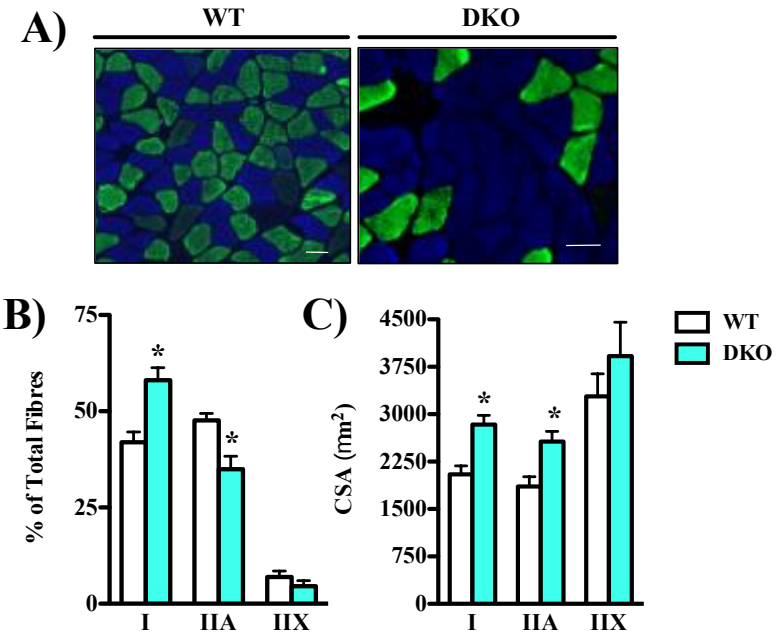

Figure 4.3. Dual ablation of SLN and PLN results in a fast-to-slow fibre-type shift and fibre-specific hypertrophy within oxidative muscle. **A)** Representative soleus (SOL) immunofluorescent cross-sectional images based on myosin heavy chain isoform staining (blue = type I, green = type IIA, black = type IIX). Scale bars are set to 50 μm. **B)** Fibre-type distribution pattern (% of total fibres) of WT (n = 10) and DKO (n = 9) SOL. **C)** Fibre-type specific cross sectional area (μm^2). * Significantly different that WT ($P < 0.05$). Values are mean ± S.E.

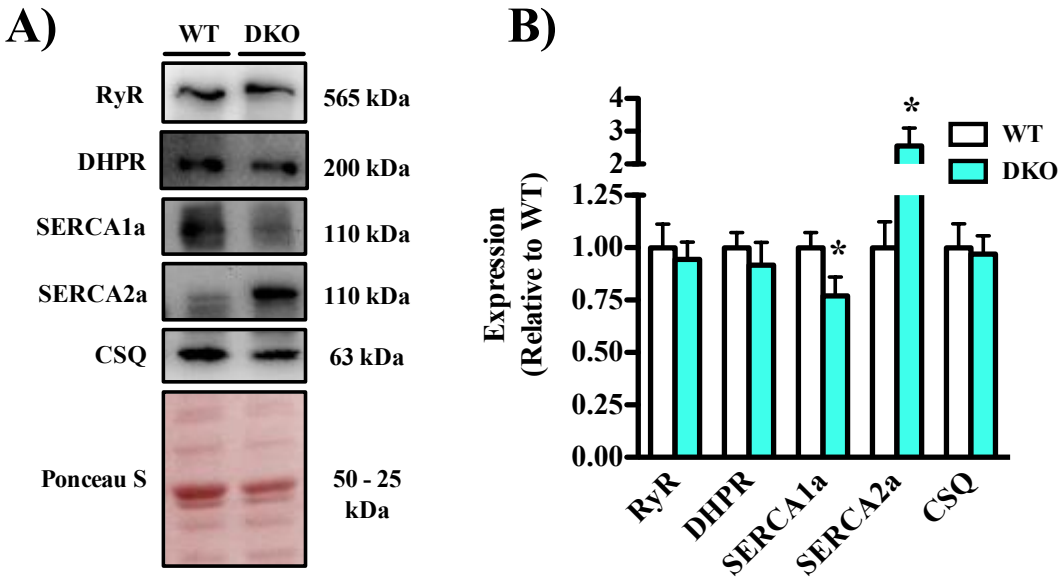

Figure 4.4. SERCA isoform expression is altered in the soleus of DKO mice. **A)** Representative Western blot of SR proteins. Equal protein load was confirmed using Ponceau S staining. **B)** SR protein expression (relative to WT) (n = 21/group). * Significantly different than WT ($P < 0.05$). Values are mean ± S.E.

SERCA Function and Ca^{2+}-Pumping Efficiency of Oxidative Muscle

SOL Ca^{2+}-dependent Ca^{2+}-ATPase activity was measured in both the absence (i.e. with Ca^{2+} ionophore) and presence (i.e. no Ca^{2+} ionophore) of a vesicular Ca^{2+} gradient (**Figure 4.5**). Surprisingly, maximal Ca^{2+}-dependent Ca^{2+}-ATPase activity (V_{Max}) in the presence of a Ca^{2+} ionophore tended ($P = 0.06$) to be lower in DKO animals (**Figure 4.5 A/B**), while in the absence of a Ca^{2+} ionophore, V_{Max} was significantly reduced ($P < 0.05$) (**Figure 4.5 C/D**). Furthermore, pCa_{50} (i.e. Ca^{2+} affinity: pCa at half V_{Max}) was not impacted by dual SLN/PLN ablation in either the presence ($P = 0.267$) or absence ($P = 0.198$) of a Ca^{2+} ionophore (**Table 4.1**).

In addition to SERCA's ATPase function, Ca^{2+}-dependent Ca^{2+}-uptake and SR Ca^{2+} leak rate within SOL muscles were measured using a fluorometric assay system in the presence (i.e. oxalate-supported) and absence (i.e. no oxalate) of a vesicular SR Ca^{2+} gradient to mimic the ATPase assay conditions (**Figure 4.6**). Consistent with the findings above, oxalate-supported Ca^{2+}-uptake rate at a pCa of 5.7 (i.e. $[Ca^{2+}]_f$ of 2000 nM) tended ($P = 0.06$) to be lower in DKO mice, whereas no differences were found at a pCa of 6.0 (i.e. $[Ca^{2+}]_f$ of 1000 nM) ($P = 0.113$), 6.3 (i.e. $[Ca^{2+}]_f$ of 500 nM) ($P = 0.168$), or 6.6 (i.e. $[Ca^{2+}]_f$ of 250 nM) ($P = 0.140$) (**Figure 4.6 A**). SR Ca^{2+} leak rate following vesicle loading and subsequent addition of CPA was not different ($P = 0.457$) between WT and DKO mice in the presence of oxalate (**Figure 4.6 B**). When oxalate was removed from the assay buffer (**Figure 4.6 C**), no difference in Ca^{2+}-uptake rate was seen between WT and DKO mice at a pCa of 5.7 ($P = 0.275$), 6.0 ($P = 0.230$), or 6.3 ($P = 0.128$). However, at a pCa of 6.6, the Ca^{2+}-uptake rate was significantly slower ($P < 0.05$) in DKO SOL (**Figure 4.6 C**). As above, dual SLN/PLN ablation did not impact (*P*

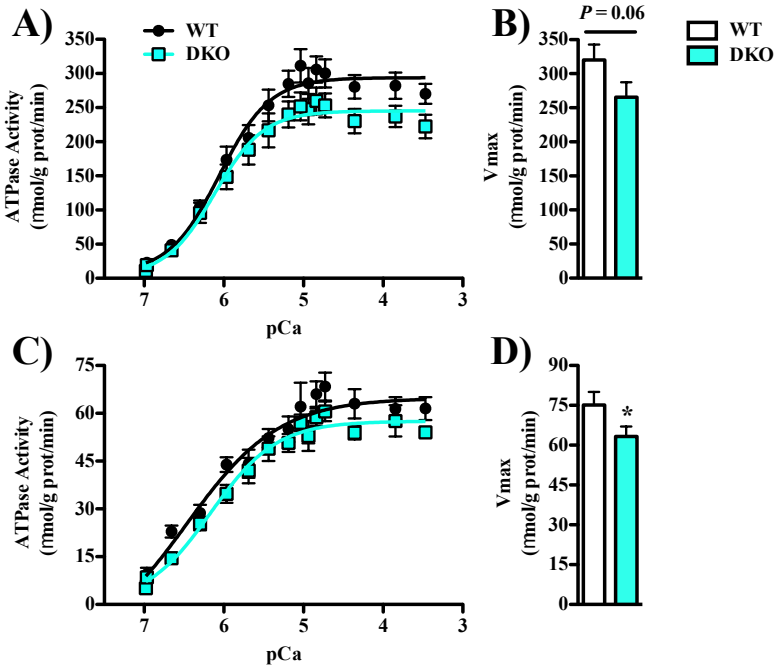

Figure 4.5. Ca^{2+}-dependent Ca^{2+}-ATPase activity (µmol/g protein/min) within soleus homogenates of wild-type (WT) and DKO mice (n = 6/group). **A)** ATPase activity curves measured in the presence of the Ca^{2+}-specific ionophore A23187 (i.e. leaky vesicles). **B)** Maximal ATPase activity (V_{Max}) of leaky vesicles. **C)** ATPase activity curves measured in the absence of the Ca^{2+}-specific ionophore A23187 (i.e. intact vesicles). **D)** V_{Max} of intact vesicles. *Significantly different (P <0.05) from WT. Values are mean ± S.E.

Table 4.1. SERCA Ca^{2+} affinity (pCa_{50}: pCa at half maximal Ca^{2+}-dependent Ca^{2+}-ATPase activity) within the soleus of wild type (WT) and double knock-out (DKO) mice (n = 6/group). ATPase activity was measured in the presence (i.e. leaky vesicles) and absence (i.e. intact vesicles) of the Ca^{2+}-specific ionophore A23187. Values are mean ± S.E.

	pCa_{50}	
Condition	**WT**	**DKO**
Leaky	6.03 ± 0.05	6.09 ± 0.06
Intact	6.28 ± 0.11	6.16 ± 0.09

= 0.543) SR Ca^{2+} leak rate following vesicle loading and subsequent inhibition of SERCA with CPA in the absence of oxalate (**Figure 4.6 D**).

To determine SERCA's Ca^{2+} pumping efficiency in the SOL (i.e. apparent coupling ratio: Ca^{2+} pumped/ATP hydrolyzed), Ca^{2+}-uptake rates were divided by ATPase rates at a pCa of 5.7, 6.0, 6.3, and 6.6. Apparent coupling ratios were determined in the absence of vesicular Ca^{2+} filling (i.e. Ca^{2+}-uptake with oxalate/ATPase with ionophore) (**Figure 4.7 A**), and in the presence of vesicular Ca^{2+} filling (i.e. Ca^{2+}-uptake without oxalate/ATPase without ionophore) (**Figure 4.7 B**). In the absence of vesicular Ca^{2+} filling, apparent coupling ratios were similar between WT and DKO animals at all measured pCa values (**Figure 4.7 A**). When Ca^{2+} was allowed to accumulate in the vesicle lumen, coupling ratios were again similar between WT and DKO mice between pCa 5.7 – 6.3 (**Figure 4.7 B**). However, at pCa 6.6 the apparent coupling ratio tended (*P* = 0.08) to be higher in DKO mice, suggesting a greater energetic efficiency at which SERCA pumps Ca^{2+}.

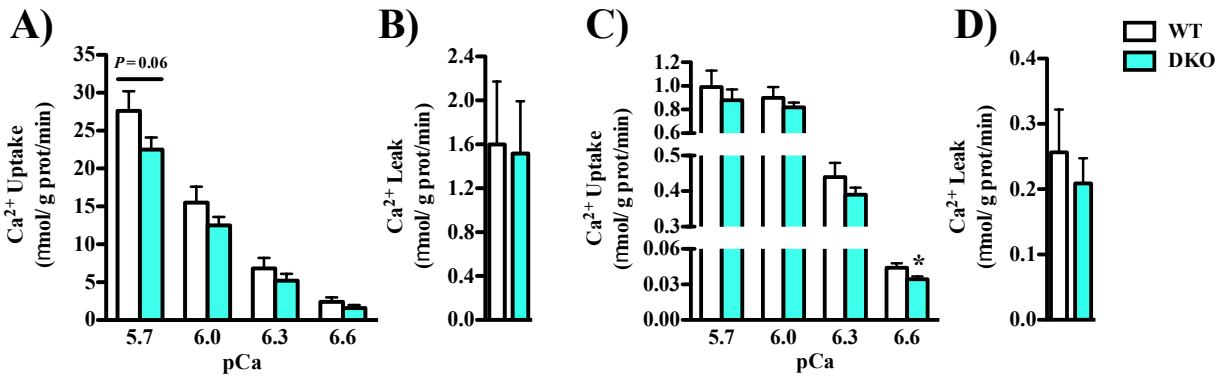

Figure 4.6. Ca^{2+}-dependent Ca^{2+}-uptake and leak rates (µmol/g protein/min) within soleus of wild-type (WT) and double knock-out (DKO) mice (n = 6/group). **A)** Oxalate-supported Ca^{2+}-uptake rates at various pCa values (i.e. $-\log[Ca^{2+}_f]$). **B)** Ca^{2+} leak rate of oxalate-supported vesicles following filling and the subsequent addition of the SERCA-specific inhibitor CPA. **C)** Ca^{2+}-uptake rates in the absence of the precipitating anion oxalate. **D)** Ca^{2+} leak in the absence of oxalate following the addition of CPA. * Significantly different than WT ($P < 0.05$). Values are mean ± S.E.

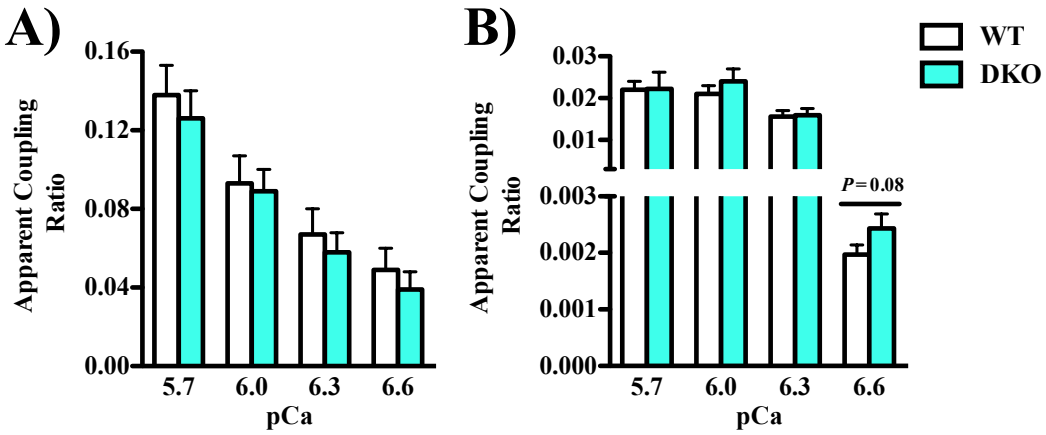

Figure 4.7. SERCA Ca^{2+}-pumping efficiency (i.e. coupling ratio: Ca^{2+}-uptake rate/ Ca^{2+}-ATPase rate) within soleus of wild-type (WT) and double knock-out (DKO) mice (n = 6/group). Coupling ratios were measured across of range of pCa values (i.e. $-\log[Ca^{2+}_f]$). **A)** SERCA efficiency measured in the presence of a vesicular Ca^{2+} gradient (i.e. presence of oxalate during Ca^{2+}-uptake and the Ca^{2+} ionophore A23187 during Ca^{2+}-ATPase measurements). **B)** SERCA efficiency measured in the absence of a vesicular Ca^{2+} gradient (i.e. absence of oxalate during Ca^{2+}-uptake and ionophore during Ca^{2+}-ATPase measurements). Values are mean ± S.E.

Discussion

Cellular Ca^{2+} is not only critical for muscular excitation-contraction coupling, but also serves as an integral second messenger in signaling processes controlling the contractile and metabolic phenotype of skeletal muscle (129, 149). SERCA is the main regulator of cytosolic and SR [Ca^{2+}] of muscle both at rest and during exercise, and as such comprises a large proportion of skeletal muscle energy expenditure (18, 42). SLN and PLN are two critical regulators of SERCA function (43), and while single gene knock-out studies show that endogenous levels of either protein do not drastically alter the morphology or phenotype of muscular tissues (49, 131), their combined expression can (108). Furthermore, heterologous expression studies using HEK-293 cells have demonstrated that a super-inhibitory ternary SLN/PLN/SERCA complex can form to regulate Ca^{2+}-handling (53, 76). Given that both proteins are endogenously expressed within oxidative skeletal muscle to regulate SERCA function (28, 65), it was of interest to determine their combined impact on Ca^{2+}-handling and muscle morphology.

Interestingly, we found that DKO mice had a higher 24-hr energy expenditure; however, this could be explained, in part, by the higher spontaneous cage activity of these animals. We also found that dual SLN/PLN ablation resulted in a fast-to-slow fibre type shift within the SOL and hypertrophy of both type I and IIA fibres, a muscular phenotype that is consistent with the activation of Ca^{2+}-dependent signaling pathways (129, 149). Despite the loss of two well-described inhibitors of the Ca^{2+}-pump, SERCA function was paradoxically reduced in DKO SOL homogenates, although this was likely due to a reduction in total SERCA density resulting from the fibre-type shift. While SERCA's pumping efficiency within the SOL of DKO mice tended to be higher, consistent with the

loss of SLN in these animals, the combined impact of dual SLN/PLN ablation on whole-body metabolism and skeletal muscle fibre-type characteristics differed from that previously shown for *Sln*$^{-/-}$ and *Pln*$^{-/-}$ models (14, 49). Thus, unlike ablation of either regulator alone, the combined regulation of SERCAs by SLN and PLN is required for the maintenance of skeletal fibre-type characteristics, muscle morphology, and Ca^{2+}-handling.

Whole-Body Metabolic Phenotype of DKO Mice

As described previously (108), gross appearance of DKO animals was similar to that of WT controls and body mass was not affected by dual SLN/PLN ablation. Given that whole-body metabolic rate is unaltered in both *Sln*$^{-/-}$ and *Pln*$^{-/-}$ mice housed at room temperature (14), it was surprising then that energy expenditure was higher in DKO mice. However, whole-body metabolic rate was only elevated when measured over a full 24-hr light/dark cycle, and tended to be higher only during active periods. These findings are consistent with the increased spontaneous cage activity of DKO mice and suggest that increased activity thermogenesis is a contributing factor to their observed greater energy expenditure when averaged over 24-hrs. A major question that is currently unclear from this study is how does loss of these SERCA regulators result in increased physical activity, especially when deletion of either SLN or PLN in isolation does not. Despite this, both body mass normalized metabolic rate and absolute heat production rate did not differ between WT and DKO animals during inactive periods, indicating that SLN/PLN ablation *per se* does not alter metabolic rate in mice held at room temperature. That energy expenditure is not altered when DKO animals are inactive is consistent with

previous findings that, despite only SLN being capable of uncoupling SERCA function (14, 55), whole-body energy expenditure is unchanged in *Sln*$^{-/-}$ animals when held at either room temperature or thermoneutrality (14, 62, 87). Thus, lack of SLN, even in DKO mice, does not result in an overt reduction in whole-body energy expenditure under control conditions and suggests other inefficient processes compensate for the absence of SLN-induced uncoupling in order to maintain metabolic rate.

An interesting finding from this study was that DKO animals displayed fasting hyperglycemia following an overnight fast. While unclear from the results herein, hepatic glucose output may need to increase following fasting in order to regulate blood glucose levels in light of spontaneous cage activity being greater in DKO mice. Although DKO mice had higher blood glucose in response to an intraperitoneal injection of glucose, this appears to be a function of fasting glucose levels being greater in these mice, and not evidence of whole-body glucose intolerance as AUC was similar between WT and DKO animals when adjusted for fasting glycaemia.

Fibre-Type Characteristics and SR Protein Expression of DKO Skeletal Muscle

One of the most striking findings of this study was the fibre-type shift within the SOL of DKO mice and subsequent impact on SERCA function. We have previously shown that, despite the presence of endogenous SLN and PLN protein expression within the SOL, neither *Sln*$^{-/-}$ or *Pln*$^{-/-}$ mice present with any alteration in morphology or fibre-type within this muscle (49). Interestingly, DKO mice show a fast-to-slow fibre type shift, as evidenced by the increase in percentage of type I fibres and concomitant decline in the percentage of type IIA fibres within the SOL; deletion of SLN and PLN also

resulted in hypertrophy of both type I and IIA fibres. While SERCA isoform expression was altered in DKO homogenate, this is likely reflective of the fibre-type shift of these animals, as SERCA2a is the main isoform in type I fibres and SERCA1a in IIA fibres. Similar to other SLN and PLN mouse models, DHPR, RyR, and CSQ protein content were unaltered in DKO SOL (12, 49, 139).

Our group has recently described a novel myopathy in Pln^{OE} mice, in which the SOL displays a pronounced increase in the percentage of type I fibres and subsequent reduction of IIA fibres (65). However, unlike DKO SOL described herein, type I fibres of Pln^{OE} mice are atrophied while compensatory hypertrophy occurs in the IIA fibres (65). The fibre-type transition observed in Pln^{OE} SOL is believed to be due to a rise of cytosolic [Ca^{2+}] and subsequent activation of Ca^{2+}-dependent signaling pathways resulting from chronic SERCA inhibition. Specifically, CaN signaling, which along with CaMKs is a major inducer of MHC I (129, 149, 151), is increased within the SOL of Pln^{OE} mice (139). While CaN promotes muscular hypertrophy (149), the activity of proteolytic enzymes including Ca^{2+}-dependent calpains, are elevated in Pln^{OE} SOL (65), which is likely to explain the atrophy of type I fibres wherein PLN overexpression occurs. DKO mice described herein provide a unique contrast to the Pln^{OE} model in that while both show a fast-to-slow fibre transition, type I and IIA fibres are hypertrophied in DKO SOL only. Although speculative, this muscular phenotype is consistent with the activation of Ca^{2+}-dependent signaling pathways. What is striking is how ablation of two SERCA inhibitory proteins could result in the activation of such pathways controlling fibre-type and size, although several possibilities may exit.

Firstly, although Ca^{2+}-affinity and V_{Max} were not improved when measured *in vitro*, we have shown relaxation rates to be faster in DKO SOL (152), suggesting enhanced SERCA function *in vivo*, possibly leading to increased SR Ca^{2+} load within oxidative muscle. In support of this, caffeine-induced Ca^{2+} release is greater in both atrial and ventricular myocytes of DKO mice (108), indicating that SR Ca^{2+} content is greater. When luminal [Ca^{2+}] is high, SR Ca^{2+} stores can leak back into the cytosol through a number of proteins including the RyR and even SERCAs themselves (153-155). Indeed, spontaneous SR Ca^{2+} release or leak events are increased in frequency and or/amplitude in response to deletion of either PLN (105-107, 109-113) or SLN (103). Furthermore, RyR hyperphosphorylation of residues associated with Ca^{2+}-leak (including those phosphorylated by CaMKII) are greater in atrial myocytes of $Sln^{-/-}$ mice as a result of SR Ca^{2+} overload (103). While no muscular phenotype is present in either $Sln^{-/-}$ or $Pln^{-/-}$ skeletal muscle, it is likely that SR Ca^{2+} load, and therefore the gradient driving SR Ca^{2+} leak, is greatest in DKO animals compared to either single gene knock-out. Although Ca^{2+} leak rate following the addition of CPA was unchanged in SOL homogenates of DKO mice relative to WT controls, the luminal Ca^{2+} content achieved using this assay is likely not reflective of that *in vivo*. Secondly, activation of cytosolic Ca^{2+} signaling proteins could occur if Ca^{2+}-pumping rate was paradoxically reduced in response to the loss of both SLN and PLN. Most surprisingly, this appears to be the case in DKO SOL (described below).

Ca^{2+}-Handling within Oxidative Skeletal Muscle

Surprisingly, SERCA activity was lower in SOL homogenate of DKO mice. Furthermore, loss of both SERCA inhibitory proteins did not increase the pCa50 within the SOL, which would be expected given that both proteins have been shown to individually reduce SERCA's Ca^{2+} affinity (76). However, in light of the fast-to-slow fibre-type shift in SOL, these findings might not be completely unexpected. Consistent with the increased number of type I fibres, SERCA2a protein expression was higher in DKO SOL, whereas SERCA1a was reduced along with the number of IIA fibres. While no intrinsic difference in the rate of Ca^{2+}-pumping exists between SERCA isoforms (30), the density of SERCA pumps is greater in fast-twitch fibres (27). Using quantitative western blotting with purified SERCA1a and 2a protein standards, Smith and colleagues (42) found the ratio of SERCA1a:SERCA2a in mouse SOL to be ~14:1; thus, ~90% of the total number of SERCA pumps in SOL is comprised of SERCA1a. Although the absolute number of SERCA1a pumps per fast-twitch fibre is not known, it is reasonable to expect that the ~13% reduction in IIA fibres within DKO SOL lowered the total number of SERCA pumps, and subsequently is reflected as a reduction in SERCA catalytic activity at higher $[Ca^{2+}]_f$. Consequently, this may mask an improvement in Ca^{2+} affinity when measuring ATPase activity given that pCa50 is dependent on V_{Max}. If SERCA function were normalized to the total SERCA content, the expected improvement in Ca^{2+} affinity within DKO SOL may be found. The scenario in oxidative skeletal muscle described herein differs considerably from that previously reported in DKO hearts whereby the V_{Max} of Ca^{2+}-uptake and Ca^{2+} affinity are drastically improved (108). Furthermore, SERCA2a is the main isoform in cardiac muscle, and its expression,

along with other Ca^{2+}-handling proteins, are not altered in DKO hearts (108). Thus, the impact of dual SLN/PLN ablation on SERCA function appears to be tissue dependent.

When Ca^{2+}-precipitating anions like oxalate or other agents that allow leak of luminal Ca^{2+} are not present when measuring SERCA function, luminal Ca^{2+} accumulation can induce "back-inhibition" of the pump, slowing SERCA catalytic activity, and even promote alternative reactions that reduce coupling (described in **Chapter 1**) (123). Not surprisingly then, SERCA ATPase and Ca^{2+}-uptake activities proceeded much slower when Ca^{2+} ions were allowed to accumulate within SR vesicles (i.e. absence of ionophore or oxalate), as has previously been observed by our group (14, 49) and others (123). Similar to that observed in the presence of Ca^{2+} ionophore, maximal Ca^{2+}-dependent Ca^{2+}-ATPase activity was also lower in DKO SOL when ionophore was removed from the reaction medium. As described above, this is likely reflective of the fast-to-slow fibre shift and accompanying reduction of total SERCA density within the homogenate of DKO SOL. Again, as pCa50 under this condition is dependent on V_{Max}, we did not observe the expected leftward shift in the ATPase activity curves of DKO mice that is indicative of enhanced SERCA Ca^{2+}-affinity with SLN/PLN ablation. In fact, we have previously shown ATPase activity curves to be rightward shifted within the SOL of *Sln*$^{-/-}$ mice (i.e. decreased SERCA Ca^{2+}-affinity) when Ca^{2+} ionophore is removed from the assay medium, which was attributed to greater back-inhibition of SERCA activity in these animals (123). Together, our current and previous findings highlight the complexities of SERCA's kinetic properties using intact SR preparations.

SERCA's energetic efficiency within skeletal muscle is reduced (i.e. uncoupled) by its physical interaction with SLN, but not PLN (14, 55); thus, when SLN is bound to SERCA, more ATP is required to pump a given amount of Ca^{2+} into the SR lumen. In our previous study with *Sln*$^{-/-}$ mice, SLN-mediated uncoupling within oxidative skeletal muscle was only observed to occur when SR vesicles from muscle homogenates were allowed to accumulate Ca^{2+} (14). Furthermore, the impact of SLN on SERCA pumping efficiency was Ca^{2+}-dependent, as SERCA was more uncoupled in WT compared to *Sln*$^{-/-}$ SOL at low free [Ca^{2+}] (i.e. pCa 6.9) (14). In agreement with our previous findings, the apparent coupling ratio (i.e. Ca^{2+}-uptake rate/ATPase rate) of DKO mice tended to be higher (i.e. more coupled) only at pCa 6.6 under conditions where Ca^{2+} was allowed to accumulate within the vesicle lumen, consistent with the deletion of SLN in DKO mice; like that of *Sln*$^{-/-}$ animals, this suggests that DKO mice too require less energy to translocate Ca^{2+} within skeletal muscle. Unfortunately, we were unable to achieve reliable Ca^{2+}-uptake rates at pCa values greater than 6.6 in the absence of oxalate, although it is reasonable to predict that SERCA would be even more coupled in DKO SOL as $[Ca^{2+}]_f$ declines further. Our findings here and previously (14) indicate that the uncoupling mechanism by SLN is dependent on the accumulation of luminal Ca^{2+} and subsequent back-inhibition of the pump. Consistent with this, Reis and colleagues (156) have found that the amount of heat released from rabbit skeletal muscle SR vesicles during Ca^{2+} pumping is increased only if vesicles are filled with Ca^{2+}. In light of Ca^{2+} pumping being more efficient in DKO skeletal muscle, one might predict that these mice are susceptible to an obesogenic phenotype similar to that of *Sln*$^{-/-}$ mice due to an

inability to recruit SLN-mediated uncoupling of SERCA; however, it is unclear whether this will occur given that they are also more spontaneously active.

Conclusion

DKO mice displayed a unique whole-body and skeletal muscle phenotype that is distinct from either *Sln*$^{-/-}$ and *Pln*$^{-/-}$ mice. While energy expenditure of DKO mice measured over 24 hours was greater than WT control mice, this could be explained, in part, by their greater spontaneous activity. Interestingly, deletion of SLN and PLN resulted in a fast-to-slow fibre-type shift and fibre hypertrophy within oxidative muscle. While mechanistically unclear how this occurs in DKO muscle, this phenotype is consistent with activation of cytosolic Ca^{2+}-dependent signaling pathways. Although mechanistically unclear how this occurs, it may involve SR Ca^{2+} leak, as SR Ca^{2+} content *in vivo* and the corresponding gradient driving Ca^{2+} efflux is expected to be greater in DKO muscle. Paradoxically, SERCA function appeared reduced in DKO skeletal muscle homogenate, although this may simply reflect a lower SERCA protein density that would accompany the fast-to-slow fibre-type shift in these mice. As hypothesized, SERCA pumping efficiency tended to be greater in DKO SOL, which is consistent with the loss of SLN specifically. Thus, both SLN and PLN, through their additive effect on SERCA and/or a super-inhibitory ternary complex, are critical for the regulation of skeletal muscle Ca^{2+}-handling, muscle fibre-type and size, and whole-body metabolism.

CHAPTER 5

Examination of Diet-Induced Obesity in Mice Lacking Both SLN and PLN

Introduction

Obesity results from a chronic energy imbalance whereby energy intake exceeds that of expenditure. The resulting accumulation of body fat can result in numerous metabolic defects including hypertension, cardiovascular disease, various cancers, and type II diabetes (2). Adaptive thermogenesis refers to the modulation of caloric expenditure in response to physiological stressors including ambient temperature and diet (4), and is believed to be involved in the regulation of body mass and pathogenesis of obesity. Dissipation of the mitochondrial proton gradient within brown adipose tissue (BAT), mediated by uncoupling protein-1 (UCP-1), is the most well-characterized mechanism of adaptive thermogenesis in rodents (3). However, skeletal muscle is now recognized as a critical contributor to adaptive thermogenesis through the action of the sarco(endo)plasmic reticulum (SR) Ca^{2+}-ATPase (SERCA) (15).

SERCAs are 110 kDa integral membrane proteins of the SR responsible for the ATP-dependent pumping of Ca^{2+} ions from the cytosol into the SR lumen (23). SERCAs contribute upwards of 48% of basal energy consumption in resting non-contracting rodent skeletal muscle (42), indicating a continual need to sequester Ca^{2+} even in idle skeletal muscles, which is not surprising given the $>10^4$ Ca^{2+} gradient across the SR favoring continual ion efflux (31, 32). Numerous sites within the SR exist whereby luminal Ca^{2+} can leak from (154), including SERCAs themselves (155). Sarcolipin (SLN) and phospholamban (PLN) are two protein regulators of SERCA function that physically interact with the pump to reduce its Ca^{2+} affinity and/or maximal pumping rate, slowing the rate of Ca^{2+}-uptake, and subsequently reducing muscular contractility (48, 49, 65, 71, 76, 77). Both regulatory proteins can reduce the peak amount of Ca^{2+}

released during muscle activation (44, 47, 59, 74, 78, 104, 108), which is believed to be the result of reduced SR Ca^{2+} content with SERCA inhibition.

SLN in particular has gained considerable attention for its role in muscle-based adaptive thermogenesis as it reduces the energetic efficiency of SERCA by uncoupling Ca^{2+} transport from ATP consumption (14, 37, 38, 54, 55). Not surprisingly then, mice lacking SLN (*Sln*$^{-/-}$) are susceptible to obesity when fed a high-fat diet (HFD) (13, 16, 17), and become hypothermic when acutely cold-challenged (12, 54). Despite PLN's structural resemblance to SLN and similar impact on Ca^{2+} pumping rate, PLN does not uncouple SERCA (55). As expected, *Pln*$^{-/-}$ mice do not develop excessive diet-induced obesity when fed a "Westernized" diet (**Chapter 3**) or hypothermia during cold-challenge (54), together indicating that unlike SLN, PLN is not involved in skeletal muscle-based adaptive thermogenesis. Thus, while these SERCA regulators have historically believed to be homologous in function, they appear to have distinct roles in muscle physiology.

Traditionally, regulation of SERCAs by SLN and PLN was thought to be mutually exclusive based on their chamber-specific expression pattern within the heart (58). However, co-expression of SLN and PLN has been reported within SR-enriched microsomes from both the atria and ventricle of mice (44). We have also found both SLN and PLN protein to be expressed endogenously within mouse oxidative muscle such as the soleus (SOL) (65, 139), although their fibre-type specific distribution in mice is yet unclear from these studies. Furthermore, despite the heterogeneous nature of skeletal muscle, we have even demonstrated co-expression of SLN and PLN within human single skeletal muscle fibres isolated from the vastus lateralis (126). Co-expression studies

using HEK-293 cells have shown that SLN and PLN can bind to one another, forming a super-inhibitory ternary complex with SERCA to reduce Ca^{2+}-uptake to a greater extent than either inhibitory protein alone (53, 76). Given that both SERCA regulators are found within the same muscle and/or muscle fibre *in vivo*, potential exists for muscular Ca^{2+}-handling to be regulated by SLN and PLN both in an additive manner and as a super-inhibitory complex.

Although ablation of either protein in mouse skeletal muscle improves SERCA function and muscular contractility without affect on muscle morphology or fibre-type (48, 49), loss of both SLN and PLN results in a more complex and tissue-specific phenotype (108). While SERCA function is markedly improved within the hearts of mice double knock-out (DKO) that lack both SLN and PLN, these animals present with left-ventricular hypertrophy and are subsequently susceptible to pressure overload in response to aortic banding (108). Furthermore, DKO SOL shows a fast-to-slow fibre-type shift, and like that of the LV myocytes (108), displays hypertrophy of type I and IIA fibres (**Chapter 4**). Although SERCA function in DKO SOL is paradoxically reduced when measured *in vitro* using crude muscle homogenates (**Chapter 4**), *ex vivo* relaxation rates and tetanic force are improved, as would be expected with the loss of SERCA inhibitors (152); this suggests that SERCA activity *in vitro* is a function a lower pump density resulting from the fibre-type shift in DKO mice, not a reduction in its activation state *in vivo*. Therefore, it is possible that SR Ca^{2+} load is greater within DKO skeletal muscle, similar to that found within the hearts of these animals (108). Together, these studies indicate that the combined action of SLN and PLN on SERCA, possibly even the

ternary super-inhibitory complex, are required for the maintenance of muscle fibre-type and size, and for the response to physiological stress.

Consistent with the loss of SLN specifically, SERCA pumping efficiency tends to be greater within oxidative skeletal muscle of DKO animals (**Chapter 4**). As such, it is reasonable to hypothesize that, like *Sln*$^{-/-}$ mice, DKO animals would be susceptible to an obesogenic phenotype due to an inability to recruit SLN-mediated uncoupling of SERCA; however, DKO mice are also more spontaneously active (**Chapter 4**). Furthermore, an increase in SR Ca^{2+} load, which is to be expected in DKO skeletal muscle *in vivo*, can affect Ca^{2+} pumping efficiency by promoting alternate reactions of SERCA's catalytic cycle (see **Chapter 1**: **Figure 1.3**); thus, it remains unclear how deletion of both SLN and PLN affects energy balance when there is a need to recruit muscle-based diet-induced thermogenesis. We hypothesized that, despite potential changes in skeletal muscle SR Ca^{2+} content and physical activity, DKO mice would develop excessive diet-induced obesity when compared to WT control animals due to the absence of SLN-mediated uncoupling of SERCA.

Methods

Experimental Animals and Genotyping

Experimental animals were group housed at room temperature (~22°C) under a 12:12-hr reverse light/dark cycle, and given *ad libitum* access to standard rodent chow (8640 Teklad 22/5 Rodent Diet, Teklad Diets, Madison, WI) and water. Animal genotyping was done as previously described in Chapters 2-4 using appropriate forward and reverse primers (**Appendix A**: **Table A1**). All experiments were conducted using 3-4 month old male WT (i.e. $Sln^{+/+}/Pln^{+/+}$) and DKO (i.e. $Sln^{-/-}/Pln^{-/-}$) mice. Following genotype identification, mice were individually housed under same environmental and feeding conditions described above. All studies were approved by the University of Waterloo Animal Care Committee and carried out in accordance with the Canadian Council on Animal Care.

Experimental Diets and Diet-Induced Obesity

Individually housed mice were given *ad libitum* access to water and either standard rodent chow (as above) or a "Westernized" high-fat diet (HFD) containing 42% kcal from fat, 42.7% kcal from carbohydrate, and 15.2% kcal from protein (TD 88137; Harlan Teklad, Madison, WI) for 8 weeks to induce obesity. Sample sizes for each group were as follows: WT chow: 21, DKO chow: 21, WT HFD: 22, and DKO HFD: 22. Body mass and food consumption were monitored weekly throughout the 8-week period. Food consumption was determined by weighing food pellets on top of the cage hopper and subtracting the difference remaining, along with any that had fallen into the cage bedding after each week. Whole-body metabolic efficiency, an indirect measurement of energy

expenditure (6, 87), was calculated by dividing the total mass gained over 8 weeks for each animal by their total food consumption (g mass gained/ MJ food consumed). To calculate this, food consumption (g) was converted to MJ using the caloric density (kcal/g) of each diet provided by the manufacturer and the conversion 1 kcal = 0.00418 MJ.

Whole-body Energy Expenditure and Glucose Tolerance

Before initiation of the dietary treatments, all animals were acclimated for one week to clear plastic cages with wire mesh bottoms, and provided powdered rodent chow and water *ad libitum* as described in Chapter 2. Prior to and following the experimental diets, animals were placed in the Comprehensive Lab Animal Monitoring System (CLAMS; Oxymax Series, Columbus Instruments, Columbus, OH) to measure O_2 consumption rate (ml O_2 consumed/kg body mass/hr), respiratory exchange ratio (RER: VCO_2/VO_2), metabolic heat production (kcal/hr/mouse), and spontaneous cage activity. Variables were expressed over 24-hours, and during states of activity and inactivity as described in **Chapters 2** to **4** and previously by our group (13). For high-fat fed animals, powdered HFD was placed in the feed canisters during post-diet CLAMS measurements.

Glucose tolerance was measured pre- and post-diet using an intraperitoneal glucose tolerance test following an overnight fast (~16 hrs). Blood (~5-10 μL) was sampled from a tail vein and analyzed for glucose using a standard diabetic glucometer (Accu-Chek Aviva, Roche Diagnostics) at 0, 30, 60, and 120 min following an injection of 10% D-glucose (1g/kg body mass) (13, 16). A detailed schematic of the experimental timeline and measurements can be found in **Appendix B** (**Figure B1**).

Blood and Tissue Collection

All chemicals were purchased from BioShop Canada Inc. (Burlington, ON, Canada) unless indicated otherwise. Post-diet, animals were fasted 4 hours prior to euthanasia by an anesthetic overdoes of sodium pentobarbital (0.65 mg/kg body mass). Blood was collected via cardiac puncture using a heparinized syringe and allowed to clot on ice for ~10 min before being centrifuged at 5000 x g for 10 min. Serum was then collected, frozen in liquid nitrogen, and stored at -80°C until required.

Epididymal (Epidid), retroperitoneal (Retro), and inguinal (Ing) fat pads were removed and weighed for the determination of adiposity. A visceral adiposity index was calculated as 100 X [(Epidi + Retro pads)/ body mass] as done previously by our group (13). Organs (kidney, heart, liver) and skeletal muscles (SOL, extensor digitorum longus (EDL)) were also removed, cleaned and weighed. Following excision, the SOL was cleared of connective tissue, weighed and placed in ice-cold phenylmethylsulfonyl fluoride (PMSF; Sigma-Aldrich, Oakville, ON, Canada) buffer (pH: 7.5). PMSF buffer contained in mM: 250 sucrose, 5 HEPES, 0.2 PMSF, and 0.2% (w/v) NaN_3 (Fisher Scientific, Fair Lawn, NJ). SOL muscles were homogenized 1:10 (w/v) in ice-cold PMSF buffer using a glass-on-glass Dounce homogenizer, aliquots frozen in liquid nitrogen and stored at -80°C until needed.

Interscapular BAT was cleared from extraneous white adipose tissue and muscle, weighed, and flash frozen in liquid nitrogen. Prior to use, BAT samples were thawed in ice-cold PMSF buffer, minced, and homogenized 1:4 (w/v) in PMSF for Western blotting (13).

Western Blotting

Primary antibodies against PLN (2D12, product #: MA3-922), RyR (34C, product #: MA3-925), DHPR α-1 subunit (1A, product #: MA3-920), CSQ (VIIID12, product #: MA3-913) and SERCA2a (2A7-A1, product #: MA3-919) were purchased from ThermoScientific (Rockford, IL), while that against SERCA1a (A52) was a generous gift from Dr. David MacLennan (University of Toronto) (125). The primary antibody directed against the C-terminal luminal tail of SLN (LVRSYQY) was from Lampire Biological Laboratories (Pipersville, PA) (65), that directed against UCP-1 (ab10983) was from Abcam Inc. (Toronto, ON, Canada), and that directed against phosphorylated Ser16/Thr17 of PLN was from Cell Signalling Technology (Danvers, MA, Product #: 8496). All appropriate secondary antibodies were purchased from Santa Cruz Biotechnology (Santa Cruz, CA). Muscle and BAT samples were solubilized in 1X Laemmli buffer containing SDS and separated on glycine or tricine gels by SDS-PAGE (**Appendix A**: **Table A2**). All proteins were wet transferred on ice for 1 hr onto polyvinylidene difluoride (PVDF) membranes (0.2 μm pore size) except SLN, which was transferred to nitrocellulose membranes (0.2 μm pore size) (28). Following transfer, membranes were blocked in TRIS-buffered saline (pH: 7.5) containing 0.1% Tween-20 (v/v) (TBST) and 5% (w/v) skim milk powder for 1 hour at room temperature. All primary, secondary, and detection conditions for each protein are outlined in **Appendix A** (**Table A2**). Densitometry analysis was done using GeneSnap software (Syngene; Frederick, MD), and protein load was confirmed using Ponceau S staining for normalization of densitometry values.

Protein content of muscle and BAT homogenates was determined by the bicinchoninic acid assay (Sigma-Aldrich, Oakville, ON, Canada) using bovine serum albumin (Sigma-Aldrich) as a standard.

Serum Catecholamines

Serum epinephrine and norepinephrine content was determined by high-performance liquid chromatography (HPLC) using the methods of Weicker and colleagues (140) as modified by Green *et al*. (141). Briefly, ~200 µl of thawed plasma was mixed in an Eppendorf tube containing 20 mg of acid washed Al_2O_3 (Sigma-Aldrich), 400 µl of buffer (pH: 8.7) containing 2 M Tris and 2% (w/v) EDTA, ~637 pg of 3,4-dihydroxybenzylamine (internal standard), and mixed for 10 min for catecholamine adsorption. Samples were then washed with distilled water and desorbed from Al_2O_3 with the addition of 0.1 M perchloric acid. Following centrifugation, 50 µl the supernatant was injected into a Waters 2465 HPLC (Mississauga, ON, Canada) at 1.2 mL/min and separated using a Supelcosil (#58230U) columun (C18, 15 cm, 5 µm particle size). The mobile phase (pH: 3.5) consisted of 50 mM sodium acetate, 20 mM citric acid, 2 mM sodium octane sulfate, 1 mM di-*n*-butylamine, 100 µM EDTA dissolved in 96:4 (v/v) water:methanol. Serum catecholamines were compared against freshly made epinephrine (Sigma-Aldrich, product #: E4375) and norepinephrine (Sigma-Aldrich, product #: A9512) standards, whose retention times were 5.26 min and 4.27 min, respectively.

Statistical Analysis

Dietary mass gain of chow- and HFD-fed animals, glucose tolerance, and CLAMS variables were analyzed using a 2-way ANOVA with repeated measures. Cumulative food intake, cumulative metabolic efficiency, tissue mass, adiposity, dietary protein expression, and serum catecholamines were analyzed with a 2-way ANOVA. When appropriate, post-hoc comparisons were made using a Newman-Keuls test to examine specific mean differences. Dietary SLN and PLN expression of WT mice (i.e. chow vs. HFD) were analyzed using a 2-tailed Student's t-test (independent samples). Statistical significance was considered at $P \leq 0.05$. All data presented are mean ± S.E.

Results

Dietary Mass Gain, Food Consumption and Metabolic Efficiency

Dietary changes in animal body mass are shown in **Figure 5.1**. Surprisingly, DKO animals were resistant to mass gain when fed either a chow or a high-fat diet (main effect of genotype: DKO < WT, $P < 0.0001$) (**Figure 5.1 A**). By week 8, DKO mice gained ~42% less mass than WT controls when fed a chow diet (WT vs. DKO: 4.6 ± 0.5 g vs. 2.7 ± 0.3 g), and ~23% less mass when given a HFD (WT vs. DKO: 16.0 ± 0.9 g vs. 12.3 ± 1.5 g). Cumulative 8-week caloric intake (MJ consumed) was significantly greater in high-fat fed animals (main effect of diet: HFD > chow, $P < 0.0001$); however, no genotype difference in food intake existed in either chow- or HFD-fed animals (**Figure 5.1 B**). While metabolic efficiency (i.e. g body mass gained/cumulative MJ food consumed) was significantly greater in high-fat fed animals (main effect of diet: HFD > chow, $P < 0.0001$) by week 8, DKO mice tended ($P = 0.106$) to have a lower metabolic efficiency than WT mice, but this was not statistically significant (**Figure 5.1 C**).

Metabolic Phenotype

Figure 5.2 displays the whole-body metabolic variables of WT and DKO mice before and after 8 weeks of the control chow diet. Body mass normalized metabolic rate (i.e. ml O_2/kg/hr) was greater (significant main effect of genotype: DKO > WT, $P < 0.01$) in DKO mice when averaged over a full 24-hour light/dark cycle and during active periods (**Figure 5.2 A/B**). Although not statistically significant, there was a trend ($P < 0.07$) towards a main effect of genotype for DKO mice to have higher body mass

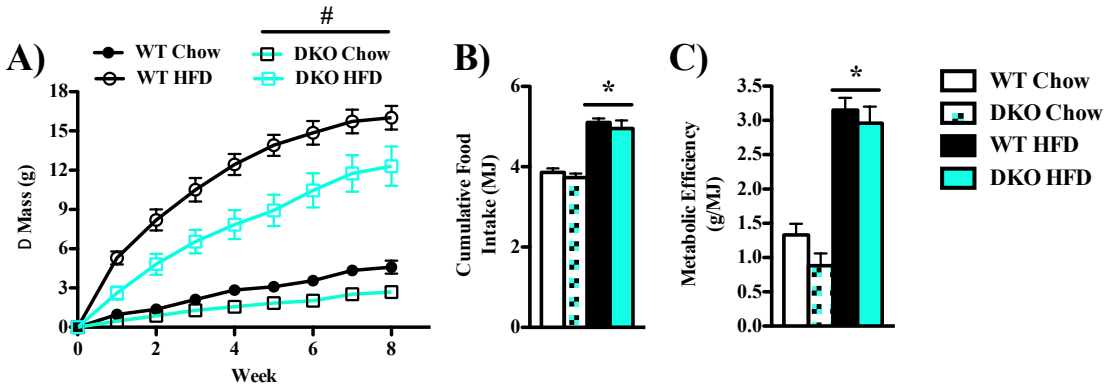

Figure 5.1. Double knock-out (DKO) mice gain less mass, regardless of diet. **A)** Dietary mass gain (g) of wild-type (WT) and DKO mice over 8 weeks of a chow or high-fat diet (HFD) (n = 21-22/group). **B**) Cumulative 8-week food consumption (MJ). **C)** Metabolic efficiency (g mass gained/MJ food consumed) following the 8 week dietary treatment. For **B)** and **C)** n = 9 -12/group. # Significant main effect ($P < 0.001$) of genotype (DKO < WT). * Significant main effect ($P < 0.0001$) of diet (HFD > chow). Values are mean ± S.E.

normalized energy expenditure during inactive periods (**Figure 5.2 A/B**). While metabolic heat production rate (kcal/hr/mouse) was not different between WT and DKO animals, there was a significant main effect ($P < 0.0001$) of the 8-week chow diet, with heat production rate being greater post-diet under all measurement periods (**Figure 5.2 C**). Unlike **Chapter 4**, total spontaneous activity (**Figure 5.2 D**) and cage ambulation (**Figure 5.2 E**) were similar between this cohort of WT and DKO mice. Lastly, no differences in RER (**Figure 5.2 F**) existed between WT and DKO mice, either before or after the 8-week chow diet.

CLAMS variables for high-fat fed animals are shown in **Figure 5.3**. Following the HFD, whole-body energy expenditure normalized to body mass was greater in DKO mice than WT controls when measured over a 24-hr period ($P < 0.001$), during states of activity ($P < 0.001$), and during states of inactivity ($P < 0.05$) (**Figure 5.3 A/B**). Interestingly, whole-body metabolic rate remained unchanged post-HFD relative to pre-diet in DKO mice, whereas it was significantly reduced ($P < 0.05$) in WT mice when measured under all three states (**Figure 5.3 B**). When expressed in absolute terms as heat production rate, energy expenditure was significantly greater post-diet (main effect of HFD: post > pre, $P < 0.0001$) by ~30%, ~26%, and ~37% when measured over 24-hrs, during states of activity, and during states of inactivity, respectively (**Figure 5.3 C**). However, no differences in absolute heat production existed between WT and DKO mice pre- or post HFD. While the HFD itself did not impact cage activity in WT or DKO animals, DKO mice surprisingly displayed significantly greater total spontaneous activity (main effect of genotype: DKO > WT, $P < 0.001$) (**Figure 5.3 D**) and cage ambulation

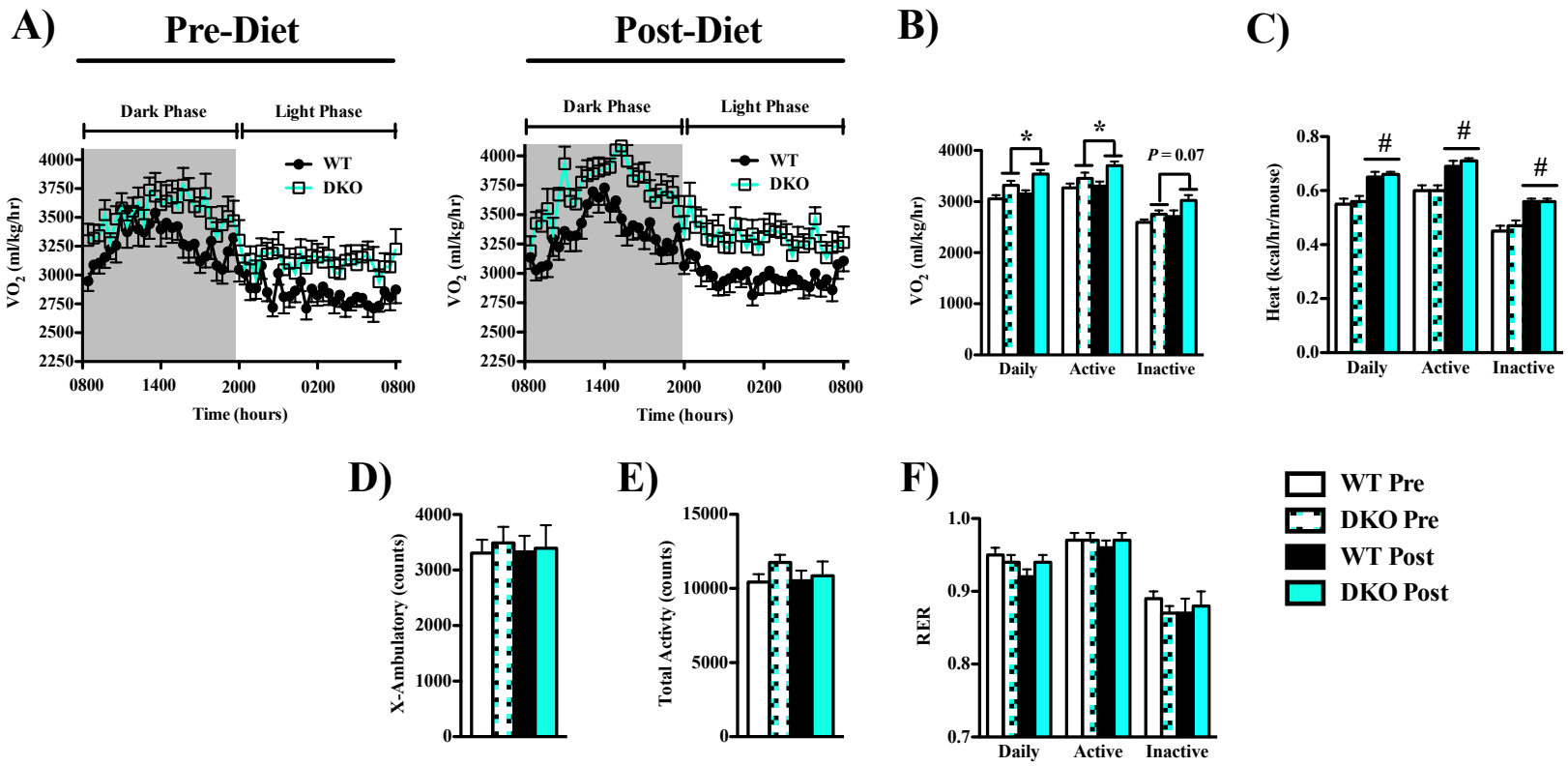

Figure 5.2. Metabolic phenotype of wild-type (WT; n = 13) and double knock-out (DKO; n = 13) mice in response to 8 weeks of chow feeding. **A)** Metabolic rate expressed as oxygen consumption rate (VO_2: ml O_2/kg body mass/hr) over as full 24 hour light/dark cycle before (Pre) and following (Post) the 8-week chow diet. **B)** VO_2 averaged over 24 hours (daily), during states of cage activity (active: 0800 hrs - 2000 hrs (dark phase), >2 ambulatory activity counts) and inactivity (inactive: 2000 hrs - 0800 hrs (light phase), ≤2 ambulatory activity counts). **C)** Metabolic rate expressed as absolute heat production rate (kcal/hr/mouse). **D**) Total spontaneous cage activity (counts) over 24-hours. **E)** Ambulatory cage activity (counts) in the X plane over 24 hours. **F)** Respiratory exchange ratio (RER: VCO_2/VO_2). * Significant main effect ($P < 0.01$) of genotype (DKO > WT). # Significant main effect ($P < 0.0001$) of diet (Post > Pre). Values are mean ± S.E.

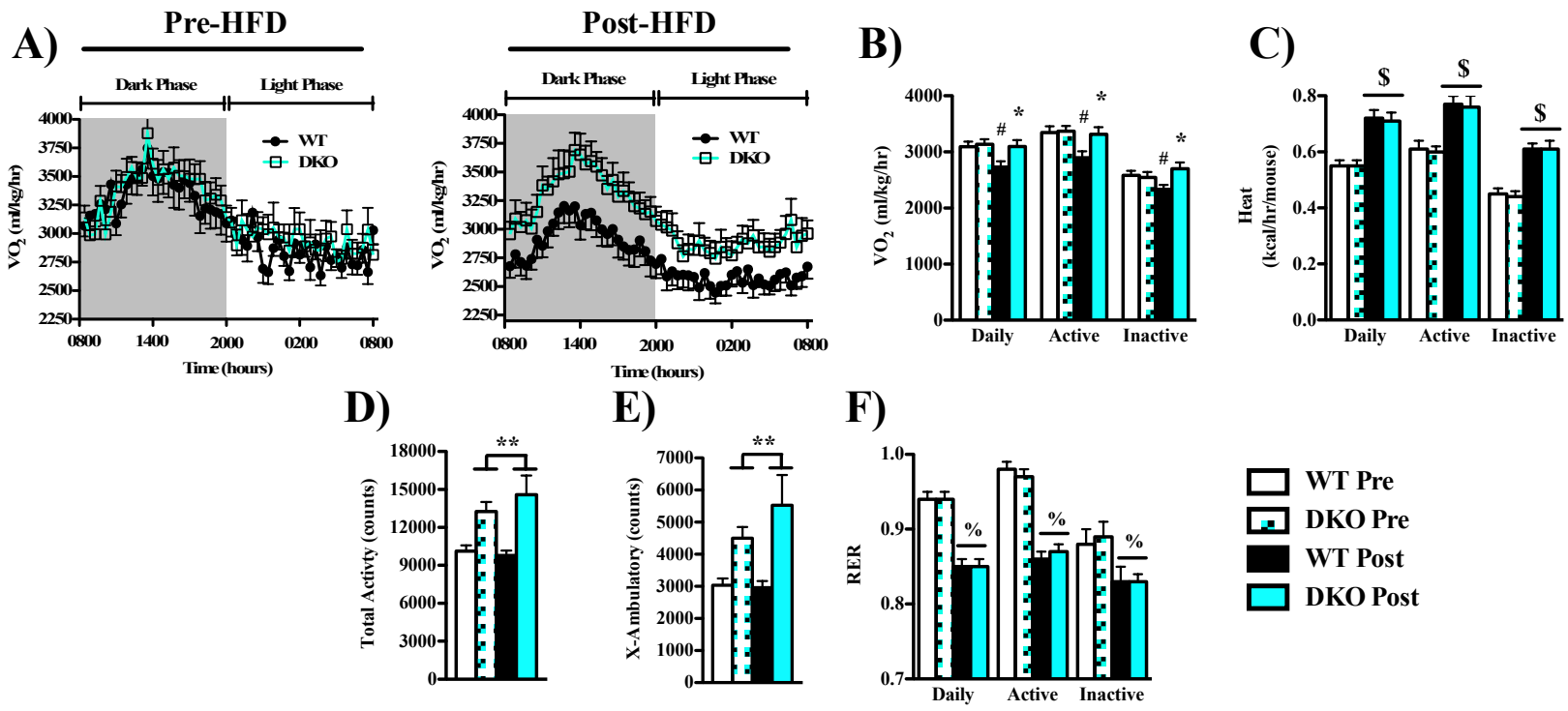

Figure 5.3. Metabolic phenotype of wild-type (WT) and double knock-out (DKO) mice in response to an 8-week high-fat diet (HFD) (n = 13/group). **A)** Metabolic rate expressed as oxygen consumption rate (VO_2: ml O_2/kg body mass/hr) over as full 24 hour light/dark cycle before (Pre) and following (Post) the 8-week HFD. **B)** VO_2 averaged over 24 hours (daily), during states of cage activity (active: 0800 hrs - 2000 hrs (dark phase), >2 ambulatory activity counts) and inactivity (inactive: 2000 hrs - 0800 hrs (light phase), ≤2 ambulatory activity counts). **C)** Metabolic rate expressed as absolute heat production rate (kcal/hr/mouse). **D**) Total spontaneous cage activity (counts) over 24-hours. **E)** Ambulatory cage activity (counts) in the X plane over 24 hours. **F)** Respiratory exchange ratio (RER: VCO_2/VO_2). * Significantly different ($P < 0.05$) than WT HFD. # Significantly different ($P < 0.05$) than WT Chow. $ Significant main effect ($P < 0.001$) of diet (Post > Pre). % Significant main effect ($P < 0.001$) effect of diet (Post < Pre). ** Significant main effect ($P < 0.05$) of genotype (DKO > WT). Values are mean ± S.E.

(**Figure 5.3 E**) compared to WT controls (main effect of genotype: DKO > WT, $P < 0.05$). Consistent with the consumption of the HFD, whole-body substrate usage indicated a shift towards greater fat oxidation during all measurement states, as RER was significantly lower post-HFD in both WT and DKO mice (main effect of HFD: post < pre, $P < 0.001$) (**Figure 5.3 F**). No differences in RER existed between WT and DKO animals, before or after the 8 week HFD (**Figure 5.3 F**).

Whole-Body Glucose Tolerance and Dietary Catecholamine Response

Interestingly, while WT mice were less glucose tolerant ($P < 0.05$) after 8 weeks of chow feeding, as shown by their greater blood glucose at all time points of the glucose tolerance test and greater AUC values relative to pre-diet, glucose tolerance of DKO animals remained unchanged after the 8-week control diet (**Figure 5.4 A/B**). Whole-body glucose tolerance pre- and post-HFD is shown in **Figure 5.5**. As expected, animals became glucose intolerant following the 8-week HFD relative to pre-dietary levels, as evidenced by the significantly greater blood glucose levels across all time points measured (main effect of HFD: post > pre, $P < 0.0001$) (**Figure 5.5 A**). This was also shown when glucose tolerance was expressed as area under the curve (AUC) (**Figure 5.5 B**), which was ~49% greater post-HFD relative to pre-dietary levels (main effect of HFD: post > pre, $P < 0.001$). No differences in blood-glucose concentration existed between WT and DKO mice at any time point pre- or post-HFD, or when glucose tolerance was expressed as AUC.

Serum epinephrine and norepinephrine following 8 weeks of chow- or high-fat feeding are shown in **Figure 5.6**. While dual ablation of SLN and PLN did not itself alter

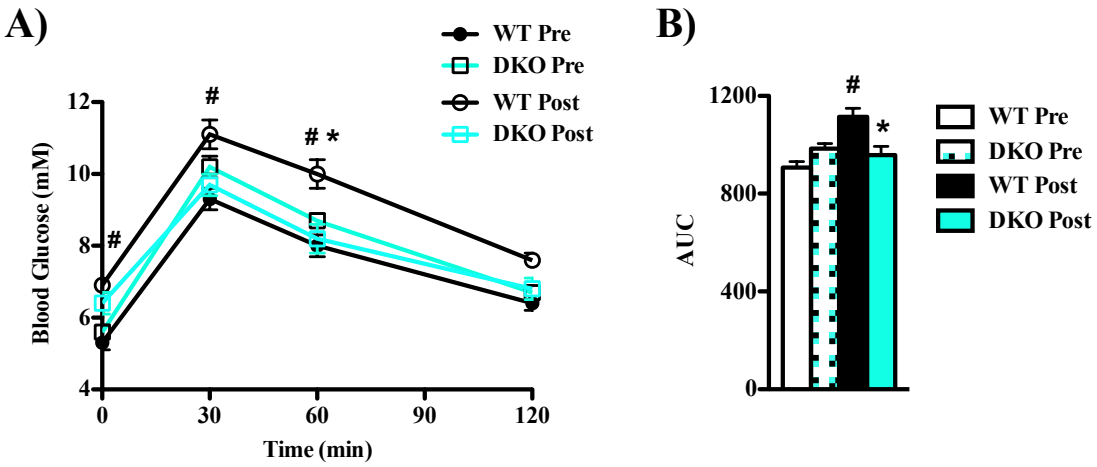

Figure 5.4. Glucose tolerance of wild-type (WT; n = 19) and double knock-out (DKO; n = 17) mice before (Pre) and after (Post) an 8-week chow diet. **A)** Blood glucose (mM) during and intraperitoneal glucose tolerance test pre- and post-diet. **B)** Glucose tolerance expressed as area under the curve (AUC) of animals pre- and post-diet. # Significantly different ($P < 0.05$) than WT Pre. * Significantly different ($P < 0.05$; WT Post vs. DKO Post). Values are mean ± S.E.

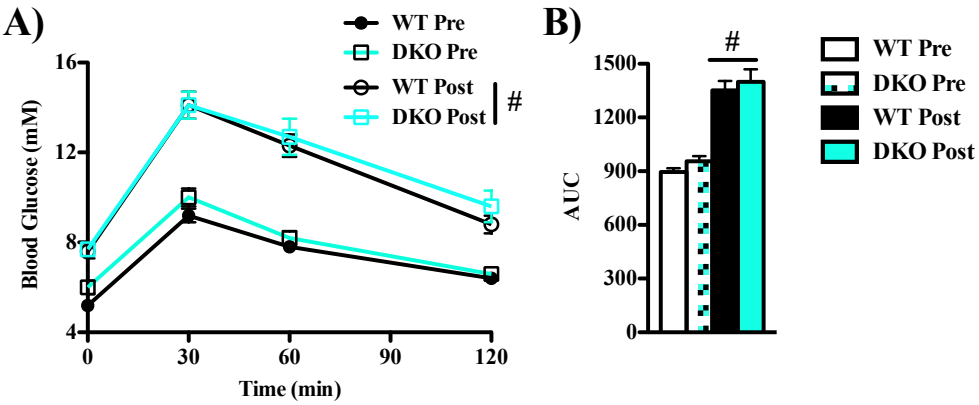

Figure 5.5. Glucose tolerance of wild-type (WT) and double knock-out (DKO) mice before (Pre) and after (Post) an 8-week high-fat diet (HFD) (n = 20/group). **A)** Blood glucose (mM) during and intraperitoneal glucose tolerance test pre- and post-HFD. **B)** Glucose tolerance expressed as area under the curve (AUC) of animals pre- and post-HFD. # Significant main effect ($P < 0.001$) of diet (Post > Pre). Values are mean ± S.E.

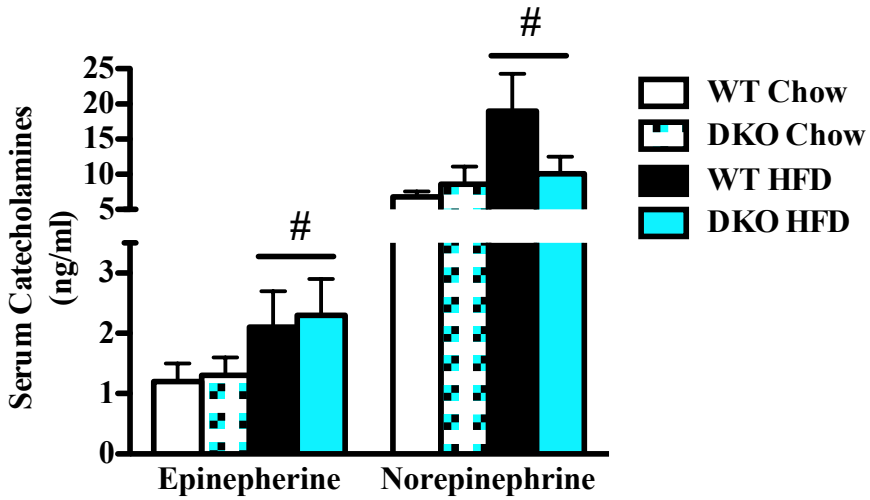

Figure 5.6. Serum epinephrine and norepinephrine concentrations (ng/ml) of wild-type (WT) and double knock-out (DKO) mice following 8 weeks of a chow or high-fat diet (HFD) (n = 9-10/group). # Significant main effect ($P < 0.05$) of diet (HFD > Chow). Values are mean ± S.E.

Table 5.1. Organ masses of WT and double knock-out (DKO) mice following 8 weeks of a chow or high-fat diet (HFD) (n = 21-22/group). Values are presented as absolute mass (g) and organ mass as a percentage of total body mass (% mass). *P*-values are listed for the main effect of genotype (WT vs. DKO), diet (Chow vs. HFD), and the genotype/diet interaction when analyzed by a 2-way ANOVA. Values are mean ± S.E.

	Chow		HFD		Genotype	Diet	Interaction
	WT	DKO	WT	DKO	*P*-Value		
Mass (g)							
Kidney	0.321 ± 0.009	0.306 ± 0.010	0.313 ± 0.009	0.321 ± 0.014	0.786	0.764	0.277
Heart	0.195 ± 0.005	0.216 ± 0.007	0.201 ± 0.006	0.240 ± 0.009	<0.0001	<0.05	0.171
Liver	1.742 ± 0.078	1.484 ± 0.044	3.398 ± 0.237	2.229 ± 0.193	<0.0001	<0.0001	<0.01
% Mass							
Kidney	0.806 ± 0.017	0.847 ± 0.023	0.588 ± 0.013	0.698 ± 0.026	<0.001	<0.0001	0.105
Heart	0.494 ± 0.016	0.598 ± 0.020	0.379 ± 0.009	0.524 ± 0.019	<0.0001	<0.0001	0.220
Liver	4.325 ± 0.073	4.090 ± 0.055	6.281 ± 0.301	4.640 ± 0.232	<0.0001	<0.0001	<0.001

serum catecholamine concentrations, high-fat feeding significantly increased serum epinephrine (main effect of diet: HFD > chow, $P < 0.05$) and norepinephrine (main effect of diet: HFD > chow, $P < 0.05$) by ~68% and ~89% relative to chow-fed animals, respectively.

Organ, Muscle and Fat Mass

Kidney, heart, and liver masses (both absolute and normalized to body mass) of chow and high-fat fed animals are listed in **Table 5.1**. Absolute kidney mass was unaffected by genotype or diet; however, relative to body mass high-fat fed animals had a significantly lower normalized kidney mass, with kidneys comprising a greater proportion of body mass in DKO mice, irrespective of dietary treatment. While high-fat feeding increased absolute and relative heart mass compared with chow-fed animals, DKO mice displayed cardiac hypertrophy as indicated by their greater absolute and relative heart mass compared to WT controls, irrespective of diet-treatment. Although high-fat feeding increased both absolute and relative liver mass in each genotype relative to chow-fed controls, high-fat fed DKO mice had smaller absolute and relative liver masses than that of WT counterparts.

SOL mass tended ($P = 0.068$) to be greater in high-fat fed mice compared to chow-fed counterparts, but did not differ by genotype (**Figure 5.7 A**). Interestingly, EDL mass was increased ($P < 0.05$) in high-fat fed WT mice relative to chow-fed counterparts, whereas no impact of diet was observed in DKO animals (**Figure 5.7 A**). No genotype differences in EDL mass existed for either chow- or HFD-fed groups.

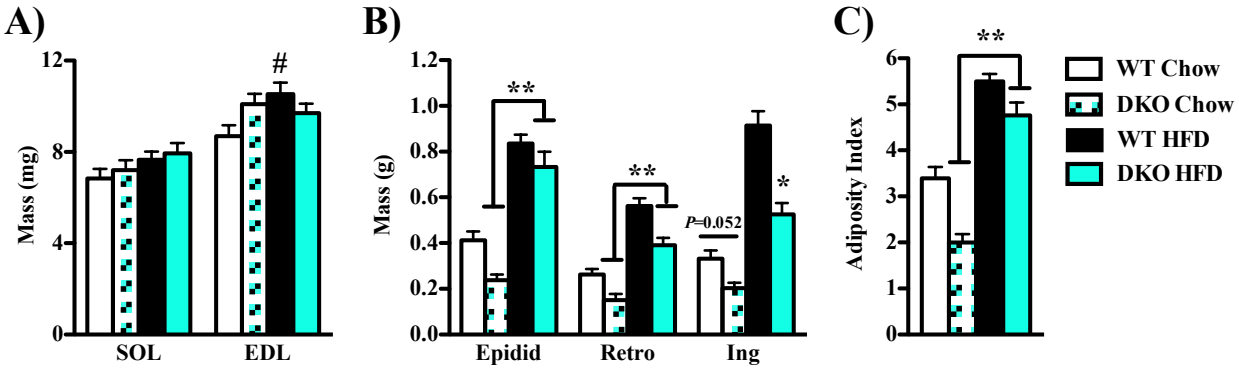

Figure 5.7. Skeletal muscle and adipose depot mass of wild-type (WT) and double knock-out (DKO) mice following 8 weeks of a chow or high-fat diet (HFD) (n = 19-21/group). **A)** Soleus (SOL) and extensor digitorum (EDL) mass (mg). **B)** Epididymal (Epidid), retroperitoneal (Retro), and inguinal (Ing) fat pad masses (g). **C)** Adiposity index (as described in "Methods"). # Significantly different than WT chow ($P < 0.05$). * Significantly different ($P < 0.001$) than WT HFD. ** Significant main effect ($P < 0.001$) of genotype (DKO < WT). Values are mean ± S.E.

As expected, high-fat feeding significantly increased (main effect of diet: HFD > chow, $P < 0.001$) the masses of the Epidid (+1.4-fold) and Retro (+1.3-fold) fat depots (**Figure 5.7 B**). Interestingly, both of these fat depots were significantly smaller in DKO mice relative to WT controls, irrespective of diet (main effect of genotype: DKO < WT, $P < 0.01$) (**Figure 5.7 B**). Similar to the other fat depots, HFD-fed mice had significantly larger ($P < 0.001$) Ing fat pads relative to their respective chow-fed controls (**Figure 5.7 B**). Compared with WT controls, the Ing fat depot of chow-fed DKO animals tended ($P = 0.052$) to be smaller, whereas it was significantly smaller ($P < 0.0001$) in high-fat fed DKO mice relative to WT counterparts (**Figure 5.7 B**). Correspondingly, the adiposity index of high-fat fed mice was greater than chow-fed controls (main effect of diet: HFD > chow, $P < 0.0001$), but DKO mice were significantly less obese, regardless of dietary treatment (main effect of genotype: DKO < WT, $P < 0.0001$) (**Figure 5.7 C**).

SR Protein Expression

SOL protein expression of RyR ($P = 0.173$), DHPR ($P = 0.353$), and CSQ ($P = 0.877$) did not differ between WT and DKO mice, irrespective of dietary intervention (**Figure 5.8 A/B**). However, there was a tendency ($P = 0.06$) for SOL DHPR expression to be increased by ~19% in HFD-fed animals relative to chow-fed control mice. While SERCA isoform expression was not altered by diet, SOL SERCA1a expression was reduced (main effect of genotype: DKO < WT, $P < 0.05$), while SERCA2a expression was correspondingly increased (main effect of genotype: DKO > WT, $P < 0.001$) in DKO

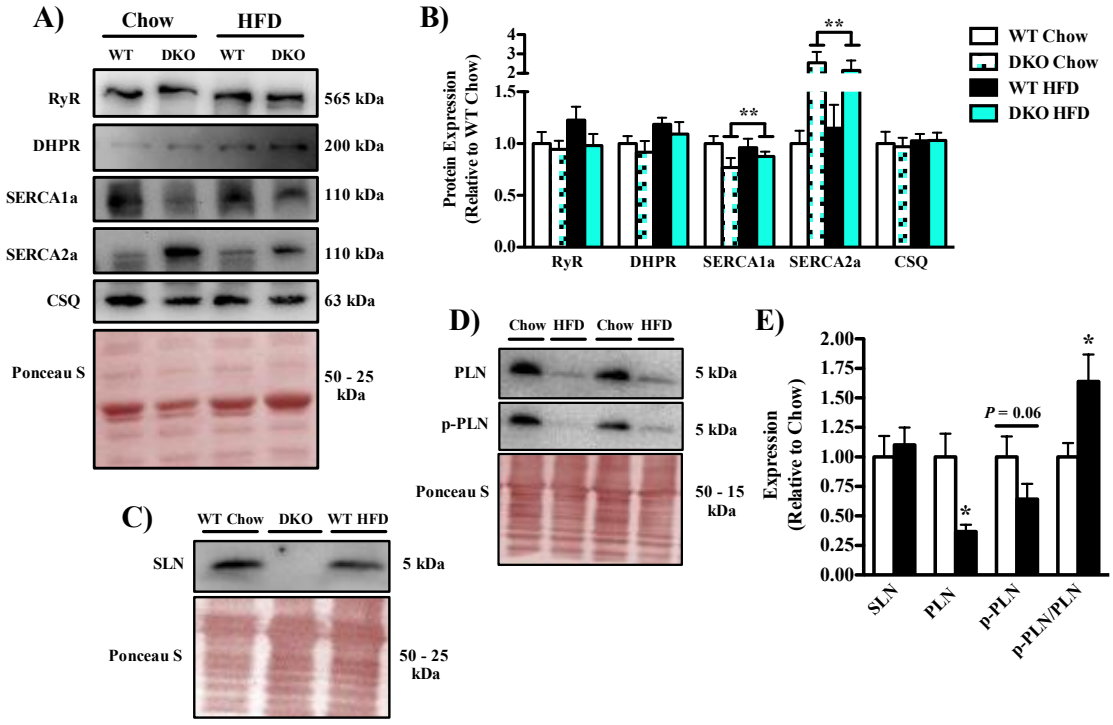

Figure 5.8. Expression of soleus Ca^{2+}-handling proteins following 8 weeks of a chow or high-fat diet (HFD). **A)** Representative Western blots of chow and high-fat fed wild type (WT) and double knock-out (DKO) mice. Equal protein load was confirmed using Ponceau S staining. **B)** Ca^{2+}-handling protein expression relative to chow-fed WT mice. **C)** Representative Western blot of SLN in chow and high-fat fed WT mice. DKO soleus was included as a negative control. **D)** Representative Western blots of monomeric PLN and phosphorylated monomeric PLN (p-PLN) of chow, and high-fat fed WT mice. **D**) SLN and PLN expression relative to chow-fed mice. N = 14-22/group for all blots. ** Significant main effect ($P < 0.05$) of genotype. * Significantly different ($P < 0.05$) from WT Chow. Values are mean ± S.E.

animals relative to WT controls (**Figure 5.8 A/B**). In WT mice, SOL SLN protein expression was unchanged ($P = 0.332$) by high-fat feeding (**Figure 5.8 C/E**), whereas PLN was significantly ($P < 0.01$) reduced by ~55% relative to chow-fed controls and phosphorylated PLN was increased by high-fat feeding (**Figure 5.8 D/E**).

BAT Mass and UCP-1 Expression

Given that DKO animals presented with a lean phenotype, it was of interest to determine if BAT-mediated thermogenesis was compensating to regulate energy balance in the absence of SLN and PLN. As expected, absolute BAT mass was significantly greater by ~1.4-fold in HFD-fed mice relative to chow-fed controls (main effect of diet: HFD > chow, $P < 0.0001$) (**Figure 5.9 A**). Similarly, BAT mass comprised a significantly greater proportion of body mass in HFD-fed mice relative to chow-fed controls (main effect of diet: HFD > chow, $P < 0.0001$) (**Figure 5.9 B**). Interestingly, both absolute and normalized BAT mass was significantly smaller in DKO mice relative to WT controls (main effect of genotype: DKO < WT, $P < 0.0001$), irrespective of diet intervention (**Figure 5.9 A/B**). As expected, high-fat feeding resulted in a ~25% increase in UCP-1 protein expression relative to chow-fed mice (main effect of diet: HFD > chow, $P < 0.01$), but was not affected by animal genotype (**Figure 5.9 C/D**).

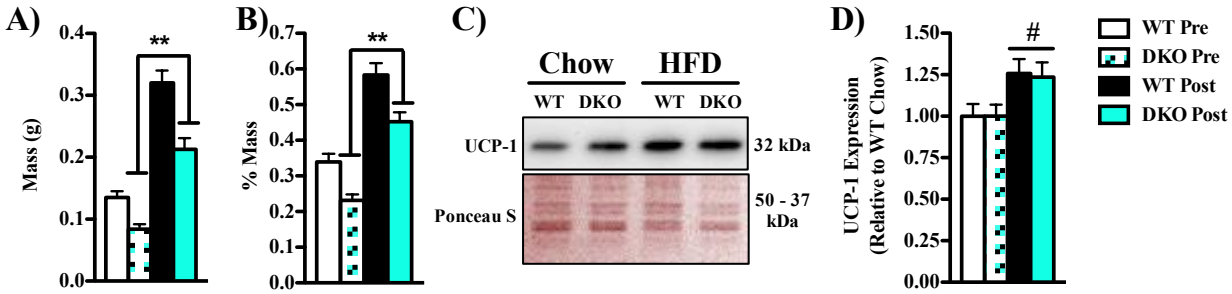

Figure 5.9. Adaptive response of brown adipose tissue (BAT) with dual SLN/PLN ablation. **A)** BAT mass (g) of wild-type (WT) and double knock-out (DKO) mice following an 8 weeks of a chow or high-fat diet (HFD). **B)** BAT mass expressed as a percentage of animal body mass (% mass). **C)** Representative Western blot of BAT UCP-1. Equal protein load was confirmed by Ponceau S staining. **D)** BAT UCP-1 protein expression relative to chow-fed WT mice. N = 19-20/group. ** Significant main effect ($P < 0.001$) of genotype (DKO < WT). # Significant main effect ($P < 0.01$) of diet (HFD > Chow). Values are mean ± S.E.

Discussion

Here, we hypothesized that DKO mice would develop excessive obesity relative to WT controls when fed a "Westernized" HFD due to their inability to uncouple SERCA function via skeletal muscle SLN. To our surprise, dual ablation of SLN and PLN was actually protective against diet-induced mass gain and adiposity in both chow- and HFD-fed animals, but did not mitigate the development of HFD-induced glucose intolerance. The lean phenotype of DKO mice was the result of their greater energy expenditure and not due to compensation by other energy balance mechanisms. Although the cohort of HFD-fed DKO mice were more spontaneously active during metabolic measurements, this was not sufficient to fully explain their reduced mass gain and adiposity, as whole-body energy expenditure was greater even during inactive periods. While SERCA isoforms were altered in DKO SOL, consistent with the fast-to-slow fibre-type shift previously reported in these animals (**Chapter 4**), expression of SR proteins involved in Ca^{2+} release and storage remained unchanged, as was BAT UCP-1. We propose herein that a futile cycling of SR Ca^{2+} may possibly explain the hypermetabolic phenotype of DKO mice, as loss of SERCA inhibitors would increase SR Ca^{2+} load, subsequently driving a gradient of Ca^{2+} leakage and re-uptake (discussed below).

Whole-Body Metabolic Phenotype of DKO Mice

The most surprising and novel finding from this study was that DKO mice were resistant to diet-induced mass gain and had correspondingly lower adiposity than WT control animals, regardless of whether they were fed a chow or HFD. These findings differ considerably to single gene KO studies of either protein. Our group (16, 17, 157)

and others (12) have demonstrated that *Sln*$^{-/-}$ mice develop excessive obesity at room temperature only when fed a HFD, whereas *Pln*$^{-/-}$ mice present with a phenotype indistinguishable to WT littermates when given either a control or HFD (**Chapter 3**). Therefore, it was reasonable to expect DKO animals to display a similar phenotype to that of *Sln*$^{-/-}$ animals, as only the SLN/SERCA relationship is thermogenic in nature (12-14, 54, 55). However, DKO animals displayed lower mass gain over 8-weeks of chow or high-fat feeding despite eating similar amounts of either diet as WT control mice, indicating their lean phenotype was not the result of lower energy intake. Subsequently, visceral and subcutaneous fat pad size was smaller in DKO animals following either diet, and when measured as an adiposity index (i.e. relative to total body mass), DKO animals were less obese irrespective of diet treatment. As food intake was similar between genotype, this would suggest the lean phenotype of DKO animals resulted from greater energy expenditure.

Metabolic efficiency is a measurement of the ability to convert consumed energy into stored mass (6, 87); thus, differences in metabolic efficiency are in part reflective of a change in energy expenditure. Despite their lower adiposity, there was only a tendency for metabolic efficiency to be lower in DKO mice following the 8-week chow or HFD. However, planned comparisons (i.e. Student's t-test) indicated that this was the case for chow-fed DKO mice relative to WT controls (WT vs. DKO: 1.33 ± 0.16 g/MJ vs. 0.88 ± 0.18 g/MJ, $P < 0.05$), but not for HFD-fed mice (WT vs. DKO: 3.15 ± 0.18 g/MJ vs. 2.96 ± 0.24 g/MJ, $P = 0.260$). However, because adaptive thermogenic mechanisms are activated by caloric surfeit (4), weekly metabolic efficiency was measured throughout the 8-week HFD to determine whether genotype differences existed that may be masked by a

terminal measurement (**Appendix D**: **Figure D1**). Indeed, DKO mice had a lower weekly metabolic efficiency between weeks 1 to 5, indicating that they were more energetically inefficient throughout this period (**Figure D1.B**). Interestingly, the weekly metabolic efficiency of WT mice steadily declined over the course of the HFD, the magnitude of which eventually matching DKO mice towards the latter end of the HFD. This suggests that diet-induced thermogenic mechanisms were being activated in WT mice to combat diet-induced obesity, whereas DKO animals did not require the need for similar diet-induced mechanisms given their greater energetic inefficiency. In fact, even chow-fed DKO mice had a lower weekly metabolic efficiency compared to WT controls (**Appendix D**: **Figure D1.A**), suggesting that dual SLN/PLN ablation increases energy expenditure even in the absence of dietary stress.

In agreement with their lower weekly metabolic efficiency, whole-body metabolic rate of chow-fed DKO animals was greater compared with WT control mice, indicating that energy expenditure was in fact greater with dual SLN/PLN ablation. However, unlike that observed in **Chapter 4**, this group of DKO mice were not more spontaneously active during CLAMS measurements. Although unclear why this was the case, it is unlikely then that the increased activity of DKO animals observed previously (**Chapter 4**) can fully explain their lean and hypermetabolic phenotype. In light of this, and our finding that energy intake was similar to that of WT mice, the attenuated mass gain and lower adiposity of chow-fed DKO mice is the result of their higher metabolic rate. Consequently, whole-body glucose tolerance post-diet remained unchanged relative to DKO animals while it was relatively impaired in WT controls, suggesting that DKO animals were protected against the age-related decline in glucose handling as a result of

their attenuated mass gain. In the HFD-fed group of mice, although pre-diet energy expenditure measurements were similar between genotype, it was greater in DKO animals relative to WT controls post-HFD during all measurement periods. Like that of chow-fed counterparts, this can explain their protection against diet-induced obesity given that calorie intake was similar between high-fat fed WT and DKO mice. As previously observed in **Chapter 4**, we observed greater spontaneous cage activity to be higher in DKO mice during CLAMS measurements pre- and post-HFD. While increased physical activity can explain, in part, their protection against obesity, it is unlikely to be the sole determinant of their greater metabolic rate for several reasons. Firstly, caloric expenditure was greater in the chow-fed DKO cohort despite similar cage activity. Lastly, DKO animals had a higher post-HFD metabolic rate even when measured during periods of inactivity.

Insulin resistance and glucose intolerance are phenotypic traits often associated with obesity; the accumulation of bioactive lipid species within insulin responsive tissues such as the liver and skeletal muscle, along with the changing profile of circulating pro-inflammatory cytokines are just several known obesity-related factors that inhibit the insulin signaling cascade (142, 143, 158). Thus, one of the more surprising findings from this study was the lack of improvement in whole-body glucose tolerance despite the lower adiposity of HFD-fed DKO mice. Our previous findings with *Sln*$^{-/-}$ and *Pln*$^{-/-}$ mice contrast with these results in that they demonstrate the expected correlation with adiposity and whole-body glucose handling (157). Specifically, the excessive diet-induced adiposity of *Sln*$^{-/-}$ mice is accompanied by excessive glucose intolerance (157), whereas *Pln*$^{-/-}$ mice present with similar diet-induced adiposity and glucose intolerance to

that of WT littermates when fed the same HFD used herein (**Chapter 3**). While it is unclear from the current study as to why DKO animals did not show the expected improvement in glucose tolerance post-HFD, several factors may explain this observation. First, the genotype disparity in HFD-induced mass gain, and thus likely adiposity, appears attenuated by week 8 between WT and DKO mice relative to earlier time points. In line with this, post-HFD adiposity of *Sln*$^{-/-}$ mice previously measured by our group was ~25% greater than WT controls (157), while that of the DKO animals measured here was only ~13% lower. It is possible an improvement in glucose tolerance in DKO mice may have been observed earlier into the HFD, wherein a greater adiposity disparity was more likely to have occurred. Lastly, circulating insulin and C-peptide were not measured during the glucose tolerance test, which would provide insight into the insulin secretory pattern in response to the glucose bolus. As the accumulation of bioactive lipids within the pancreas can impair β-cell function with obesity (159), it is possible that pancreatic glucose-induced insulin secretion of DKO mice may be lower, indicating a lower pancreatic burden to regulate glycaemia. It is important to note that insulin sensitivity of WT and DKO animals cannot be inferred from these data. While impaired glucose tolerance and insulin sensitivity can often accompany one another in rodent studies of diet-induced obesity, this is not always the case. Despite the development of excessive diet-induced glucose intolerance in *Sln*$^{-/-}$ mice, these animals surprisingly are not insulin resistant as assessed by an intraperitnoeal insulin tolerance test (12, 157). If, as discussed above, the greater diet-induced obesity of WT mice resulted in compensatory hyperinsulinemia to regulate blood glucose, it is possible then

that measurement of insulin sensitivity directly may reveal DKO mice to be more insulin sensitive post-HFD, as would be predicted by their lean phenotype.

Organ and Muscle Mass

In agreement with Shanmugam and colleagues (108), we observed cardiac hypertrophy in DKO mice, as evidenced by both higher absolute and relative heart mass. Cardiac hypertrophy in these animals has previously been shown to be specific to the ventricle, as gross atrial mass and myocyte size are unaltered while those of the left ventricle are (108), an interesting finding given that this same group has reported co-expression of SLN and PLN in microsomal fractions enriched with SR from both atria and ventricle (44). Regardless of the chamber-specific response, the cardiac hypertrophy observed here and previously (108) is consistent with the larger cross sectional area of type I and IIA fibres of DKO SOL reported in **Chapter 4**, a muscle that we also find to endogenously express SLN and PLN (65). Although unclear exactly how loss of both SERCA inhibitors can result in cardiac hypertrophy, DKO hearts display altered gene expression patterns of extracellular matrix proteins indicative of cardiac remodeling, along with alterations in the phosphoinositide 3-kinase/Akt pathway, which is implicated in both adaptive and maladaptive cardiac hypertrophy (108).

While the absolute and relative liver masses were unchanged between WT and DKO mice following chow feeding, this was not the case for high-fat fed animals. Although HFD-fed mice expectedly displayed larger absolute and relative liver masses compared to chow-fed controls, DKO animals had both lower absolute and relative liver masses relative to WT counterparts following the HFD. Our finding that liver size was

unchanged in chow-fed DKO animals despite their lower adiposity and mass gain may not be entirely surprising given that excessive accumulation of lipids within the liver is unlikely with this control diet. However, the lower absolute and relative liver mass of HFD-fed DKO mice may likely indicate that they are protected against hepatic accumulation of lipids, and is consistent with the protection of DKO mice from diet-induced obesity.

Absolute kidney mass was unaffected by dual SLN/PLN ablation or diet; however, relative kidney mass was lower in HFD-fed mice compared to chow-fed controls, which is to be expected from the development of obesity with high-fat feeding. Furthermore, the finding that DKO mice had a lower relative kidney mass is simply reflective of their lower body mass following both chow- and high-fat diets.

Despite greater cross sectional area of type I and IIA fibres (**Chapter 4**), gross SOL mass was unchanged in DKO mice. Similar findings have been shown in the SOL of both *Sln*$^{-/-}$ (16, 130) and *Pln*$^{-/-}$ (**Chapter 3**) mice fed the same control or HFD. However, the tendency of HFD-fed animals to have greater SOL mass is possibly an adaptation reflective of the greater load experienced by this muscle with obesity. Although the EDL mass of chow-fed animals remained unchanged by dual SLN/PLN ablation, only WT mice displayed an increase in EDL size in response to the HFD. This hypertrophy is again likely the result of an increased load experienced by this muscle in response to the excessive mass gain by HFD-fed WT mice.

Skeletal Muscle and BAT Protein Expression

Here, SERCA2a protein expression was increased and SERCA1a concomitantly reduced within SOL of both chow- and HFD-fed DKO mice. These changes in SERCA isoform content are consistent with the fast-to-slow fibre type shift previously reported in **Chapter 4**. Despite this muscular distinction in SERCA isoform expression of DKO mice, it is unlikely to explain their lean phenotype. Using SR vesicles derived from rabbit red (i.e. SERCA2a) and white (i.e. SERCA1a) skeletal muscle, Ca^{2+} transport was shown to be more coupled to ATP cleavage (i.e. more efficient) within red muscle, resulting in lower heat release during Ca^{2+} pumping compared to that of white muscle (160); this indicates that SERCA2a is the more energetically efficient skeletal muscle isoform, and if anything, its greater content within DKO oxidative muscle would predispose these animals to obesity. Similar to that described for DKO atria and ventricles (108), we found SOL RyR, DHPRα1 and CSQ protein expression to be unaltered in DKO mice, suggesting no intrinsic changes in the capacity for Ca^{2+} release or storage in these animals. Together, our western blotting results do not explain the phenotype of DKO animals. Recently, a number of new SERCA regulatory proteins bearing structural and functional resemblance to SLN/PLN have been discovered (56, 161), some of which have been demonstrated to uncouple SERCA function (114). While we cannot rule out that alternate SERCA regulatory proteins are induced to compensate for the lack of both SLN and PLN within DKO muscle, compensation by another uncoupler of SERCA seems unlikely given that Ca^{2+} pumping efficiency tends to be higher in DKO animals (**Chapter 4**).

Interestingly, there was a tendency for DHPRα1 protein content to be higher in HFD-fed mice. Although not statistically significant, SOL DHPRα1 protein expression

measured in **Chapter 3** was also elevated ~37% in HFD-fed animals (main effect of diet: $P = 0.149$). This is not the first study to report a diet-induced change in DHPR expression. In male Wistar rats, calorie restriction was shown to reduce cardiac DHPR protein expression by ~28% (162). Interestingly, calorie restriction also prevents the age related decline of DHPR content within oxidative skeletal muscle (163). Several studies have demonstrated that obesity and diabetes results in abnormal Ca^{2+}-handling and depressed skeletal muscle function in rodents (67, 164-166). Although the physiological significance of the diet-induced change in DHPR protein found herein is unclear, it may be an adaptation to mitigate contractile dysfunction with diet-induced obesity.

Surprisingly, SOL SLN protein expression of WT mice was unaltered by diet. High-fat feeding has previously been shown to increase SLN content ~3-4 fold within this muscle group in C57BL/6J mice (12, 157), while in **Chapter 3**, SLN expression declined in response to this same HFD. Our findings herein should not negate the established importance of skeletal muscle SLN in adaptive diet-induced thermogenesis, as has been demonstrated by our group and others using both loss- and gain-of-function approaches *in vivo* (12, 14, 16, 17, 54, 55, 62, 87, 88, 157). As described in **Chapter 3**, a direct correlation of oxidative skeletal muscle SLN protein content and SERCA-uncoupling is not always observed. Furthermore, the seemingly diverse diet-induced responses of SLN protein expression within oxidative muscle may also relate to the differing genetic backgrounds of the mice used within each study. However, like that observed in **Chapter 3**, SOL PLN protein expression was again reduced in response to diet-induced obesity, an adaptation that appears to be preserved across differing murine genetic backgrounds. Furthermore, PLN phosphorylation was increased in WT mice

with high-fat feeding. Together, the decrease in monomeric PLN content and increase in its phosphorylation status indicates that prolonged caloric surfeit diminishes the physical interaction between PLN and SERCA within oxidative skeletal muscle. These findings are in line with the notion that PLN differs functionally from SLN in that it is not involved in skeletal muscle adaptive thermogenesis by uncoupling SERCA function through its physical interaction with the pump (54, 55, 132).

Interestingly, serum epinephrine and norepinephrine concentrations were greater in HFD-fed animals, possibly as a mechanism to activate thermogenesis in peripheral tissues (i.e. BAT, skeletal muscle). This catecholamine response was consistent with the increase in PLN Ser16/Thr17 phosphorylation in high-fat fed WT mice. PLN is a well-described phosphorylation target of PKA (43); thus, its phosphorylation suggests the HFD resulted in sympathetic activation of skeletal muscle. However, as skeletal muscle is innervated by sympathetic neurons, it cannot be assumed that circulating catecholamines are solely responsible for the adrenergic activation of skeletal muscle leading to PLN phosphorylation. While there was a tendency for the HFD to increase PLN Ser16/Thr17 phosphorylation in **Chapter 3**, this occurred without an increase in circulating catecholamine content. The HFD-induced rise in serum epinephrine/norepinephrine found herein may simply be related to the greater adiposity disparity between HFD-fed mice relative to chow-fed controls in this study compared to those of **Chapter 3**.

BAT mitochondrial uncoupling is critical for adaptive diet-induced thermogenesis in rodents (3, 6). As DKO mice were resistant to mass gain and adiposity, it was necessary to determine whether compensatory adaptations in BAT/UCP-1 existed in

these animals that could explain this phenotype. Although the lower absolute and relative BAT mass of DKO mice would suggest a lower capacity for BAT-mediated thermogenesis (3), this would presumably render these mice susceptible to diet-induced obesity, which was clearly not the case. In fact, BAT UCP-1 protein expression was similar between WT and DKO mice and was increased equally by the high-fat diet, indicating that the adaptive response of BAT UCP-1 remained intact despite a reduced capacity for BAT thermogenesis in DKO animals. The similar induction of UCP-1 protein expression is consistent with the rise in serum catecholamines of both WT and DKO mice, particularly norepinephrine, which directly activates UCP-1 gene expression though PKA and cAMP response element-binding protein (3). It is possible that the need for BAT thermogenesis is reduced in DKO mice due to alternate sources of inefficient metabolism, resulting in a reduced need to maintain BAT mass. Alternately, while BAT is not a major storage site of fat, the lower absolute and relative BAT mass of DKO mice may be reflective of reduced intracellular lipid accumulation within this tissue bed, particularly given that whole-body energy expenditure is greater in these animals. Regardless, it does not appear that an enhanced ability of UCP-1 mediated mitochondrial uncoupling can explain the lean DKO phenotype.

Potential Mechanism Mediating the Lean DKO Phenotype

A major question remaining is how does the loss of two SERCA inhibitory proteins render mice protected against diet-induced mass gain and adiposity, as this appears paradoxical in light of SLN's demonstrated role in diet-induced thermogenesis. The inhibitory role of PLN and SLN on SERCA function is well documented. In

cardiomyocytes, both SLN (44, 59, 78) and PLN (47, 74) reduce the Ca^{2+} transient amplitude during muscle stimulation, which is believed to be the result of lower SR Ca^{2+} load due to a reduced rate of Ca^{2+}-uptake in the presence of either regulatory protein. Not surprisingly then, SR Ca^{2+} load is greater in both atrial and ventricular myocytes of DKO mice (108). SR [Ca^{2+}] is highly regulated and dependent not just on SERCA-mediated Ca^{2+}-uptake, but luminal Ca^{2+} buffering, SR Ca^{2+} leak pathways, store operated Ca^{2+} entry, and Ca^{2+} release via the RyR/DHPR complex to name but a few. If SR Ca^{2+} load is increased in DKO oxidative muscle *in vivo*, as would be expected by the loss of both SLN and PLN, the accumulated luminal Ca^{2+} may enhance the already large ion gradient favoring SR Ca^{2+} efflux. As a result, SERCA would consume more total ATP in an effort to maintain cytosolic [Ca^{2+}], a mechanism akin to the futile Ca^{2+} cycling seen in heater organs of deep sea diving fishes (84). Several studies have indirectly shown that such a mechanism may exist. Indeed, deletion of either PLN (105-107, 109-113) or SLN (103) increases the loss of Ca^{2+} from SR. Furthermore, mouse flexor digitorum brevis (FDB), which does not participate in shivering thermogenesis, displays increased markers of RyR-mediated Ca^{2+} leak (e.g. calstabin-1 depletion, RyR1 hyperphosphorylation) and increased basal cytosolic [Ca^{2+}], along with activating mitochondrial biogenesis following acclimation of mice to 4°C (85, 86). Any leaked SR Ca^{2+} in these instances would require continual re-uptake from SERCA to regulate cytosolic [Ca^{2+}], and thus the consumption of ATP. In **Chapter 4**, we observed a fast-to-slow fibre type shift, along with hypertrophy of type I and IIA fibres within the SOL of DKO mice. This muscular phenotype is consistent with activation of cytosolic Ca^{2+}-dependent signaling pathways mediated by CaN and CaMKs (129, 149). While speculative, reducing the interaction of

SERCA with both SLN and PLN could indirectly drive the release and futile cycling of Ca^{2+} ions across the SR by promoting Ca^{2+} leak and subsequent SERCA activation, thus explaining both the muscular and metabolic phenotype of DKO animals.

Conclusion

Despite the established role of SLN in mediating skeletal muscle adaptive thermogenesis, mice lacking both SLN and PLN were paradoxically resistant to diet-induced mass gain and adiposity compared to WT control mice when fed either standard rodent chow or a HFD for 8 weeks. The lean phenotype of DKO mice was the result of their greater whole-body energy expenditure, even during states of physical inactivity. Although SERCA isoform expression was altered in DKO SOL, which is likely reflective of the fast-to-slow fibre type transition previously observed in these mice (**Chapter 4**), no compensatory changes of SR or BAT protein expression were found. In light of the role of either protein in reducing SR Ca^{2+}-uptake and subsequently SR Ca^{2+} load, we propose that such protection of DKO mice against diet-induced mass gain and adiposity may originate from a futile cycling of Ca^{2+} ions across the SR within skeletal muscle *in vivo*.

CHAPTER 6

Conclusions, Perspectives, and Future Directions

Recap of Major Findings and Conclusion

There were several major objectives of this thesis. In light of PLN's sequence homology and similar biochemical action on SERCA function as SLN, we wanted to determine whether physiological levels of PLN protein expression uncoupled Ca^{2+} transport from ATP hydrolysis within skeletal muscle. Furthermore, we sought to determine whether the PLN/SERCA relationship was involved in diet-induced thermogenesis, and ultimately protective against obesity. Using *Pln*$^{-/-}$ mice, SERCA pumping efficiency was found to be unaffected by its interaction with PLN within oxidative skeletal muscle. Not surprisingly then, when *Pln*$^{-/-}$ mice were challenged by a "Westernized" HFD for 8 weeks, they became equally as obese and glucose intolerant as WT littermates. Lack of an excessively obese phenotype was not due to compensation by skeletal muscle SLN or BAT UCP-1 expression in the absence of PLN, nor was energy intake altered in *Pln*$^{-/-}$ mice. Surprisingly, SOL PLN protein expression was reduced and phosphorylation increased by the HFD in WT mice, a finding that was replicated in **Chapter 5** using a different mouse strain. **Chapter 2** and **3** revealed that skeletal muscle PLN is functionally distinct from that of SLN, and while responsive to diet, PLN serves a different role in diet-induced obesity other than regulating SERCA efficiency and thermogenesis through its physical interaction with the pump.

SLN and PLN can form a ternary super-inhibitory complex with SERCA, in which Ca^{2+}-uptake activity is inhibited to a greater extent than by either regulator alone (53, 76). Although SLN and PLN have previously been thought to regulate SERCA in a mutually exclusive manner based on their tissue distribution, several reports have found their expression within the same muscle group and even within the same single skeletal

muscle fibre (28, 65). Moreover, deletion of both SLN and PLN results in cardiac hypertrophy and susceptibility to cardiac dysfunction, despite improved SERCA function (108). Thus, these studies suggest that SLN and PLN, through their additive effect and/or super-inhibition of SERCA, are critical for regulating muscular Ca^{2+}-handling. Given that both are present endogenously within oxidative muscle, the other major objective of this thesis was to characterize the impact of dual SLN/PLN ablation on muscular Ca^{2+}-handling and whole-body metabolism. Interestingly, the SOL of DKO mice displayed a fast-to-slow fibre type shift, including hypertrophy of I and IIA fibres. As neither *Sln*$^{-/-}$ nor *Pln*$^{-/-}$ SOL display a change in fibre type or morphology (**Chapter 2**, 49), this suggests that ablation of either regulator may be compensated in action by the other. Consistent with the fibre type shift of DKO animals, SERCA2a protein expression was elevated in SOL homogenates, whereas SERCA1a was depressed. To our surprise, SERCA catalytic activity was reduced despite the loss of SLN and PLN, although this likely reflected the reduction in SERCA pump density accompanying the increased proportion of type I fibres within DKO SOL. As expected with the loss of SLN, SERCA pumping efficiency tended to be greater in DKO SOL, suggesting a lower ATP demand to transport Ca^{2+}. In light of their more efficient Ca^{2+}-handling, it was reasonable then to hypothesize that DKO animals would be susceptible to diet-induced obesity due to the absence specifically of SLN. Strikingly, DKO animals gained less mass and had a lower adiposity than WT control mice following both 8-weeks of chow or high-fat feeding, a lean phenotype that was the result of greater energy expenditure of these mice. Dual SLN/PLN ablation did not result in any compensatory changes in food intake, muscle SR or BAT protein expression that could explain this unique phenotype. **Chapter 4** and **5**

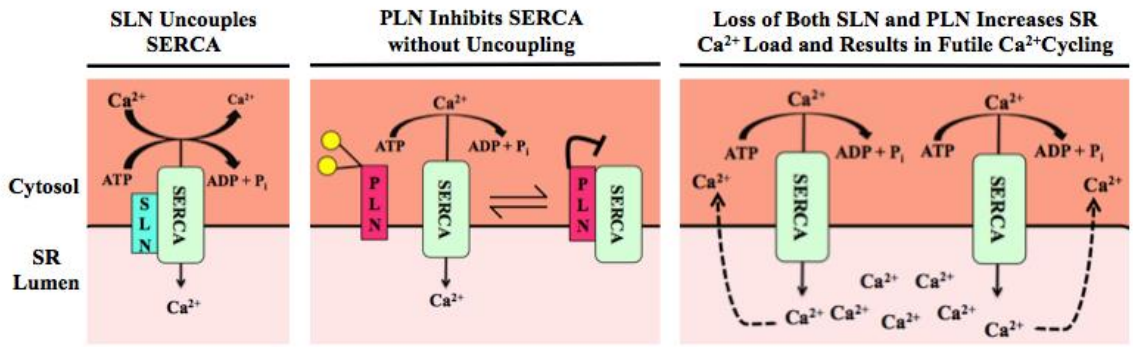

Figure 6.1. Conceptual figure illustrating the regulation of SERCA thermogenesis by different mechanisms. SLN uncouples Ca^{2+} transport from ATP hydrolysis by inducing "slippage" of Ca^{2+} ions from the pump (left). Although PLN inhibits the rate of SERCA activity when bound, it does not reduce transport efficiency (middle). In the absence of both SERCA inhibitors, Ca^{2+} transport in improved *in vivo* and as a result of the greater SR Ca^{2+} content, Ca^{2+} leak (dashed lines) is subsequently increased generating a futile Ca^{2+} cycle (right).

revealed that the combined action of SLN and PLN on SERCA is critical for the regulation of skeletal muscle fibre type/size and metabolism. In light of this, we propose that both the fibre type transition and lean phenotype of DKO mice may be the result of a futile cycle of chronic SR Ca^{2+} leak and re-uptake, as loss of SERCA inhibitors is likely to increase SR Ca^{2+} load, subsequently driving the loss of luminal Ca^{2+} and activation of SERCA activity (**Figure 6.1**).

Critical Differences Between SLN and PLN

Despite similarities in their sequence and ability to inhibit SERCA, several notable differences between SLN and PLN may explain why only the SLN/SERCA interaction is thermogenic in nature, particularly in their N-terminal cytosolic domains. The N-terminus of PLN is much larger and contains two domains, namely IA (AAs 1-20) and IB (AAs 21-30) (**Figure 1.4**). PLN's phosphorylation sites (serine-16 and threonine-17) are located within the IA domain and are responsible for regulating its responsiveness to β-adrenergic and Ca^{2+}-mediated signals via PKA and CaMKII, respectively (43). Although several reports have proposed threonine -5 on SLN as a site of reversible phosphorylation/dephosphorylation in regulating cardiac contractility in response to β – agonism (44, 60), this has not been demonstrated as a mechanism regulating skeletal muscle SLN like that of PLN (68, 71). To this end, the physical interaction of PLN with SERCA will be abolished under physiological states associated with increased sympathetic activation of skeletal muscle, such as exercise, cold exposure, and obesity. Therefore, the reversible nature of PLN regulation makes it conceptually incompatible as

an adaptive uncoupler of SERCA given that β-adrenergic signaling is a major component of adaptive thermogenesis.

Consistent with differences in their cytosolic region, Sahoo and colleagues (55) have shown that deletion of SLN's N-terminus completely abolishes its ability to uncouple SERCA function, while a chimeric protein consisting of SLN with its N-terminus switched for that of PLN's also does not uncouple SERCA, instead behaving more like that of native PLN. The importance of SLN's cytosolic N-terminus may reside in its ability to create a structural re-arrangement within SERCA's transmembrane domain, specifically with the M4 helix. M4 contains a cytosolic portion that extends into SERCAs stalk region (referred to as M4S4), and when bound to SLN, exhibits a 17° axial tilt relative to that of PLN-bound SERCA (167). Crystal structures of SERCA-SLN contain a bifurcated salt bridge that forms between residue E2 of SLN and both R324 and K328 within M4S4, a feature not present in the SERCA-PLN complex; therefore, this distinction is the likely explanation of the 17° tilt when bound to SLN (167). Interestingly, deletion of SLN's N-terminus produces an M4S4 tilt angle equivalent to that of PLN-bound SERCA (167). This structural re-arrangement caused by SLN is independent of its regulation of Ca^{2+} affinity, as SERCA's Ca^{2+} binding site geometry remains similar to that of PLN regardless of the M4S4 tilt angle (167), suggesting instead that it is specific to uncoupling *per se*. Autry and colleagues (167) have hypothesized the importance of the tilt caused by SLN is critical in promoting SERCA uncoupling because M4S4 is directly connected to the Ca^{2+}-binding residue (comprising the second binding site on SERCA) on M4, which transmits the Ca^{2+} bound signal resulting in

autophosphoryaltion of Asp351 within SERCA's phosphorylation domain (**Figure 1.2**) (168, 169).

Furthermore, cross-linking studies have revealed distinct differences in the ability of either regulatory protein to bind to different kinetic states of SERCA (54, 55). While PLN binding to SERCA is mutually exclusive with Ca^{2+}, SLN is capable of binding to all major kinetic intermediates of SERCA's reaction cycle, including Ca^{2+}-bound states (54). Interaction of SLN with nucleotide-bound SERCA in both the presence and absence of Ca^{2+} would be a requisite for SLN to induce "slippage" as this is predicted to occur during the E1 to E2 transition (**Figure 1.3**), whereas the mutually exclusive nature of PLN binding to SERCA with Ca^{2+} would preclude its ability to reduce pumping efficiency by a similar mechanism. In light of these distinctions between the two SERCA regulators, it is not surprising then that skeletal muscle PLN does not uncouple Ca^{2+}-transport from ATP hydrolysis (**Chapter 2**).

PLN is Regulated by Physiological Stimuli

Perhaps one of the more pressing questions resulting from this thesis is what physiological role does a reduction in muscle PLN expression serve with diet-induced obesity. While this finding was somewhat unexpected in light of the dietary response previously shown for SLN (13), it is remarkably consistent with other physiological states in which a change in energy expenditure occurs. Both shivering and non-shivering thermogenenic mechanisms are induced by acute and chronic cold exposure in order to protect core body temperature. Prolonged cold acclimation of rabbits (i.e. 4°C for 72 hrs) results in a reduction of cardiac PLN protein expression, increased phospho-PLN content,

and increased SERCA2a protein expression (94). More surprisingly, cold-acclimated rabbits displayed an increase in the amount of heat released from cardiac SR vesicles while Ca^{2+}-pumping (94), suggesting that these SR changes not only facilitate an improvement of cardiac contractility, but are also thermogenic in nature. Cold exposure also appears to impact the SR of oxidative skeletal muscle in a similar manner. Within the SOL of rabbits, exposure to 4°C for 10 days increases SERCA1a protein expression and the amount of heat released from the SR during Ca^{2+}-pumping (101), although no examination of PLN was made in this study. While it is unclear whether the presence of SLN could explain the thermogenic effect observed in cold exposed rabbits, both the rates of ATP hydrolysis and Ca^{2+}-uptake were higher following cold exposure (94, 101), indicating that an enhanced interaction of SLN with SERCA is unlikely. The response of SR proteins to cold exposure are mediated, in part, by an increase in circulating thyroid hormones (94), which are themselves regulators of muscular Ca^{2+}-handling (91). In fact, experimentally inducing hypothyroidism completely abolishes the adaptive thermogenic response of rabbit skeletal muscle SR to cold exposure (101).

States of thyroid dysfunction (i.e. hypo- and hyperthyroidism) can themselves change whole-body metabolic rate (92). Induction of hyperthyroidism (i.e. a hypermetabolic state) by administration of L-thyroxine (T4) in experimental animals decreases PLN expression and increases phospho-PLN content within both cardiac and oxidative skeletal muscle (93, 94, 97, 148). As is observed with cold-acclimation in rabbits, the amount of heat released by SR vesicles during Ca^{2+}-pumping is increased in cardiac and skeletal muscle with T4 administration (94, 100). Not surprisingly then, propylthiouracil induced hypothyroidism (i.e. a hypometabolic state) increases PLN

protein expression and concomitantly decreases its unphopshorylated form, while reducing the amount of heat released from the SR during Ca^{2+}-pumping within cardiac muscle (94). The results from these previous studies and that of this thesis demonstrate that PLN appears to display an adaptive response to physiological/hormonal signals such that its interaction with SERCA is diminished during an adaptive rise in energy expenditure. While removal of PLN-mediated inhibition of SERCA will facilitate Ca^{2+} cycling during muscular shivering when animals are acutely cold exposed, shivering gradually diminishes with longer exposure times and non-shivering thermogenic mechanisms become the predominate heat source (3). To this end, it is unclear if skeletal muscle PLN protein expression displays a similar reduction like that in the heart with prolonged periods of cold exposure, and if so, what physiological purpose this would serve. As both diet-induced obesity and hyperthyroidism, states not associated with an adaptive increase in muscular contracture, diminish the interaction of skeletal muscle PLN with SERCA, the possibility arises that this in itself might represent an adaptive mechanism controlling SERCA thermogenesis, potentially by allowing SR filling and subsequently promoting SERCA's alternate reactions (**Figure 1.3**).

Potential Signaling Mechanism Mediating Dietary Response of Skeletal Muscle PLN

The action of circulating thyroid hormones on peripheral tissues is controlled by deiodinase isoforms, which convert circulating T4 into triiodothyronine (T3) (170). In mice, expression of deiodinase-2 mRNA and enzymatic activity are higher in slow- compared to fast-twitch hind limb skeletal muscle (171, 172), and is activated by acute and chronic cold exposure (173, 174). Interestingly, 2 weeks of calorie restriction

reduces skeletal muscle deiodinase-2 protein expression, in addition to slowing the rate of muscle relaxation compared with *ad libitum* fed control rats (175). While a reduction of SERCA2a protein can, in part, explain why muscle function was reduced (175), it is possible that PLN expression may have also increased in response to caloric restriction in light of reduced muscle deiodinase-2 activity. Conversely, SOL deiodinase-2 gene expression has been reported to be increased almost 3-fold by high-fat feeding (176). As these studies show that both cold and diet can modulate muscular thyroid signaling with downstream effects on Ca^{2+}-handling, it is a reasonable hypothesis that diet-induced obesity could reduce skeletal muscle PLN protein expression via the activation of muscular deiodinase-2 expression/activity. In agreement with the importance of peripheral tissue thyroid signaling in regulating adaptive thermogenesis, mice deficient in diodinase-2 develop and excessive diet-induced obesity phenotype (176, 177). Although BAT UCP-1 expression is lower in diodinase-2 KO mice (177), it is likely that impaired skeletal muscle thermogenesis also contributes to this phenotype, although the contribution of SR proteins has not specifically been examined.

Future Directions

As discussed above, several studies have shown an association between a reduction in PLN's interaction with SERCA and increased SERCA thermogenesis (94, 100). Furthermore, improving SERCA function can result in SR Ca^{2+} leak in cardiac muscle (103, 105-107, 109-113), which will indirectly increase energy turnover by continuously cycling Ca^{2+} ions across the SR; however, it is unclear whether this occurs within skeletal muscle in response to the loss of SERCA inhibitory proteins. Although

this thesis examined the stoichiometric ratio of SERCA pumping in *Pln*$^{-/-}$ and DKO mice, this variable may not be the only important determinant of SR thermogenesis affected by SERCA regulatory proteins *in vivo*. To determine whether ablation of PLN, SLN, or both SERCA inhibitory proteins results in SR Ca^{2+} leakage, studies utilizing mechanically skinned single skeletal muscle fibres in which the SR remains intact (155), should be employed in conjunction with high-fat feeding in *Pln*$^{-/-}$, *Sln*$^{-/-}$, and DKO models. This technique involves exposing fibres to solutions of various [Ca^{2+}] for a defined period of time to allow SR Ca^{2+}-uptake. Fibres are then placed in a solution in both the presence and absence of compounds that block Ca^{2+} leak, and then exposed to a "release" solution, in which the generated force is used to calculate SR Ca^{2+} content. These experiments will enable proof-of-concept studies of SERCA regulation and SR Ca^{2+} load in the context of diet-induced obesity, and will be critical in examining whether futile Ca^{2+} cycling is a mechanism explaining the phenotype of DKO mice found in **Chapter 4** and **5**.

In addition to controlling the expression of SR proteins, peripheral thyroid signaling is modulated by diet (described above); therefore, muscle specific thyroid signaling is a potentially strong candidate mechanism regulating the adaptive dietary response of PLN protein. To assess the role of muscle-specific thyroid signaling on PLN with diet-induced obesity, future studies can utilize skeletal muscle-specific diodenase-2 KO mice, which are currently available (172, 178). If thyroid signaling through diodenase-2 is responsible for controlling the adaptive decline of PLN observed in this thesis, then deletion of diodenase-2 would be expected to attenuate or completely block this response. As discussed above, thyroid hormone can induce SERCA thermogenesis,

possibly by diminishing its interaction with PLN in order to promote its alternate reactions. If then, the diet-induced reduction of skeletal muscle PLN is an adaptive mechanism to promote SERCA thermogenesis, it stands to reason that *Pln*$^{-/-}$ mice would be protected against diet-induced obesity, which was not the case (**Chapter 3**). Interestingly, diodinase-2 KO mice are in fact susceptible to diet-induced obesity, but only when housed at thermoneutrality (177). In light of this, one major limitation was that our studies were carried out at room temperature, which may have prevented an observable metabolic phenotype with PLN ablation. Given that room temperature housing is in itself a thermal stress, metabolic rate must rise in order to compensate for continual heat loss, potentially masking a genotype difference in energy expenditure between WT and *Pln*$^{-/-}$ littermates. Therefore, high-fat feeding studies should be repeated with *Pln*$^{-/-}$ animals to determine whether a metabolic phenotype exists in the absence of ambient thermal stress to gain greater insight into the adaptive PLN response reported herein. Additionally, the role of PLN in mediating the muscle-specific and whole-body metabolic repose to thyroid hormone is completely unknown. To examine this, future studies can manipulate thyroid status by injection of *Pln*$^{-/-}$ mice with T4 or PTU.

The role of PLN in muscular contractility is well documented, and within the heart, reducing PLN's interaction with SERCA has long been proposed as a method of improving contractility in the failing myocardium. However, the impact of diet-induced obesity on skeletal muscle function is incompletely understood, although several reports have shown a number of contractile variables to be impaired by obesity (67, 164, 166, 179). Furthermore, it remains unclear from our studies how SERCA enzyme function is affected by prolonged high-fat feeding. This will be critical to assess, as SERCA activity

can be modulated by oxidative stress and SR lipid composition, factors that are altered by obesity (145, 180-183). It is tempting then to speculate that adaptive response of PLN to high-fat feeding described herein may function to mitigate contractile dysfunction caused by obesity in an effort to regulate SR Ca^{2+} load. To further elucidate the physiological role of the adaptive decline in PLN protein expression, future studies should examine SERCA and oxidative muscle function in WT and *Pln*$^{-/-}$ mice in response to diet-induced obesity.

References

1. **Withrow, D., and Alter, D. A. (2011) The economic burden of obesity worldwide: a systematic review of the direct costs of obesity. *Obes Rev* 12, 131-141**
2. **(2000) Obesity: preventing and managing the global epidemic. Report of a WHO consultation. *World Health Organ Tech Rep Ser* 894, i-xii, 1-253**
3. **Cannon, B., and Nedergaard, J. (2004) Brown adipose tissue: function and physiological significance. *Physiol Rev* 84, 277-359**
4. **Lowell, B. B., and Spiegelman, B. M. (2000) Towards a molecular understanding of adaptive thermogenesis. *Nature* 404, 652-660**
5. **Enerback, S., Jacobsson, A., Simpson, E. M., Guerra, C., Yamashita, H., Harper, M. E., and Kozak, L. P. (1997) Mice lacking mitochondrial uncoupling protein are cold-sensitive but not obese. *Nature* 387, 90-94**
6. **Feldmann, H. M., Golozoubova, V., Cannon, B., and Nedergaard, J. (2009) UCP1 ablation induces obesity and abolishes diet-induced thermogenesis in mice exempt from thermal stress by living at thermoneutrality. *Cell Metab* 9, 203-209**
7. **Saito, M., Okamatsu-Ogura, Y., Matsushita, M., Watanabe, K., Yoneshiro, T., Nio-Kobayashi, J., Iwanaga, T., Miyagawa, M., Kameya, T., Nakada, K., Kawai, Y., and Tsujisaki, M. (2009) High incidence of metabolically active brown adipose tissue in healthy adult humans: effects of cold exposure and adiposity. *Diabetes* 58, 1526-1531**
8. **Zingaretti, M. C., Crosta, F., Vitali, A., Guerrieri, M., Frontini, A., Cannon, B., Nedergaard, J., and Cinti, S. (2009) The presence of UCP1 demonstrates that metabolically active adipose tissue in the neck of adult humans truly represents brown adipose tissue. *FASEB J* 23, 3113-3120**
9. **Muzik, O., Mangner, T. J., Leonard, W. R., Kumar, A., Janisse, J., and Granneman, J. G. (2013) 15O PET measurement of blood flow and oxygen consumption in cold-activated human brown fat. *J Nucl Med* 54, 523-531**
10. **Porter, C., Chondronikola, M., and Sidossis, L. S. (2015) The Therapeutic Potential of Brown Adipocytes in Humans. *Front Endocrinol (Lausanne)* 6, 156**
11. **Warner, A., and Mittag, J. (2016) Breaking BAT: can browning create a better white? *J Endocrinol* 228, R19-29**
12. **Bal, N. C., Maurya, S. K., Sopariwala, D. H., Sahoo, S. K., Gupta, S. C., Shaikh, S. A., Pant, M., Rowland, L. A., Bombardier, E., Goonasekera, S. A., Tupling, A. R., Molkentin, J. D., and Periasamy, M. (2012) Sarcolipin is a newly identified regulator of muscle-based thermogenesis in mammals. *Nat Med* 18, 1575-1579**
13. **Bombardier, E., Smith, I. C., Gamu, D., Fajardo, V. A., Vigna, C., Sayer, R. A., Gupta, S. C., Bal, N. C., Periasamy, M., and Tupling, A. R. (2013)**

Sarcolipin trumps beta-adrenergic receptor signaling as the favored mechanism for muscle-based diet-induced thermogenesis. ***FASEB J***

14. **Bombardier, E., Smith, I. C., Vigna, C., Fajardo, V. A., and Tupling, A. R. (2013) Ablation of sarcolipin decreases the energy requirements for Ca(2+) transport by sarco(endo)plasmic reticulum Ca(2+)-ATPases in resting skeletal muscle.** ***FEBS Lett*** **587, 1687-1692**
15. **Gamu, D., Bombardier, E., Smith, I. C., Fajardo, V. A., and Tupling, A. R. (2014) Sarcolipin provides a novel muscle-based mechanism for adaptive thermogenesis.** ***Exerc Sport Sci Rev*** **42, 136-142**
16. **Gamu, D., Trinh, A., Bombardier, E., and Tupling, A. R. (2015) Persistence of diet-induced obesity despite access to voluntary activity in mice lacking sarcolipin.** ***Physiol Rep*** **3**
17. **MacPherson, R. E., Gamu, D., Frendo-Cumbo, S., Castellani, L., Kwon, F., Tupling, A. R., and Wright, D. C. (2016) Sarcolipin knockout mice fed a high-fat diet exhibit altered indices of adipose tissue inflammation and remodeling.** ***Obesity (Silver Spring)*** **24, 1499-1505**
18. **Rolfe, D. F., and Brown, G. C. (1997) Cellular energy utilization and molecular origin of standard metabolic rate in mammals.** ***Physiol Rev*** **77, 731-758**
19. **Dulhunty, A. F. (2006) Excitation-contraction coupling from the 1950s into the new millennium.** ***Clin Exp Pharmacol Physiol*** **33, 763-772**
20. **MacIntosh, B. R., Holash, R. J., and Renaud, J. M. (2012) Skeletal muscle fatigue--regulation of excitation-contraction coupling to avoid metabolic catastrophe.** ***J Cell Sci*** **125, 2105-2114**
21. **Tupling, A. R. (2004) The sarcoplasmic reticulum in muscle fatigue and disease: role of the sarco(endo)plasmic reticulum Ca2+-ATPase.** ***Can J Appl Physiol*** **29, 308-329**
22. **Clausen, T. (2003) Na+-K+ pump regulation and skeletal muscle contractility.** ***Physiol Rev*** **83, 1269-1324**
23. **Vandecaetsbeek, I., Vangheluwe, P., Raeymaekers, L., Wuytack, F., and Vanoevelen, J. (2011) The Ca2+ pumps of the endoplasmic reticulum and Golgi apparatus.** ***Cold Spring Harb Perspect Biol*** **3**
24. **Brini, M., and Carafoli, E. (2009) Calcium pumps in health and disease.** ***Physiol Rev*** **89, 1341-1378**
25. **Hovnanian, A. (2007) SERCA pumps and human diseases.** ***Subcell Biochem*** **45, 337-363**
26. **Periasamy, M., and Kalyanasundaram, A. (2007) SERCA pump isoforms: their role in calcium transport and disease.** ***Muscle Nerve*** **35, 430-442**
27. **Wu, K. D., and Lytton, J. (1993) Molecular cloning and quantification of sarcoplasmic reticulum Ca(2+)-ATPase isoforms in rat muscles.** ***Am J Physiol*** **264, C333-341**
28. **Fajardo, V. A., Bombardier, E., Vigna, C., Devji, T., Bloemberg, D., Gamu, D., Gramolini, A. O., Quadrilatero, J., and Tupling, A. R. (2013) Co-Expression of SERCA Isoforms, Phospholamban and Sarcolipin in Human Skeletal Muscle Fibers.** ***PLoS One*** **8, e84304**

29. **Wuytack, F., Raeymaekers, L., and Missiaen, L. (2002) Molecular physiology of the SERCA and SPCA pumps. *Cell Calcium* 32, 279-305**
30. **Lytton, J., Westlin, M., Burk, S. E., Shull, G. E., and MacLennan, D. H. (1992) Functional comparisons between isoforms of the sarcoplasmic or endoplasmic reticulum family of calcium pumps. *J Biol Chem* 267, 14483-14489**
31. **MacLennan, D. H. (1990) Molecular tools to elucidate problems in excitation-contraction coupling. *Biophys J* 58, 1355-1365**
32. **Toyoshima, C. (2008) Structural aspects of ion pumping by Ca2+-ATPase of sarcoplasmic reticulum. *Arch Biochem Biophys* 476, 3-11**
33. **Toyoshima, C. (2007) Ion pumping by calcium ATPase of sarcoplasmic reticulum. *Adv Exp Med Biol* 592, 295-303**
34. **MacLennan, D. H., Rice, W. J., and Green, N. M. (1997) The mechanism of Ca2+ transport by sarco(endo)plasmic reticulum Ca2+-ATPases. *J Biol Chem* 272, 28815-28818**
35. **Berman, M. C. (2001) Slippage and uncoupling in P-type cation pumps; implications for energy transduction mechanisms and regulation of metabolism. *Biochim Biophys Acta* 1513, 95-121**
36. **de Meis, L. (2001) Role of the sarcoplasmic reticulum Ca2+-ATPase on heat production and thermogenesis. *Biosci Rep* 21, 113-137**
37. **Smith, W. S., Broadbridge, R., East, J. M., and Lee, A. G. (2002) Sarcolipin uncouples hydrolysis of ATP from accumulation of Ca2+ by the Ca2+-ATPase of skeletal-muscle sarcoplasmic reticulum. *Biochem J* 361, 277-286**
38. **Mall, S., Broadbridge, R., Harrison, S. L., Gore, M. G., Lee, A. G., and East, J. M. (2006) The presence of sarcolipin results in increased heat production by Ca(2+)-ATPase. *J Biol Chem* 281, 36597-36602**
39. **Chinet, A., Decrouy, A., and Even, P. C. (1992) Ca(2+)-dependent heat production under basal and near-basal conditions in the mouse soleus muscle. *J Physiol* 455, 663-678**
40. **Decrouy, A., Even, P. C., and Chinet, A. (1993) Decreased rates of Ca(2+)-dependent heat production in slow- and fast-twitch muscles from the dystrophic (mdx) mouse. *Experientia* 49, 843-849**
41. **Dulloo, A. G., Decrouy, A., and Chinet, A. (1994) Suppression of Ca(2+)-dependent heat production in mouse skeletal muscle by high fish oil consumption. *Metabolism* 43, 931-934**
42. **Smith, I. C., Bombardier, E., Vigna, C., and Tupling, A.R. (2013) ATP consumption by sarcoplasmic reticulum Ca2+ pumps accounts for 40-50% of resting metabolic rate in mouse fast and slow twitch skeletal muscle. *PLoS One* 8, e68924**
43. **Bhupathy, P., Babu, G. J., and Periasamy, M. (2007) Sarcolipin and phospholamban as regulators of cardiac sarcoplasmic reticulum Ca2+ ATPase. *J Mol Cell Cardiol* 42, 903-911**
44. **Babu, G. J., Bhupathy, P., Timofeyev, V., Petrashevskaya, N. N., Reiser, P. J., Chiamvimonvat, N., and Periasamy, M. (2007) Ablation of sarcolipin**

enhances sarcoplasmic reticulum calcium transport and atrial contractility. *Proc Natl Acad Sci U S A* 104, 17867-17872

45. Luo, W., Grupp, I. L., Harrer, J., Ponniah, S., Grupp, G., Duffy, J. J., Doetschman, T., and Kranias, E. G. (1994) Targeted ablation of the phospholamban gene is associated with markedly enhanced myocardial contractility and loss of beta-agonist stimulation. *Circ Res* 75, 401-409

46. Chu, G., Ferguson, D. G., Edes, I., Kiss, E., Sato, Y., and Kranias, E. G. (1998) Phospholamban ablation and compensatory responses in the mammalian heart. *Ann N Y Acad Sci* 853, 49-62

47. Wolska, B. M., Stojanovic, M. O., Luo, W., Kranias, E. G., and Solaro, R. J. (1996) Effect of ablation of phospholamban on dynamics of cardiac myocyte contraction and intracellular Ca2+. *Am J Physiol* 271, C391-397

48. Slack, J. P., Grupp, I. L., Luo, W., and Kranias, E. G. (1997) Phospholamban ablation enhances relaxation in the murine soleus. *Am J Physiol* 273, C1-6

49. Tupling, A. R., Bombardier, E., Gupta, S. C., Hussain, D., Vigna, C., Bloemberg, D., Quadrilatero, J., Trivieri, M. G., Babu, G. J., Backx, P. H., Periasamy, M., MacLennan, D. H., and Gramolini, A. O. (2011) Enhanced Ca2+ transport and muscle relaxation in skeletal muscle from sarcolipin-null mice. *Am J Physiol Cell Physiol* 301, C841-849

50. Arkin, I. T., Adams, P. D., Brunger, A. T., Smith, S. O., and Engelman, D. M. (1997) Structural perspectives of phospholamban, a helical transmembrane pentamer. *Annu Rev Biophys Biomol Struct* 26, 157-179

51. Cao, Y., Wu, X., Yang, R., Wang, X., Sun, H., and Lee, I. (2017) Self-assembling study of sarcolipin and its mutants in multiple molecular dynamic simulations. *Proteins* 85, 1065-1077

52. Autry, J. M., Rubin, J. E., Pietrini, S. D., Winters, D. L., Robia, S. L., and Thomas, D. D. (2011) Oligomeric interactions of sarcolipin and the Ca-ATPase. *J Biol Chem* 286, 31697-31706

53. Asahi, M., Sugita, Y., Kurzydlowski, K., De Leon, S., Tada, M., Toyoshima, C., and MacLennan, D. H. (2003) Sarcolipin regulates sarco(endo)plasmic reticulum Ca2+-ATPase (SERCA) by binding to transmembrane helices alone or in association with phospholamban. *Proc Natl Acad Sci U S A* 100, 5040-5045

54. Sahoo, S. K., Shaikh, S. A., Sopariwala, D. H., Bal, N. C., and Periasamy, M. (2013) Sarcolipin protein interaction with sarco(endo)plasmic reticulum Ca2+ ATPase (SERCA) is distinct from phospholamban protein, and only sarcolipin can promote uncoupling of the SERCA pump. *J Biol Chem* 288, 6881-6889

55. Sahoo, S. K., Shaikh, S. A., Sopariwala, D. H., Bal, N. C., Bruhn, D. S., Kopec, W., Khandelia, H., and Periasamy, M. (2015) The N Terminus of Sarcolipin Plays an Important Role in Uncoupling Sarco-endoplasmic Reticulum Ca2+-ATPase (SERCA) ATP Hydrolysis from Ca2+ Transport. *J Biol Chem* 290, 14057-14067

56. Anderson, D. M., Anderson, K. M., Chang, C. L., Makarewich, C. A., Nelson, B. R., McAnally, J. R., Kasaragod, P., Shelton, J. M., Liou, J., Bassel-Duby, R.,

and Olson, E. N. (2015) A micropeptide encoded by a putative long noncoding RNA regulates muscle performance. *Cell* 160, 595-606
57. Traaseth, N. J., Ha, K. N., Verardi, R., Shi, L., Buffy, J. J., Masterson, L. R., and Veglia, G. (2008) Structural and dynamic basis of phospholamban and sarcolipin inhibition of Ca(2+)-ATPase. *Biochemistry* 47, 3-13
58. Periasamy, M., Bhupathy, P., and Babu, G. J. (2008) Regulation of sarcoplasmic reticulum Ca2+ ATPase pump expression and its relevance to cardiac muscle physiology and pathology. *Cardiovasc Res* 77, 265-273
59. Babu, G. J., Bhupathy, P., Petrashevskaya, N. N., Wang, H., Raman, S., Wheeler, D., Jagatheesan, G., Wieczorek, D., Schwartz, A., Janssen, P. M., Ziolo, M. T., and Periasamy, M. (2006) Targeted overexpression of sarcolipin in the mouse heart decreases sarcoplasmic reticulum calcium transport and cardiac contractility. *J Biol Chem* 281, 3972-3979
60. Bhupathy, P., Babu, G. J., Ito, M., and Periasamy, M. (2009) Threonine-5 at the N-terminus can modulate sarcolipin function in cardiac myocytes. *J Mol Cell Cardiol* 47, 723-729
61. Vangheluwe, P., Schuermans, M., Zador, E., Waelkens, E., Raeymaekers, L., and Wuytack, F. (2005) Sarcolipin and phospholamban mRNA and protein expression in cardiac and skeletal muscle of different species. *Biochem J* 389, 151-159
62. Rowland, L. A., Bal, N. C., Kozak, L. P., and Periasamy, M. (2015) Uncoupling Protein 1 and Sarcolipin Are Required to Maintain Optimal Thermogenesis, and Loss of Both Systems Compromises Survival of Mice under Cold Stress. *J Biol Chem* 290, 12282-12289
63. Bal, N. C., Maurya, S. K., Singh, S., Wehrens, X. H., and Periasamy, M. (2016) Increased Reliance on Muscle-based Thermogenesis upon Acute Minimization of Brown Adipose Tissue Function. *J Biol Chem* 291, 17247-17257
64. Sopariwala, D. H., Pant, M., Shaikh, S. A., Goonasekera, S. A., Molkentin, J. D., Weisleder, N., Ma, J., Pan, Z., and Periasamy, M. (2015) Sarcolipin overexpression improves muscle energetics and reduces fatigue. *J Appl Physiol (1985)* 118, 1050-1058
65. Fajardo, V. A., Bombardier, E., McMillan, E., Tran, K., Wadsworth, B. J., Gamu, D., Hopf, A., Vigna, C., Smith, I. C., Bellissimo, C., Michel, R. N., Tarnopolsky, M. A., Quadrilatero, J., and Tupling, A. R. (2015) Phospholamban overexpression in mice causes a centronuclear myopathy-like phenotype. *Dis Model Mech* 8, 999-1009
66. Summermatter, S., Thurnheer, R., Santos, G., Mosca, B., Baum, O., Treves, S., Hoppeler, H., Zorzato, F., and Handschin, C. (2012) Remodeling of calcium handling in skeletal muscle through PGC-1alpha: impact on force, fatigability, and fiber type. *Am J Physiol Cell Physiol* 302, C88-99
67. Ciapaite, J., van den Berg, S. A., Houten, S. M., Nicolay, K., van Dijk, K. W., and Jeneson, J. A. (2015) Fiber-type-specific sensitivities and phenotypic adaptations to dietary fat overload differentially impact

fast- versus slow-twitch muscle contractile function in C57BL/6J mice. *J Nutr Biochem* 26, 155-164
68. Song, Q., Young, K. B., Chu, G., Gulick, J., Gerst, M., Grupp, I. L., Robbins, J., and Kranias, E. G. (2004) Overexpression of phospholamban in slow-twitch skeletal muscle is associated with depressed contractile function and muscle remodeling. *FASEB J* 18, 974-976
69. Odermatt, A., Becker, S., Khanna, V. K., Kurzydlowski, K., Leisner, E., Pette, D., and MacLennan, D. H. (1998) Sarcolipin regulates the activity of SERCA1, the fast-twitch skeletal muscle sarcoplasmic reticulum Ca2+-ATPase. *J Biol Chem* 273, 12360-12369
70. Akin, B. L., Hurley, T. D., Chen, Z., and Jones, L. R. (2013) The structural basis for phospholamban inhibition of the calcium pump in sarcoplasmic reticulum. *J Biol Chem* 288, 30181-30191
71. Slack, J. P., Grupp, I. L., Ferguson, D. G., Rosenthal, N., and Kranias, E. G. (1997) Ectopic expression of phospholamban in fast-twitch skeletal muscle alters sarcoplasmic reticulum Ca2+ transport and muscle relaxation. *J Biol Chem* 272, 18862-18868
72. Gustavsson, M., Verardi, R., Mullen, D. G., Mote, K. R., Traaseth, N. J., Gopinath, T., and Veglia, G. (2013) Allosteric regulation of SERCA by phosphorylation-mediated conformational shift of phospholamban. *Proc Natl Acad Sci U S A* 110, 17338-17343
73. Gorski, P. A., Glaves, J. P., Vangheluwe, P., and Young, H. S. (2013) Sarco(endo)plasmic reticulum calcium ATPase (SERCA) inhibition by sarcolipin is encoded in its luminal tail. *J Biol Chem* 288, 8456-8467
74. Kadambi, V. J., Ponniah, S., Harrer, J. M., Hoit, B. D., Dorn, G. W., 2nd, Walsh, R. A., and Kranias, E. G. (1996) Cardiac-specific overexpression of phospholamban alters calcium kinetics and resultant cardiomyocyte mechanics in transgenic mice. *J Clin Invest* 97, 533-539
75. Pattison, J. S., Waggoner, J. R., James, J., Martin, L., Gulick, J., Osinska, H., Klevitsky, R., Kranias, E. G., and Robbins, J. (2008) Phospholamban overexpression in transgenic rabbits. *Transgenic Res* 17, 157-170
76. Asahi, M., Kurzydlowski, K., Tada, M., and MacLennan, D. H. (2002) Sarcolipin inhibits polymerization of phospholamban to induce superinhibition of sarco(endo)plasmic reticulum Ca2+-ATPases (SERCAs). *J Biol Chem* 277, 26725-26728
77. Tupling, A. R., Asahi, M., and MacLennan, D. H. (2002) Sarcolipin overexpression in rat slow twitch muscle inhibits sarcoplasmic reticulum Ca2+ uptake and impairs contractile function. *J Biol Chem* 277, 44740-44746
78. Asahi, M., Otsu, K., Nakayama, H., Hikoso, S., Takeda, T., Gramolini, A. O., Trivieri, M. G., Oudit, G. Y., Morita, T., Kusakari, Y., Hirano, S., Hongo, K., Hirotani, S., Yamaguchi, O., Peterson, A., Backx, P. H., Kurihara, S., Hori, M., and MacLennan, D. H. (2004) Cardiac-specific overexpression of sarcolipin inhibits sarco(endo)plasmic reticulum Ca2+ ATPase (SERCA2a) activity and impairs cardiac function in mice. *Proc Natl Acad Sci U S A* 101, 9199-9204

79. **Shannon, T. R., Chu, G., Kranias, E. G., and Bers, D. M. (2001) Phospholamban decreases the energetic efficiency of the sarcoplasmic reticulum Ca pump.** ***J Biol Chem*** **276, 7195-7201**
80. **Frank, K., Tilgmann, C., Shannon, T. R., Bers, D. M., and Kranias, E. G. (2000) Regulatory role of phospholamban in the efficiency of cardiac sarcoplasmic reticulum Ca2+ transport.** ***Biochemistry*** **39, 14176-14182**
81. **Gramolini, A. O., Trivieri, M. G., Oudit, G. Y., Kislinger, T., Li, W., Patel, M. M., Emili, A., Kranias, E. G., Backx, P. H., and Maclennan, D. H. (2006) Cardiac-specific overexpression of sarcolipin in phospholamban null mice impairs myocyte function that is restored by phosphorylation.** ***Proc Natl Acad Sci U S A*** **103, 2446-2451**
82. **Haghighi, K., Schmidt, A. G., Hoit, B. D., Brittsan, A. G., Yatani, A., Lester, J. W., Zhai, J., Kimura, Y., Dorn, G. W., 2nd, MacLennan, D. H., and Kranias, E. G. (2001) Superinhibition of sarcoplasmic reticulum function by phospholamban induces cardiac contractile failure.** ***J Biol Chem*** **276, 24145-24152**
83. **Maclennan, D. H., and Zvaritch, E. (2011) Mechanistic models for muscle diseases and disorders originating in the sarcoplasmic reticulum.** ***Biochim Biophys Acta*** **1813, 948-964**
84. **Morrissette, J. M., Franck, J. P., and Block, B. A. (2003) Characterization of ryanodine receptor and Ca2+-ATPase isoforms in the thermogenic heater organ of blue marlin (Makaira nigricans).** ***J Exp Biol*** **206, 805-812**
85. **Bruton, J. D., Aydin, J., Yamada, T., Shabalina, I. G., Ivarsson, N., Zhang, S. J., Wada, M., Tavi, P., Nedergaard, J., Katz, A., and Westerblad, H. (2010) Increased fatigue resistance linked to Ca2+-stimulated mitochondrial biogenesis in muscle fibres of cold-acclimated mice.** ***J Physiol*** **588, 4275-4288**
86. **Aydin, J., Shabalina, I. G., Place, N., Reiken, S., Zhang, S. J., Bellinger, A. M., Nedergaard, J., Cannon, B., Marks, A. R., Bruton, J. D., and Westerblad, H. (2008) Nonshivering thermogenesis protects against defective calcium handling in muscle.** ***FASEB J*** **22, 3919-3924**
87. **Rowland, L. A., Maurya, S. K., Bal, N. C., Kozak, L., and Periasamy, M. (2016) Sarcolipin and uncoupling protein 1 play distinct roles in diet-induced thermogenesis and do not compensate for one another.** ***Obesity (Silver Spring)*** **24, 1430-1433**
88. **Maurya, S. K., Bal, N. C., Sopariwala, D. H., Pant, M., Rowland, L. A., Shaikh, S. A., and Periasamy, M. (2015) Sarcolipin Is a Key Determinant of the Basal Metabolic Rate, and Its Overexpression Enhances Energy Expenditure and Resistance against Diet-induced Obesity.** ***J Biol Chem*** **290, 10840-10849**
89. **Chu, G., Luo, W., Slack, J. P., Tilgmann, C., Sweet, W. E., Spindler, M., Saupe, K. W., Boivin, G. P., Moravec, C. S., Matlib, M. A., Grupp, I. L., Ingwall, J. S., and Kranias, E. G. (1996) Compensatory mechanisms associated with the hyperdynamic function of phospholamban-deficient mouse hearts.** ***Circ Res*** **79, 1064-1076**

90. **Kadambi, V. J., Ball, N., Kranias, E. G., Walsh, R. A., and Hoit, B. D. (1999) Modulation of force-frequency relation by phospholamban in genetically engineered mice.** ***Am J Physiol*** **276, H2245-2250**
91. **Carr, A. N., and Kranias, E. G. (2002) Thyroid hormone regulation of calcium cycling proteins.** ***Thyroid*** **12, 453-457**
92. **Freake, H. C., and Oppenheimer, J. H. (1995) Thermogenesis and thyroid function.** ***Annu Rev Nutr*** **15, 263-291**
93. **Arai, M., Otsu, K., MacLennan, D. H., Alpert, N. R., and Periasamy, M. (1991) Effect of thyroid hormone on the expression of mRNA encoding sarcoplasmic reticulum proteins.** ***Circ Res*** **69, 266-276**
94. **Ketzer, L. A., Arruda, A. P., Carvalho, D. P., and de Meis, L. (2009) Cardiac sarcoplasmic reticulum Ca2+-ATPase: heat production and phospholamban alterations promoted by cold exposure and thyroid hormone.** ***Am J Physiol Heart Circ Physiol*** **297, H556-563**
95. **Ojamaa, K., Kenessey, A., and Klein, I. (2000) Thyroid hormone regulation of phospholamban phosphorylation in the rat heart.** ***Endocrinology*** **141, 2139-2144**
96. **Jiang, M., Xu, A., Jones, D. L., and Narayanan, N. (2004) Coordinate downregulation of CaM kinase II and phospholamban accompanies contractile phenotype transition in the hyperthyroid rabbit soleus.** ***Am J Physiol Cell Physiol*** **287, C622-632**
97. **Holt, E., Sjaastad, I., Lunde, P. K., Christensen, G., and Sejersted, O. M. (1999) Thyroid hormone control of contraction and the Ca(2+)-ATPase/phospholamban complex in adult rat ventricular myocytes.** ***J Mol Cell Cardiol*** **31, 645-656**
98. **Trivieri, M. G., Oudit, G. Y., Sah, R., Kerfant, B. G., Sun, H., Gramolini, A. O., Pan, Y., Wickenden, A. D., Croteau, W., Morreale de Escobar, G., Pekhletski, R., St Germain, D., Maclennan, D. H., and Backx, P. H. (2006) Cardiac-specific elevations in thyroid hormone enhance contractility and prevent pressure overload-induced cardiac dysfunction.** ***Proc Natl Acad Sci U S A*** **103, 6043-6048**
99. **Minamisawa, S., Uemura, N., Sato, Y., Yokoyama, U., Yamaguchi, T., Inoue, K., Nakagome, M., Bai, Y., Hori, H., Shimizu, M., Mochizuki, S., and Ishikawa, Y. (2006) Post-transcriptional downregulation of sarcolipin mRNA by triiodothyronine in the atrial myocardium.** ***FEBS Lett*** **580, 2247-2252**
100. **Arruda, A. P., Da-Silva, W. S., Carvalho, D. P., and De Meis, L. (2003) Hyperthyroidism increases the uncoupled ATPase activity and heat production by the sarcoplasmic reticulum Ca2+-ATPase.** ***Biochem J*** **375, 753-760**
101. **Arruda, A. P., Ketzer, L. A., Nigro, M., Galina, A., Carvalho, D. P., and de Meis, L. (2008) Cold tolerance in hypothyroid rabbits: role of skeletal muscle mitochondria and sarcoplasmic reticulum Ca2+ ATPase isoform 1 heat production.** ***Endocrinology*** **149, 6262-6271**

102. Mirit, E., Palmon, A., Hasin, Y., and Horowitz, M. (1999) Heat acclimation induces changes in cardiac mechanical performance: the role of thyroid hormone. ***Am J Physiol*** **276, R550-558**
103. Xie, L. H., Shanmugam, M., Park, J. Y., Zhao, Z., Wen, H., Tian, B., Periasamy, M., and Babu, G. J. (2012) Ablation of sarcolipin results in atrial remodeling. ***Am J Physiol Cell Physiol*** **302, C1762-1771**
104. Davia, K., Hajjar, R. J., Terracciano, C. M., Kent, N. S., Ranu, H. K., O'Gara, P., Rosenzweig, A., and Harding, S. E. (1999) Functional alterations in adult rat myocytes after overexpression of phospholamban with use of adenovirus. ***Physiol Genomics*** **1, 41-50**
105. Huser, J., Bers, D. M., and Blatter, L. A. (1998) Subcellular properties of [Ca2+]i transients in phospholamban-deficient mouse ventricular cells. ***Am J Physiol*** **274, H1800-1811**
106. Lukyanenko, V., Viatchenko-Karpinski, S., Smirnov, A., Wiesner, T. F., and Gyorke, S. (2001) Dynamic regulation of sarcoplasmic reticulum Ca(2+) content and release by luminal Ca(2+)-sensitive leak in rat ventricular myocytes. ***Biophys J*** **81, 785-798**
107. Santana, L. F., Kranias, E. G., and Lederer, W. J. (1997) Calcium sparks and excitation-contraction coupling in phospholamban-deficient mouse ventricular myocytes. ***J Physiol*** **503 (Pt 1), 21-29**
108. Shanmugam, M., Gao, S., Hong, C., Fefelova, N., Nowycky, M. C., Xie, L. H., Periasamy, M., and Babu, G. J. (2011) Ablation of phospholamban and sarcolipin results in cardiac hypertrophy and decreased cardiac contractility. ***Cardiovasc Res*** **89, 353-361**
109. Wellman, G. C., Santana, L. F., Bonev, A. D., and Nelson, M. T. (2001) Role of phospholamban in the modulation of arterial Ca(2+) sparks and Ca(2+)-activated K(+) channels by cAMP. ***Am J Physiol Cell Physiol*** **281, C1029-1037**
110. Chan, Y. H., Tsai, W. C., Song, Z., Ko, C. Y., Qu, Z., Weiss, J. N., Lin, S. F., Chen, P. S., Jones, L. R., and Chen, Z. (2015) Acute reversal of phospholamban inhibition facilitates the rhythmic whole-cell propagating calcium waves in isolated ventricular myocytes. ***J Mol Cell Cardiol*** **80, 126-135**
111. Sirenko, S., Maltsev, V. A., Maltseva, L. A., Yang, D., Lukyanenko, Y., Vinogradova, T. M., Jones, L. R., and Lakatta, E. G. (2014) Sarcoplasmic reticulum Ca2+ cycling protein phosphorylation in a physiologic Ca2+ milieu unleashes a high-power, rhythmic Ca2+ clock in ventricular myocytes: relevance to arrhythmias and bio-pacemaker design. ***J Mol Cell Cardiol*** **66, 106-115**
112. Zhang, T., Guo, T., Mishra, S., Dalton, N. D., Kranias, E. G., Peterson, K. L., Bers, D. M., and Brown, J. H. (2010) Phospholamban ablation rescues sarcoplasmic reticulum Ca(2+) handling but exacerbates cardiac dysfunction in CaMKIIdelta(C) transgenic mice. ***Circ Res*** **106, 354-362**
113. Aschar-Sobbi, R., Emmett, T. L., Kargacin, G. J., and Kargacin, M. E. (2012) Phospholamban phosphorylation increases the passive calcium leak from cardiac sarcoplasmic reticulum. ***Pflugers Arch*** **464, 295-305**

114. Moraru, A., Cakan-Akdogan, G., Strassburger, K., Males, M., Mueller, S., Jabs, M., Muelleder, M., Frejno, M., Braeckman, B. P., Ralser, M., and Teleman, A. A. (2017) THADA Regulates the Organismal Balance between Energy Storage and Heat Production. ***Dev Cell*** **41, 72-81 e76**
115. Leberer, E., Hartner, K. T., Brandl, C. J., Fujii, J., Tada, M., MacLennan, D. H., and Pette, D. (1989) Slow/cardiac sarcoplasmic reticulum Ca2+-ATPase and phospholamban mRNAs are expressed in chronically stimulated rabbit fast-twitch muscle. ***Eur J Biochem*** **185, 51-54**
116. Arai, M., Otsu, K., MacLennan, D. H., and Periasamy, M. (1992) Regulation of sarcoplasmic reticulum gene expression during cardiac and skeletal muscle development. ***Am J Physiol*** **262, C614-620**
117. Wu, H., Kanatous, S. B., Thurmond, F. A., Gallardo, T., Isotani, E., Bassel-Duby, R., and Williams, R. S. (2002) Regulation of mitochondrial biogenesis in skeletal muscle by CaMK. ***Science*** **296, 349-352**
118. Parsons, S. A., Wilkins, B. J., Bueno, O. F., and Molkentin, J. D. (2003) Altered skeletal muscle phenotypes in calcineurin Aalpha and Abeta gene-targeted mice. ***Mol Cell Biol*** **23, 4331-4343**
119. Chen, G., Carroll, S., Racay, P., Dick, J., Pette, D., Traub, I., Vrbova, G., Eggli, P., Celio, M., and Schwaller, B. (2001) Deficiency in parvalbumin increases fatigue resistance in fast-twitch muscle and upregulates mitochondria. ***Am J Physiol Cell Physiol*** **281, C114-122**
120. Racay, P., Gregory, P., and Schwaller, B. (2006) Parvalbumin deficiency in fast-twitch muscles leads to increased 'slow-twitch type' mitochondria, but does not affect the expression of fiber specific proteins. ***FEBS J*** **273, 96-108**
121. Chin, E. R., Grange, R. W., Viau, F., Simard, A. R., Humphries, C., Shelton, J., Bassel-Duby, R., Williams, R. S., and Michel, R. N. (2003) Alterations in slow-twitch muscle phenotype in transgenic mice overexpressing the Ca2+ buffering protein parvalbumin. ***J Physiol*** **547, 649-663**
122. Duhamel, T. A., Stewart, R. D., Tupling, A. R., Ouyang, J., and Green, H. J. (2007) Muscle sarcoplasmic reticulum calcium regulation in humans during consecutive days of exercise and recovery. ***J Appl Physiol (1985)*** **103, 1212-1220**
123. Inesi, G., and de Meis, L. (1989) Regulation of steady state filling in sarcoplasmic reticulum. Roles of back-inhibition, leakage, and slippage of the calcium pump. ***J Biol Chem*** **264, 5929-5936**
124. Grynkiewicz, G., Poenie, M., and Tsien, R. Y. (1985) A new generation of Ca2+ indicators with greatly improved fluorescence properties. ***J Biol Chem*** **260, 3440-3450**
125. Zubrzycka-Gaarn, E., MacDonald, G., Phillips, L., Jorgensen, A. O., and MacLennan, D. H. (1984) Monoclonal antibodies to the Ca2+ + Mg2+-dependent ATPase of sarcoplasmic reticulum identify polymorphic forms of the enzyme and indicate the presence in the enzyme of a classical high-affinity Ca2+ binding site. ***J Bioenerg Biomembr*** **16, 441-464**

126. Fajardo, V. A., Bombardier, E., Vigna, C., Devji, T., Bloemberg, D., Gamu, D., Gramolini, A.O., Quadrilatero, J., and Tupling, A.R. (2013) Co-expression of SERCA isoforms, phospholamban and sarcolipin in human muscle fibers. ***PLoS One*** **PONE-D-13-25403**

127. Bloemberg, D., and Quadrilatero, J. (2012) Rapid determination of myosin heavy chain expression in rat, mouse, and human skeletal muscle using multicolor immunofluorescence analysis. ***PLoS One*** **7, e35273**

128. Damiani, E., Sacchetto, R., and Margreth, A. (2000) Variation of phospholamban in slow-twitch muscle sarcoplasmic reticulum between mammalian species and a link to the substrate specificity of endogenous Ca(2+)-calmodulin-dependent protein kinase. ***Biochim Biophys Acta*** **1464, 231-241**

129. Chin, E. R. (2004) The role of calcium and calcium/calmodulin-dependent kinases in skeletal muscle plasticity and mitochondrial biogenesis. ***Proc Nutr Soc*** **63, 279-286**

130. Fajardo, V. A., Rietze, B. A., Chambers, P. J., Bellissimo, C., Bombardier, E., Quadrilatero, J., and Tupling, A. R. (2017) Effects of sarcolipin deletion on skeletal muscle adaptive responses to functional overload and unload. ***Am J Physiol Cell Physiol*****, ajpcell 00291 02016**

131. Gamu, D., Trinh, A., Fajardo, V. A., Bombardier, E., and Tupling, A. R. (2017) Sarcolipin expression is not required for the mitochondrial enzymatic response to physical activity or diet. ***J Appl Physiol (1985)*** **122, 1276-1283**

132. Shaikh, S. A., Sahoo, S. K., and Periasamy, M. (2016) Phospholamban and sarcolipin: Are they functionally redundant or distinct regulators of the Sarco(Endo)Plasmic Reticulum Calcium ATPase? ***J Mol Cell Cardiol*** **91, 81-91**

133. Wu, J., Cohen, P., and Spiegelman, B. M. (2013) Adaptive thermogenesis in adipocytes: is beige the new brown? ***Genes Dev*** **27, 234-250**

134. Boss, O., Samec, S., Paoloni-Giacobino, A., Rossier, C., Dulloo, A., Seydoux, J., Muzzin, P., and Giacobino, J. P. (1997) Uncoupling protein-3: a new member of the mitochondrial carrier family with tissue-specific expression. ***FEBS Lett*** **408, 39-42**

135. Gong, D. W., Monemdjou, S., Gavrilova, O., Leon, L. R., Marcus-Samuels, B., Chou, C. J., Everett, C., Kozak, L. P., Li, C., Deng, C., Harper, M. E., and Reitman, M. L. (2000) Lack of obesity and normal response to fasting and thyroid hormone in mice lacking uncoupling protein-3. ***J Biol Chem*** **275, 16251-16257**

136. Vidal-Puig, A. J., Grujic, D., Zhang, C. Y., Hagen, T., Boss, O., Ido, Y., Szczepanik, A., Wade, J., Mootha, V., Cortright, R., Muoio, D. M., and Lowell, B. B. (2000) Energy metabolism in uncoupling protein 3 gene knockout mice. ***J Biol Chem*** **275, 16258-16266**

137. MacLennan, D. H., Asahi, M., and Tupling, A. R. (2003) The regulation of SERCA-type pumps by phospholamban and sarcolipin. ***Ann N Y Acad Sci*** **986, 472-480**

138. Rose, A. J., Kiens, B., and Richter, E. A. (2006) Ca2+-calmodulin-dependent protein kinase expression and signalling in skeletal muscle during exercise. ***J Physiol*** **574, 889-903**
139. Fajardo, V. A., Gamu, D., Mitchell, A., Bloemberg, D., Bombardier, E., Chambers, P. J., Bellissimo, C., Quadrilatero, J., and Tupling, A. R. (2017) Sarcolipin deletion exacerbates soleus muscle atrophy and weakness in phospholamban overexpressing mice. ***PLoS One*** **12, e0173708**
140. Weicker, H., Feraudi, M., Hagele, H., and Pluto, R. (1984) Electrochemical detection of catecholamines in urine and plasma after separation with HPLC. ***Clin Chim Acta*** **141, 17-25**
141. Green, H. J., Jones, S., Ball-Burnett, M., and Fraser, I. (1991) Early adaptations in blood substrates, metabolites, and hormones to prolonged exercise training in man. ***Can J Physiol Pharmacol*** **69, 1222-1229**
142. Cooney, G. J., Thompson, A. L., Furler, S. M., Ye, J., and Kraegen, E. W. (2002) Muscle long-chain acyl CoA esters and insulin resistance. ***Ann N Y Acad Sci*** **967, 196-207**
143. Smith, M. M., and Minson, C. T. (2012) Obesity and adipokines: effects on sympathetic overactivity. ***J Physiol*** **590, 1787-1801**
144. Butler, J., Smyth, N., Broadbridge, R., Council, C. E., Lee, A. G., Stocker, C. J., Hislop, D. C., Arch, J. R., Cawthorne, M. A., and Malcolm East, J. (2015) The effects of sarcolipin over-expression in mouse skeletal muscle on metabolic activity. ***Arch Biochem Biophys*** **569, 26-31**
145. Paran, C. W., Verkerke, A. R., Heden, T. D., Park, S., Zou, K., Lawson, H. A., Song, H., Turk, J., Houmard, J. A., and Funai, K. (2015) Reduced efficiency of sarcolipin-dependent respiration in myocytes from humans with severe obesity. ***Obesity (Silver Spring)*** **23, 1440-1449**
146. Fajardo, V. A. (2016) The Role of Phospholamban and Sarcolipin in Skeletal Muscle Disease. ***University of Waterloo: PhD Thesis***
147. Almundarij, T. I., Gavini, C. K., and Novak, C. M. (2017) Suppressed sympathetic outflow to skeletal muscle, muscle thermogenesis, and activity energy expenditure with calorie restriction. ***Physiol Rep*** **5**
148. Kaasik, A., Paju, K., Vetter, R., and Seppet, E. K. (1997) Thyroid hormones increase the contractility but suppress the effects of beta-adrenergic agonist by decreasing phospholamban expression in rat atria. ***Cardiovasc Res*** **35, 106-112**
149. Michel, R. N., Dunn, S. E., and Chin, E. R. (2004) Calcineurin and skeletal muscle growth. ***Proc Nutr Soc*** **63, 341-349**
150. Moraru, A., Cakan-Akdogan, G., Strassburger, K., Males, M., Mueller, S., Jabs, M., Muelleder, M., Frejno, M., Braeckman, B. P., Ralser, M., and Teleman, A. A. (2017) THADA Regulates the Organismal Balance between Energy Storage and Heat Production. ***Dev Cell*** **41, 450**
151. Chin, E. R. (2005) Role of Ca2+/calmodulin-dependent kinases in skeletal muscle plasticity. ***J Appl Physiol (1985)*** **99, 414-423**

152. Gamu, D., Wadsworth, B. J., Bombardier, E., Smith, I. C., and Tupling, A. R. (2014) Dual ablation of phospholamban and sarcolipin enhance skeletal muscle contractility. *Appl Physiol Nutr Metab* 39, S19
153. Bers, D. M. (2014) Cardiac sarcoplasmic reticulum calcium leak: basis and roles in cardiac dysfunction. *Annu Rev Physiol* 76, 107-127
154. Camello, C., Lomax, R., Petersen, O. H., and Tepikin, A. V. (2002) Calcium leak from intracellular stores--the enigma of calcium signalling. *Cell Calcium* 32, 355-361
155. Murphy, R. M., Larkins, N. T., Mollica, J. P., Beard, N. A., and Lamb, G. D. (2009) Calsequestrin content and SERCA determine normal and maximal Ca2+ storage levels in sarcoplasmic reticulum of fast- and slow-twitch fibres of rat. *J Physiol* 587, 443-460
156. Reis, M., Farage, M., and de Meis, L. (2002) Thermogenesis and energy expenditure: control of heat production by the Ca(2+)-ATPase of fast and slow muscle. *Mol Membr Biol* 19, 301-310
157. Bombardier, E., Smith, I. C., Gamu, D., Fajardo, V. A., Vigna, C., Sayer, R. A., Gupta, S. C., Bal, N. C., Periasamy, M., and Tupling, A. R. (2013) Sarcolipin trumps beta-adrenergic receptor signaling as the favored mechanism for muscle-based diet-induced thermogenesis. *FASEB J* 27, 3871-3878
158. Chavez, J. A., Knotts, T. A., Wang, L. P., Li, G., Dobrowsky, R. T., Florant, G. L., and Summers, S. A. (2003) A role for ceramide, but not diacylglycerol, in the antagonism of insulin signal transduction by saturated fatty acids. *J Biol Chem* 278, 10297-10303
159. Giacca, A., Xiao, C., Oprescu, A. I., Carpentier, A. C., and Lewis, G. F. (2011) Lipid-induced pancreatic beta-cell dysfunction: focus on in vivo studies. *Am J Physiol Endocrinol Metab* 300, E255-262
160. de Meis, L., Arruda, A. P., da-Silva, W. S., Reis, M., and Carvalho, D. P. (2003) The thermogenic function of the sarcoplasmic reticulum Ca2+-ATPase of normal and hyperthyroid rabbit. *Ann N Y Acad Sci* 986, 481-488
161. Anderson, D. M., Makarewich, C. A., Anderson, K. M., Shelton, J. M., Bezprozvannaya, S., Bassel-Duby, R., and Olson, E. N. (2016) Widespread control of calcium signaling by a family of SERCA-inhibiting micropeptides. *Sci Signal* 9, ra119
162. De Tomasi, L. C., Bruno, A., Sugizaki, M. M., Lima-Leopoldo, A. P., Nascimento, A. F., Junior, S. A., Pinotti, M. F., Padovani, C. R., Leopoldo, A. S., and Cicogna, A. C. (2009) Food restriction promotes downregulation of myocardial L-type Ca2+ channels. *Can J Physiol Pharmacol* 87, 426-431
163. Mayhew, M., Renganathan, M., and Delbono, O. (1998) Effectiveness of caloric restriction in preventing age-related changes in rat skeletal muscle. *Biochem Biophys Res Commun* 251, 95-99
164. Bruton, J. D., Katz, A., Lannergren, J., Abbate, F., and Westerblad, H. (2002) Regulation of myoplasmic Ca(2+) in genetically obese (ob/ob) mouse single skeletal muscle fibres. *Pflugers Arch* 444, 692-699

165. Cotter, M. A., Cameron, N. E., Robertson, S., and Ewing, I. (1993) Polyol pathway-related skeletal muscle contractile and morphological abnormalities in diabetic rats. *Exp Physiol* 78, 139-155
166. Warmington, S. A., Tolan, R., and McBennett, S. (2000) Functional and histological characteristics of skeletal muscle and the effects of leptin in the genetically obese (ob/ob) mouse. *Int J Obes Relat Metab Disord* 24, 1040-1050
167. Autry, J. M., Thomas, D. D., and Espinoza-Fonseca, L. M. (2016) Sarcolipin Promotes Uncoupling of the SERCA Ca2+ Pump by Inducing a Structural Rearrangement in the Energy-Transduction Domain. *Biochemistry* 55, 6083-6086
168. Clausen, J. D., Bublitz, M., Arnou, B., Montigny, C., Jaxel, C., Moller, J. V., Nissen, P., Andersen, J. P., and le Maire, M. (2013) SERCA mutant E309Q binds two Ca(2+) ions but adopts a catalytically incompetent conformation. *EMBO J* 32, 3231-3243
169. Inesi, G., Ma, H., Lewis, D., and Xu, C. (2004) Ca2+ occlusion and gating function of Glu309 in the ADP-fluoroaluminate analog of the Ca2+-ATPase phosphoenzyme intermediate. *J Biol Chem* 279, 31629-31637
170. Bianco, A. C., Maia, A. L., da Silva, W. S., and Christoffolete, M. A. (2005) Adaptive activation of thyroid hormone and energy expenditure. *Biosci Rep* 25, 191-208
171. Marsili, A., Ramadan, W., Harney, J. W., Mulcahey, M., Castroneves, L. A., Goemann, I. M., Wajner, S. M., Huang, S. A., Zavacki, A. M., Maia, A. L., Dentice, M., Salvatore, D., Silva, J. E., and Larsen, P. R. (2010) Type 2 iodothyronine deiodinase levels are higher in slow-twitch than fast-twitch mouse skeletal muscle and are increased in hypothyroidism. *Endocrinology* 151, 5952-5960
172. Werneck-de-Castro, J. P., Fonseca, T. L., Ignacio, D. L., Fernandes, G. W., Andrade-Feraud, C. M., Lartey, L. J., Ribeiro, M. B., Ribeiro, M. O., Gereben, B., and Bianco, A. C. (2015) Thyroid Hormone Signaling in Male Mouse Skeletal Muscle Is Largely Independent of D2 in Myocytes. *Endocrinology* 156, 3842-3852
173. Louzada, R. A., Santos, M. C., Cavalcanti-de-Albuquerque, J. P., Rangel, I. F., Ferreira, A. C., Galina, A., Werneck-de-Castro, J. P., and Carvalho, D. P. (2014) Type 2 iodothyronine deiodinase is upregulated in rat slow- and fast-twitch skeletal muscle during cold exposure. *Am J Physiol Endocrinol Metab* 307, E1020-1029
174. Ramadan, W., Marsili, A., Larsen, P. R., Zavacki, A. M., and Silva, J. E. (2011) Type-2 iodothyronine 5'deiodinase (D2) in skeletal muscle of C57Bl/6 mice. II. Evidence for a role of D2 in the hypermetabolism of thyroid hormone receptor alpha-deficient mice. *Endocrinology* 152, 3093-3102
175. De Andrade, P. B., Neff, L. A., Strosova, M. K., Arsenijevic, D., Patthey-Vuadens, O., Scapozza, L., Montani, J. P., Ruegg, U. T., Dulloo, A. G., and Dorchies, O. M. (2015) Caloric restriction induces energy-sparing alterations in skeletal muscle contraction, fiber composition and local

thyroid hormone metabolism that persist during catch-up fat upon refeeding. *Front Physiol* 6, 254

176. Marsili, A., Aguayo-Mazzucato, C., Chen, T., Kumar, A., Chung, M., Lunsford, E. P., Harney, J. W., Van-Tran, T., Gianetti, E., Ramadan, W., Chou, C., Bonner-Weir, S., Larsen, P. R., Silva, J. E., and Zavacki, A. M. (2011) Mice with a targeted deletion of the type 2 deiodinase are insulin resistant and susceptible to diet induced obesity. *PLoS One* 6, e20832

177. Castillo, M., Hall, J. A., Correa-Medina, M., Ueta, C., Kang, H. W., Cohen, D. E., and Bianco, A. C. (2011) Disruption of thyroid hormone activation in type 2 deiodinase knockout mice causes obesity with glucose intolerance and liver steatosis only at thermoneutrality. *Diabetes* 60, 1082-1089

178. Fonseca, T. L., Werneck-De-Castro, J. P., Castillo, M., Bocco, B. M., Fernandes, G. W., McAninch, E. A., Ignacio, D. L., Moises, C. C., Ferreira, A. R., Gereben, B., and Bianco, A. C. (2014) Tissue-specific inactivation of type 2 deiodinase reveals multilevel control of fatty acid oxidation by thyroid hormone in the mouse. *Diabetes* 63, 1594-1604

179. Shortreed, K. E., Krause, M. P., Huang, J. H., Dhanani, D., Moradi, J., Ceddia, R. B., and Hawke, T. J. (2009) Muscle-specific adaptations, impaired oxidative capacity and maintenance of contractile function characterize diet-induced obese mouse skeletal muscle. *PLoS One* 4, e7293

180. Fu, M. H., and Tupling, A. R. (2009) Protective effects of Hsp70 on the structure and function of SERCA2a expressed in HEK-293 cells during heat stress. *Am J Physiol Heart Circ Physiol* 296, H1175-1183

181. Tupling, A. R., Bombardier, E., Vigna, C., Quadrilatero, J., and Fu, M. (2008) Interaction between Hsp70 and the SR Ca2+ pump: a potential mechanism for cytoprotection in heart and skeletal muscle. *Appl Physiol Nutr Metab* 33, 1023-1032

182. Tupling, A. R., Gramolini, A. O., Duhamel, T. A., Kondo, H., Asahi, M., Tsuchiya, S. C., Borrelli, M. J., Lepock, J. R., Otsu, K., Hori, M., MacLennan, D. H., and Green, H. J. (2004) HSP70 binds to the fast-twitch skeletal muscle sarco(endo)plasmic reticulum Ca2+ -ATPase (SERCA1a) and prevents thermal inactivation. *J Biol Chem* 279, 52382-52389

183. Fajardo, V. A., Bombardier, E., Tran, K., Metherel, A. H., Irvine, T., Holloway, G. P., Green, H. J., Stark, K. D., and Tupling, A. R. (2015) Sarcoplasmic Reticulum Phospholipid Fatty Acid Composition and Sarcolipin Content in Rat Skeletal Muscle. *J Membr Biol* 248, 1089-1096

Appendix A

Table A1. Primer sequences for genotyping of wild-type (WT) phopholamban (PLN), sarcolipin (SLN), or corresponding targeted knock-out sequences.

Genotype	Primer Name	Sequence
***Pln*$^{+/+}$**	27 WT Forward	5'-CACGTCAGAATCTCCAGAACC-3'
	27 WT Rreverse	5'-TCCCCCTTTAACTCTCATAAGC-3'
***Pln*$^{-/-}$**	MMRRC Line 27 HLT7	5'-TGTGGGTTGCAAAGTTAGGC-3'
	L27 NEO	5'-TCCTCGTGCTTTACGGTATC-3'
***Sln*$^{+/+}$**	SLN-WT Forward	5'-TGTCCTCATCACCGTTCTCCT-3'
	SLN-WT Reverse	5'-GCTGGAGCATCTTGGCTAATC-3'
***Sln*$^{-/-}$**	SLN-null Forward	5'-GTGGCCAGAGCTTTCCAATA-3'
	SLN-null Reverse	5'-CAAAACCAAATTAAGGGCCA-3'

Appendix A

$$ATP + Ca^{2+}\,(EVS) \xrightarrow{SERCA} ADP + P_i + Ca^{2+}\,(lumen)$$

$$ADP + phosphoenolpyruvate \xrightarrow{PK} ATP + pyruvate$$

$$pyruvate + NADH \xrightarrow{LDH} lactate + NAD^{+}$$

Figure A1. Ca^{2+}-ATPase assay reaction schematic. SERCA transports Ca^{2+} ions from the extravesicular space (EVS) into the vesicle lumen in an ATP-dependent manner. The ADP produced from this reaction serves as a substrate along with excess phosphoenolpyruvate for the auxiliary enzyme pyruvate kinase (PK), forming an ATP-regenerating system. Pyruvate formed from the PK reaction serves as a reactant along with excess NADH for the second auxiliary enzyme lactate dehydrogenase (LDH). The consumption of NADH is measured spectrophotometically as it is stoichiometrically coupled 1:1 to the consumption of ATP.

Appendix A

Table A2. Western blotting details. Samples were transferred to either polyvinylidene difluoride (PVDF) or nitrocellulose (NC) membranes. Antibody incubations occurred at room temperature (RT) or overnight (ON).

Protein	Gel % (Type)	Membrane	Blocking Agent	1° (Time/Temp)	2° (Time/Temp)	ECL Substrate
SERCA1a	7.5% (Glycine)	PVDF	5% Skim Milk	1:10000 (1hr/RT)	1:20000 (1hr/RT)	Bio Vision
SERCA2a	7.5% (Glycine)	PVDF	5% Skim Milk	1:2000 (1hr/RT)	1:20000 (1hr/RT)	Luminata Forte
RyR	6% (Glycine)	PVDF	5% Skim Milk	1:1000 (1hr/RT)	1:4000 (1hr/RT)	Luminata Forte
DHPR	6% (Glycine)	PVDF	5% Skim Milk	1:1000 (1hr/RT)	1:4000 (1hr/RT)	Bio Vision
CSQ	7.5% (Glycine)	PVDF	5% Skim Milk	1:1000 (1hr/RT)	1:4000 (1hr/RT)	Bio Vision
SLN	13% (Tricine)	NC	5% Skim Milk	1:50 (ON/4°C)	1:2000 (1hr/RT)	Super Signal
PLN	13% (Tricine)	PVDF	5% Skim Milk	1:1000 (ON/4°C)	1:2000 (1hr/RT)	Luminata Forte
phos-PLN	13% (Tricine)	PVDF	5% Skim Milk	1:1000 (ON/4°C)	1:2000 (1hr/RT)	Luminata Forte
UCP-1	10% (Glycine)	PVDF	5% Skim Milk	1:2000 (ON/4°C)	1:10000 (1hr/RT)	Bio Vision

-ECL: enhanced chemiluminescence

Appendix A

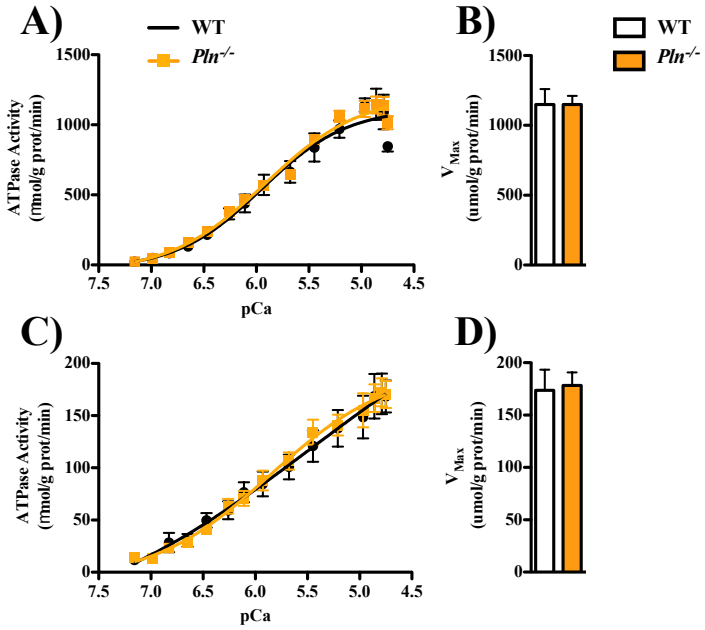

Figure A2. Ca^{2+}-dependent Ca^{2+}-ATPase activity (µmol/g protein/min) within extensor digitorum longus homogenates of wild-type (WT) and *Pln*$^{-/-}$ mice (n = 5/group). **A)** ATPase activity curves measured in the presence of the Ca^{2+}-specific ionophore A23187 (i.e. leaky vesicles). **B)** Maximal ATPase activity (V_{Max}) of leaky vesicles. **C)** ATPase activity curves measured in the absence of the Ca^{2+}-specific ionophore A23187 (i.e. intact vesicles). **D)** V_{Max} of intact vesicles. Values mean ± S.E.

Appendix A

Table A3. EDL Ca^{2+} affinity (i.e. pCa_{50}: pCa at half maximal ATPase activity) of wild-type (WT) and *Pln*$^{-/-}$ mice (n = 5/group) in the presence (i.e. leaky vesicles) and absence (i.e. intact vesicles) of the Ca^{2+}-specific ionophore A23187.

	pCa_{50}	
Condition	**WT**	***Pln*$^{-/-}$**
Leaky	5.94 ± 0.06	5.92 ± 0.03
Intact	5.77 ± 0.19	5.80 ± 0.04

Appendix B

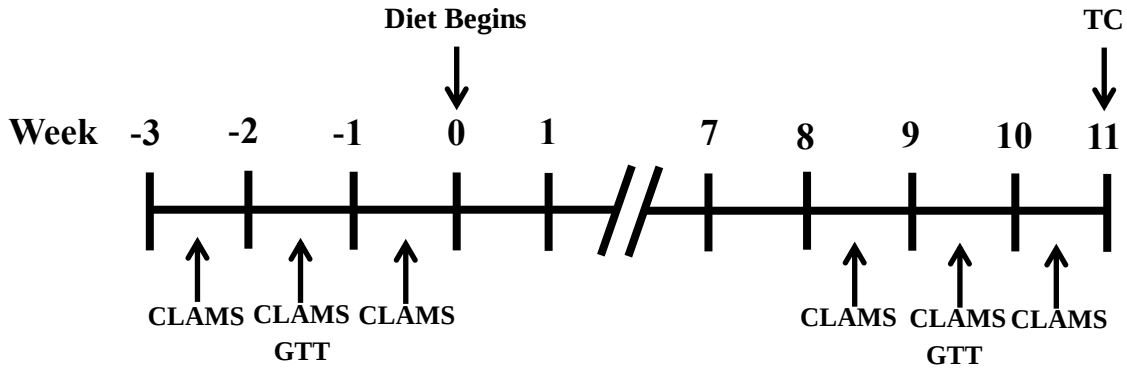

Figure B1. Measurement timeline of control and high-fat fed animals pre- and post-diet. CLAMS: Comprehensive Lab Animal Monitoring System, GTT: glucose tolerance test, TC: tissue collection.

Appendix B

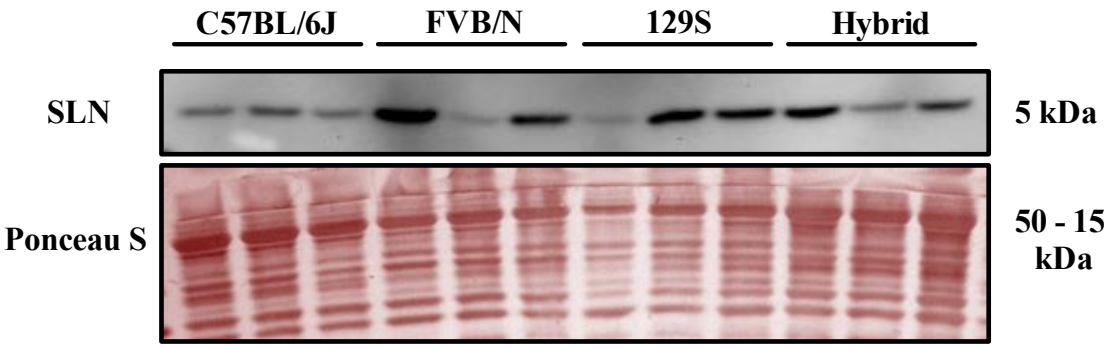

Figure B2. SOL SLN protein expression of WT mice (4-6 months old) across different strains. 20 μg of protein was resolved on a 13% tricine gel.

Appendix C

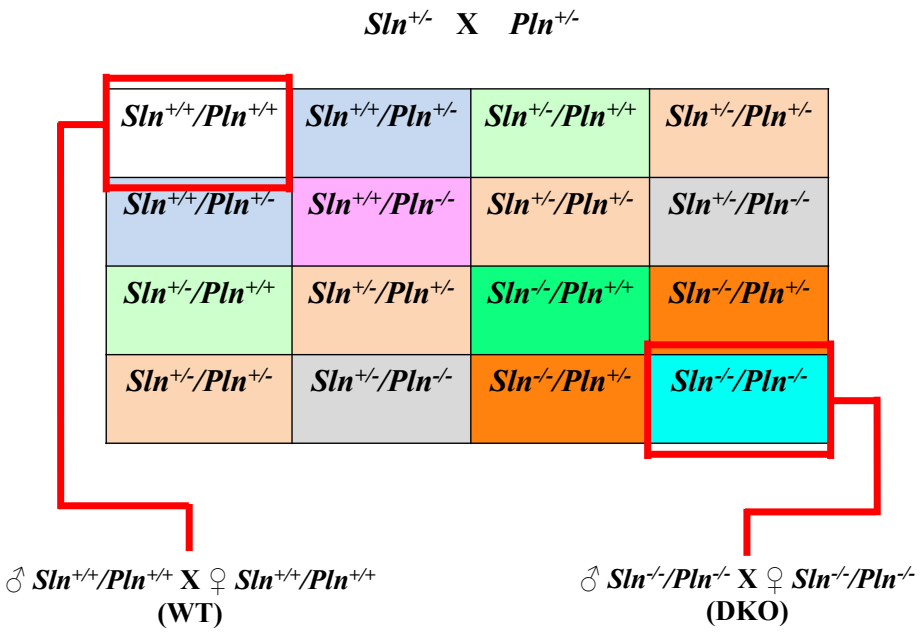

Figure C1. Breeding schematic used to establish double knock-out (DKO) and wild-type (WT) control colonies. Different colours denote various genotypes from crossing of heterozygous mice from established *Sln* and *Pln* colonies.

Appendix C

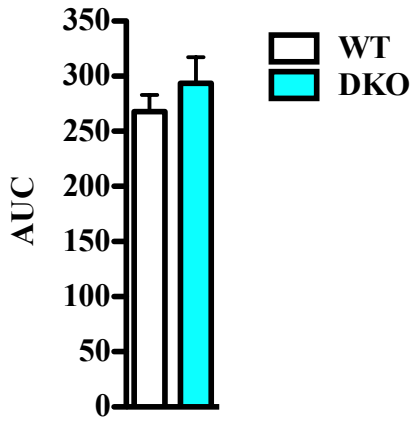

Figure C2. Area under the curve (AUC) measured during a glucose tolerance test and adjusted for fasting blood glucose. Values are mean ± S.E.

Appendix D

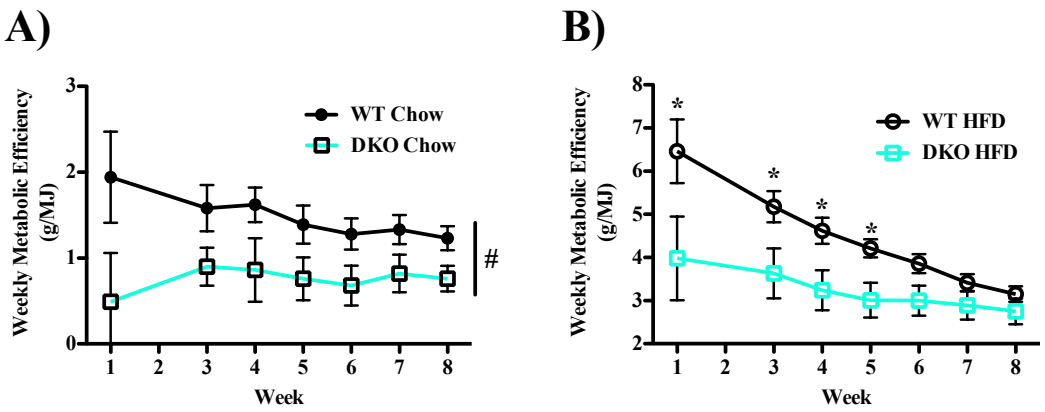

Figure D1. Weekly metabolic efficiency (g mass gained/MJ food consumed) of **A)** chow (n = 8-10/group) and **B)** HFD-fed (n = 12/group) wild-type (WT) and double knock-out (DKO) mice. Week 2 was removed due to incomplete data for all mice. # Significant main effect ($P < 0.05$) of genotype (WT > DKO). * Significantly different ($P < 0.05$) than corresponding DKO. Values are mean ± S.E.